

Northeastern Iranian loess and its palaeoclimatic implications

Inaugural-Dissertation

zur

Erlangung des Doktorgrades

der Mathematisch-Naturwissenschaftlichen Fakultät

der Universität zu Köln

vorgelegt von

Stefan Vlaminck

aus Köln

Köln 2018

Berichterstatter/Gutachter: PD Dr. Martin Kehl
Prof. Dr. Frank Schäbitz

Tag der Abschlussprüfung: 05.05.2017

Abstract

Loess-palaeosol sequences (LPS) are valuable terrestrial archives for the characterization and reconstruction of late Pleistocene climate dynamics over wide areas. Within the Eurasian loess belt most scientific attention was attributed to the loess successions of southeastern Europe and Central Asia. Thus, considerable knowledge gaps remain to be closed for other regions. The loess deposits and LPS of northern Iran represent an important link between these two areas. However, previous investigations were based on coarse-meshed sampling and analyses and therefore provided only limited insights into the lithological properties of loess deposits, intercalated palaeosols and the resulting pedostratigraphy. This applies also to the provenance of loess, the degree of weathering and the genetic interpretation of palaeosols. Consequently, insights into palaeoclimate of northeastern Iran and its last interglacial-glacial landscape evolution are limited, impeding regional as well as supraregional correlations with palaeoclimatic archives and LPS from western and central Asia.

The present dissertation aims at elaborating new records of lithological and palaeopedological properties of northeastern Iranian loess. Relative wind velocities during the periods of loess formation and the distance from the dust source are inferred from highly resolved grain-size analyses. The dust source itself is tentatively localized by means of immobile major elements. Moreover, palaeosols are to be identified and characterized in order to establish a regional pedostratigraphy of northeastern Iran. One focus is put on the detection of weakly developed palaeosols, as little is known about their existence and potential correlations with interstadials of MIS 3. A second focus is put on the thorough characterization of the MIS 5 pedo-complex. These foci provide evidence in order to distinguish between syngenetic and post-sedimentary palaeosols. Furthermore, marker horizons are identified and supplemented by luminescence dating results to establish a chronostratigraphic scheme and regional correlation of the LPS. Based on the results of the present dissertation the northeastern Iranian LPS are compared with palaeoclimatic archives from western and central Asia.

This requires improved stratigraphical investigations and high-resolution sampling of three newly discovered loess exposures. The studied loess deposits are found along a modern precipitation gradient, since the profiles of Neka-Abelou and Toshan are located in the subhumid foreland of the Alborz Mountain range, whereas the Agh Band (Agh 1/2) profile is located in the so called Iranian loess plateau (ILP). The considerable number of sediment samples (~4500) was used to provide new records on grain-size (laser-diffractometry), soil color (VIS spectrometry), carbonate content (MIRS) and rock magnetism (magnetic susceptibility) which are combined with micromorphological and geochemical findings. The correlation of the northeastern Iranian LPS with marine isotope stages is based on a discussion of the luminescence dating result from these sections.

Accordingly, the LPS of Neka-Abelou and Toshan are structured by numerous weakly to strongly developed palaeosols. These sections may be well correlated with other LPS along the northern declivity of the Alborz Mountains, which are known from the scientific literature. The MIS 5 pedocomplex, composed of three strongly developed palaeosols (Bt[k] and Bw[k]-horizons) has proven to be highly suited for correlation. The uppermost of these palaeosols

is overlain by weakly weathered MIS 4 loess, which may be well recognized in numerous exposures of the region. The MIS 5 pedocomplex and the MIS 4-loess thus provide excellent stratigraphic marker horizons. Moreover, a tephra layer could be detected at the base of the MIS 4-loess, which might yield independent age control. Additionally, last glacial loess deposits are structured by several syngenetic palaeosols (CB and Bw-horizons), which have formed during the interstadial periods of MIS 3 and 2. The boundaries between these incipient palaeosols and underlying and overlying loess strata are marked by gradual transitions in texture, soil color and magnetic susceptibility. The comparatively fine texture of these soils indicates decreasing wind velocities, while magnetic susceptibility signals weakly enhanced weathering intensities. The latter, however, resulted merely in partial decalcification of the deposits. Hence, the interstadial palaeosols likely developed under relatively dry and dusty climatic conditions, corresponding with increased wind energy and proximal sediment supply. It is assumed that these interstadial palaeosols are the result of millennial scale fluctuations, which are covered by the standard deviation of luminescence dating and thus impede any correlation with the marine record.

Conversely, the palaeosol of the MIS 5 pedo-complex formed postgenetically on glacial loess under reduced and distal or absent dust accumulation. These soils are completely decalcified and exhibit abrupt lower boundaries in the form of distinct carbonate enrichment horizons. The transitions into subsequent stadials are again characterized by intervals of syngenetic soil formation, indicating a gradual aridization. From MIS 4 to 2 a distinct coarsening trend of loess texture is apparent, indicating steeper atmospheric pressure gradients and proximal sediment supply. The major phase of loess formation presumably coincides with MIS 3.

The ratio of immobile major elements $\text{Al}_2\text{O}_3/\text{TiO}_2$ reveals a different provenance of loess along the northern declivity of the Alborz Mountains as compared to loess in the ILP. It is assumed that dust, forming the loess deposits of these areas originates from the alluvial plains of the respective rivers Gorgan and Atrek.

The palaeosols of the Agh1/2 profile are composed of strongly developed Bwyk-horizons, which could be correlated with MIS 7. Previous findings suggesting a correlation with MIS 5 may therefore be rejected. Moreover, no incipient palaeosols of the last pleniglacial could be detected in Agh Band. Hence the correlation of the Agh Band profile (Agh 1/2) with LPS of Neka-Abelou and Toshan is afflicted with considerable uncertainties.

Based on its highly detailed stratigraphy and the exceptional amount of available data, the Toshan section is defined as northern Iranian key sequence. The MIS 5 pedo-complex may be well correlated with loess sections from southern Europe, Armenia and central Asia. This palaeosol triple also reflects palaeoclimatic fluctuations of MIS which are recorded in other climatic archives from (e.g.) the Mediterranean, Lake Van and Lake Urmia. Furthermore, northern Iranian loess and its six interstadial palaeosols seem to offer more differentiated insights into the last glacial than the loess deposits from the other above mentioned regions.

Kurzzusammenfassung

Löss-Paläobodensequenzen (LPS) stellen wertvolle terrestrische Archive dar, um die Dynamik des spätpleistozänen Klimas zu kennzeichnen und großräumig nachvollziehen zu können. Innerhalb des Eurasischen Lössgürtels befanden sich vor allem die Lössabfolgen Südosteuropas und Zentralasiens im Brennpunkt der bisherigen Forschung, so dass große regionale Kenntnislücken existieren. Die im Nordostiran vorkommenden Löss- und LPS stellen ein wichtiges Bindeglied zwischen diesen Großräumen dar, allerdings lieferten bisherige Untersuchungen aufgrund der grobmaschigen Beprobung und Analyse nur wenig Befunde über die lithologischen Eigenschaften der Löss- und eingeschalteten Böden sowie über die hieraus abzuleitende Pedostratigraphie. Dies gilt auch für das Herkunftsgebiet der lössbildenden Stäube sowie für den Verwitterungsgrad und die genetische Deutung der Paläoböden. Daher sind auch derzeit nur eingeschränkte Einblicke in das Paläoklima des Nordostirans und dessen Landschaftsentwicklung während des letzten Interglazial-Glazial-Zyklus möglich und regionale als auch eine überregionale Korrelation mit anderen Klimaarchiven und LPS aus West- und Zentralasien erschwert.

Die vorliegende Arbeit setzt sich zum Ziel, neue Records der lithologischen und paläopedologischen Eigenschaften des nordostiranischen Lösses zu erarbeiten. Aus der hochaufgelöst bestimmten Korngrößenzusammensetzung sollen die während des Staubtransports herrschenden Windgeschwindigkeiten bzw. die Entfernung vom Quellgebiet abgeleitet werden. Letzteres soll mit Hilfe mobiler Hauptelemente eingegrenzt werden.

Weitere Ziele bestehen in der Kennzeichnung der Paläoböden und Ableitung einer regionalen Pedostratigraphie. Schwerpunkte bilden hierbei einerseits schwache Bodenbildungen, über deren Existenz und mögliche Korrelation mit Interstadialen des MIS 3 kaum etwas bekannt ist und andererseits der aus kräftigen Böden bestehende Pedokomplex des MIS 5. Hierzu sollen auch Hinweise zur Unterscheidung von syn- und postsedimentärer Bodenbildung erarbeitet werden. Außerdem besteht ein Ziel darin, stratigraphische Leithorizonte zu identifizieren, die – in Kombination mit den Lumineszenzdatierungen – eine chronostratigraphische Einordnung und Korrelation der LPS ermöglichen. Die Arbeitsergebnisse sollen schließlich zur Korrelation der nordostiranischen LPS mit West- und Zentralasiatischen Klimaarchiven herangezogen werden.

Dies erforderte zunächst eine feinstratigraphische Aufnahme und hochauflösende Beprobung der Löss- und LPS, die in drei neu angelegten Stufenprofilen von repräsentativen Aufschlüssen in verschiedenen Teilregionen erfolgte. Mit der Auswahl der Aufschlüsse wurde ein rezenter Klimagradient abgedeckt, da die Profile von Neka-Abelou und Toshan im subhumiden nördlichen Vorland des Elbursgebirges liegen, während das Profil Agh Band (Agh1/2) im semiariden Gebiet des sog. Iranischen Lössplateaus (ILP) angelegt wurde. An dem umfangreichen Material (~4500 Sedimentproben) wurden neue Records der Korngröße (Laser-Diffraktometrie), Bodenfarbe (VIS-Spektrometrie), des Karbonatgehalts (MIRS) und der Gesteinsmagnetik (magnetische Suszeptibilität) erarbeitet und mit Ergebnissen mikromorphologischer Untersuchungen sowie geochemischer Analysen kombiniert. Zur Korrelation der LPS mit dem Klimakalender wurden zudem Ergebnisse von Lumineszenzdatierungen diskutiert, die an gleichen Profilen erarbeitet worden sind.

Demnach sind die LPS Neka-Abelou und Toshan durch zahlreiche stark bis schwach entwickelte Paläoböden gegliedert, die sich mit weiteren in der Literatur beschriebenen LPS

der Elburs-Nordabdachung gut korrelieren lassen. Dies gilt insbesondere für den Pedokomplex des MIS 5. Dieser besteht aus drei kräftig entwickelten Paläoböden, die durch Bt(k) und Bw(k)-Horizonte gekennzeichnet sind. Der oberste Boden wird im Hangenden durch schwach pedogen überprägten Löss des MIS 4 überdeckt, der in zahlreichen Aufschlüssen gut zu erkennen ist und gemeinsam mit dem Bodentripel hervorragende stratigraphische Marker bildet. An der Basis des MIS 4-Lösses konnte zudem eine Tephralage nachgewiesen werden, die unabhängige Altersdaten liefern könnte. Zudem ist der letztglaziale Löss durch mehrere syngenetische Böden gegliedert (CBk und Bwk-Horizonte), die sich während der Interstadiale des MIS 3 und 2 gebildet haben. Diese Böden sind durch graduelle Übergänge der Textur, Farbe und magnetischen Suszeptibilität zu den hangenden und liegenden Lössen gekennzeichnet. Die relative feine Textur dieser Böden zeigt abnehmende Windgeschwindigkeiten an, während die magnetische Suszeptibilität schwach zunehmende Verwitterungsintensitäten signalisiert, die jedoch nur zu einer partiellen Kalkverarmung führten. Diese Interstadialböden bildeten sich vermutlich während trockener und staubiger Klimabedingungen, die mit relativ hohen Windgeschwindigkeiten und proximaler Sedimentanlieferung korrespondierten. Es wird vermutet, dass diese Paläoböden auf kurzfristige Klimaschwankungen zurückzuführen sind, die zeitlich durch die Standardabweichung der Lumineszenzdatierung abgedeckt werden und sich somit einer Korrelation entziehen.

Demgegenüber bildeten sich die Böden des MIS 5-Pedokomplexes unter reduzierter, distaler oder fehlender Staubakkumulation postgenetisch aus kaltzeitlichem Löss. Diese Böden sind vollständig entkalkt und besitzen scharfe Untergrenzen in Form deutlicher Karbonatanreicherungs-horizonte. Die Übergänge zu nachfolgenden Stadien sind erneut durch Phasen der syngenetischen Bodenbildung gekennzeichnet und signalisieren eine graduelle Aridisierung. Insgesamt zeigt eine deutliche Vergröberungstendenz der Löss-textur während der MIS 4 bis 2 eine Zunahme atmosphärischer Druckgradienten bzw. eine proximale Sedimentanlieferung an. Die Hauptphase der Lössbildung ereignete sich vermutlich während des MIS 3. Das Verhältnis der immobilen Hauptelemente Al_2O_3/TiO_2 lässt zudem vermuten, dass sich das Quellgebiet der Lösses entlang der Elbursnordabdachung von dem des ILP unterscheidet. Es wird angenommen, dass der Staub aus dem sich die Lössvorkommen dieser beiden Räume bildete den alluvialen Schwemmebenen der jeweiligen Flusssysteme des Gorgans und des Atreks entstammt.

Die Paläoböden des Profils Agh 1/2 bestehen aus kräftig entwickelten Bwyk-Horizonten, die entgegen vorheriger Ergebnisse nicht dem MIS 5 sondern dem MIS 7 zuzuordnen sind. Zudem konnte keinen initialen Paläoböden des letzten Pleniglazials in Agh Band gefunden werden. Die Korrelation des Profils Agh Band (Agh 1/2) mit den LPS Neka-Abelou und Toshan ist daher gegenwärtig mit Unsicherheiten behaftet.

Aufgrund der detaillierten Stratigraphie und der herausragenden Datenverfügbarkeit wurde das Profil Toshan als nordiranische Schlüsselsequenz definiert. Der MIS 5-Pedokomplex lässt sich gut mit Lössprofilen Südeuropas, Armeniens und Zentralasiens korrelieren und spiegelt die auch in anderen Klimaarchiven z.B. des Mittelmeeres, des Vansees und des Urmiasees dokumentierten Klimaschwankungen des MIS 5 wider. Mit bis zu sechs interstadialen Böden erlaubt der Löss Nordirans zudem eine bessere pedostratigraphische Differenzierung des letzten Glazials, als dies in den o.g. Regionen bisher möglich scheint.

Acknowledgements

The present dissertation marks the end of a time full of new impressions (that I will always keep in good memory) and particularly mountains of work to climb. In doing so I was supported by a multitude of different people, whose human abilities and scientific skills contributed to the completion of this thesis.

I want to express my deep gratitude to my supervisor and scientific mentor PD Dr. Martin Kehl for his patience, many fruitful scientific and friendly discussions and his guidance in loess research and during field work.

I want to thank:

- Prof. Dr. Manfred Frechen and PD. Dr. Eva Lehndorff for critical thoughts and comments on my manuscripts and valuable scientific advice
- Prof. Farhad Khormali for generous logistic support during field campaigns to Iran
- Dr. Tobias Lauer for his friendship and mutual support during field campaigns and an introduction to luminescence dating
- Dr. Ali Shahriari and Jafar Sharifi for their help during field work and for introducing me to the fascinating culture of Iran
- Dr. Sven-Oliver Franz for fruitful discussions on questions related to geochemistry and mineralogy
- Dr. Christian Rolf for scientific advice related to rock magnetism and his kind invitations to Grubenhagen
- Dr. Eileen Eckmeier for introducing me to VIS
- Prof. Dr. Frank Schäbitz for co-supervising this thesis

During the past four years I have invested countless hours of work in different laboratories to generate highly resolved records. However, the large amount of samples could not have been handled by one single person. Workload was, therefore, distributed among several research facilities, each of which was in charge of analyses matching their respective practical and theoretical expertise. In this context, I wish to express my gratitude to: Sonja Riemenschneider and Astrid Jaeckel from the Leibniz-Institute for Applied Geophysics (LIAG) for performing grain-size analyses and Katrin Worm and Lena Wallbrecht for doing rock magnetic analyses.

I address particular thanks to Katrin and Horst Worm for inviting me to their home after laboratory work in Grubenhagen.

I thank Michael Wagner and Lars Emde for their deep friendship and their ability to make me laugh. Special thanks go to Alexandra, Angela and Frank Wagner, Brigitte Caster and Herbert Emde for their friendship and honesty. I would like to address special thanks to Julia Gehendges and her parents Marga and Jürgen who have filled significant parts of my life with love and joy.

I want to express my deepest gratitude to my wonderful family, for their love and patience. Finally I want to address my deepest gratitude to my beloved Susanne for giving me love and hope.

Table of Contents

Abstract.....	I
Kurzzusammenfassung.....	III
Acknowledgements ..	V
Table of Contents.....	VI
List of Figures.....	X
List of Tables.....	XVII
 Chapter 1 Introduction	 1
1.1 Definitions and formation of loess	3
1.2 Loess as an archive of palaeoclimate research	7
1.3 Loess in northern Iran	11
1.4 Knowledge gaps and scope of the thesis	13
1.5 Analytical approach	15
1.6 Geographical setting.....	18
 Chapter 2 Loess-soil sequence at Toshan (Northern Iran): Insights into late Pleistocene climate change	 21
Abstract	22
2.1 Introduction.....	22
2.2 Study area	24
2.3 Materials and Methods.....	25
2.3.1 Field sampling and micromorphology	25
2.3.2 Granulometric analysis	26
2.3.3 Mid-infrared spectroscopic measurements	27
2.3.4 Spectrophotometric analysis.....	28
2.4 Results	29
2.4.1 Field description and micromorphology	29
Unit 6 (25.73-22.51 m below surface)	29
Unit 5 (22.50-15.41 m below surface)	30
Units 4 to 2 (15.40-1.47 m below surface).....	31
Unit 1 (1.46-0.00 m below surface)	32
2.4.2 Grain-size	33
2.4.3 Soil color	35
2.4.4 Carbonate content.....	36
2.5 Discussion	36
2.5.1 Granulometric properties of loess and its implications for changes in wind velocity and dust source area	36
2.5.2 Palaeosols at Toshan: implications for morphodynamic processes and differential soil formation.....	38
2.5.3 Stratigraphic comparison with other palaeoclimatic archives	40
2.6 Conclusions	43
2.7 Acknowledgements.....	43

Chapter 3	The Agh Band loess-palaeosol sequence – A terrestrial archive for climatic shifts during the last and penultimate glacial-interglacial cycles in a semiarid region in northern Iran	44
	Abstract	45
	3.1 Introduction.....	45
	3.2 Geographical Setting	47
	3.3 Methods... ..	48
	3.3.1 Preparation of the profile and sampling	48
	3.3.2 Luminescence dating.....	49
	3.3.3 Determination of carbonate content – Mid-infrared spectroscopic measurements	51
	3.3.4 Grain-size measurements.....	53
	3.3.5 Magnetic susceptibility.....	53
	3.4 Results and discussion	54
	3.4.1 Lithological/pedological field description	54
	Unit 4	55
	Units 3-2 and 3-1	56
	Unit 2	57
	Unit 1	57
	3.4.2 Luminescence dating results	58
	Dose recovery and fading	58
	Chronological framework of the sediment units.....	59
	3.4.3 Carbonate content.....	61
	3.4.4 Patterns of high resolution grain size analyses	62
	3.4.5 Interpretation of magnetic susceptibility	64
	3.4.6 Hiatuses within the Agh Band profile	65
	3.4.7 Relation of the Agh Band loess-palaeosol sequence to other loess profiles in northern Iran	67
	3.5 Summary and conclusion.....	68
	3.6 Acknowledgements.....	69
	Appendix	69
 Chapter 4	 130.000 years of loess and palaeosol formation: Geochemical and rock magnetic properties of the Toshan loess-soil sequence (NE Iran)	 71
	Abstract	72
	4.1 Introduction.....	72
	4.2 Study area	75
	4.2.1 The loess-soil sequence at Toshan	76
	4.3 Materials and methods.....	78
	4.3.1 Magnetic susceptibility.....	78
	4.3.2 Geochemical and mineralogical analysis	78
	4.3.3 Geochemical parameters and ratios	78
	4.4 Results	80
	4.4.1 Mineral assemblage	80
	4.4.2 Composition of major elements	81

4.4.3 Trace elements and UCC-normalized Spidergrams.....	82
4.4.4 Mass and frequency dependent susceptibility.....	84
4.5 Discussion	85
4.5.1 Loess composition and provenance in NE Iran deduced from major and trace elements abundances.....	85
4.5.2 Weathering and soil formation in loess	88
4.5.3 Interstadial pedogenesis during MIS 3 inferred from the rock magnetic properties of the loess-soil sequence at Toshan	90
4.6 Conclusions	93
4.7 Acknowledgements.....	94
Appendix	95
 Chapter 5 The loess-soil sequence at Neka-Abelou and its palaeoclimatic implications: towards a pedostratigraphic model of northeastern Iran.....	 97
Abstract	98
5.1 Introduction.....	98
5.2 The Neka-Abelou exposure	100
5.3 Materials and methods.....	102
5.3.1 Field sampling	102
5.4 Results	103
5.4.1 Field description	103
Unit 3 (22.25-13.38 m below surface).....	103
Unit 2 (13.38-6.14 m below surface).....	105
Unit 1 (0.00-8.19 m below surface).....	106
5.4.2 Carbonate content.....	107
5.4.3 Grain-size	108
5.5 Discussion	110
5.5.1 Relative changes in wind velocity and dust source area deduced from textural composition of loess	110
5.5.2 Palaeosols at Neka-Abelou: implications for polygenesis and differential soil formation.....	111
5.5.3 Pedostratigraphy of northern Iranian loess along the northern declivity of the Alborz Mountains	115
5.6 Conclusions	119
 Chapter 6 Comprehensive discussion	 121
6.1 Pedostratigraphic improvements based on high-resolution proxy records of loess and palaeosols	122
6.2 The nature of upper and lower boundaries of palaeosols and their implications for morphodynamics, differential soil formation and palaeoclimate	124
6.3 Granulometric properties of northeastern Iranian loess: implications for relative wind energy.....	127
6.4 Geochemical characteristics of the dust source	127

6.5 Loess deposits along the northern declivity of the Alborz Mountains and in the Iranian Loess Plateau – is there a pedostratigraphic connection?.....	128
6.6 Northeastern Iranian loess in a supraregional context.....	130
Last interglacial and interstadials of the early glacial	132
MIS 4 and last pleniglacial.....	136
6.7 High-resolution sampling and multi-proxy analysis: a review of pros and cons	138
Mid-infrared spectroscopy	139
Visible spectroscopy.....	139
Laser diffractometry.....	140
Magnetic susceptibility	141
Chapter 7 Conclusion.....	142
References.....	144
Eigenbeteiligung an den Veröffentlichungen.....	162
Erklärung.....	163
Curriculum vitae.....	164

List of Figures

Fig. 1.1: Formation of different fabrics binding single grains, mainly silt particles in loess (redrawn from Smalley and Markovic, 2014).	5
Fig. 1.2: Summary of the principal modes of aeolian sediment transport (redrawn from Pye, 1995).	7
Fig. 1.3: Palaeosols intercalated in loess at Neka 3. The palaeosols are clearly distinguishable from loess by their brownish color (Photo taken by Stefan Vlaminc, 2014).	10
Fig. 1.4: Simplified geomorphological map of northern Iran supplemented by the location of loess-palaeosol sequences (based on geomorphological map of Iran, scale 1:2,500,000, Busche et al., 1990).	11
Fig. 1.5: Climate diagrams of selected meteorological stations of northern Iran and Tehran (Meteorological Organization of Iran, 2016).	19
Fig. 2.1 A & B: Northern Iran with locations of loess-soil sequences studied by Kehl (2010) and own section. The section at Toshan is located within the suburban zone of Gorgan City. B: Central Asia with locations of Lake Van (Litt et al., 2014), Lake Urmia (Djamali et al., 2008) and loess-palaeosol sequences of Remisowka (Machalett et al., 2008) and Tagidjar (Mestdagh et al., 1999).	24
Fig. 2.2 A & B: Cross-sectional view showing an idealized horizontal and vertical succession of the sequence at Toshan.	26
Fig. 2.3: Discontinuous sampling at Toshan. The 5 discrete step-like profiles, overlapping one another are indicated by the capitals A, B, D, E, and F. The dashed lines represent the lower convex shaped boundary of a Bt- and a Bw-horizon respectively. These fossil soil horizons delineate a former hill surface.	26
Fig. 2.4: Prediction of CaCO_3 from MIRS and partial least square regression (MIRS-PLSR) compared to CaCO_3 content determined by the Scheibler method based on the volumetric release of CO_2 (as based on data from Kehl, 2010).	28
Fig. 2.5: Results of the granulometric analysis. Red lines indicate dates within the profile. The results are supplemented by the distinct subprofiles A, B, D, E and F. The pedostratigraphic units 1 to 6 hereafter do not demand to correspond with certain marine isotope stages, but serve for a comprehensible structure of the following statements. Age control is provided by Lauer et al. (this issue). The quoted results are pIRIR ₂₉₀ -luminescence ages (fine grain). The grain-size records are superimposed by black curves indicating a moving average over four intervals. Red rectangles to the right of the profile indicate the position of samples extracted for micromorphological analysis. Thin sections will be relevant for future scientific contributions. Culminations in clay sized particles (<5.5 μm) minima in U-ratios and median grain-size match the stratigraphic position of palaeosols. Loess layers exhibit an opposite trend.	31
Fig. 2.6 A and B: Loess groundmass under plain and crossed polarized light. The thin section was extracted from 15.65 m. C and D: Clay domains and precipitations of pedogenic iron oxides within Bt-horizon (22.43 m).	33

Fig. 2.7: Results of the colorimetric and MIRS analysis indicating a strong correlation with the physical stratigraphy. Palaeosols are depleted in CaCO_3 and enriched in Fe_t . Maxima in a^* , b^* and RI attributed to fossil soil horizons indicate abundance of particles promoting reddish and yellowish soil color respectively.	34
Fig. 2.8: Comparison of textural properties of selected loess layers, palaeosol and modern soil horizons. The histogram was determined by averaging the respective grain-size fractions of the entire strata denominated as loess.	35
Fig. 2.9: Preliminary pedostratigraphic correlation of loess-soil sequences in NE Iran (Kehl et al., 2005; Frechen et al., 2009).	41
Fig. 2.10: Preliminary supraregional correlation of the section at Toshan with the loess-palaeosol sequences at Remisowka (Machalett et al., 2008), Tagidjar (Mestdagh et al., 1999), as well as the pollen records from Lake Urmia (Djamali et al., 2008) and Lake Van (Litt et al., 2014). This correlation is based on stratigraphical estimates.	42
Fig. 3.1: Study area; map showing the distribution of loess in northern Iran and the locations of loess sections studied before on the foothills of the Alborz Mountains and in the so-called loess-plateau of Northern Iran. The new section at Agh Band presented here, is located at less than 100 m distance from locations studied by Kehl et al. (2005) and Frechen et al. (2009).	46
Fig. 3.2: Picture of the northern Iranian loess “plateau” with > 60 m thick loess deposits (left), characterized by steep hillslopes. Head cut of one of the frequent gullies (right). Sheep trails mark the present day land surface and the intensive usage of the loess-hills accelerates erosion. The recent landscape has no plateau-character and it is debated when the incision of the valleys started and if land surfaces of the past had been plateau-like.	47
Fig. 3.3: Agh Band loess-palaeosol sequence with the 2 sub-profiles Agh 1 and Agh 2. Profile Agh 1 describes an about 30 m thick loess succession, profile Agh 2 an about 20 m thick sequence. The location of the lower part of profile Agh Band as studied by Kehl et al. (2005) and Frechen et al. (2009) is marked with a circle.	48
Fig. 3.4: Prediction of CaCO_3 from MIRS analyses and partial least square regression, compared to the CaCO_3 content obtained by the Scheibler method.	51
Fig. 3.5: Litho/ pedostratigraphic column and pIRIR_{290} luminescence age estimates of the Agh Band profile.	52
Fig. 3.6: Lowermost soil of the Agh Band loess sequence (subprofile Agh 2; soil Agh 4). The Bwyk-horizon grades into a CByk-horizon. The smooth transition marks climatic shift towards most likely increased aridity and dust accumulation.	56
Fig. 3.7: Palaeosol Agh S3 (See Figure 5). The Bwy-horizon grades into a CBy-horizon indicating a climatic shift towards less soil-forming intensity and most likely dryer climate conditions. There is no sharp boundary between the soil horizons and the transition towards the overlying loess. The dashed black line marks tectonic disturbance of the soil pointing to tectonic activity after the soil had been formed.	56

- Fig. 3.8:** Banded loess-deposits (Unit 3-1); 30.18-31.20 m depth. The dashed lines (left) mark the orientation of the banded features. The black numbers (e.g. 3120) mark the total profile depth within sub-profile Agh 1. The genesis of the bands is still under debate but might be linked to former biogenetic crusts preserved at that part of the Agh Band profile. The horizontal orientation of the bands with only a minor inclination represents the palaeosurface and shows that the steep slope, characterizing the present day landscape, was not developed while unit 3-1 was formed. 57
- Fig. 3.9:** Results of dose recovery tests. 59
- Fig. 3.10:** pIRIR₂₉₀-dose residuals plotted against the corresponding equivalent doses. The intercept dose residual of about 15 Gy should be similar to dose residuals at time of deposition. 59
- Fig. 3.11:** IR₅₀ and pIRIR₂₉₀ g-values. 61
- Fig. 3.12:** Subprofile Agh 2; selected grain-size data, magnetic susceptibility and carbonate values. The U-ratio is according to Vandenberghe et al. (1985) and takes into account the ratio of medium silt to fine silt. 63
- Fig. 3.13:** Subprofile Agh 1; Selected grain-size data, magnetic susceptibility- and carbonate values. The disturbed upper unit 1 was not investigated for magnetic properties. 63
- Fig. 3.14:** Averaged mean grain-size curves from Agh 1 (14-17 m and 25 - 28 m profile depth) in comparison with loess from Toshan (see Vlamincx et al., 2016). The Agh Band loess shows, in contrast to the Toshan loess, a uni-modal distribution and is substantially coarser than the Toshan loess. 64
- Fig. 3.15:** Frequency depended susceptibility (K_{fd}) against low field susceptibility (K_{lf}) after the idea of Heller et al. (1991) for data from Agh Band in comparison to data from the western part of the CLP (Baichaoyuan). Both locations are characterized by semi-arid climate and the susceptibility data confirm climatic analogy. 65
- Fig. 3.16:** Left; pIRIR₂₉₀-luminescence age estimates plotted against profile-depth. The green box indicates the chronological gap found in subprofile Agh 2. The age framed by the black circle is interpreted as underestimated. Right: Benthic $\delta^{18}O$ record including marine isotope stages modified after Lisiecki (2005). 66
- Fig. 3.17:** Attempt of a correlation between the loess-sequences Agh Band (loess-plateau) and Toshan (foothills of the Alborz-mountains) based on pIRIR₂₉₀-luminescence age estimates. It is illustrated, that in periods during which the Toshan loess was strongly affected by soil-formation, the Agh Band area was most likely too dry and hence characterized by intense dust accumulation and almost no soil-formation. 67
- Fig. 4.1:** Simplified geological map 1:1000000 of North-eastern Iran, displaying the different lithologies in the vicinity of the loess-soils sequences at Neka, Toshan, Now Deh and Agh Band (modified from Geological Survey of Iran, 1991). 76
- Fig. 4.2 A:** X-ray diffractogram showing the main mineral assemblage in loess at Toshan as parent material for soil formation. This sediment at a depth of 13.19 m is attributed to MIS 4 and represents

the most “typical” loess at Toshan (Vlaminck et al., 2016; Lauer et al. 2017a). **B:** X-ray diffractogram indicating the assemblage of main minerals within soil 5-3b. This Bt-horizon is believed to be the most strongly weathered soil of the entire loess-soil sequence at Toshan and possibly formed during MIS 5e (Vlaminck et al. 2016, Lauer et al. 2017a). The X-ray diffractograms were evaluated using MacDiff 4.2.5 software. The primary peaks in this diffractogram are labeled with an abbreviation of the minerals identified. The abbreviation used for labeling is referred only to the mineral exhibiting the highest intensity within the respective 2Theta interval. In order to maintain visual clarity interfering minerals were excluded from labeling. 80

Fig. 4.3: Biplots comparing the K_2O/Al_2O_3 vs. TiO_2/Al_2O_3 ; K_2O/Al_2O_3 ratios of loess and palaeosols from the sections at Neka, Now Deh, Agh Band and Toshan with respect to the composition of the upper continental crust (UCC) and shales. The major elements composition of Neka and Now Deh loess and palaeosols was taken from Kehl (2010) and the data for UCC and shales was taken from McLennan (2001). Palaeosols are illustrated by geometric forms being entirely filled with one color, whereas the fill color of symbols indicating loess is white. 81

Fig. 4.4: Determination of quantitative alteration of major elements in palaeosols with respect to loess as based on Garrels and Mackenzie, (1971). The calculation was done by dividing the content of a given element from altered material (palaeosol) by the respective content from the relatively unaltered sediment (loess) ([oxide palaeosol/oxide loess] * 100). 82

Fig. 4.5: Spidergrams showing the composition of major and trace elements in loess (**A**) and palaeosols (**B to D**) normalized to the average geochemical composition of the upper continental crust. The element abundances of UCC used for normalization were taken from McLennan (2001). The number of interfering curves was restricted to a number of 4 in order to maintain readability. Each curve represents an arithmetic mean of the data set of the respective strata. Conversely, the data referring to palaeosols 6-1 and 6-2 (**D**) were converted directly, since there was merely one sample analyzed for each of both palaeosols. Please note that, Cs-value for palaeosol 6-2 (**D**) was beyond detection limit and is hence missing in this spidergram. 83

Fig. 4.6: Stratigraphy of the Toshan loess-soils sequence supplemented by records of magnetic susceptibility, the chemical proxy of alteration (CPA), the chemical index of alteration (CIA). The chronological framework was taken from Lauer et al. (2017a). 84

Fig. 4.7: Biplot of Na_2O/Al_2O_3 vs. K_2O/Al_2O_3 indicating the geochemical maturity of bulk loess in NE Iran. Particularly the Na_2O/Al_2O_3 ratio displays a gradient showing increasing Na_2O depletion from the semi-arid climate in the Iranian loess plateau (Agh Band) towards subhumid climatic conditions at Neka. The positions of igneous rocks, Chinese loess and the shale trend were taken from Muhs and Budahn (2006). NE Iranian loess thereafter group close to Chinese loess and the shale trend testifying to a degree of enhanced chemical maturity in relation to igneous rocks. 86

Fig. 4.8: A-CN-K diagram according to Nesbitt and Young (1984) of the loess-soil sequence at Toshan (n=52). CaO^* represents Ca bound to silica such as feldspars. This ternary diagram reveals overall CIA-values of 60 to 73. Accordingly, data points plot close to the plagioclase weathering trend, suggesting that element mobility is governed by plagioclase depletion. 88

Fig. 4.9: Stratigraphy of the Toshan loess-soil sequence supplemented by the record of magnetic susceptibility, ratios of Fe/Mg, Ti/Mg, Ti/Sr and Ba/Sr. 91

- Fig. 4.10:** Frequency dependent susceptibility (K_{fd}) against low field susceptibility (K_{lf}) according to the idea of Heller et al. (1991). Rock magnetic properties of the loess soil-sequence at Toshan (A) as compared to those of the Xifeng loess and palaeosol sequence (B) located in the central part of the Chinese Loess Plateau. Both locations are characterized by mean annual precipitation amounts of approx. 550 mm. Our susceptibility data confirm climatic analogy. 93
- Fig. 5.1:** Map of northeastern Iran showing the locations of the hitherto known loess-soil sequences and the occurrence of loess deposits supplemented by other geomorphological features in the region (based on National Iranian Oil Company, 1978). The location of loess deposits in the southwestern part of the study area have not been mapped yet and are therefore missing. 100
- Fig. 5.2 Top:** Panoramic picture displaying the palaeo-morphology of the Neka 3 loess-soil sequence. The lower concave line might be a hint at the formation of a palaeo-channel, which truncated palaeosols underneath soil 3-1. Picture **B** illustrates the unconformable contact of the MIS 5 pedo-complex (soils 2-1, 2-2 and 3-1) with underlying palaeosol horizons which are indicated by dashed lines. Pictures **C**, **D** and **E** show the location of sample extraction (panoramic picture and pictures A and B were taken by Martin Kehl in 2014; Pictures C and D were taken by Stefan Vlaminc in 2014; Picture E was taken by Stefan Vlaminc in 2015). 101
- Fig. 5.3 A:** Photograph of the Neka3 section, showing the arrangement of profiles C, D, E and F penetrating in a northeastern facing wall within the partly collapsed quarry. Profile B is hidden behind collapsed blocks, while profile A was prepared on the reverse side of the quarry. **B:** The undisturbed modern soil (profile M) was found around 30 m to the east of the area displayed on the present photograph (photos taken by Martin Kehl, 2015). 103
- Fig. 5.4:** Pedostratigraphy of the Neka3 loess-palaeosol sequence supplemented by granulometric proxies and CaCO₃-content. The black curves superimposing the grain-size records, represent a moving average. The luminescence ages given in the present figure were determined by Dr. Tobias Lauer for preliminary age estimation. Fifteen new samples for luminescence dating were taken and twenty-three samples for micromorphological analyses. 109
- Fig. 5.5 A:** Histogram showing the average particle size distribution (PSD) of loess at the Neka3 loess-palaeosol sequence. This average distribution is superimposed by PSD of distinct loess layers (L1 to L5) in order to illustrate compositional differences. **B:** Histogram displaying the average particle-size distribution of loess deposits in the Neka3 section, superimposed by granulometric composition of the Toshan, Now Deh and Agh Band sections. 111
- Fig. 5.6:** Palaeosols 2-2 and 2-1 allocated to unit 2. Both palaeosols are characterized by gradual upper boundaries. To the top of palaeosol 2-1 thick charcoal pieces were found (A). B: decalcified Bw-horizon belonging to pedo-complex (PC) 2-2. C: relatively unweathered loess, separating PC 2-2 from 2-1. D: recalcified ABk-horizon belonging to PC 2-2. 113
- Fig. 5.7:** Shape of upper boundaries of soils 2-2 and 2-1. The present curve was extracted from the running mean of the clay-contents graph shown in Fig. 5.4. While the transition from soil 2-2 into the overlying loess is gradual in nature, the upper boundary of soil 2-1 exhibits a gradual decrease, interrupted by 4 clay “pulses”. 114

Fig. 5.8: Pedostratigraphy of northern Iranian loess sequences along the northern declivity of the Alborz Mountains. The MIS 5 pedo-complex is indicated by the greyish zone. This pedo-complex and the overlying layer of relatively unweathered loess combined constitute an excellent stratigraphic marker. Last pleniglacial loess hosts at least 3 weakly developed interstadial palaeosols. Due to large uncertainties in geochronological dating the intercorrelation of these fossil soil horizons as well as their allocation to distinct Greenland Interstadials (GI) remain unclear. 117

Fig. 5.9: Statistical relationship between the volumetric median and the geographical latitude of the loess-soil sequences located along the northern foot slopes of the Alborz Mountain range supplemented by data from the Agh Band section in the Iranian Loess Plateau. The volumetric median given in the present figure represents an arithmetic mean of all volumetric median values from all layers denominated as loess (C) in the respective loess section. The strong coefficient of determination is valid on a confidence interval of >0.95. 119

Fig. 6.1: Multimodal particle-size distribution of **A:** the Neka3 tephra in relation to the average grain-size distribution of loess from the Neka3 section. **B:** Multimodal particle-size distribution of a potential tephra at the Toshan loess-palaeosol sequence in relation to the average granulometric composition of Toshan loess. 123

Fig. 6.2: Photograph taken from the Neka3 section in a south-western direction. The buildings in the foreground belong to the town of Neka. In the background the 5600 m high Damavand volcano is in visual range. It is located at a distance of ~135 km to the southwest of the Neka3 section (photo was taken by Martin Kehl, 2015). 124

Fig. 6.3: Photographs from **A:** Erosional contact of the ABk-horizon belonging to palaeosol 5-2 and the overlying loess strata at the Toshan section, as indicated by the irregularly shaped boundary between the two strata. **B:** Palaeosols 2-1 and 2-2 from the Neka section, characterized by a gradual upper boundary. **C:** Soil Agh S4 from the Agh Band section exhibits a gradual upper boundary (all photos were taken by Stefan Vlaminck, A and B in 2013 and C in 2014). 125

Fig. 6.4 A: Comparison of age increase of Agh Band and Toshan loess. **B:** at Toshan age increase with depth shows a consistent trend, whilst **C:** the age increase curve belonging to the Agh Band section is characterized by numerous inversions. OSL age estimates given were determined by Lauer et al. (2017b) and clearly illustrate the hiatuses in the sequence. The grey shaded area indicates the standard deviation of luminescence ages. 129

Fig. 6.5: Loess distribution map of central Asia and parts of western Asia according to Machalett et al. (2008), supplemented by the location of pollen sequences and by data from Lateef (1988) for loess deposits in northwestern Iran, Kehl (2010) and own field observations and Wolf et al. (2016) for loess in Armenia. 131

Fig. 6.6: Surprearegional correlation of northeastern Iranian loess deposits (Toshan section) with loess-palaeosol sequences from Armenia (BL), Kazakhstan (Remisowka) and Tajikistan (Tagidjar) and pollen records from Lake Urmia (Iran), Lake Van (Turkey) and Tenaghi Phillipon (Greece). For a location of the respective archives the reader is referred to Fig. 6.6. The age estimates included into the pollen record from Lake Urmia are ²³⁰Th ages and were taken from Steven et al. (2012). 134

Fig. 6.7: Simplified map illustrating the extent of subaerially exposed shelf sediments in response to Atel regression as postulated by Kroonenberg et al. (1997); Svitoch (1997); Dolukhanov et al. (2009),

Yanina et al. (2012, 2014); Tudryn et al. (2013). The palaeocoastline was taken from Zickel et al. (2016). 136

Fig. 6.8: Age increase of the Toshan section as a function of depth below surface. Luminescence dating result were taken from Lauer et al., (2017a). White dots indicate average age estimates showing consistent age increase with increasing depth, while red dots represent inversive ages. The grey surface in the background illustrates age uncertainties (Lauer et al., 2017a). The transitional zones between our luminescence results are provided with numbers representing the average age increase per 2cm sampling increment in years. These values were inferred from linear interpolation from two succeeding average age estimates. The brownish and vertical bars crossing the age estimates indicate the position of weakly developed interstadial palaeosols 3-1, 3-1a, 3-2 and 3-2b..... 137

List of Tables

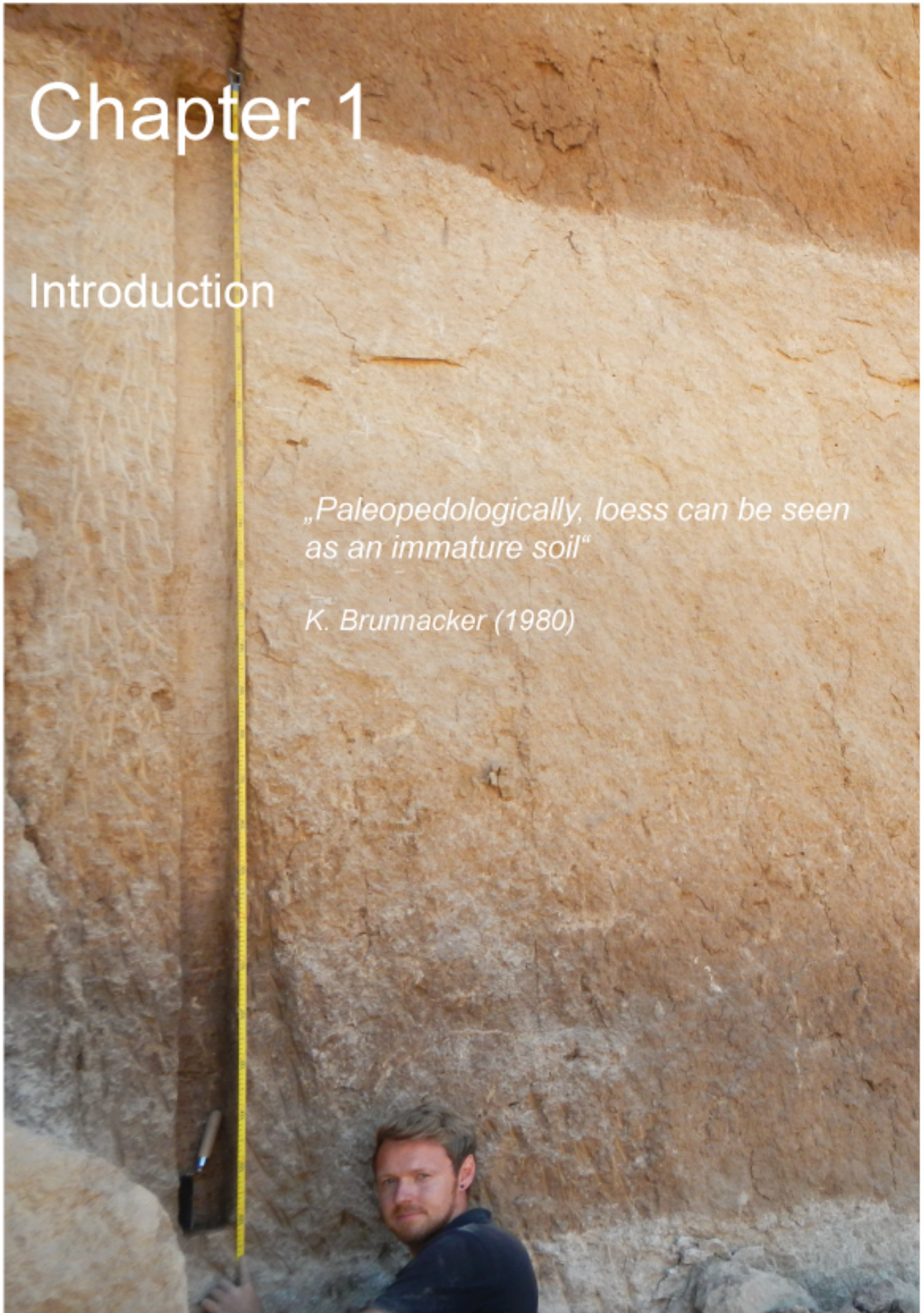
Table 2.1: Model parameters and statistical indices for prediction of CaCO_3	27
Table 3.1: Results from gamma spectroscopy and luminescence dating including non-fading corrected pIRIR ₂₀₉ ages. Abbreviations: DR = dose rate; De = equivalent dose. The right column shows the number of measured aliquots and the amount of accepted aliquots. As acceptance criteria, aliquots showing recycling ratios deviating > 10% from unity were rejected.	50
Table 3.2: IR ₅₀ and pIRIR ₂₉₀ g-values and corresponding luminescence ages (fading-uncorrected and fading-corrected). For the calculation of fading corrected luminescence ages, the R-luminescence package was used (Dietze et al., 2013). For sample Agh S8 b, the fading corrected age was not calculated due to significant scatter among obtained g-values (see Figure 3.11).	60
Table app. 3.1: Stratigraphy of the Agh Band loess-palaeosol sequence. The table gives an overview about the thickness of the sedimentological layer and intercalated palaeosols. Please note that a more specific classification of the pedogenetic processes based on results of micromorphological studies colorimetric and MIRS analysis will be published elsewhere.	69
Table 4.1: Brief description of palaeosols (3-1 to 6-2) and the modern soil (1-1). The soil horizons were denominated according to WRB (2007). The palaeosols were numbered depending on their allocated stratigraphic unit and their position within this unit. Hence, the first palaeosol of unit 3 is referred to as soil 3-1. Structure, pedofeatures and the estimated degree of soil development are based on field findings and micromorphological analyses (Vlaminck et al., 2016). Loess strata (L1 to L4) were excluded from this description due to their homogeneous characteristics in terms of color, CaCO_3 -content and structure. This holds true also for CBk-horizons. These horizons are characterized by partial decalcification, coherent to subangular blocky structure, thus representing a transitional stage between C and B horizons in which features of the parental loess still prevail. For a thorough description of the Toshan loess-soil sequence the reader is referred to Vlaminck et al. (2016).	77
Table app. 4.2: Composition of major element given in wt% supplemented by lithological information. LOI = Loss On Ignition at 1100°C.	95
Table app. 4.3: Composition of trace elements given in ppm. <BDL = beyond detection limit.	96
Table 6.1: Summary of major differences between postgenetic and syngenetic soils.	126

Chapter 1

Introduction

*„Paleopedologically, loess can be seen
as an immature soil“*

K. Brunnacker (1980)



The Quaternary encompasses the past ca. 2.6 Ma and is colloquially known as the “Ice Age”. It was a period of long-term and global climate fluctuations promoting glacier extension during cold phases of stadials alternating with warm interstadial or interglacial episodes triggering glacier retreat. These cycles were modulated by changes in Earth’s orbital parameters affecting the budget of incoming solar radiation on astronomical timescales (Berger, 2009).

However, during the last interglacial-glacial cycle orbitally forced changes in global ice volume were superimposed by short-lived and cyclical transitions between stadial and interstadial conditions active on millennial to even centennial timescales (Heinrich, 1988; Bond et al., 1992, 1993; Hemming, 2004; Mogensen, 2009; Gottschalk et al., 2015; Markle et al., 2017). These oscillations often referred to as Dansgaard-Oeschger (D-O) events are believed to arise from perturbations in the Atlantic Meridional Overturning Circulation (AMOC), which are reflected in the Greenland ice-core stratigraphy (Rasmussen et al., 2014; Gottschalk et al., 2015). Twenty-four of these D-O cycles are known, being most abundant during the last pleniglacial. Evidence is growing that these oscillations occurred globally (Mogensen, 2009; Gottschalk et al., 2015; Markle et al., 2017).

The formation of loess is traditionally attributed to stadials and involves a series of processes governed by climate such as the production and aeolian transportation of silt-sized particles, their deposition as well as syn- and postsedimentary alterations (Kehl, 2010). The latter may include the formation of palaeosols during moist and probably warm interglacials and interstadial intervals. Thus, the alternation of dry/cold and warm/moist phases resulted in the formation of LPS, which provide significant insights into the dynamics of Quaternary climate changes (Vandenberge, 2006; Muhs, 2012; Zeeden et al., 2017). While astronomically driven moist phases may be well recognized in most loess sections by means of intercalated palaeosols, millennial scale fluctuations require favorable conditions to be recorded in loess (Bokhorst, 2009; Muhs, 2012; Marković et al., 2015; Zeeden et al., 2017). These include morphodynamic stability and particularly climatic conditions conducive to soil formation such as sufficiently high levels of edaphic moisture availability in relation to dust deposition. The correlation of millennial scale fluctuations from LPS with the Greenland ice-core stratigraphy is subject to considerable difficulties due to relatively high uncertainties in geochronological dating (Bokhorst, 2009; Marković et al., 2015).

In northeastern Iran, loess deposits are found on the northern declivity of the Alborz Mountains bordering the Caspian Lowland. There, westerly cyclones, the Siberian anticyclone, subtropical and polar air masses and local front systems constitute a complex synoptic climate pattern, promoting dust storms as well as a steep hydroclimatic gradient (Alijani and Harman, 1985; Orlovsky, 2005). Thus, it is likely that dust deposition and precipitation have reacted sensitively to long- and short-termed climate fluctuations during the late Pleistocene and that these changes have left differentiated marks in the loess deposits of northeastern Iran.

1.1 Definitions and formation of loess

Since the first scientific characterization of loess by Karl Caesar von Leonhard in 1820 manifold criteria have emerged from the scientific discourse aiming at a consistent definition of loess. The most recent publication reviving the discussion on the nature of loess is the one by Sprafke and Obreht (2016), which is entitled “Loess: Rock, sediment or soil – What is missing for its definition?” The title itself indicates that loess research still lacks a uniform definition of its proper object of research and that the pursuit of a consensus is an ongoing issue. Hence, this chapter briefly outlines major problems related to the definition of the term “loess”. A thorough characterization of loess-like sediments is not included in this chapter. For additional information the reader is referred to e.g. Pye (1987), Pye (1995), Pécsi and Richter (1996), Haase et al. (2007) and Sprafke et al. (2013).

Loess may be considered a geomorphological entity and as such its formation encompasses a chain of processes (Smith et al., 2002 and Smalley et al., 2009), such as i) the production of silt-sized particles whose mineral assemblage is dominated by quartz ii) their aeolian transport as dust from proximal or distal source areas iii) the entrapment of airborne particles by a protective vegetation cover inducing their deposition and promoting preservation of the sediment, and iv) modification by syn-depositional and/or post-depositional processes (Smith et al., 2002; Kehl, 2010). Kehl (2010) summarizes that the specific lithology of the dust source and the environmental conditions prevailing during the formation of the respective loess deposit may lead to large variations in thickness, grain-size, mineralogy, geochemical properties and structure of different loess deposits on the globe.

In comparison to “primary loess deposits” or “typical” loess as defined by Pécsi (1990) loess derivatives exhibit similar morphological properties and thus complicate a clear identification of distinctive features (Pécsi and Richter, 1996). Loess derivatives may have undergone a polygenetic formation in which the primary loess deposit was subject to secondary transportation by e.g. gravitational processes along hill or mountain slopes resulting in the deposition at considerable distance from its origin (Sprafke and Obreht, 2016). This process is documented e.g. in the weakly stratified „derasional loess“ of Hungary which was related to solifluction or in the “solifluction loess” found in the Krems region whose admixture of gravels testifies to a gravitational displacement (Pécsi and Richter, 1996; Sprafke et al., 2013; Sprafke and Obreht, 2016).

The search for a distinctive element to demarcate loess from loess derivatives, lead Pye (1987) to define (“primary”) loess as “[...] a terrestrial windblown silt deposit consisting chiefly of quartz, feldspar, mica, clay minerals and carbonate grains in varying proportions”. This sedimentological definition emphasizes the aeolian origin of particles to form “primary loess” which was first expressed by Ferdinand von Richthofen in 1882 (Smalley, 2001). In his well-known publication “Loess is not just the accumulation of dust” Pécsi (1990) advocated for an in situ formation of loess and identified 10 criteria that may qualify the eventual loess deposit as “typical” loess. The main criteria were summarized as follows, “[...] true (typical) loess can be described as a loose deposit with coarse silt predominant in grain size, unstratified, porous, permeable, stable in steep walls, easily erodible by water, „structured light loam“ of pale yellow colour due to finely dispersed limonite (iron hydroxide), quartz as main mineral constituent (40-80%), subordinate feldspar content, variable amounts of clay minerals (5-20%) and carbonates (1-20%)”. The in situ theory of Pécsi (1990 and 1995) requires the

transformation of the silty aeolian deposit into loess through diagenetic processes in a specific geographical environment (Pécsi, 1995; Smalley et al., 2011). This initial diagenesis is often referred to as “loessification”. In this context, Smalley and Marković (2014) distinguish “petit loessification” (pL loessification) from “grand loessification” (gL loessification), where the former designates the view of loess formation held by Pécsi (1990). “Grand loessification” is associated with the concept of loess formation of Berg (1916), postulating that loess is exclusively a product of weathering/pedogenesis irrespective of the parent geology (Sprafke and Obreht, 2016). This theory, antithetical to the aeolian theory of v. Richthofen (1882) and Pye (1987) becomes manifest in the citation of Berg “As to the aeolian theory of loess I flatly deny it”.

Although the sedimentological definition of Pye (1987) has gained wide acceptance (Muhs et al., 2013) loessification is acknowledged as a significant part in the genesis of loess, since it provides particularly silt dominated sediments with the typical appearance and structure of loess (Pécsi, 1990, 1995; Smalley et al., 2011; Svirčev et al., 2013; Smalley and Marković, 2014; Sprafke and Obreht, 2016). However, loessification still lacks resilient theories to unravel and explain the processes involved. Smalley and Marković (2014) state that the collapsibility is one of the key defining factors of loess. The acquisition of collapsibility depends on the presence of clay minerals and calcite. As collapsibility is acquired in a post-depositional manner Smalley and Marković (2014) considered it a process of pL loessification. The associated process of hydroconsolidation is illustrated in fig. 1.1 as based on a study of loess from Kent (England) by Smalley and Marković (2014).

After the aeolian deposition of dust on a vegetated land surface clay minerals may develop pillar-like structures by direct deposition on menisci of porewater resulting in clay bonds between these silt particles (fig. 1.1 A). These bonds may be reinforced by calcite or dolomite cementing after the clay bridges have formed (fig. 1.1 C). Conversely, fine needle-like calcite may develop bridges between single silt grains prior to the development of clay bonds, promoting subsequent entrapment of clay minerals (fig. 1.1 B). Thus, there is little direct contact between single particles, causing high voids ratio in loess of up to 1.0 (Assallay et al., 1997; Cilek, 2001; Smalley and Marković, 2014). The destruction of clay bridges or calcite bridges due to e.g. increasing mechanical load, results in the collapse of this loose silt structure. Single grains collapse in the inter-particle zone and cause further consolidation. Moreover, shrinking and swelling of clay minerals may favour the breakage of clay and calcite bridges (Smalley and Marković, 2014). Thus, loess can appear as a strong and brittle material but can lose its resistivity to mechanical stress when wetted (Assallay et al., 1997; Smalley and Marković, 2014).

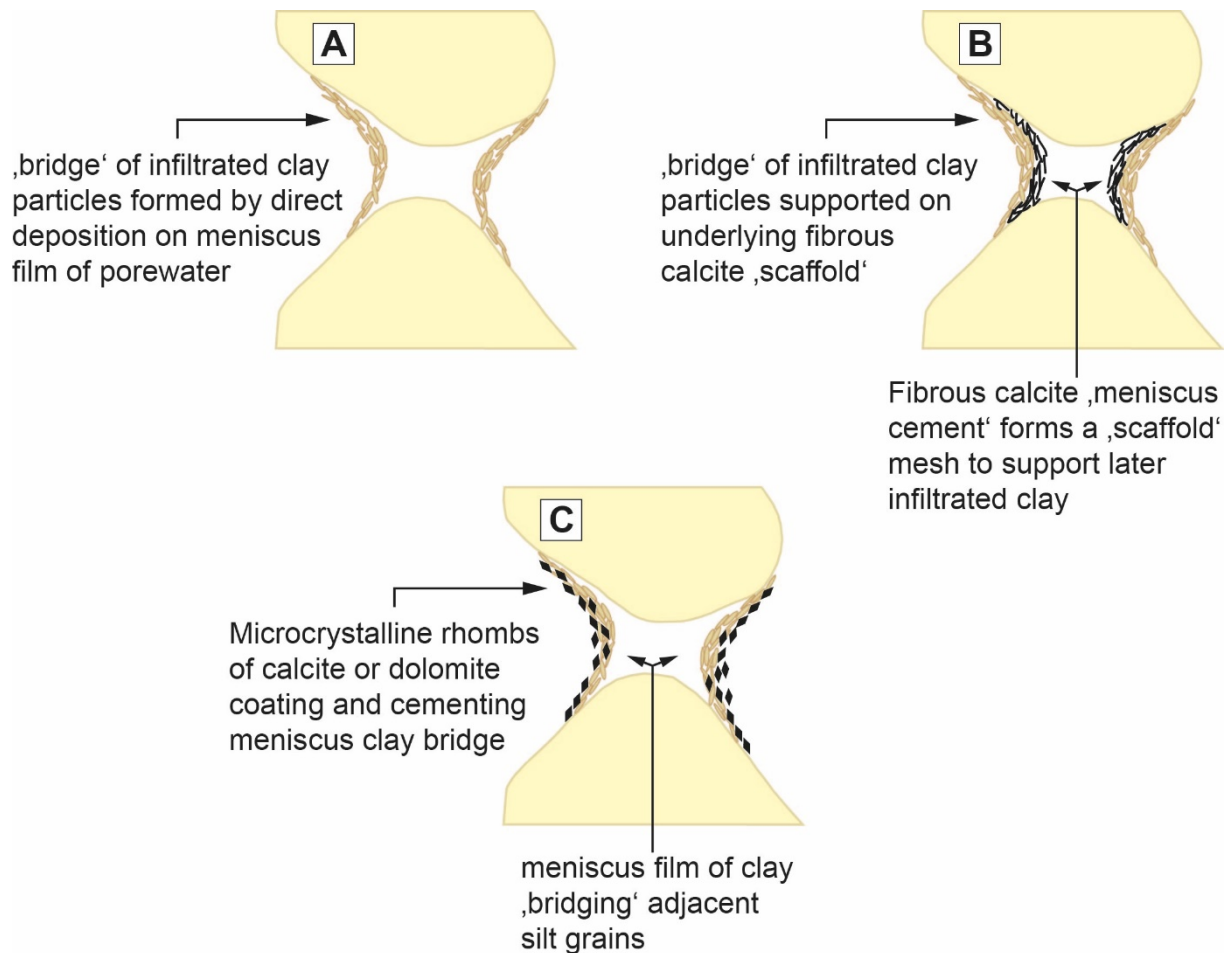


Fig. 1.1: Formation of different fabrics binding single grains, mainly silt particles in loess (redrawn from Smalley and Markovic, 2014).

Cilek (2001) argued that loessification must be a rapid process, since the unconsolidated dust with its high porosity could not be preserved if loessification operated on large temporal scales. Besides these abiotic processes Smalley et al. (2011) and Svirčev et al. (2013) suggest to include the formation of biological loess crusts (BLC) in the list of processes associated with loessification. This pioneer biological colonisation of loess by cyanobacterial activity may play a crucial role in trapping airborne dust particles and protect the encrusted surface from erosion (Svirčev et al., 2013). However, it is not clear whether the different processes involved in loessification are present across different ecosystems such as e.g. semi-arid, tundra or steppe environments and thus are universal in nature as suggested by Pécsi (1990).

Sprafke and Obreht (2016) argue that loessification is not classified as a pedogenic process, since its influence is considered too weak to form a soil. On the other hand loessification processes occur close to the ground surface in certain ecosystems and thus are not purely lithospheric (Sprafke and Obreht, 2016). Due to this controversial relationship they suggest to use the terms quasi-pedogenic and/or quasi diagenetic to classify loessification. Depending on the scientific background of the researcher and whether the emphasis is put on an aeolian origin or a post sedimentary origin, loess is commonly classified as soft rock, sediment or soil (Pye, 1987; Pécsi, 1990).

Another discussion that paralleled the search for a consistent definition of loess focused on the characterization of loess as based on the origin of its (silt sized) particles. Smalley and Derbyshire (1990) claimed that “[...] the place of particle origin names the loess type.” Thus, loess types such as perimontane loess (Pye, 1995), mountain loess (Smalley and Derbyshire, 1990), ice-sheet and periglacial/glacial (Smalley and Derbyshire, 1990; Pye, 1990, Smalley et al., 2009) or desert loess (Coudé-Gaussen, 1990; Yaalon and Dan, 1974; Smith et al., 2002) have emerged from scientific discussions. Each place of particle origin is associated with a geomorphological process capable of producing quartz silt particles (Smith et al., 2002). Hence, the term desert loess implies that clastic debris is generated in and deflated from warm deserts.

It was argued that loess found on the semi-arid margins of lowland deserts are scarce owing to the limited efficiency of geomorphological processes operating in these environments such as aeolian particle attrition and salt-weathering (Smalley and Krinsley, 1978; Pye, 1987; Sun, 2002). However, Smith et al. (2002) state that the absence of loess in an area does not necessarily mean that silt is absent in the respective environment. The scarcity of peridesert loess might be partly due to the lack of dust traps in the form of a (dense) vegetation cover in desert margin areas. Silty deposits, thus, may be readily remobilized by the wind (Tsoar and Pye, 1987; Smith et al., 2002). Based on simulated attrition of angular quartz grains in a laboratory environment Whalley et al. (1982) and Wright et al. (1998) could show that silt and clay-sized fragments were generated by point impacts of angular particles in the course of aeolian abrasion. Although the relative importance of these processes in nature is still inadequately known, Crouvi et al. (2008) showed that desert loess may be found in the Negev desert of southern Israel (Crouvi et al., 2010). The coarse silt fraction of this desert loess likely stems from aeolian particle comminution active in the adjacent Sinai-Negev sand sea (Crouvi et al., 2010). Smalley et al. (2005) acknowledge that vast loess deposits are associated with deserts; however they seriously doubt that aeolian processes constitute an effective silt producing mechanism and hence do not consider deserts a place of particle generation. Instead, deserts represent areas where this clastic debris is stored after physical weathering in mountainous regions and subsequent fluvial transport into lowland deserts (Sun, 2002; Smalley et al., 2005).

Perimontane or mountain loess is found e.g. in Europe (Smalley et al., 2009). In the Alps the bedrock is thought to have been affected by high altitude frost shattering, grinding by mountain glaciers, and fluvial comminution which was most intense during glacial intervals. The resulting clastic debris was transported by large river systems such as Rhine River and deposited as floodwater sediments. These fine-grained, unconsolidated and moderately sorted sediments were exposed to deflation, leading to the deposition of loess on both sides of the river in periglacial environment (Smalley et al., 2009). Similar to loess originating from mountainous regions, glacial loess implies a subglacial or periglacial environment, where particle comminution is largely provided by protruding continental ice shields (Smalley et al., 2009; Kehl, 2010). Haldorsen (1981) state that the capability of those ice masses to produce silt size particles depends on the subglacial bedload, since sand and silt represent final and resistant products of this geomorphological process (Smith et al., 2002). Siltstones are prominent within the geological record and thus considerable volumes of silt are associated with pre-Quaternary and extra-glacial environments (Nahon and Trompette, 1982). It was argued that a mere glacial origin of loess-sized material may not account for the vast

amounts of silt in the geological record, since the occurrence of large continental ice-sheets is restricted in space and time. Wright (2001, 2007) stresses the role of chemical weathering in creating quartz silt during subtropical tertiary or interglacial palaeoclimates. Hence, the assemblage of the subglacial bedload might also contain significant amounts of pre-Quaternary or interglacial sediments, reworked by glaciers (Wright, 2001; Smith et al., 2002). In order to circumvent the problem of classifying loess based on the origin of its particles (Smalley and Derbyshire, 1990), Wright (2001a) suggested referring glacial/cold loess to the climatic interval during which loess was formed. Most loess deposits on the globe are related to cold glacial palaeoclimates of the Pleistocene. However, loess formation may also occur during interglacial periods as evidenced by loess deposits from semi-arid regions of the northeastern Tibetan Plateau, which are of Holocene age (Lehmkuhl et al., 2014; Muhs et al., 2013).

1.2 Loess as an archive of palaeoclimate research

In the present chapter the basic processes, behind the development of particle-size distribution of loess and palaeosols, the formation of structure, color and mineralogical alteration are briefly outlined.

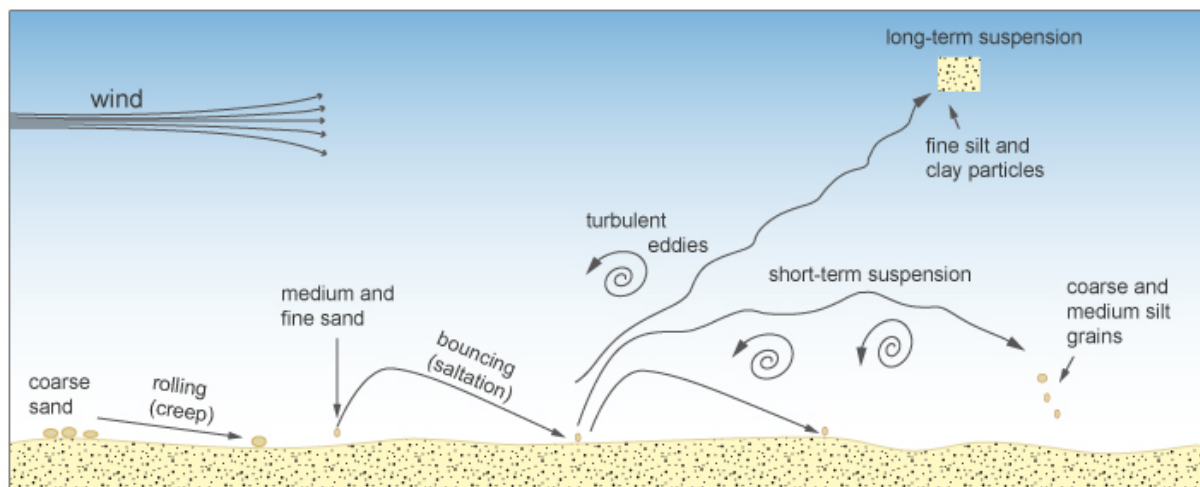


Fig. 1.2: Summary of the principal modes of aeolian sediment transport (redrawn from Pye, 1995).

Since loess basically forms in response to the deposition of airborne dust, its particle-size distribution is one of the most widely used proxies of palaeoclimate change in loess research (e.g. Vandenberghe et al., 1997; Weltje, 1997; Sun et al., 2002, 2004; Vandenberghe et al., 2006; Prins et al., 2007; Bokhorst, 2009). Dust particles smaller than 50 μm are transported in short-term and long-term suspension, respectively (Fig. 1.2). The length of this suspension is governed by the settling velocity, and the turbulence and velocity of the air flow (Tsoar and Pye, 1987; Greeley and Iversen, 1987). The settling velocity (U_f in $\text{cm}\cdot\text{s}^{-1}$) of particles decreases with decreasing grain-size. It can be calculated by approximation according to Stokes' Law:

$$[1] \quad U_f = (\rho_s g / 18\mu) \cdot D^2$$

where D is the particle diameter in cm, ρ_s represents the particle density, g is the Earth's gravitational acceleration and μ denominates the dynamic viscosity of the air (Tsoar and Pye, 1987). The latter is highly dependent on air temperature (Greeley and Iversen, 1987). Accordingly, finest particles such as the clay to fine silt fraction possess the lowest settling velocity and have the highest potential to be transported in long-term suspension (Tsoar and Pye, 1987). Consequently, clay and fine silt are predominantly dispersed to high atmospheric levels and transported over large horizontal distances (Fig. 1.2) of up to interhemispheric dimension (Derbyshire et al., 1998; Tsoar and Pye, 1987; Machalett et al., 2008). The presence of fine particles ($<16\ \mu\text{m}$) may thus indicate aeolian entrainment from distal source areas and/or lower wind energy. Conversely, coarse and medium silt are transported in lower altitudes and over smaller distances in the form of short-term suspension cascades (Fig. 1.2). Their presence is indicative of a proximal sediment supply and/or stronger air currents. If the grain-size distribution of several loess-palaeosol sequences is known, gradients in median particle-size could represent an indicator of palaeowind directions (Vandenberghe et al., 2006).

“Primary” loess deposits host considerable amounts of detrital carbonates, particularly calcite (CaCO_3) and dolomite ($\text{CaMg}[\text{CO}_3]_2$) (Gallet et al., 1998). Both minerals act as a chemical buffer to soil pH-value. Due to the presence of soil biota, the soil air is particularly enriched in CO_2 . Meteoric water percolating through loess or soils may incorporate this soil-borne CO_2 to form carbonic acid (H_2CO_3) and dissolve primary carbonates. The dissolution of calcite and dolomite at pH-values of around 7 is considered a prerequisite for the preferential weathering of silicate minerals (soil pH of 6) and the subsequent formation of pedogenic oxides and hydroxides (Scheffer/Schachtschabel, 2009). Hence, most palaeosols are significantly depleted in calcite with respect to parental loess, while the strata subjacent to these palaeosols constitute a zone of secondary carbonate precipitations.

Besides its original carbonate content loess is composed of varying amounts of quartz, feldspar, mica, siliceous clay, and trace minerals (Gallet et al., 1998; Újvári et al., 2008) and may therefore be considered a polymineral sedimentary entity. Each mineral in loess consists of characteristic major and trace elements. The relative abundance of these minerals and subsequently the geochemical inventory of loess are governed by the geological conditions of the dust source. Major and trace elements that have lowest amounts in natural waters such as e.g. TiO_2 , Al_2O_3 or Zr and Y may be considered resistant to chemical weathering and are thus suited as provenance indicator (Jahn et al., 2001). In contrast, increasing precipitation amounts promote enhanced chemical alteration of rapidly weathered primary silicate minerals (e.g. feldspar, mica, amphibole) resulting in the formation of palaeosols.

Palaeosols represent past land surfaces and have formed on loess under moister and likely also warmer (interglacial/interstadial) palaeoclimatic conditions. Depending on the soil environmental conditions prevailing during and/or after the time of formation, palaeosols are often perceived as e.g. brownish, reddish or greyish layers (Aitkenhead et al., 2013). Palaeosols are characterized by finer textural properties than loess. The finer texture of palaeosols may be due to i) detrital inheritance from parental dust deposits if the palaeosol under consideration is believed to have formed under ongoing dust deposition or ii)

neof ormation of siliceous clay at the expense of e.g. larger feldspar and micaceous mineral particles (Nesbitt and Young, 1989). The neof ormation of clay sized-particles occurs subsequent to the dissolution of primary carbonates, preferably at soil pH of ~6. Secondary clay mineral formation is particularly the result of chemical weathering involving the hydrolytic exchange of metal cations such as e.g. K^+ , Ca^{2+} , Na^+ from feldspars with protons from percolating waters. This protonation leads to the breakup of oxygen bridges and the release of ions favoring the neof ormation of (pedogenic) minerals. Secondary clay minerals may form from the reaction of released Al-hydroxides and silicic acid (Scheffer/Schachtschabel, 2009). In the course of continuing pedogenesis and changing pedo-chemical conditions, previously formed clay minerals may be transformed by mobilization or incorporation of cations from/into the interlayer region of these minerals (Wilson, 1999). For instance smectite may form by the release of interlayer K^+ from illite and micaceous minerals (Khormali et al., 2011). Thus, pedogenesis corresponds with leaching of soluble and mobile elements and the selective enrichment of less soluble and immobile elements.

Chemical weathering also affects visual appearance of palaeosols (Fig. 1.3). The colorimetric properties of loess and palaeosols are largely governed by the pigmenting effects of iron hydroxides and oxides such as ferrihydrite, goethite and hematite, which form from weathering of iron containing silicate minerals. In most iron-bearing minerals, Fe is bound in the bivalent state. In the presence of O_2 and H_2O the released bivalent iron is oxidized to Fe(III) and hydrolyzed to form Fe(III) oxides and hydroxides (Cornell and Schwertmann, 2003). In immature palaeosols, characterized by incipient soil formation the most abundant Fe-hydroxide is the amorphous ferrihydrite ($Fe_5HO_2 \cdot 4H_2O$), which gives a pale brownish colour to the substrate. In more mature palaeosols crystalline goethite ($\alpha\text{-FeOOH}$) and hematite ($\alpha\text{-Fe}_2O_3$) may predominate (Cornell and Schwertmann, 2003; Buggle et al., 2014). The pigmenting effect caused by hematite promotes a reddish color in a given soil (Barrón and Torrent, 1986), whilst increasing goethite contents favor the formation of a brownish-yellowish soil color (Cornell and Schwertmann, 2003). Hematite may e.g. form by dehydration of amorphous pedogenic iron hydroxides such as ferrihydrite and conversion of iron oxides e.g. goethite (Cornell and Schwertmann, 2003). This transformation requires a sufficiently long soil forming period and pronounced seasonal variations in temperature and soil moisture availability. Hence, iron-oxide crystallinity is indicative of soil maturity and pedogenic intensity. Conversely, under reducing conditions trivalent Fe is reduced to Fe(II), which enters soil solution and may be leached. Thus, brownish pigments are dissolved, resulting in greyish soil colour. Besides iron-hydroxides, soil color depends on the amount of soil organic matter, and $CaCO_3$ preserved in the substrate (Aitkenhead et al., 2013; Buggle et al., 2014). For example organic matter provides blackish pigments to soils (Eckmeier et al., 2012), whereas the presence of calcite leads to a more whitish color.

Soil structure is basically determined by different properties of soil constituents and by environmental conditions (Bullinger-Weber et al., 2007). The aggregation of soil particles, forming structural units depends particularly on the amount as well as the type of clay minerals, which in turn are of primary and secondary nature (Horn et al., 1994). Initially, pre-existing bonds between single particles must be destructed. This is achieved by dissolution of carbonates, which form bridges between loess particles as shown in chapter 1.1. Dispersed particles in the range of clay to silt may be pulled together by the tension forces of

water menisci in a given soil. Thus, clusters of particles are combined to form micro-aggregates (Dexter, 1988). Under the presence of expendable clay minerals such as e.g. smectite, repeated drying and wetting cycles will develop cracks which define the boundaries of the aggregates as secondary pores. Peptized clay particles are able to migrate into these pores, forming clay coatings. Secondary and primary clay minerals within a given aggregate may be translocated towards its outer part.



Fig. 1.3: Palaeosols intercalated in loess at Neka-Abelou. The palaeosols are clearly distinguishable from loess by their brownish color (Photo taken by Stefan Vlamincx, 2014).

Thus, the inner part of soil aggregates has a lower clay content and is more porous. Each wetting of the soil causes swelling pressures tending to consolidate the aggregates (Dexter, 1988; Bronick and Lal, 2005). After manifold wetting and drying cycles the characteristics defining the aggregates are more pronounced until a natural state of aggregation is developed (Dexter, 1988). Incipient palaeosols, therefore, have a weakly developed or coherent soil structure, while strongly developed palaeosols are composed of distinct aggregates. Furthermore, pedogenic iron hydroxides that formed on the outer part of micro and macro-pores tend to increase structural stability of palaeosols. Likewise, secondary carbonates originating from leaching of overlying loess strata, may precipitate and form e.g. pseudomycelia in the void matrix between soil aggregates and cement parts of a palaeosol (Bullinger-Weber et al., 2007). Hence, significant information on soil environmental conditions may be inferred from soil micro and macro- structure.

Optically stimulated luminescence dating represents one of the most widely used techniques in dating loess deposits since loess has proven to be well suited for application of OSL (e.g. Fuchs and Owen, 2008; Thrasher et al., 2009; Roberts 2008, 2015). This absolute dating method determines the last exposure of mineral grains to sunlight. As the dust particles are transported by the wind they are exposed to sunlight, and potentially remaining luminescence signals in mineral grains such as quartz and potassium feldspar are reset. When these mineral grains settle they are covered by other dust particles from subsequent sedimentation. Once excluded from sunlight naturally occurring ionizing radiation in the surrounding sediment causes the entrapment of electrons in lattice defects of quartz and feldspar. The buried sediment thereby acquires an absorbed radiation dose (equivalent dose) which increases with time of exposure to radiogenic elements such as K, U, Th and Rb (Aitken, 1998). The trapped electrons are released by applying an artificial stimulus in the

form of visible light or infrared radiation. The released electrons emit photons which are counted by means of a photomultiplier (Roberts, 2015). Thus, the total equivalent dose is determined. Once, the natural dose rate is known numerical ages may be obtained by dividing the equivalent dose by the natural dose rate (Roberts, 2015). Quartz is reported to saturate at lower equivalent dose than potassium feldspar. Therefore, luminescence signals from feldspars yield potentially higher ages than those from quartz (Roberts, 2015). In contrast to quartz, feldspars may suffer an anomalous loss of trapped charge denominated as anomalous fading. Commonly, the fine fraction of loess ranging from 4-11 μm is extracted for analysis. This fraction implies a comparatively long-distance transport, assuming that sunlight exposure was sufficiently long to reset any residual luminescence signal of the quartz and feldspar minerals to zero. Hence, in the present dissertation OSL age estimates are based on the quartz as well as the potassium feldspar (polyminerall) content of the 4-11 μm fraction in northeastern Iranian loess (Lauer et al., 2017a, 2017b).

1.3 Loess in northern Iran

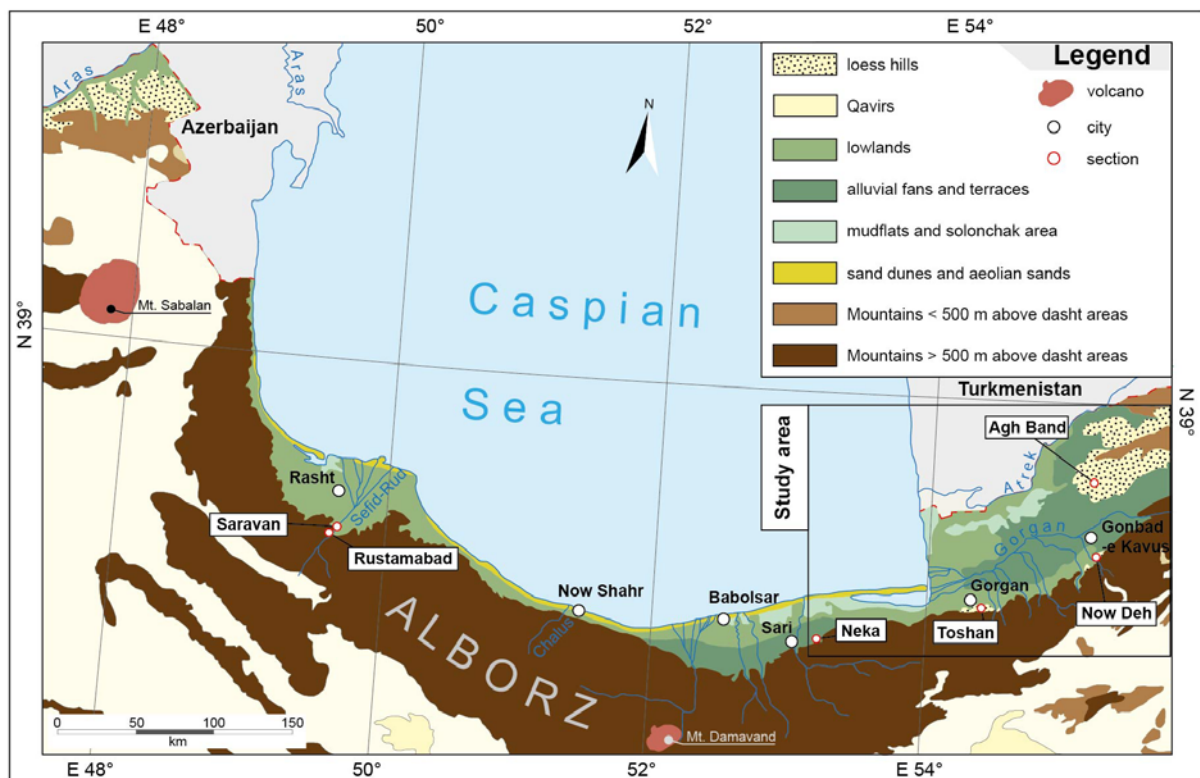


Fig. 1.4: Simplified geomorphological map of northern Iran supplemented by the location of loess-palaeosol sequences (based on geomorphological map of Iran, scale 1:2,500,000, Busche et al., 1990).

The loess deposits of the northern hemisphere extend from the maritime regions of north-western Europe (France, Belgium) and central Europe (Germany) over the Russian plain and south-eastern Europe (Ukraine, Serbia) to the loess deposits of western Asia (Armenia, Iran, Azerbaijan, Turkmenistan), central Asia (Tajikistan, Kazakhstan, Uzbekistan) and eastern Asia (China, Mongolia) (Pécsi, 1990; Haase et al., 2007; Muhs, 2012). The meridional extent of loess is primarily confined to the mid-latitudes particularly between 30° and 55° north, thus

forming a belt-like structure whose northernmost boundary runs south of the major advance of Pleistocene ice sheets. Especially loess in North America and on the Russian Plain is thought to represent glacial loess since it is associated with silt deflation from fluvio-glacial deposits (Smalley et al., 2009). Regions formerly covered by continental glaciers such as e.g. Scandinavia lack significant loess deposits (Muhs, 2012). Conversely, the loess deposits ranging from the Near East to northern China are located far to the south of this Pleistocene glacier frontline. Dodonov and Baiguzina (1995) state that these loess areas are closely related to the vicinity of deserts, constituting an elongated subtropical and temperate loess-desert zone located between 30° and 45°N.

In comparison to other loess areas on the globe, the Iranian loess deposits have attracted merely intermittent scientific attention during the last century. Field observations of loess in Iran were first conducted in the late nineteenth century (Tietze, 1877) followed by further studies being performed over the course of the twentieth century (Stahl, 1923; Bobek, 1937; Rieben, 1966; Ehlers, 1971; Lateef, 1988). While these authors provide short descriptions on Iranian loess, recent scientific progress on the nature, chronology, origin and the palaeoclimatic significance of Iranian loess deposits could be substantially advanced by Okhravi and Amini (2001); Kehl et al. (2005a, b); Frechen et al. (2009); Kehl (2009), Karimi et al. (2009); Kehl (2010); Khormali and Kehl (2011); Karimi et al. (2011); Khormali et al. (2012); Asadi et al. (2013); Vlamincx et al. (2016); Lauer et al. (2017a, b); Shahriari et al. (2017); Taheri et al. (2016); Wang et al. (2016a, b); Ghafarpour et al. (2016). In northeastern Iran, loess forms smooth hills adjoining the Gorgan and Atrek Rivers in Golestan Province (Fig. 1.4, Kehl 2010).

Lateef (1988) reports on the absence of loess on the southern Caspian Sea front starting from Gorgan for a distance of 550 km into a western direction. However, the hitherto existing findings of Kehl et al. (2005a) and own field observations suggest that the borderline of loess absence is to be displaced to the west of the city of Sari. Hence, discontinuous loess covers along the Alborz and Kopeh Dagh Mountains may be found between Minoodasht and Sari. The loess-soil sequences Neka, Toshan, Now Deh associated with this mountain range are structured by up to 11 palaeosols (Kehl et al., 2005a; Vlamincx et al., 2016) encompassing at least the last glacial-interglacial cycle (Frechen et al., 2009; Lauer et al., 2017a). The clastic material building up loess in these sequences is likely derived from physical weathering in the Alborz Mountains and was presumably reworked and distributed to the piedmonts by the Gorgan River and its tributaries, where alluvial fans and floodplain deposits provided a proximal source of airborne dust. However, the clayey nature of these loess deposits suggests also a sediment supply from remote areas such as e.g. the dune fields of the Karakum desert in Turkmenistan. This assumption was already mentioned by Lateef (1988).

To the north of Golestan Province the so called Iranian loess Plateau (ILP) is located close to the Kopet Dagh Mountains neighbouring Turkmenistan and the border river Atrek (Fig. 1.4). Here, the Agh Band loess-palaeosol sequence hosts 3 palaeosols representing a palaeoclimatic archive for the late Pleistocene namely the last and penultimate glacial-interglacial cycles (Lauer et al., 2017b). Detailed information on the above mentioned sections is included in the following chapters. The late Pleistocene loess deposits at Agh Band are disconformably underlain by highly weathered loess deposits resembling the Chinese Red Clay. Magnetostratigraphic investigations of this series revealed that loess accumulation in the region began around 2.4 to 1.8 million years ago. These sediments,

therefore, are considered the oldest loess deposits of arid central Asia (Wang et al., 2016b). Analogous to the loess deposits situated along the Alborz Mountains, part of the clastic sediment may be derived from the Kopet Dagh Mountains and entrained by the wind from the floodplains of the Atrek River. Due to its considerable fine sand content Wang et al. (2016a, b) assume that dust forming loess at Agh Band originates from the dune fields of the Karakum desert to the north of the ILP.

Other loess deposits in northern Iran are found in the central and western parts of the Alborz Mountains, e.g. on fluvial terraces of the Chalus and Sefid Rud Rivers, respectively (Ehlers, 1971; Kehl, 2010; Fig. 1.4). First pedostratigraphic and chronological results on Sefid Rud loess are provided by Kehl (2010) for the sections of Rustamabad, Saravan and Barrage Tarik. Accordingly, Rustamabad section was prepared in a road cut, located 50 m above the valley floor. The section hosts 7 dark brown palaeosols, which are intercalated in loess and loess-like sediments. A first sample for luminescence dating extracted from underneath the first palaeosol yielded an age of around 130.000 years (Kehl, 2010). In contrast to Rustamabad section the Saravan loess-palaeosol sequence is situated 25 to 30 m above the lower terrace of the Sefid Rud River. Kehl (2010) found three palaeosols, which have formed between 22.000 and 47.000 years and subsequently cover MIS 3. In northwestern Iran further loess deposits are found south of the River Aras in east Azerbaijan Province (Kehl, 2010). On the northeastern footslopes of the Kopet Dagh Mountains and in intramontane basins loess occurrences of rather local extent may be found such as e.g. loess of the Gharatikan watershed (Okhravi and Amini, 2001) and several sections in the vicinity of Mashad (Karimi et al., 2009, 2011).

1.4 Knowledge gaps and scope of the thesis

The northeastern Iranian loess deposits represent the most complete and best structured successions of loess and palaeosols in northern Iran as a greater region (Kehl, 2010). Therefore these deposits are believed to offer the greatest potential for detailed insights into the dynamics of late Pleistocene climate change in the region, covering particularly the last interglacial-glacial cycle. Conversely, the loess sequences in northwestern Iran give fragmentary evidence of palaeoclimate change covering merely certain time slices of the targeted interval. Previous results of northeastern Iranian loess are based on low resolution analysis. Hence, the current pedostratigraphies are not appropriately corroborated by analytical data. Moreover, a northeastern Iranian key loess sequence is missing which might be placed into a broader spatial context to foster a deeper understanding of palaeoclimate in northern Iran and the Eurasian loess belt. Therefore, the present dissertation aims at:

(Objective 1) Elaboration of highly detailed loess records of northeastern Iran by high-resolution sampling and analyses in order to provide a key section for the last interglacial-glacial cycle

The spatial extent of palaeoclimatic fluctuations is hitherto not sufficiently constrained. For instance lithostratigraphic and chronological findings from the Saravan loess section located in the Sefid-Rud valley (Fig. 1.4) revealed the presence of weakly developed palaeosols that

formed during MIS 3 (Kehl, 2010). However, analogous palaeosols have currently not been documented for the northeastern Iranian region. Furthermore, this region lacks the definition of one or more stratigraphical marker horizons to facilitate intercorrelation of the loess-palaeosol sequences. Hence, it is crucial to:

(Objective 2) Scrutinize the hitherto existing litho- and pedostratigraphy by detection of additional marker horizons including interstadial palaeosols

Traditionally, palaeosols are thought to form on loess, which has been deposited during the previous stadials. This static postgenetic approach was challenged by Liu (1985) and Kemp (2001), who suggested that palaeosols might also form during continuous, but reduced dust deposition and thus represent the result of syngenetic (also known as accretionary) soil formation. When the balance of calcareous dust deposition outweighs the chemical weathering potential of soil moisture availability, soil formation is retarded or inhibited. Thus, soil formation and dust deposition may be considered two competing processes. We assume that these shifts can be detectable by means of the nature of the upper and lower boundaries of palaeosols. Furthermore, these boundaries host information on morphodynamic activity. The question of post- or syngenetic soil formation bears significant palaeoclimatic implications. Thus, another objective of this doctoral thesis is to:

(Objective 3) Decipher the nature of upper and lower boundaries of palaeosols and their implication for differential soil formation, morphodynamic conditions and palaeoclimate

The shifts in the texture of loess are indicative of changing wind strength and/or changing sink to source distances. This approach is also applicable to potential palaeosols that formed under ongoing dust deposition and might thus offer the opportunity to compare atmospheric dynamics during phases of soil formation and loess formation. To address this issue highly resolved records of grain-size are required, which were lacking to date. As a part of the present results considerable effort was dedicated to the:

(Objective 4) Deduction of relative wind strength from the textural properties of loess and palaeosols

Most global loess deposits originate from source rocks/sediments that have experienced at least one cycle of erosion, transportation and sedimentation (Gallet et al., 1998; Muhs and Budahn, 2006). Due to extensive silt production combined with its aeolian transport, the assemblage of major and trace elements in loess is thought to approximate the average geochemical composition of the upper continental crust (Taylor, 1983; Taylor and McLennan, 1995; Ujvári et al., 2008). Hitherto, it is not clear whether northeastern Iranian loess originates from well-mixed sediments and/or sedimentary rocks. Frechen et al. (2009) state that the spatial extent of loess deposits in north eastern Iran is closely related to the vicinity of rivers in Golestan Province, suggesting that the floodplains of the rivers might at least represent the proximal dust source of the loess deposits at the sections Neka, Toshan, Now Deh and Agh Band. Therefore, geochemical investigations are carried out,:

(Objective 5) *Providing further evidence for the provenance of northeastern Iranian loess*

Kehl (2010) provides a first pedostratigraphic scheme of northeastern Iran, comparing the section at Neka, Now Deh, and Agh Band. This comparison is done primarily by means of pedostratigraphic estimates based on rough age control. However, a differentiated pedostratigraphy of northeastern Iran is important in order to gain deeper insights into the spatial extent of palaeoclimatic fluctuations and to establish a key loess sequence, being representative of the region. Thus, the present thesis aims at:

(Objective 6) *Elaboration of a new pedostratigraphic model for northeastern Iran by intercorrelation of the respective loess-palaeosol sequences*

The loess region of northeastern Iran is the missing link to correlate palaeoclimatic findings from western and central Asian loess-palaeosol sequences. Furthermore, several highly resolved pollen records from lacustrine sediments exist in the vicinity of northern Iran. In order to close this spatio-temporal gap the final aim is a:

(Objective 7) *Comparison of the key loess-sequence of Northern Iran with other archives of Quaternary climate change on a supraregional scale*

1.5 Analytical approach

Fluctuations in climatic parameters such as temperature, precipitation and wind velocity may promote changes in the physical and chemical properties of loess, which can be preserved over large parts of the Quaternary period. Within the present dissertation three new sections of northeastern Iranian loess have been studied, based upon a multi-proxy study of inorganic compounds, which encompass color, CaCO_3 -content, grain-size, mineralogy and geochemistry, magnetic susceptibility, and micromorphology. These fluctuations are detectable by means of numerous different biotic and abiotic proxies. Proxies are, therefore, considered the preserved physical and chemical characteristics of past environments. However, the application of biotic proxies is beyond the scope of the thesis. These proxies include the analysis of biomarkers such as e.g. leave derived n-alkanes and their stable carbon isotope composition as well as stable carbon and nitrogen isotopes of soil organic matter in order to reconstruct the former vegetation cover (e.g. Lei et al., 2010; Zech et al., 2010; Schatz et al., 2011; Zech et al., 2013; Shahriari et al. 2017).

All loess sections presented in this dissertation were sampled in 2 cm increments. During field description the emphasis was placed on soil structure, mottling, precipitation of secondary carbonate, soil color and the nature of upper and lower boundaries of the respective strata. The different soil horizons were classified according to the WRB (IUSS Working Group WRB, 2007). Micromorphology was used to corroborate the preliminary field findings and soil classification.

Palaeosols belong to the most eye-catching changes in the physical properties of loess (Fig. 1.3). The description of the colorimetric properties represents a valuable method allowing for

the distinction between palaeosols and loess (Fig. 1.2). However, weakly developed palaeosols may cause only subtle color differences as compared to loess layers thus impeding a visual detection. The soil color is usually determined by visual matching between the color as perceived in the field and the Munsell soil color chart. Such a determination is prone to errors, since it is highly dependent on soil moisture conditions, the light conditions (unclouded or clouded), and the researcher's perception (Melville and Atkinson, 1985). In order to circumvent subjective perception as a source of errors the colorimetric properties of loess and palaeosols are determined by means of VIS (visible) spectroscopy under laboratory conditions. The spectrophotometric analysis covers the spectral range of visible light from 360 to 740 nm (Eckmeier et al., 2013). The spectral information is then converted to the CIE (L^* , a^* , b^*) color space (CIE 1978). For an explanation of the measurement technique, the reader is referred to chapter 2.3.4. The $L^*a^*b^*$ data is used to calculate the redness index (RI). The RI represents a proxy of relative hematite contents, which was empirically defined by Barrón and Torrent (1986). Thus, the RI indicates relative soil maturity as well as seasonal variations in temperature and precipitation prevailing during pedogenesis (Buggle et al., 2014).

The textural properties of loess and palaeosol samples were determined using laser diffractometry. It offers considerable advantages over the classical sieve and pipette method, as it is less time consuming and thus suited for analysis of large sample sets. Moreover laser-diffractometry has become a standard measurement technique in loess research and our results of particle-size distribution may thus be compared with those from other researchers. The texture of relatively unweathered loess is used as a proxy of wind energy and the relative distance between dust sources and sinks. However, the particle-size distribution of loess may be affected by chemical weathering processes after deposition, which might result in an enrichment of secondary clay minerals. Vandenberghe et al. (1985), therefore, introduced the U-ratio that takes into account the ratio of medium silt (16-44 μm) and fine silt (5.5-16 μm) and disregards the clay fraction (<5.5 μm). The interpretation potential of the U-ratio, however, is subject to restrictions which are discussed in chapter 2.5.1. While the U-ratio is used as proxy of relative wind strength the clay fraction serves to mirror soil formation (Machalett et al., 2008).

The development of palaeosol horizons corresponds with decomposition of readily weatherable minerals such as e.g. plagioclase and the neoformation of secondary minerals (clay minerals). As a result soluble elements (Ca, Mg, Sr) are leached, whereas less soluble (e.g. Al, Sc, Ti) or immobile (K, Pb) elements are enriched (Buggle et al., 2011). The mineralogical composition is determined by X-ray diffractometry (XRD), while the geochemical composition of the bulk samples was investigated using X-ray fluorescence (XRF). As both analyzing techniques require extensive pretreatments prior to the respective measurements, XRF and XRD were carried out in low resolution. Geochemical proxies of palaeoclimate are based on the relation between immobile/insoluble elements and soluble/mobile counterparts, hosted by the same mineral. For example the chemical index of alteration (CIA) gives a quantitative measure of feldspar weathering as it relies on the mobility of CaO (Ca bound to silica), Na₂O and K₂O, whilst Al₂O₃ is enriched in the weathering residuals of feldspars (Nesbitt and Young, 1982; Buggle et al., 2011). Furthermore canonical ratios are formed based on the same principles. Fe and Mg are

abundant in amphiboles, where Fe forms insoluble hydrolysates under oxidizing conditions after its release from the mother mineral. Conversely, Mg is soluble and may be leached from the weathering profile. The down-profile variations of geochemical weathering proxies are therefore used as proxy of moist or dry palaeoclimatic conditions. The combination of insoluble major elements such as Al_2O_3 and TiO_2 are thought to form invariant ratios depending on the source rock. These elements are used as a provenance indicator of northeastern Iranian loess.

Moreover, chemical weathering promotes the formation of magnetizable minerals such as magnetite and maghemite (Heller et al., 1991). These minerals are most abundant in palaeosols and can be determined by analyzing the magnetic susceptibility of loess and palaeosols. Thus, the magnetic susceptibility is found enhanced in palaeosols, while loess layers exhibit low amounts of magnetite and maghemite (Evans and Heller, 2003). The rock magnetic properties of loess-palaeosol sequence are considered a proxy of palaeoprecipitation and palaeoweathering.

The CaCO_3 -content was determined by means of mid-infrared spectroscopy (MIRS), whose fast measurement routine is suited for the analysis of large sample sets. As shown in chapter 1.2, the dissolution of primary carbonates is a first phase of pedogenesis on loess. The determination of CaCO_3 contents, therefore, serves as a proxy of pedogenesis in order to distinguish between loess and palaeosols and allows for the characterization of loess layers. However, palaeosols may also be partly or completely recalcified by CaCO_3 originating from overlying loess layers. Secondary carbonate metabolism is detectable by its morphological characteristics in the form of e.g. pseudomycelia or powdery lime being found between soil aggregates. These features may be observed macroscopically in the field and microscopically by means of micromorphology. The down-profile variations in CaCO_3 -content bear implications for polygenetic influences on palaeosol formation.

The data from palaeoclimatic proxies, briefly outlined in this chapter, may be used to correlate the northeastern Iranian loess-palaeosol sequences located at Neka, Toshan, Agh Band and Now Deh. Thus, local findings are combined to elaborate a regional model of the late Pleistocene climate dynamics in northeastern Iran. The correlation of loess soil-sequences may be achieved by using characteristic culminations from proxy-records or, where available, tephra layers as chronological tie points (Roberts, 2015). The application of this correlative technique requires continuous sedimentation rates and morphodynamic stability (Roberts, 2015). However, numerous luminescence dating studies have revealed highly varying sedimentation rates of airborne dust and erosional unconformities in loess-palaeosol sequences in terrestrial records of the late Pleistocene (e.g. Antoine et al., 2001; Frechen et al., 2001; Roberts et al., 2003). Consequently, a resilient correlation requires not only the bare palaeoclimatic data, but also high-resolution dating results in order to unravel former sedimentation regimes, detect hiatuses and correlate proxy-data from stratigraphical units, that formed at a similar time. Although dating is beyond the scope of this doctoral thesis, the results from optically stimulated luminescence dating (OSL) determined by Lauer et al. (2017a, b) and Frechen et al. (2009) are used. For a summary of the basic principles of OSL-dating the reader is referred to chapter 1.2.

1.6 Geographical setting

Iran is comprised of continental blocks that were located along the northern margin of Gondwana forming the southern boundary of the palaeo-Tethys ocean during the Paleozoic (Allen et al., 2003; Castro et al., 2013). The formation of the Neo-Tethys caused these blocks and other geotectonic units to separate from Gondwana in Permian times. The separated landmass denominated as the Cimmerian terranes, drifted northwards and thus widened the Neo-Tethys at the expense of the oceanic crust of the palaeo-Tethys, which was continuously subducted beneath the southern margin of the Eurasian Plate (Allen et al., 2003; Castro et al., 2013; and Robert et al., 2014). The collision of the Cimmerian terranes with the southern continental margin of Eurasia, the Turan platform, induced the Cimmeride orogeny during the Late Triassic. According to Castro et al. (2013) the Cimmeride orogeny constitutes the initial compressional event in the formation of the Alborz Mountain range. Conversely, the Kopeh Dagh was formed as an intracontinental basin between the stable Turan platform and central Iranian block. Thus, the rock succession of the Kopeh Dagh suggests a closing ocean basin, being uplifted and formed during the Cenozoic (Mortazavi et al., 2013). These rocks structurally differ from those of the Alborz Mountains, since they belong to the Turan platform, a geologically distinct unit (Hollingsworth et al., 2006). As part of the Alpine Himalayan Belt, the Alborz and Kopeh Dagh Mountains represent an active fold and thrust belt, since the continued convergence of the Arabian and Eurasian lithospheric plates still effects intra-continental deformation.

These Paleozoic and Cenozoic orogenic belts demarcate a narrow coastal strip from the remaining landmass of Iran, which is known as the Caspian Lowland (Fig. 1.4). Located between the Alborz Mountains to the south and the Caspian Sea to the north, the Caspian Lowland is considered the smallest climatic region of Iran (Molanejad et al., 2015). The Caspian Lowland is particularly characterized by culminating annual precipitation amounts in its southwestern part, where the meteorological station at Rasht records around 1400 mm of precipitation per year and average annual temperatures of 15.8 °C (Fig. 1.5). Owing to gradually increasing continental climate in an eastward direction, annual precipitation amounts decrease correspondingly to 690 mm at Sari and 515 mm at Gorgan (Fig. 1.5), while average temperatures rise to 16.7 and 17.8°C, respectively (Alijani and Harman, 1985). The absence of continuous mountain barriers to the north of the Caspian Lowland enables a meridional transfer of northern air masses into the southern coastal area of the Caspian Sea (Alijani and Harman, 1985; Molavi-Arabshahi et al., 2016). Although the Caspian Lowland stands out from the mostly semi-arid and arid climate in Iran, its climatic controls are closely linked to atmospheric conditions over the entire country and neighboring regions making its synoptic climatology complex (Molavi-Arabshahi et al., 2016). Iran is located at the eastern edge of the Mediterranean Sea and found in a region of general atmospheric subsidence (Stevens et al., 2012). It extends approximately from 25°N to 40°N and is, therefore, influenced by two features of the general atmospheric circulation i.e. the subtropical jet stream and the polar front jet, whose latitudinal position vary with seasonal shifts in solar irradiation.

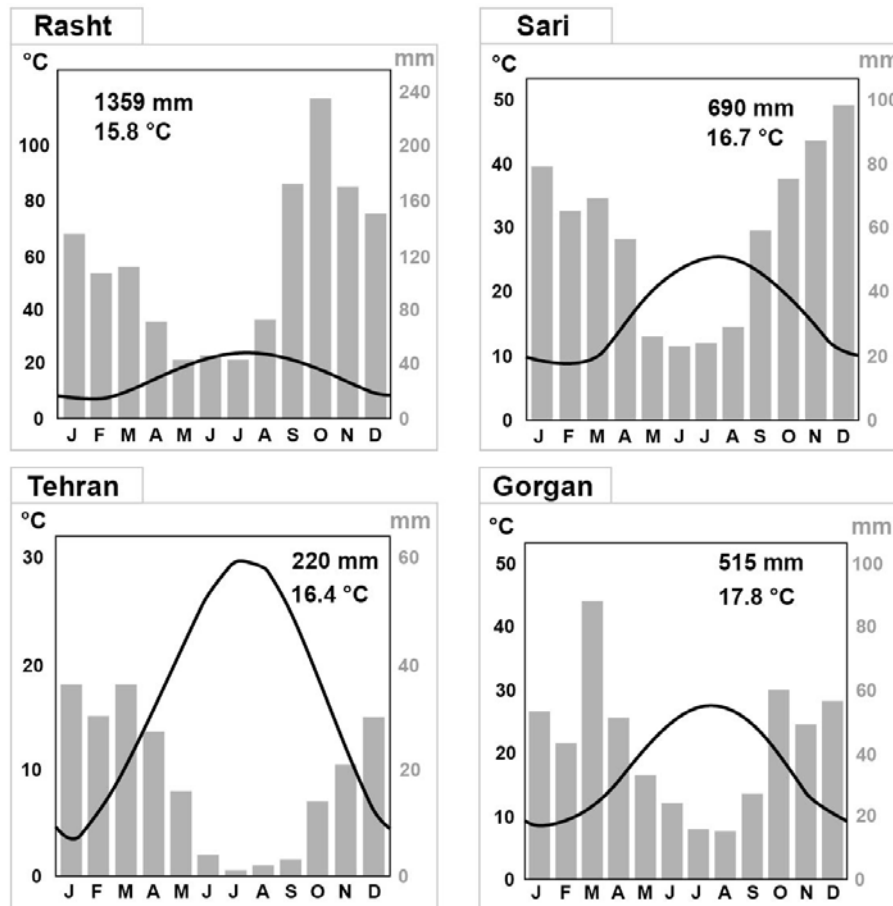


Fig. 1.5: Climate diagrams of selected meteorological stations of northern Iran and Tehran (Meteorological Organization of Iran, 2016).

Synoptical climate from September to March

During autumn and winter when latitudinal temperature and pressure contrasts intensify the Caspian Lowland is influenced by zonal and meridional air mass flows, as the subtropical and the polar front jet relocate southward. The formation of the Siberian anticyclone causes cold north to north-easterly winds to invade the Caspian Lowland. These winds are modified by sweeping the surface of the Caspian Sea thus bringing moisture to northern Iran, particularly to the northwestern part of the Caspian Lowland. Along the Alborz Mountain range these cold air masses may confront foehn-like winds descending from its northern footslopes, creating frontal systems of local and regional extent and high amounts of precipitation (Leroy et al., 2011). Furthermore, westerly winds may transport moisture from the Mediterranean Sea and the Atlantic Ocean to northern Iran (Molanejad et al., 2015). According to Molavi-Arabshahi et al. (2016) this zonal air mass flow is favored by an Omega (named according to Ω -shape of the 500 hPa contour) circulation anomaly over central Europe, redirecting moisture laden winds and cyclonic disturbances from the Atlantic Ocean and the Mediterranean Sea into the southern Caspian area. These cyclones may be directed eastward by the polar front, which is well developed along the Alborz Mountains during wintertime (Stevens et al., 2012). Thus, the polar front, also known as the Iranian front

causes increased precipitation and storminess in the Caspian Lowland (Orlowsky et al., 2005; Machalett et al., 2008; Molavi-Arabshahi et al., 2016).

The western declivity of the Zagros and Alborz Mountains, however, precludes most extratropical cyclones from penetrating into the Caspian Lowland (Machalett et al., 2008; Molavi-Arabshahi et al., 2016). Additionally, the southwestern branch of the Siberian Anticyclone may extend to the southeast of Iran and effectively block the penetration of zonal moisture bearing air masses in February (Dando, 2005). These maritime winds are considered responsible for a significant portion of annual precipitation in the Caspian Lowland (Dando, 2005; Stevens et al., 2012; Molanejad et al., 2015), whilst other authors tend to place the emphasis on north and north-easterly winds originating from the Siberian anticyclone (Leroy et al., 2011; Molavi-Arabshahi et al., 2016).

Synoptical climate from April to August

During summertime the tropical jet stream and the subtropical high-pressure belt move to a position over northern Iran, favoring subsiding air masses and subsequently clear skies (Alijani and Harman, 1985; Molanejad et al., 2015). Thus, development of storms is largely suppressed and summer is the driest season in Iran (Fig. 1.5). In the Caspian Lowland, however, thermal interaction in the form of a land-sea breeze system between the Caspian Sea as a regional source of water vapor and its southern coast line may cause convective precipitation events. Therefore, seasonal differences in rainfall may be attenuated in the Caspian Lowland and are more pronounced in the southern parts of the country (Ganji, 1968; Alijani and Harman, 1985).

Chapter 2

Loess-soil sequence at Toshan (Northern Iran): Insights into late Pleistocene climate change

Vlaminck, S.^a, Kehl, M.^a, Lauer, T.^b, Shahriari, A.^c, Sharifi, J.^c, Eckmeier, E.^e, Lehndorff, E.^d, Khormali, F.^c, Frechen, M.^b

^a Institute of Geography, University of Cologne, Albertus Magnus Platz, 50923, Cologne, Germany

^b Leibniz Institute for Applied Geophysics (LIAG), Stilleweg 2, 30655, Hannover, Germany

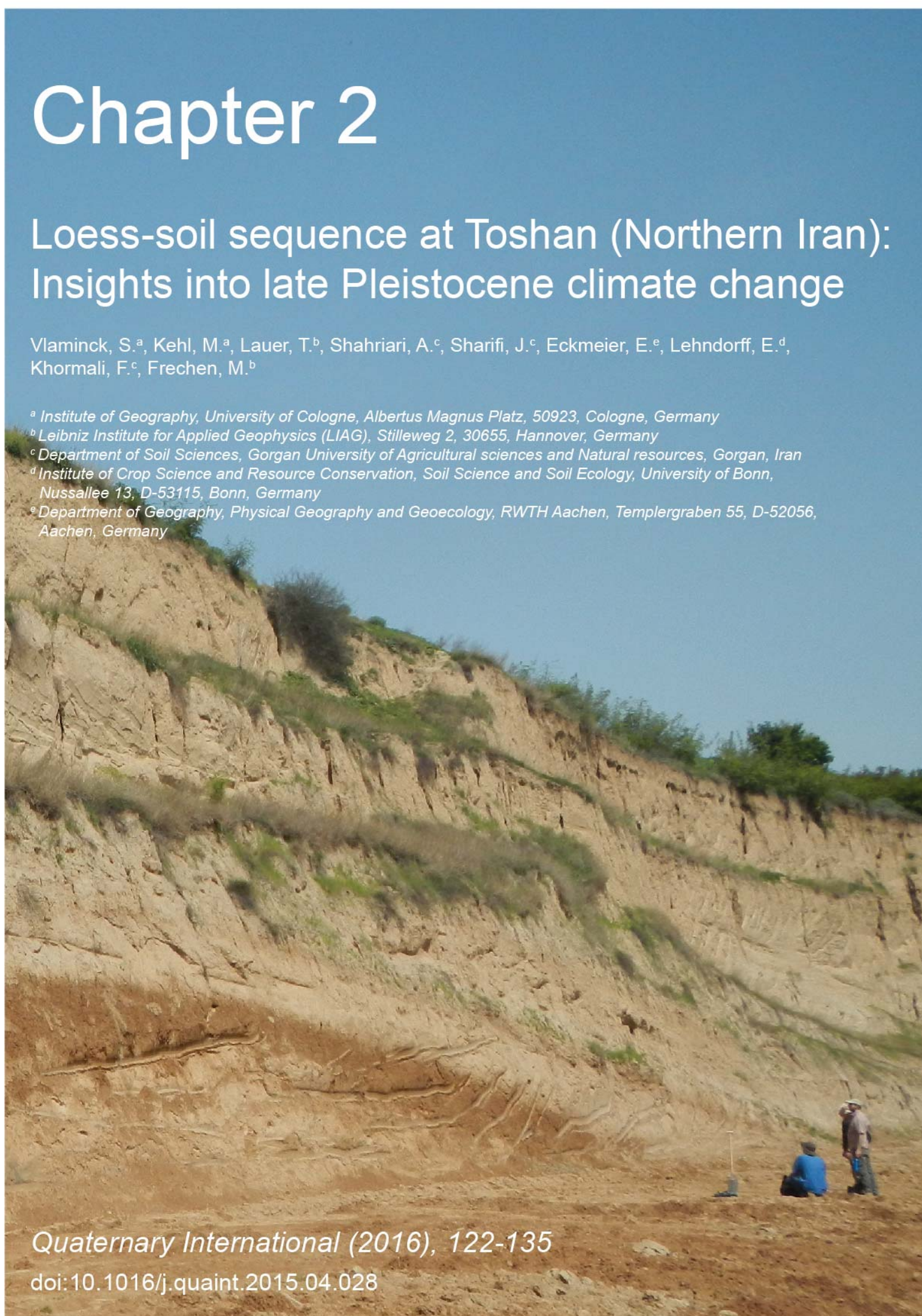
^c Department of Soil Sciences, Gorgan University of Agricultural sciences and Natural resources, Gorgan, Iran

^d Institute of Crop Science and Resource Conservation, Soil Science and Soil Ecology, University of Bonn, Nussallee 13, D-53115, Bonn, Germany

^e Department of Geography, Physical Geography and Geoecology, RWTH Aachen, Templergraben 55, D-52056, Aachen, Germany

Quaternary International (2016), 122-135

doi:10.1016/j.quaint.2015.04.028



-Formatting and orthography of the publication are adapted to the dissertation style-

Abstract

The knowledge of palaeoclimate in Iran is still limited. However, insight into the timing and the dynamics of Quaternary climate change in Iran might offer valuable information to improve the global palaeoclimate record. The loess-soil sequence of Toshan provides the first high-resolution record of late Pleistocene climate dynamics in Iran and complements the hitherto known sections at Neka, Now Deh and Agh Band to establish a pedostratigraphic record of the north-eastern Caspian Lowland. Our spectroscopic and grain-size analysis are combined to propose (i) a pedostratigraphical scheme for the sequence at Toshan, (ii) describe and estimate the degree of soil development of selected stratigraphical units, (iii) infer palaeoclimatic information, and provide (iv) a correlation with previous loess-palaeosol records of N-Iran as based on pedostratigraphic assumptions. The section at Toshan hosts a strongly developed reddish-brown argillic palaeosol (Bt) as well as eight moderately to weakly developed brownish palaeosol horizons lacking clay illuviation features (Bw/Bwk). These remnants of fossil soils are separated by finely textured loess and horizons that host characteristics of both loess and mineral subsoils (CB/CBk), giving evidence for syngenetic soil formation. The stratigraphical succession of palaeosols, loess and syngenetically altered sediments, covering the last ca.130k years, gives evidence for recurrent climate changes as well as fluctuations between dominance of soil formation or dust accumulation in relation to changes in moisture regime. The formation of Bt and Bw/Bwk-horizons is related to relatively humid and warm conditions likely corresponding with interglacial and interstadial climate.

Keywords: Loess, palaeoclimate, Iran, palaeosol

2.1 Introduction

Loess deposits constitute a sensitive terrestrial archive, as their formation involves processes governed by climate such as the production and deflation of (mainly) silt-sized particles, their aeolian transport and deposition as well as syn- and post-depositional alterations (e.g. Kemp, 2001; Smalley et al., 2005; Pécsi 1990). Traditionally the accumulation of dust forming loess is thought to occur mainly during cold and arid intervals of glacial periods (stadials) (Kemp, 2001). In contrast climatic conditions during interglacials and interstadials are characterized by higher average temperature and precipitation, which promoted the growth of vegetation, the intensity of chemical weathering and pedogenesis. Hence, under relatively stable geomorphodynamic conditions, soils formed on the dust covered landscapes of the past. Their burial under new layers of dust resulted in vertical successions of loess layers and intercalated palaeosols often preserved as remnants of the original soil. The kind and intensity of soil forming processes are mainly driven by climatic and soil-environmental conditions.

According to Jenny (1941) soil-formation is a function of climate, organic activity, relief, parent material and time, which is expressed by, e.g. the function $S=f(\text{climate [cl]}, \text{organic matter [o]}, \text{relief [r]}, \text{parent material [p]})$. Though afflicted with restrictions, palaeoclimatic

inferences can be drawn from comparison of palaeosols with the modern (Holocene) soil, forming under known climatic conditions (Kehl, 2010). In order to study the effect of climate on soil formation other factors of pedogenesis than climate have to be kept constant (Khormali and Kehl, 2011). Kemp (2001) states that the differentiation of a climatic influence from other soil-forming factors within the “clorpt”-concept of Jenny (1941) is subjected to problems. A differentiation is justified if the modern Holocene soil has derived from a substrate (=pt) in a comparative geomorphic position (=r), with a similar granulometric and mineralogical composition like the parent material of the intercalated palaeosols (Kehl, 2010; Kehl et al., 2005). Hence, if the factors “r” and “pt” are constant the function of Jenny (1941) can be simplified to $S=f(cl,o)$, and soils can be defined as climatophytomorphic (Bronger et al., 1994, 1998).

Within the Eurasian loess belt most scientific attention has been attributed to loess-soil sequences of south-eastern (SE) Europe and Central Asia (e.g. Frechen and Dodonov, 1998; Mestdagh et al., 1999; Machalett et al., 2008; Markovic et al., 2008; Antoine et al., 2009; Buggle et al., 2009; Markovic et al., 2009), while comparatively little information is available about respective terrestrial archives in Iran (Kehl et al., 2005; Frechen et al., 2009). However, additional analysis of northern Iranian loess-soil sequences may play a crucial role in correlating European and Central Asian findings, and thus closing this spatio-temporal gap. Therefore, an elaborate and well understood pedostratigraphy of north-eastern (NE) Iran is necessary, consisting of several loess-soil sequences. The loess-soil sequence at Toshan completes the pedostratigraphic record of the Caspian Lowland (NE Iran) and is described in detail below.

Within the glacial intervals of the Quaternary, northern Iran represented an extensive depositional environment for windblown dust and loess formation (Frechen et al., 2009), covering particularly the northern foot slopes of the Alborz Mountains. Descriptions of the hitherto known loess-soil sequences of the Caspian Lowland were provided by Kehl et al. (2005), Frechen et al. (2009), and Kehl (2010) while modern soils formed on loess were described by Khormali and Kehl (2011) and Khormali et al. (2012). The profiles Neka, Now Deh and Agh Band are located along a climatic gradient, ranging from subhumid conditions in the west near Neka to semiarid conditions towards the north and north-east at Agh Band (Fig. 2.1). The profiles represent a climosequence including climatophytomorphic modern soils which show differential degrees of soil formation, as expressed by their respective morphology, clay mineralogy and their physicochemical properties corresponding to decreasing humidity from W to E (Khormali and Kehl, 2011). Moreover Kehl et al. (2005) and Kehl (2010) identified differences in grain size distribution and thickness of loess layers, as well as the amount and type of palaeosols along this transect. The profile at Agh Band hosts a moderately developed Bw(t) horizon, whilst a strongly developed Bt horizon and strongly developed AhBtk horizons were found in Now Deh and the section at Neka, respectively (Kehl et al., 2005; Kehl, 2010). According to IRSL-age estimates of Frechen et al. (2009), these soils are covered by thick deposits of last glacial loess and probably formed during the last interglacial period. Their different degrees of development suggest an increased soil development during the last interglacial from Agh Band to Neka, whereas dust accumulation rates during the last glacial experienced the opposite trend (Kehl et al., 2005).

The recently studied climosequence of loess and soil sequences is now supplemented by detailed loess-soil investigations for the section at Toshan, located near the City of Gorgan.

In this paper, we give the first lithological and pedological descriptions of the sequence, including preliminary results of micromorphology, high resolution records of grain-size distribution, color and the CaCO_3 content. The aim of this study is to propose (i) a pedostratigraphical scheme for the sequence, (ii) describe and estimate the degree of soil formation of selected stratigraphical units, (iii) compare Toshan section with previously published loess-soil sequences in Northern Iran, the loess profiles at Remisowka, Kazakhstan (Machalett et al., 2008) and Tagidjar, Tajikistan (Mestdagh et al., 1999), as well as pollen records from Lake Urmia, Iran (Djamali et al., 2008) and Lake Van, Turkey (Litt et al., 2014), and (iv) infer palaeoclimatic information from the sequence at Toshan. The chronological framework of the sequence as based on a luminescence dating study is discussed by Lauer et al. (this issue).

2.2 Study area

In the NE of Iran, near the City of Gorgan the loess deposits of the Caspian Lowland form smooth hills covering the northward facing slopes of the Alborz mountain range (Fig. 2.1). The landscape is dissected by the River Gorgan and its tributaries, draining the Alborz Mountains. The geological basement consists mainly of Paleozoic and Mesozoic limestone. Loess serves as raw material for brick production and is intensively quarried. Thus local geomorphology is shaped by the interaction of anthropogenic and natural processes. The loess-soil sequence of Toshan (N 36°49'01"/E 54°25'25") is located on a watershed position in a quarry south-west of the City of Gorgan, 145 m above sea level. In this area, the loess deposits attain thicknesses of at least 30 m as exposed e.g. in the sequence investigated. Situated in a hill slope the quarry itself comprises an upper and a lower level. The upper part was investigated within this study.



Fig. 2.1 A: Northern Iran with locations of loess-soil sequences studied by Kehl (2010) and own sections. The section at Toshan is located within the suburban zone of Gorgan City. **B:** Central Asia with locations of Lake Van (Litt et al., 2014), Lake Urmia (Djamali et al., 2008) and loess-palaeosol sequences of Remisowka (Machalett et al., 2008) and Tagidjar (Mestdagh et al., 1999).

The Caspian Lowland itself represents a basin of subsidence (Brunet et al., 2003), providing an extensive accommodation space for marine and alluvial sediments such as the fluvial deposits of the River Atrek, separating Iran from Turkmenistan and the River Gorgan near

the City of the same name. Their runoff characteristics alternated, owing to variations in the context of Quaternary climate shifts (Frechen et al., 2009) and base-level variations due to fluctuations of the Caspian Sea-level (Forte and Cowgill, 2013). Fluvial sediments likely served as partial source for local loess strata. In this context, Frechen et al. (2009) state that the thicknesses of loess deposits in the Caspian Lowland are closely related to the vicinity to the rivers. This observation was already made by Lateef (1988).

Further to the North, the Caspian Lowland merges into the Turkmen steppe. The arid regions of Central Asia and the subhumid foreland of the Alborz Mountains constitute a zone of climate transition. This area has most likely reacted sensitively to fluctuations of Quaternary climate (Kehl, 2010).

The present climate at Gorgan is subhumid with a mean annual precipitation of 600 mm as measured at the meteorological station at Gorgan. Towards the Turkmen steppe, precipitation rates quickly decline to an annual mean of 200 mm. Near the section at Neka, situated to the west of Gorgan, average precipitation attains 750 mm per year. The annual mean temperature in the Caspian Lowland is at approx. 17 °C (Kehl et al., 2005).

The main wind patterns in Iran are largely governed by seasonal pressure differences between the Caspian Sea and the Iranian Highlands. In the Iranian plateau a high pressure cell develops during the cold winter months, whilst the surface water of the Caspian Sea exhibits relatively low pressure, owing to its thermal inertia (Ganji, 1968). The distribution of pressure causes air masses to flow from the Iranian plateau towards the Caspian Sea. During the hot summer months the high pressure cell in the Iranian plateau is replaced by a strong heat depression, whereas a relative center of high pressure forms above the Caspian Sea, leading to an opposite wind direction (Ganji, 1968).

2.3 Materials and Methods

2.3.1 Field sampling and micromorphology

The quarry at Toshan comprises several palaeosol horizons forming convex shaped interfaces with the loess layers. The palaeosols dip with an angle of approx. 15° towards the north and 3-5° to the east (Fig. 2.2 and 2.3). In order to gain access to the whole sequence and to establish a complete pedostratigraphy, five discrete profiles were prepared. These overlap as depicted in Figures 2.2 and 2.3. All profiles were created as step-like profiles. Care was taken to reach for layers undisturbed by quarrying or recent reworking. However, dipping angles cause a virtual increase in the thickness of respective strata. Pristine sample material could be extracted from the entire sequence in 2 cm intervals, accounting for a total of 1300 samples for yielding high resolution records of grain-size. Color and carbonate content were determined for every second sample. All samples were dried in a drying chamber at a temperature of 40°C.

Additionally, 32 samples for micromorphological analysis were taken from selected strata and uncovered thin sections, 45 x 45 mm in size and 30 µm thick were prepared. The thin sections were studied under ordinary polarized light and under crossed polarizers using a petrographic microscope. For description of thin sections, the terminology of Stoops (2003)

was used. A detailed micromorphological analysis is beyond the scope of this article, but thin sections are used as an ancillary method for the identification of pedogenic processes. During field description particular attention was paid to the soil structure, visual estimation of soil color, mottling, precipitation of secondary carbonate and the nature of lower and upper boundaries of the respective strata. The classification of the different soil horizons is based on the WRB (IUSS Working Group WRB, 2007).

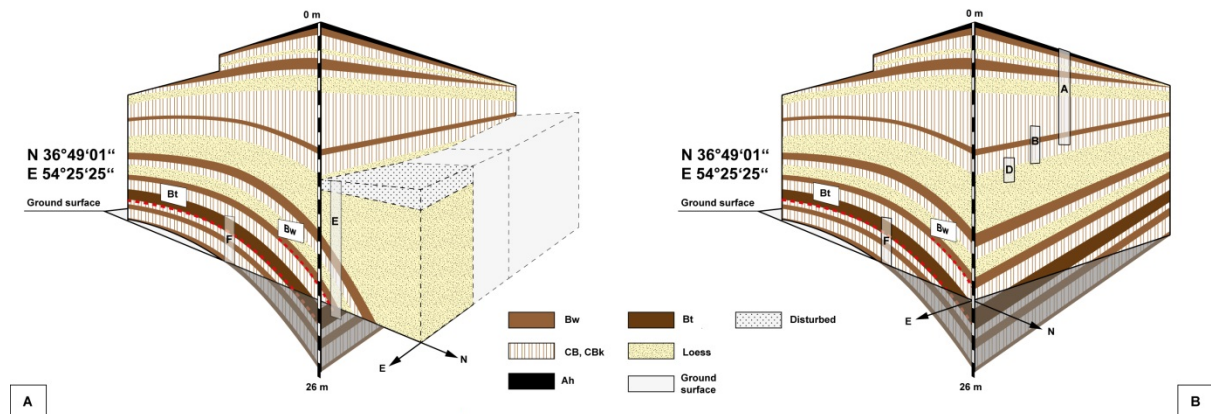


Fig. 2.2 A & B: Cross-sectional view showing an idealized horizontal and vertical succession of the sequence at Toshan.

2.3.2 Granulometric analysis

Determination of particle-size distribution (PSD) was carried out by means of laser diffraction analysis using a Beckman-Coulter LS 13320 PIDS. It offers several advantages over the classical sieve and pipette method, such as the necessity for only small amounts of sample

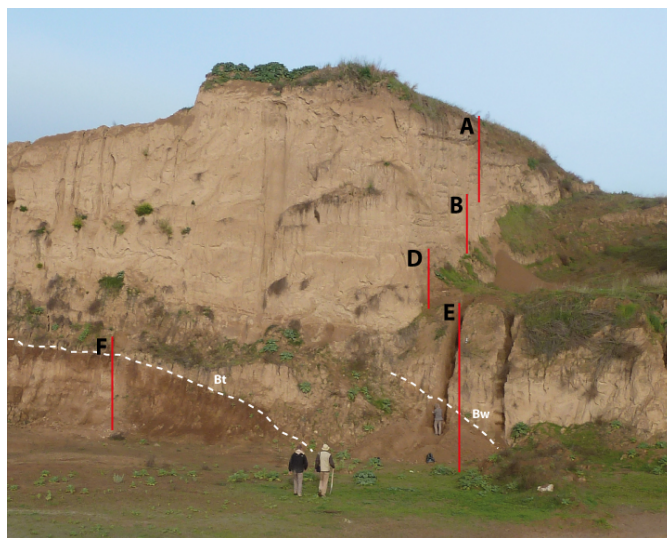


Fig. 2.3: Discontinuous sampling at Toshan. The 5 discrete step-like profiles, overlapping one another are indicated by the capitals A, B, D, E, and F. The dashed lines represent the lower convex shaped boundary of a Bt- and a Bw-horizon respectively. These fossil soil horizons delineate a former hill surface.

material, and a wide particle spectrum ranging from 0.4 to 2000 μm in diameter. Moreover PSD is measured within a short time and its results offer a reliable reproducibility (Beuselinck et al., 1998; Machalett et al., 2008). Nevertheless the detection of clay-sized particles may be subject to certain underestimations, owing to variations in particle mineralogy and morphology (Beuselinck et al., 1998). We therefore chose the sum of particles with less than 5.5 μm in diameter as an estimate of clay percentage.

The determination of particle-size distribution was conducted according to the standard sample protocol of Machalett et al. (2008) using

Fraunhofer theory for evaluating the grain-size spectra. Removal of organic matter was rejected since its portion is expected to be <2% within loess and palaeosols, thus exerting a negligible effect on PSD measurements (Machalett et al., 2008). CaCO_3 was not removed from the samples prior to the determination of PSD. In addition to secondary carbonates it involves primary carbonates, regarded to be a main component of the sediments deposited in the loess-soil sequences of the Caspian Lowland. Furthermore, there is no method available for the selective destruction of secondary carbonates.

One test sample out of every profile step was chosen. Five aliquots of each test sample were measured to identify an optimal parameterization in terms of sample weight for different types of sediments. Aggregates were dispersed by spiking each sample with 1% ammonium hydroxide (NH_4OH) in order to prevent possible reaggregation, cleavage of weak mineral grains and the formation of air bubbles during an alternative ultrasonic pretreatment (Machalett et al., 2008). In addition the tubes containing the sample material were placed on a rotator for 12 hours prior to measurements.

In order to test the reproducibility of the measurements the PSD of the same samples was determined using the adjusted sample weight. Three subsamples with five aliquots respectively were analyzed again, resulting in 15 grain-size spectra for each sample. Comparing these results, the measurement protocol was accepted if the standard deviation for all grain-size spectra (and all grain-sizes classes) accounted for less than 5%. Usually, our reproducibility tests yielded results with standard deviations ranging from 1.2 to 2.2%.

2.3.3 Mid-infrared spectroscopic measurements

Mid-infrared spectroscopy (MIRS) is based on laboratory-analysis “ground-truth” data and the reflectance of a sample, combined to predict the concentrations of e.g. carbonate and organic matter. MIRS offers considerable advantages compared to the conventional volumetric analysis of CaCO_3 since it requires only a small amount of sample material (15-25 mg). Furthermore, it is less time-consuming, which qualifies MIRS for determining the amounts of specific components for a large number of samples.

Table 2.1:

Model parameters and statistical indices for prediction of CaCO_3 .

Fraction	Spectra (n)	Maverick (n)	R^2	RMSECV ^a	RPD ^b	EF ^c
CaCO_3 [%]	406	9	0.98	1.1	8.95	0.92

^aRoot mean square error of cross validation

^bRelative percent deviation

^cModelling efficiency

Dried and homogenized sample material was given to a micro plate and compacted by means of a plunger in order to create a plain and dense surface for measuring its diffuse reflectance. Altogether 650 samples with 5 aliquots each were measured from the section at Toshan. Their diffuse reflectance spectra were recorded using a Bruker Tensor 27. This mid-infrared spectrometer is fitted with a liquid N_2 -cooled mercury-cadmium telluride (MCT)

detector and a broadband KBr splitter, providing a measurable spectral range from 8000-600 cm^{-1} (1250-16.700 nm). Within a single run spectra were recorded in 4 cm^{-1} increments.

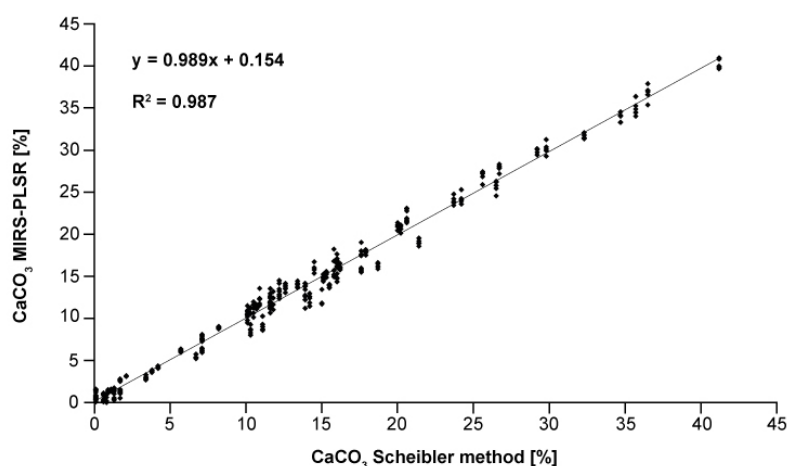


Fig. 2.4: Prediction of CaCO_3 from MIRS and partial least square regression (MIRS-PLSR) compared to CaCO_3 content determined by the Scheibler method based on the volumetric release of CO_2 (as based on data from Kehl, 2010).

A set of 83 samples of Northern Iranian loess and palaeosols (Kehl et al., 2010) was used to calibrate a statistical model for predicting the amount of CaCO_3 . For ground truth measurements of CaCO_3 the Scheibler method was applied. Hence, the samples were treated with HCl to determine their carbonate content according to the volumetric release of CO_2 . The predictive power of the applied model is supported by the CaCO_3

within loess and palaeosol horizons that were sampled across a climosequence in previous studies (Kehl et al., 2010). The quantification was conducted by means of OPUS QUANT software (©Bruker, 2006), applying partial least square regression (PLSR). The OPUS QUANT software provides an automated routine, testing combinations of diverse spectral ranges and data treatment for the best possible prediction power of the model (Bornemann et al., 2008). Thus the spectral ranges from 1997.8 to 1216.8 cm^{-1} and 6853.6 to 2653.5 cm^{-1} were suggested. A manual adjustment of the spectral range was not performed. The measurement protocol, the spectral pretreatment and the statistical analysis followed the routine of Bornemann et al. (2008). The high accuracy of this prediction is reflected by a close correlation between measured and predicted values (Fig. 2.4) and by statistical parameters listed in Table 1. The quality of the applied model was hereafter described by the coefficient of determination (R^2), the root mean square error of cross validation (RMSECV), the relative percent deviation (RPD) and the modeling efficiency (EF). The RPD represents the ratio of the standard deviation of the reference data and the standard error of the calibration procedure (Bornemann et al., 2008). The EF considers the relative deviation of the data determined in the lab in comparison to variation within the predicted data (Loague and Green, 1991). The EF should be as close to one as possible (Bornemann et al., 2008).

2.3.4 Spectrophotometric analysis

The determination of the colorimetric properties was conducted by measuring the diffused reflected light for the fraction <2 mm from 650 samples, using a Konica Minolta CM-5 spectrophotometer. The measurements followed a standardized procedure (2° standard observer and illuminant C) according to Eckmeier et al. (2013). Spectrophotometric analysis applied within this study covers a spectral range in the visible light from 360 to 740 nm. The obtained spectral information was converted to the CIE (L^* , a^* , b^*) (CIE 1976) and Munsell

color systems, respectively, utilizing the SpectraMagic NX software (Konica Minolta). The L^* values represent the luminance of the sample material on a scale from L^*0 (maximum extinction of light, black) to L^*100 (maximum luminance, white). Positive a^* values indicate redness and greenness when reaching negative values. On the other hand b^* values lying in a positive range indicate yellowness, whereas negative values represent blueness. When both a^* and b^* are zero, greyness can be inferred (Barrón and Torrent, 1986).

Data obtained by colorimetric analyses is used for detecting gradual or abrupt transions between different strata. The Redness Index (RI), which was empirically defined for the CIE ($L^* a^* b^*$) color space by Barrón and Torrent (1986), was calculated to evaluate the presence of iron oxides:

$$RI = a^* (a^{*2} + b^{*2})^{0.5} 10^{10}/b^* L^{*6}$$

This index largely takes into account the pigmenting effects of hematite (Fe_2O_3) to the soil color. Although we did not determine any absolute Fe_2O_3 , the application of the RI assumes that the intra-sequential differences may reflect relative differences in iron oxide mineralogy based on different soil environmental conditions. Nevertheless the RI is insensitive to goethite, owing to its lower pigmenting effect (Barrón and Torrent, 1986).

2.4 Results

A schematic column of the section at Toshan is shown in Fig. 2.5. According to an IRSL-dating study of Frechen et al. (2009) the first strongly developed B horizons at the sections Neka, Now Deh and Agh Band likely correlate with marine isotope stage 5e (MIS 5e), the last interglacial. Based on the assumption that the first Bt-horizon within the sequence at Toshan tentatively correlates with the last interglacial as well, six pedostratigraphic units were identified by “counting from the top”. The pedostratigraphic units hereafter do not demand to correspond with certain marine isotope stages, but serve for a comprehensible structure of the following statements. In addition, palaeosol horizons were consecutively numbered, depending on their allocated pedostratigraphic unit and their position within this unit. Hence, the first palaeosol allocated to unit 3 is referred to as soil 3-1.

Selected dating results from Lauer et al. (2017a) are added to our stratigraphic Figures. The quoted results are pIRIR₂₉₀-luminescence ages (fine grain). The evaluation of the luminescence age estimates is explained in detail in Lauer et al. (2017a).

2.4.1 Field description and micromorphology

Unit 6 (25.73-22.51 m below surface)

The basal stratum, of the sequence from 25.73–25.53 m is formed by a moderately brownish Bwk-horizon (6-2), exhibiting a subangular blocky structure. The aggregate surfaces are mottled by manganese (Mn) and $CaCO_3$ has precipitated within the secondary pores, forming pseudomycelia. This horizon merges into a stratum denominated as CBk-horizon (25.53-24.18 m), since it shows less browning and considerably smaller aggregates than the

subjacent Bwk. CBk-horizons show only partial decalcification, thus representing a transitional stage between C and B horizons in which features of the parent material still prevail. The present CBk-horizon is subject to a heterogeneous distribution of secondary carbonate. It is delimited by a sharp boundary, separating the CBk from an overlying Bwk (6-1; 24.18-23.43 m). Analogous to the first Bwk (6-2) within the sequence, it is moderately brown with a subangular blocky structure. Its thick aggregates are sparsely coated with Mn-oxides and soft powdery carbonate. Furthermore, we found several loess dolls within the Bwk-horizon (6-2). It gradually merges into an overlying CBk-horizon (23.43-22.71 m). The CBk comprises small aggregates, forming a weakly developed subangular blocky structure, on which a dense network of pseudomycelia was detected. In a depth of 22.69 m below surface a 18 cm thick calcrete has formed referred to as Ckm-horizon.

Unit 5 (22.50-15.41 m below surface)

From 22.49-21.79 m a strongly developed reddish-brown Bt-horizon (5-3b) was found constituting the basal segment of unit 5. It is clearly distinguishable along its sharp lower boundary from the subjacent Ckm-horizon. Based on visual detection in the field and supplemented by micromorphological analyses an angular blocky to prismatic structure is apparent. Moreover we were able to identify well developed clay coatings in this horizon under the microscope. Some of them have been destructed and incorporated into the ground mass as depicted in Fig. 6 c and d. Clay domains are often covered by iron oxide (Fig. 2.6 c, d). Although thin sections suggest the Bt-horizon to be devoid of secondary carbonates, powdery lime could be detected in the field. The Bt-horizon (5-3b) merges into a brownish and partly recalcified Bw-horizon (5-3a) lying in a depth of 21.77-21.13 m below the surface. Its aggregates form an angular blocky structure analogous to the underlying Bt-horizon (5-3b). Moreover it shows clay content, comparable to the subjacent Bt-horizon. Conversely, micromorphological analysis revealed the absence of clay illuviation features within the Bw-horizon (5-3b) in contrast to the Bt-horizon (5-3a). From 21.13-20.71 m a layer designated as CB-horizon gradually follows the stratum situated below. Contrary to the following CBk (20.71-19.73 m), the CB-horizon was not recalcified. The CBk-horizon itself has been affected by a pronounced secondary carbonate metabolism, in the form of pseudomycelia. Both horizons show signs of weak browning and coherent and partially fine subangular blocky structure, indicating an incipient soil formation. At 19.73 m, differences in texture and structure mark the sharp lower boundary of a strongly brownish Bwk-horizon (5-2), extending to 19.49 m. It exhibits a subangular to angular blocky structure. The aggregate surfaces are weakly mottled by Mn-concretions. The Bwk-horizon (5-2) is more brownish in its lower part, while the degree of browning seems to decrease to the top where it merges into a moderately brownish ABwk-horizon (5-2; 19.47-18.93 m) showing a subangular blocky structure. This horizon is overlain by a loess layer extending from 18.91 to 17.59 m. The loess exhibits a typical coherent structure, while small Mn-mottles dispersed within the stratum point to a weak pedogenic imprint. To the top the loess gradually merges into a CBk-horizon (17.57-16.65 m). In a depth of 16.63 m the CBk-horizon is delimited by a sharp upper boundary from a light brownish Bwk-horizon (5-1) extending to 15.95 m. The Bwk-horizon (5-1) comprises small subangular blocky aggregates and a dense network of pseudomycelia

within its secondary pores. From 15.93-15.63 m the Bwk is overlain by another CBk-horizon. In a depth of 15.61 m we found a second, thin Bwk-horizon (5-1; 15.61-15.41 m). It is light brownish and consists of small subangular blocky aggregates. These two weakly developed Bwk-horizons are summarized and referred to as soil 5-1.

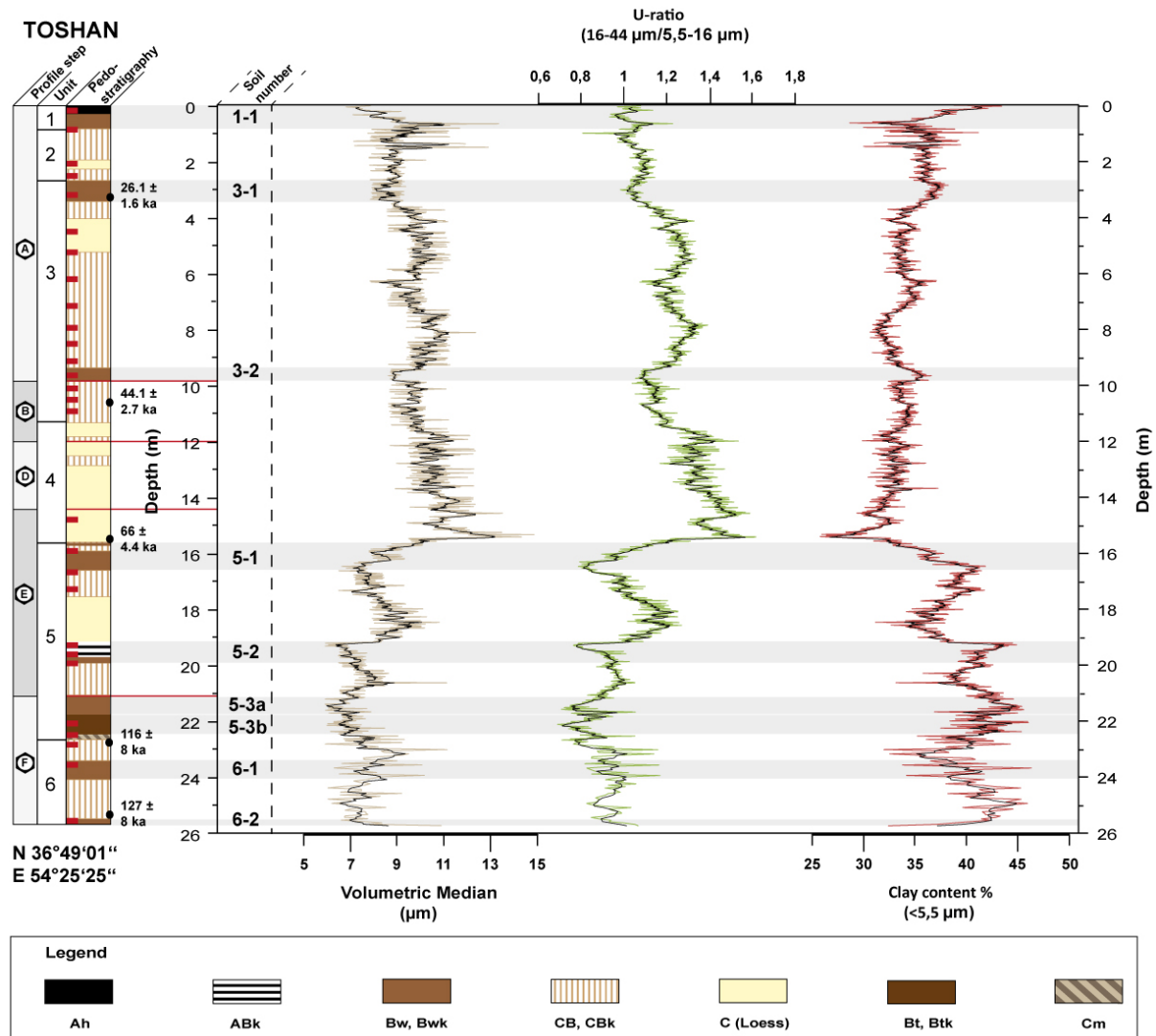


Fig. 2.5: Results of the granulometric analysis. Red lines indicate dates within the profile. The results are supplemented by the distinct subprofiles A, B, D, E and F. The pedostratigraphic units 1 to 6 hereafter do not demand to correspond with certain marine isotope stages, but serve for a comprehensible structure of the following statements. Age control is provided by Lauer et al. (this issue). The quoted results are pIRIR₂₉₀-luminescence ages (fine grain). The grain-size records are superimposed by black curves indicating a moving average over four intervals. Red rectangles to the right of the profile indicate the position of samples extracted for micromorphological analysis. Culminations in clay sized particles (<5.5 µm) minima in U-ratios and median grain-size match the stratigraphic position of palaeosols. Loess layers exhibit an opposite trend.

Units 4 to 2 (15.40-1.47 m below surface)

Unit 4, denominated as loess (15.40-11.35 m) forms a comparatively sharp boundary with the underlying stratum. The loess layer is characterized by a coherent structure and a dull yellowish color. A thin section extracted from 15.65 m (Fig. 2.6 a and b) indicates the

presence of manifold primary calcite grains and mollusk shells, which are dispersed within large parts of the stratum. Additionally, the thin section indicates signs of partial decalcification and subsequent iron oxide mottling. From 12.87-12.57 m and 11.97-11.89 m respectively, two thin CBk-horizons are intersected in the loess, showing a coherent to subangular blocky structure and a slightly browner color. Underneath these horizons the loess appears weakly enriched in CaCO_3 , as evidenced by precipitations of secondary carbonates.

The loess layer gradually merges into a CBk-horizon (11.33-9.85 m) bearing small subangular aggregates within a partially decalcified and coherent matrix. At a depth of 9.83-9.41 m a light brownish and weakly developed Bwk-horizon (3-2) was found forming a subtle lower boundary with the subjacent stratum. Nevertheless the latter Bwk-horizon (3-2) clearly contrasts with the strata situated above and below in terms of structure. Contrary to the strongly developed soil horizons mentioned above (Bt [5-3b] and Bw/ABwk [5-3a] within unit 5) the Bwk (3-2) comprises small subangular aggregates and was subject to weak recalcification. To the top a gradual transition from the Bwk (3-2) into a thick CBk-horizon situated in a depth of 9.39-5.27 m is apparent. The CBk-horizon has a coherent structure with low portions of small subangular aggregates included within the matrix. The entire stratum appears homogeneously yellowish brown and is intermingled by pseudomycelia.

The CBk gradually merges into a layer denominated as loess (5.25-3.89 m), as shown by a coherent structure, a more yellowish color as well as a coarser texture. Furthermore, the loess layer was affected by a weak secondary carbonate metabolism and bioturbation within the upper part of the stratum as indicated by finely dispersed CaCO_3 -concretions and krotovina, respectively. At a depth of 3.87 m the proportion of small subangular aggregates shows a slight increase until 3.49 m. Moreover a dense network of pseudomycelia was detected. The horizon, denominated as CBk is overlain by a weakly developed, light brownish Bwk-horizon (3-1; 3.47-2.73 m). The Bwk (3-1) exhibits a subangular blocky structure while the voids are entirely refilled with precipitations of secondary carbonate. The Bwk-horizon (3-1) hosts bioturbation features in the form of krotovina. To the top the Bwk (3-1) is delimited by an overlying CBk-horizon (2.71-2.31 m) in terms of soil color, structure and texture. This also holds true for a CBk-horizon found between 2.03 and 1.47 m. Both CBk-horizons are separated by a thin loess layer extending from 2.29-2.05 m. The transitions between the above mentioned strata are gradual in nature. The loess compares to the subjacent loess layer (5.25-3.89 m), since it comprises a coherent structure and coarsening of particle size distribution supplemented by dull yellowish colour.

Unit 1 (1.46-0.00 m below surface)

At a depth of 1.45-0.87 m a strongly recalcified CBk-horizon with a coherent to subangular structure was detected. It is overlain by a Bwk-horizon (1-1; 0.85-0.34 m), representing the modern soil. The modern Bwk-horizon (1-1) is strongly developed and comprises angular to subangular blocky aggregates, covered by powdery lime. Both the Bwk and the overlying Ah-horizon (1-1; 0.32-0.00 m) are subject to bioturbation disturbance, as indicated by krotovina and a dense network of root channels dissecting the solum. The thickness of the mollic topsoil horizon serves as diagnostic feature allowing for the distinction between Cambisols

and Kastanozems. If the solum exceeds a total thickness of 75 cm the Ah-horizon requires a vertical extension of ≥ 25 cm (WRB 2007) in order to classify the soil as Kastanozem. Hence, the recent soil is denominated as calcic Kastanozem according to the WRB (2007) soil classification system. Additionally, Khormali and Kehl (2011) and Khormali (2012) report on Bt-horizons found within Luvi-calcic-Chernozems and calcic Luvisols, respectively, situated near Shast-e-Kholar, in the vicinity of the study area at Toshan. These clay illuviation horizons have formed under mean annual precipitation rates of 600-700 mm.

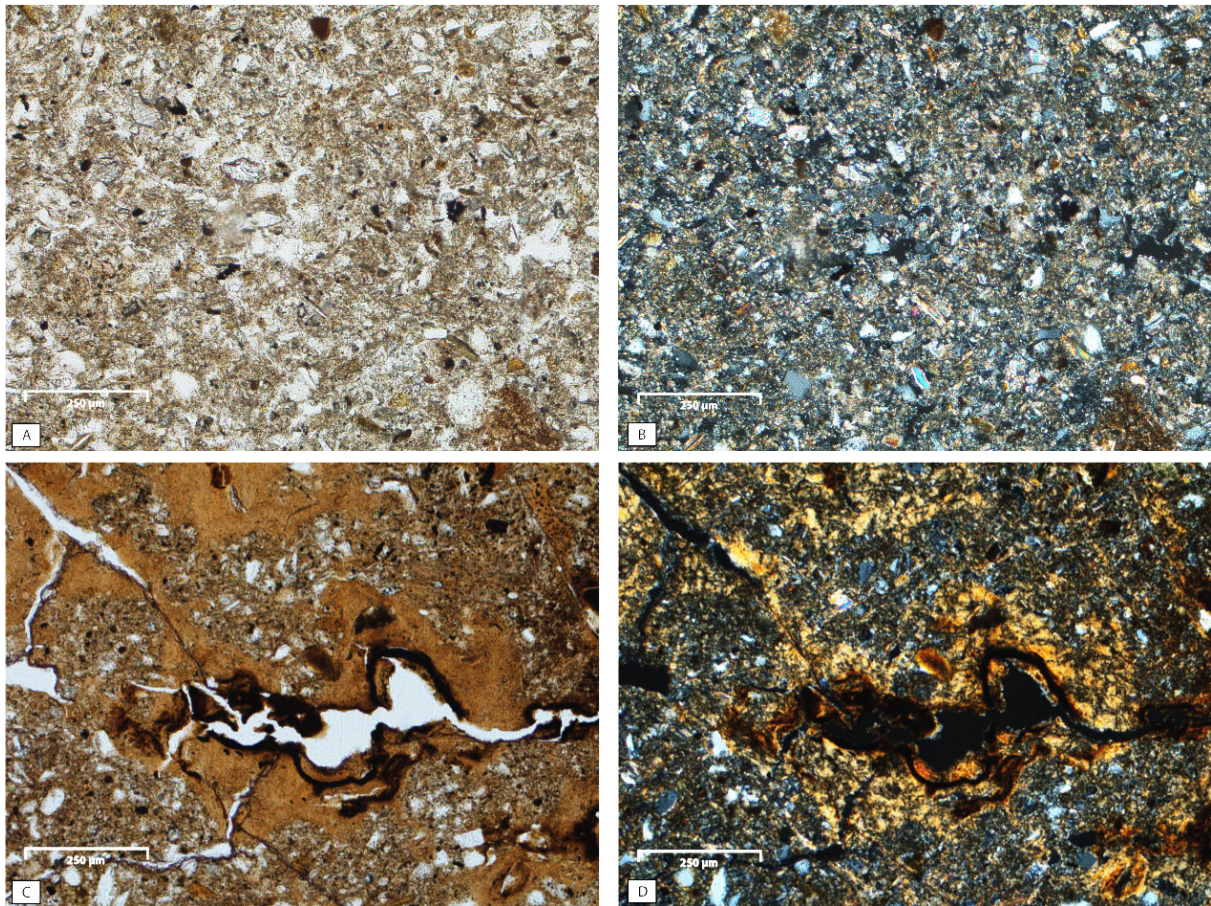


Fig. 2.6 A and B: Loess groundmass under plain and crossed polarized light. The thin section was extracted from 15.65 m. C and D: Clay domains and precipitations of pedogenic iron oxides within Bt-horizon (22.43 m).

2.4.2 Grain-size

Based on the granulometric record (Fig. 2.5), the loess-soil sequence at Toshan may be divided into a lower, finer part and an upper, coarser part. The stratigraphic units 6 and 5 constitute the averagely finer segment, whilst units 4 to 2 comprise sediment and soil horizons exhibiting coarser textural properties.

Palaeosol horizons in terms of ABwk, Bw, Bwk and Bt attributed to units 6 and 5 show clay portions ($< 5.5 \mu\text{m}$) between 38 and 46% (Fig. 2.5). Corresponding medians span the range of 6 to 9 μm and respective U-ratios attain values of 0.7-0.9 (Fig. 2.5). The highest proportion of clay-sized particles ($< 5.5 \mu\text{m}$) was determined for the Bt-horizon (5-3b) between 22.49 and 21.79 m with an amount of 46.5% (Fig. 2.3). The Bw (5-2) and Bwk (5-3a) horizons,

overlying the Bt (5-3b) show a gradual decrease in clay contents towards the top of unit 5, whereas median grain-size and U-ratio show an opposite trend. The loess layer in unit 5 (18.91-17.59 m) exhibits a median particle-size distribution of 11 μm and U-ratios of up to 1.2. These parameters progressively decrease towards the overlying CBk-horizon (Fig. 2.5). In contrast clay content ($< 5.5 \mu\text{m}$) attains values of 30% in the lower part of the loess. CB and CBk-horizons of units 6 and 5 hold an intermediate position between the comparatively fine-grained palaeosol horizons and the loess layer. Corresponding range of median particle-size distribution lay between 6 and 11 μm . Moreover CB and CBK show U-ratios of 0.8-1.0 and clay contents ($< 5.5 \mu\text{m}$) between 33 and 45% (Fig. 2.5).

Last glacial loess layers (Lauer et al. this issue) of units 4 to 2 are considerably coarser than subjacent loess in unit 5. At a depth of 15.50 m the median and U-ratio attain peak values of 15 μm and 1.6, respectively, forming the coarsest part of Toshan section. Consequently, the lowest clay content ($< 5.5 \mu\text{m}$) was determined yielding values of 25.5% (Fig. 2.5). Despite this culmination, textural properties of loess are relatively constant, exhibiting median of 11 μm , U-ratios of 1.2 and clay contents of around 34%. Differences in particle-size between palaeosol-horizons and loess layers in units 4 to 2 are rather subtle in nature. The thick loess layer found in unit 4 represents the least weathered loess within the whole sequence. According to the chronological results of Lauer et al. (2017a) it largely correlates with MIS 4.

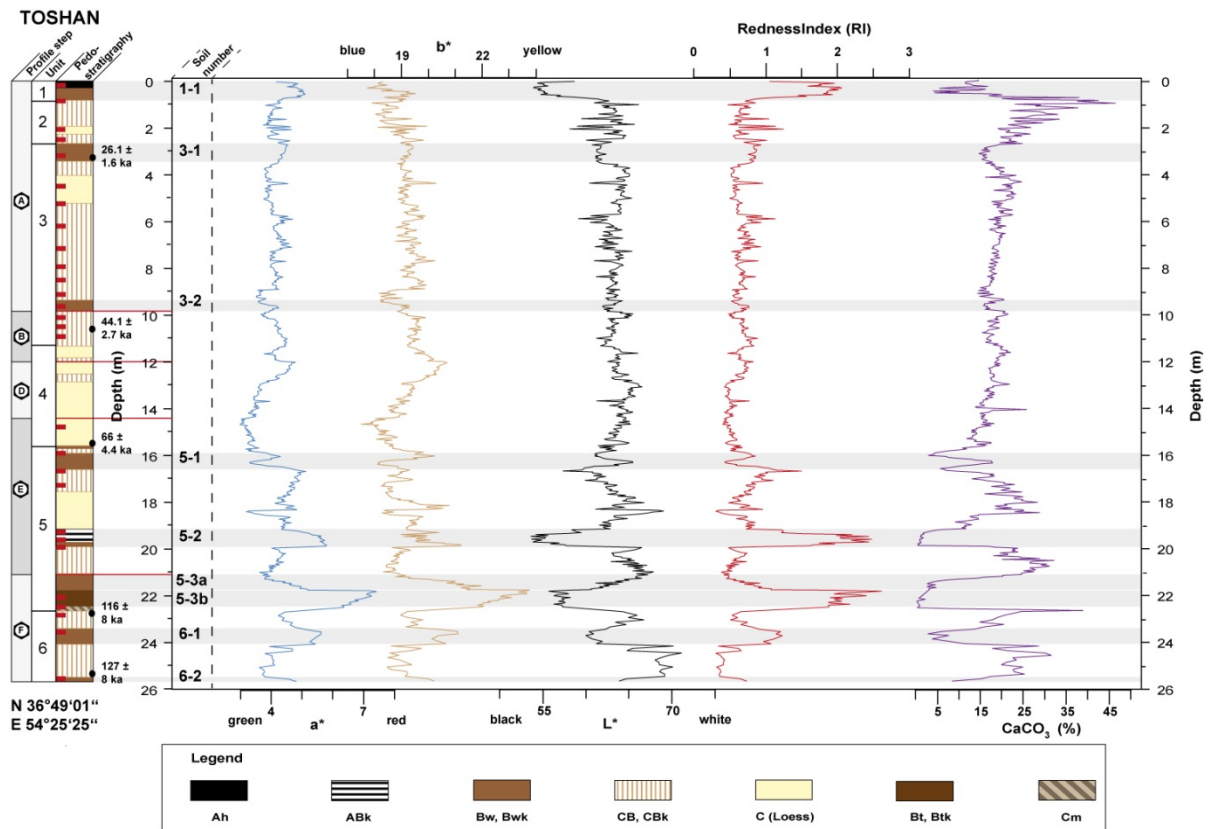


Fig. 2.7: Results of the colorimetric and MIRS analysis indicating a strong correlation with the physical stratigraphy. Palaeosols are depleted in CaCO_3 and enriched in Fe. Maxima in a^* , b^* and RI attributed to fossil soil horizons indicate abundance of particles promoting reddish and yellowish soil color respectively.

In order to define the loess found at Toshan, averaged particle size distribution of loess was determined comprising the entire grain-size data set of the layers denominated as loess. In

addition the histogram reflecting the “average loess” from Toshan is overlain by selected grain-size spectra from single loess layers (Fig. 2.8 a), palaeosol and modern soil horizons (Fig. 2.8 b). The “average loess” has a polymodal grain-size distribution. It hosts considerable maxima within the silt fraction as shown by shoulder peaks within the range of fine silt (5.5-16 μm) and the transition from coarse silt to fine sand. Moreover, a pronounced culmination constituting the medium silt fraction is recognizable, while clay content (< 5.5 μm) gradually increases attaining values of slightly more than 30%. The grain-size spectra from four selected loess strata exhibit negligible differences in clay and fine silt contents as compared to the averaged particle-size distribution. Loess at Toshan therefore represents a relatively homogenous sediment providing equivalent granulometric conditions for soil formation. It is classified as clayey loess owing to its high clay content (< 5.5 μm) at an average of 30%. Fig. 2.8 b shows that palaeosols have lower amounts of coarse particle fractions such as medium silt to fine sand as compared to the averaged loess. Conversely, the palaeosols show a particular increase in fine silt and clay sized particles.

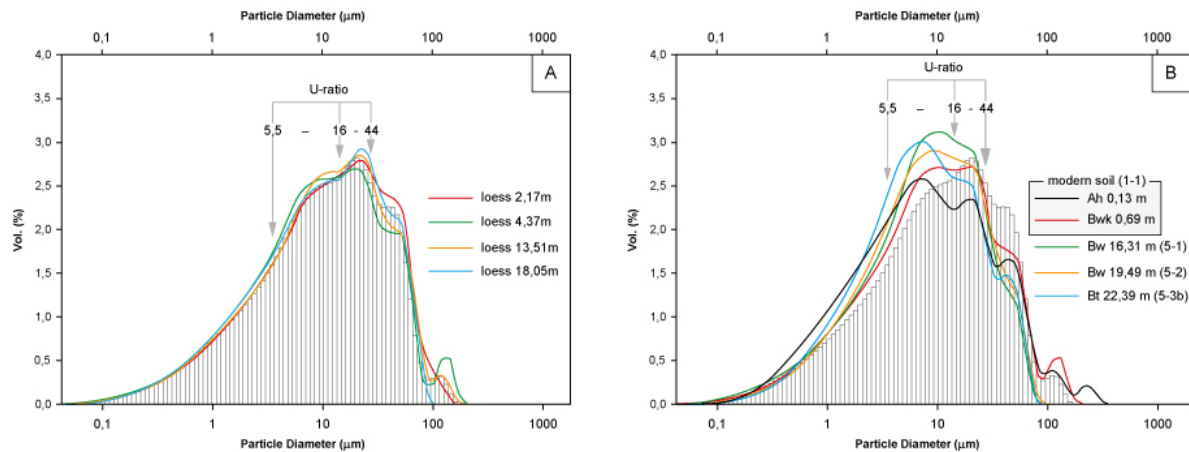


Fig. 2.8: Comparison of textural properties of selected loess layers, palaeosol and modern soil horizons. The histogram was determined by averaging the respective grain-size fractions of the entire strata denominated as loess.

2.4.3 Soil colour

Colorimetric analysis of the section at Toshan reveals clear differences in soil colour between palaeosols, loess and CB and CBk-horizons within units 6, 5 and 1.

This holds particularly true for the Bwk-horizons (6-2 and 6-1) in unit 6 as well as for the Bt (5-3b) and the overlying Bw-ABwk-horizon (5-2) found between 19.73 and 18.93 m (Fig. 2.7). The Bw-horizons reach a^* - and b^* -values of 5.5-6 and 19-20, respectively, as compared to the Bt-horizon exhibiting a^* -values of >7 and b^* -values of > 23. Thus the Bt (5-3b) comprises the largest amount of particles promoting pronouncedly reddish and yellowish soil color values within the loess-soil sequence at Toshan. Hence, these palaeosols are marked by relatively high RI and luminance towards dark brown color (Fig. 2.7). Spectrophotometric data determined for loess layers show lower a^* -values of 3-4.5 and b^* -values of 17.5-20 corresponding with low average RI (Fig. 2.7). In addition the highest luminance of the Toshan section refers to loess deposits, ranging between 60 and 70 (Fig. 2.7).

Determination of soil color yields intermediate colorimetric properties for CB- and CBk-horizons corresponding with a^* of 3.5-4.8, b^* of 18-20.5 and RI between 0.5 and 1. Luminance attains values ranging from L^* 60 to 70 (Fig. 2.7). In general CB- as well as CBk-horizons bracket the palaeosol horizons and thus basically mark the transition in a pedostratigraphic as well as in a colorimetric respect from loess to palaeosols. Hence, CB and CBk gradually merge into palaeosol-horizons and loess strata, respectively. Conversely, the transitions from the Bw-ABwk (5-2) at 19.73-18.93 m and the Bw (5-1) at 16.63-15.63 m are abrupt in nature owing to the lack of CB-horizons (Fig. 2.7). Units 4 to 2 reveal merely weak differences in soil color impeding clear differentiation between palaeosols, CB-horizons and loess layers (Fig. 2.7).

2.4.4 Carbonate content

CaCO_3 - and clay contents serve as proxies for soil formation, since decalcification constitutes a precondition for secondary clay formation.

The palaeosols attributed to unit 5 as well as the modern soil are strongly depleted in CaCO_3 attaining portions of about 2-3%. Thus the Bt-horizon (5-3b) and the Bw-ABwk (5-2) considerably contrast with loess deposits in Toshan section, which have contents of mainly primary CaCO_3 ranging between 15 and 20% (Fig. 2.5). CBk-horizons exhibit carbonate contents similar to those of loess layers, though possibly being the result of a pronounced secondary carbonate metabolism. The Bwk-horizon (3-1) separating unit 3 from unit 2 is moderately depleted in CaCO_3 exhibiting portions of 10% as opposed to the Bwk (3-2) situated in 9.83-9.41 m. The latter one shows a CaCO_3 content of ca. 15% (Fig. 2.7).

2.5 Discussion

2.5.1 Granulometric properties of loess and its implications for changes in wind velocity and dust source area

The granulometric composition of loess basically depends on wind intensity and distance from the main sediment source/sources (Novothy et al., 2011). In addition, the grain-size distribution of exposed sediments in the dust source area will determine the grain size of dust accumulations. The U-ratio ($16-44 \mu\text{m}/5.5-16 \mu\text{m}$) takes into account the ratio of medium silt to fine silt (Vandenberghe et al., 1985). It disregards pedogenic neoformation of siliceous clay and translocation of sand mainly by saltation (Vandenberghe et al., 1997). However, the application of this ratio as a proxy for relative wind speed is afflicted with restrictions. This restriction holds particularly true for major phases of pedogenesis during interglacials or interstadials. This implies associated soils to be basically syngenetic in nature. Moreover it is questionable whether thick accretionary soils are able to develop under conditions of reduced dust supply as postulated by Tsoar and Pye (1987) for deposition of aeolian sediments during the Holocene in central Asia. It appears likely that soils at Toshan have formed from dust being deposited during glacials and stadials, respectively. Hence, the U-ratio does not primarily reflect reduced wind speeds during phases of soil formation, but rather textural alterations of the parent material, causing depletion in medium silt and

enrichment in fine silt and thus changes the ratio between these grain-size fractions as shown in Fig. 2.8 b. Therefore soil genesis is believed to be mainly the result of descendant decalcification of loess promoting neoformation of fine silt, clay-sized particles and pedogenic oxides and hydroxides. Nevertheless a (minor) syngenetic contribution to the genesis of these soils cannot be excluded. Hence, within this study the application of the U-ratio is used for the determination of morphodynamic stability and extension or retreat of proximal dust source regions in relation to the Toshan section. In general the accumulation of coarser particles is imputed to cold phases such as glacials and stadials when winds were stronger and potential dust source areas extended owing to reduced landsurface stability (Tsoar and Pye, 1987). In contrast warm phases did not provide favorable conditions for strong winds. Tsoar and Pye (1987) state that silt production was reduced during the Holocene, while climate provided suitable habitat conditions for trees and plants effecting increased morphodynamic stability and thus a retreat of dust source areas. Consequently, higher U-ratios indicate glacial or stadial climate and lower U-ratios correspond with interglacial or interstadial climatic conditions.

The polymodal grain-size distribution within the loess in Toshan involves a variety of different particle fractions as described in section 4.2. Assuming that medium to coarse silt and clay to fine silt have undergone aeolian fractionation, the deposition of dust forming loess at Toshan is possibly the result of the interaction between several sediment sources. These imply to different degrees both distal and proximal sediment supply. The averaged modal grain-size of loess at Toshan is 10 μm . According to Kehl (2010) median grain-size of loess determined by sieve and pipette method is 9 μm at Neka, 11 μm at Now Deh and 29 μm at Agh Band (for locations see Fig. 2.1). This suggests a predominantly distal dust supply for the sections at Neka, Toshan and Now Deh i.e., a reference for a gentle gradient in granulometric median from west to east. The particle-size distribution at Agh Band is possibly governed by proximal sediment transport to a larger extent. Hence, our results are in good agreement with the findings of Lateef (1988), Kehl et al. (2005) and Kehl (2010) postulating increasing grain-size from west to east and from south to north, respectively.

Recurrent phases of coarsening and refining are indicated by the U-ratio. These imply repeated extensions of proximal dust source areas possibly corresponding with changes in density of vegetation cover allowing for predominantly medium silt airborne sediments to be mobilized. However, the grain-size signal may be biased by the physico-chemical behavior of colloids such as clay-sized particles which is mainly governed by its surface charge prevailing over the bare particle mass. Consequently, the electrostatic properties of clay may provoke the development of micro-aggregates and their accretion to silt-sized grains forming larger pseudo-particles. Secondary carbonates not being removed during the sample pretreatment might have a similar effect.

Lateef (1988) and Frechen et al. (2009) assume that loess-thickness in the Caspian Lowland is closely related to the vicinity of the Rivers Gorgan and Atrek. Yet, the source areas of loess at Toshan remain unknown. Further research is needed in order to localize the spatial origin of dust forming loess in Toshan.

2.5.2 Palaeosols at Toshan: Implications for morphodynamic processes and differential soil formation

Spectrophotometric determination of soil color is suited for analytical differentiation from gradual or abrupt transitions between different strata. Hence, it supplements field description merely based on visual perception and provides a more objective framework especially helpful for detecting subtle changes in soil color. In this context the nature of upper and lower boundaries of palaeosols within the sequence investigated are of particular interest. In general these constitute either an abrupt change or a smooth transition from palaeosols to overlying strata. The question whether these boundaries are abrupt or gradual can be elucidated by means of our high-resolution color record.

Abrupt changes are found between the Bt-horizon (5-3b) and the overlying Bw (5-3a) at 21.79 m as indicated by sharp alterations of a^* , b^* and L^* -values (Fig. 2.7). This Bt (5-3b) represents the most strongly developed palaeosol within the sequence at Toshan. It has clay amounts of up to 46.5% ($< 5.5 \mu\text{m}$), whereas the other Kastanozem-like Bw-ABwk (5-2) exhibit clay contents in the range of 40-45% (Fig. 2.5). As the Bwk (5-3a) overlying the Bt (5-3b) has comparable amounts in clay, it is unlikely that it constitutes a former elluvial horizon (E) associated with leaching and translocation of peptized clay into the Bt (5-3b). The Bw (5-3a) is considered to be the remnant of an independent soil, genetically not related to the Bt-horizon (5-3b). Therefore, the abrupt change in soil color between both palaeosols suggests several cycles of dust accumulation and soil formation, comprising both the accumulation of airborne dust, pedogenesis, and erosion of the topsoil, dust accumulation and again soil formation. From a pedostratigraphical point of view the sequence of formation is in good agreement with the findings of Kehl (2010) for the tentatively last interglacial soil (MIS 5e) at the Now Deh section comprising a Bt superimposed by a moderately developed Bw. This holds true also for the Bw-ABwk-horizon (5-2; 19.73-18.93 m) unconformably covered by a loess layer (Fig. 2.5). The abrupt transition from the Bw-ABwk (5-2) into the overlying loess points to the truncation of the Ah-horizon during a phase of geomorphodynamic activity. Subsequently, the upper part of the preserved subsoil was buried and recalcified by carbonates originating from overlying loess deposits.

Considering a^* , b^* and RI of the palaeosols within unit 5, a gradual decrease in proportions of pigments promoting reddish soil color and yellowish soil color is apparent (Fig. 2.7). In a pedogenic context, the a^* - and b^* -values of the CIE-lab color space model correspond with the relative abundance of pedogenic iron oxides affecting colorimetric soil properties (Yang and Ding, 2003). It is unlikely, that formation of these moderately to strongly developed palaeosols was affected by constant deposition of calcite-rich aeolian sediments since the input of CaCO_3 might have counteracted decalcification and thereby inhibited soil formation, as depicted in Fig. 2.7. This implies an interruption or a weakening of calcareous dust sedimentation during phases of major soil formation (Mestdagh et al., 1999).

Soil color suggests that the uppermost Bwk-horizons (5-1; 16.63-15.95 m and 15.61-15.41 m) situated in unit 5 constitute a twin peak-pattern in a^* , b^* , L^* and RI-values (Fig. 2.7). These horizons possibly reflect a longer and a shorter phase of pedogenesis interrupted by dust accumulation. The duration and/or intensity of soil formation are likely indicated by the different thicknesses of the palaeosols. Nevertheless micromorphological analysis of the upper part of the thicker Bwk (5-1; 15.80 m) reveals a soil structure, which is partly spongy in

nature and typical of Ah-horizons (Bronger et al., 1994). However, its macroscopic appearance does not exhibit clear differences in color caused by the pigmentation effect of organic matter. The organic compounds were possibly decomposed during mineralization, merely preserving the structure of a potential Ah-horizon. The chronology of Lauer et al. (this issue) yields an age of 66 ± 4.4 ka representing a *terminus ante quem* for the formation of the two Bwk-horizons (5-1; Fig. 2.5). Recently, Rasmussen et al. (2014) published a new chronological framework for the last glacial period based on a synchronization of NGRIP, GRIP and GISP2 ice-core records. Provided that the fluctuations of soil formation and the deposition of airborne dust recorded in the Toshan section reflect a global climate signal, both palaeosols (5-1) have formed during Greenland Interstadials (GI) 19.1 and 19.2, respectively.

In contrast gradual transitions were detected in unit 3, consisting of thick CBk-horizons intersected by two weakly developed Bwk-horizons (3-2 and 3-1) and thin loess deposits. This unit most likely correlates with MIS 3 (Lauer et al., 2017a). Additionally, the color of these palaeosols is characterized by distinct culminations both of RI, a^* and b^* values. Soil color is therefore affected by reddish and yellowish pigments. CaCO_3 is depleted in the Bwk (3-2 and 3-1) relative to loess and the CBk horizons, albeit the palaeosols have been subjected to postpedogenic recalcification originating from overlying deposits. We assume that the CBk is the result of syngenetically altered aeolian accumulations forming a thick accretionary horizon. Environmental conditions likely were characterized by deposition of airborne dust holding pace with the former moisture regime and allowing for partial decalcification and incipient soil formation. The gradual transitions from CBk-horizons into loess and *vice versa* in terms of grain-size and color records imply an interruption of this sedimentary equilibrium. Assuming constant or enhanced average dust supply in relation to decreases in moisture availability may lead to accumulation of relatively unaltered sediments denominated as loess. Subsequently, constant or increased average moisture compared to reduced accumulation of aeolian sediments may provoke the opposite effect favoring initial soil formation as observed within CBk-horizons or enhanced soil formation resulting in weakly developed Bwk-horizons (3-2 and 3-1). Hence, boundaries between syngenetically altered substrate are gradual in nature. Our findings compare to the genesis of the Brady Soil from the Great Plains (Mason et al. 2008). This soil is believed to have formed in response to a gradual change from drier and dusty environmental conditions towards a period of reduced dust accumulation and enhanced edaphic moisture.

In general, luminance is expected to decrease with the presence of soil organic matter. However, the mineralization of soil organic compounds or the truncation of the topsoils associated with the palaeosols counteracts clear colorimetric signals. Additionally, the pronounced precipitation of (whitish) secondary carbonates tends to superimpose pedogenic pigmentation effects affected by respective iron oxides and hydroxides and impedes the detection of fossil soil horizons.

The Redness-Index suggests highest relative amounts in iron oxides, or presence of hematite within the Bt (5-3b), a slight decrease towards the following Bw-ABwk (5-2), and an enhanced decline in the uppermost Bw-horizons (5-1) of the unit. Considering the absolute a^* and b^* values of the intermediate Bw-ABwk (5-2), its high RI is rather the arithmetic consequence of increased reddish (up to 6) in relation to yellowish (up to 21) soil color values. Compared to the Bw-ABwk (5-2) the Bt-horizon (5-3b) shows a^* -values of 7.6 and b^* -

values of 23.8, corresponding with more reddish soil color due to enhanced pigmentation by hematite. Theoretically, the mere leaching of CaCO_3 without any neoformation of pedogenic iron oxides would result in low L^* -values due to the loss of whitish pigments and low a^* - and b^* -values in response to the absence of pedogenic iron oxides. As part of the denominator within the RI-function (Barron and Torrent, 1986), low L^* -values in relation to a^* - and b^* -values could result in an arithmetic increase of RI-values.

Cornell and Schwertmann (2003) state that hematite ($\alpha\text{-Fe}_2\text{O}_3$) may e.g. form by dehydration of amorphous pedogenic iron hydroxides such as ferrihydrite ($\text{Fe}_5\text{HO}_8 \cdot 4\text{H}_2\text{O}$) and conversion of iron oxides e.g. goethite ($\alpha\text{-FeOOH}$). This transformation requires pronounced seasonal variations in temperature and soil moisture availability (Cornell and Schwertmann 2003). Torrent and Cabedo (1986) postulate that the formation of ferrihydrite may be favored by wet and cold winters, while the transformation of ferrihydrite to hematite takes place during warm and dry summers. Thus enhanced formation of hematite within the Bt (5-3b) suggests relatively high average temperatures during the time of formation as compared to the overlying Bw-horizons (5-2 and 5-1). Additionally annual precipitation must have been sufficient in order to allow for the removal of primary calcite, the neoformation of clay and the development of clay coatings as observed in the field. It is therefore likely that the Bt (5-3b) formed under comparatively subhumid climatic conditions with a pronounced seasonality in terms of moist winters and dry summers. This is confirmed by first micromorphological investigations (Fig. 2.4 c and d), pointing to high shrink and swell dynamics of the Bt (5-3b) during moist and dry seasons, respectively. Consequently clay coatings were partly disrupted and incorporated into the soil matrix. As a result the soil was initially compacted, inhibiting water to percolate through the solum. This compaction created redoximorphic conditions allowing for the reduction and reprecipitation of iron oxides within secondary pores (Fig. 2.4 c and d).

From a chrono-sequential point of view this polygenetic Luvisol-like palaeosol is more mature than the other Kastanozem-like palaeosols within that unit. As stated in section 4.1.4 it is known, that recent soils in the region at Toshan have undergone clay illuviation as well. Thus it appears likely that the Bt (5-3b) formed under environmental conditions comparable with the present climate. We tentatively correlate this Bt (5-3b) with MIS 5e by means of pedostratigraphy. However, based on the OSL-dating study carried out by Lauer et al. (2014), the basal part of the Bt-horizon (5-3b) at Toshan yields an age of 116 ± 8 ka. This age represents a *terminus post quem* for the onset of the formation of this palaeosol. Compared to our pedostratigraphical estimations and the stratigraphic framework of Rasmussen et al. (2014), the luminescence dating-results suggest either an age underestimation or a later phase of soil-development than MIS 5e.

2.5.3 Stratigraphic comparison with other palaeoclimatic archives

The loess-soil sequence at Toshan reveals both recurrent fluctuations of cold and comparatively arid glacial and stadial climate coinciding with dust accumulation or incipient soil formation as well as possibly warmer and moister environmental conditions during interglacials and interstadials corresponding with major phases of soil formation. The

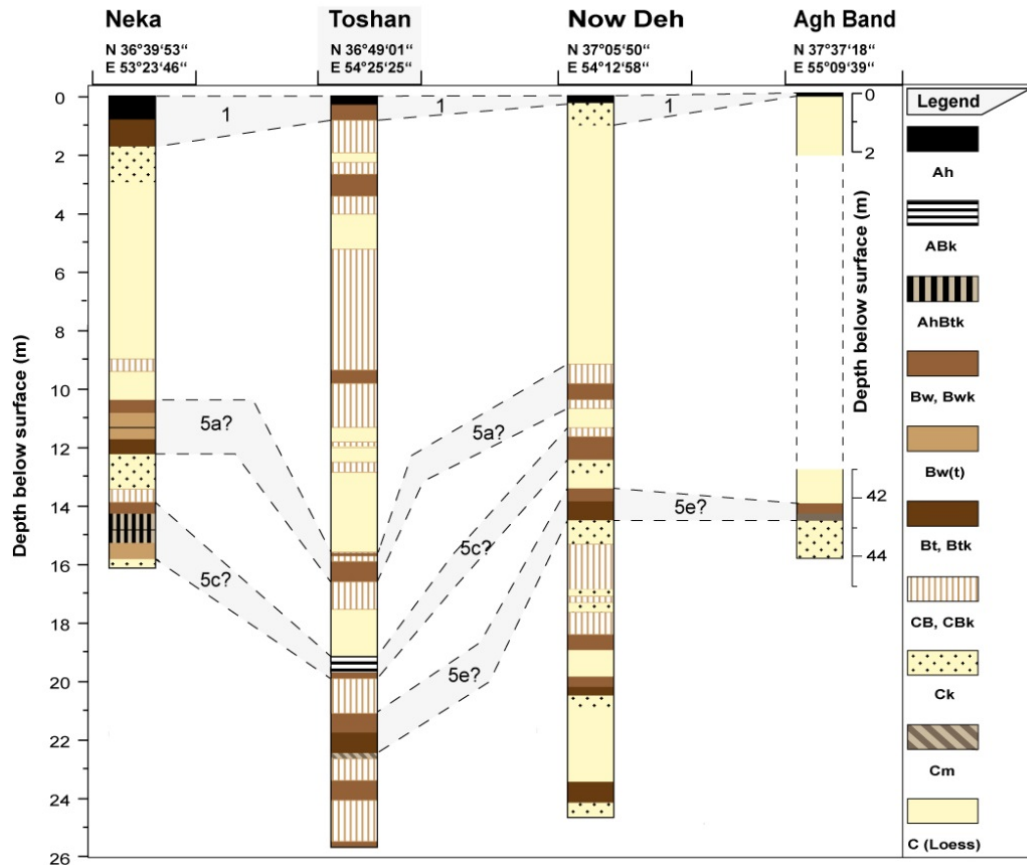


Fig. 2.9: Preliminary pedostratigraphic correlation of loess-soil sequences in NE Iran (Kehl et al., 2005; Frechen et al., 2009).

textural properties of loess at Toshan compare to the fine loess facies of the north-eastern Iranian sections at Neka and Now Deh (Kehl et al., 2005). This implies comparable source to sink distances of airborne dust and equivalent wind velocities. However, loess at Agh Band encompassing a spectrum of considerably coarser particle-sizes points to relative proximity to the dust source region and higher wind energy. Hence, north to north-easterly winds are suggested.

We assume that the formation of the Bt-horizon (5-3b) within the Toshan section is in temporal coincidence with the Btk-horizon in Now Deh and a Bw(t) in Agh Band (Fig. 2.9) representing the most strongly developed palaeosols of the respective sections (Kehl et al., 2005; Kehl, 2010). The pedostratigraphical correlation with the AhBtk studied at Neka is less clear, because new field evidence suggest that below this palaeosol a similar palaeosol follows, which shows similar degree of soil development (Fig. 2.9). The differential degrees of soil formation suggest an increased humidity from east to west and from north to south during the present and the last interglacial. Possibly, the climatic gradient as recently observed in north-eastern Iran existed in the late Pleistocene as well. Based on the tentatively last interglacial palaeosols an upward decrease in intensity of pedogenesis with time is apparent for each of the loess-soil sections mentioned, indicating decreasing magnitude of chemical weathering. These intervals are replaced by a subsequent phase of loess accumulation (Fig. 2.9). Thus loess and palaeosols at Toshan reveal a recurrent pattern, which matches the stratigraphic record of Neka, Now Deh and Agh Band sections (Kehl et al., 2005; Kehl, 2010).

Determination of grain-size distribution in loess and palaeosols at Remisowka sequence in Kazakhstan yields a correlation of relatively high U-ratios with glacials and stadials, and low values imputed to intervals of pedogenesis (Machalett et al., 2008), which coincide in their relative intensities with our results (Fig 2.10). This holds true also for the findings of Mestdagh et al. (1999) from Tagidjar, Tadjikistan (Fig. 2.10). Determination of magnetic susceptibility of loess derived palaeosols at Tagidjar in central Asia indicates that weathering decreased in magnitude from MIS 5e to substage 5a (Mestdagh et al., 1999).

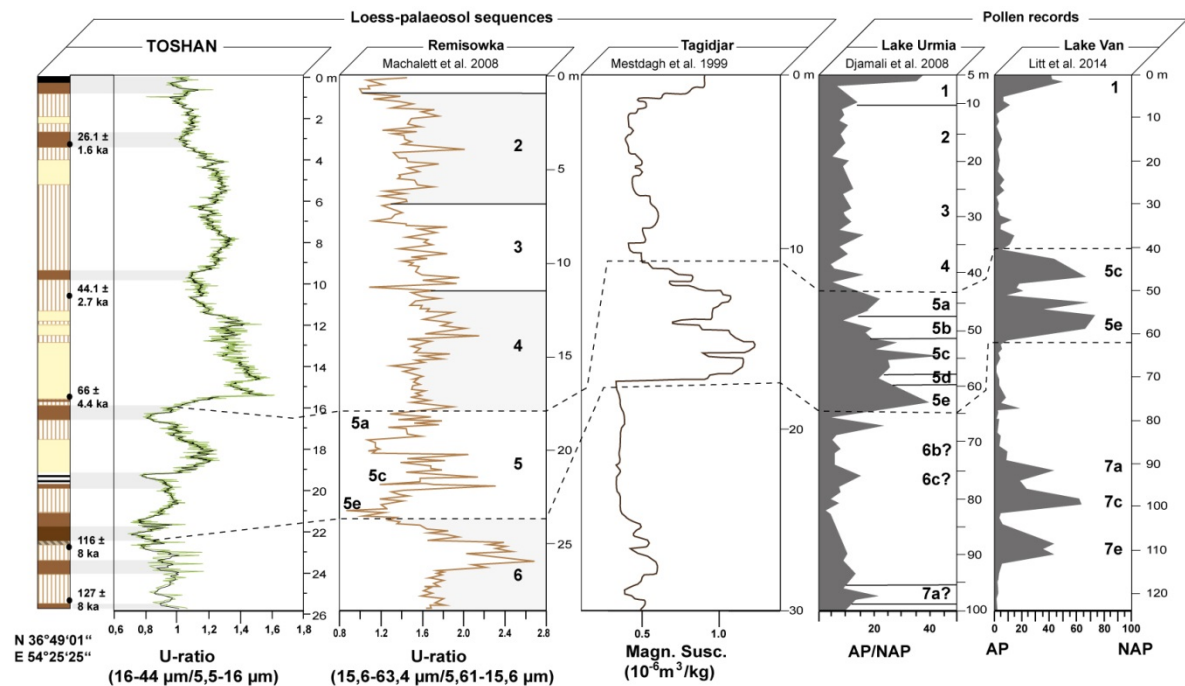


Fig. 2.10: Preliminary supraregional correlation of the section at Toshan with the loess-palaeosol sequences at Remisowka (Machalett et al. 2008), Tagidjar (Mestdagh et al. 1999), as well as the pollen records from Lake Urmia (Djamali et al. 2008) and Lake Van (Litt et al. 2014). This correlation is based on stratigraphical estimates.

Based on palynological investigations, Djamali et al. (2008) and Litt et al. (2014) yield three distinct peaks in the ratio of arboreal (AP) to non-arboreal pollen (NAP) for the MIS 5 (Fig. 2.10). Highest ratios were determined for the last interglacial substage 5e in Lake Urmia (NW Iran) and Lake Van (Anatolia, Turkey), whereas the amount of AP decreases towards the substages 5c and 5a respectively (Fig. 2.10). Conversely the stadials 5d and 5b are characterized by a pronounced increase in NAP indicating cold and arid environmental conditions. Our results revealed a similar pattern of repeated changes for the eastern Caspian Lowland, yielding an age range of 66 ± 4.4 ka to 116 ± 8 ka (Fig. 2.10).

The comparison of the Toshan section with loess-soil sequences from central Asia and the Caspian Lowland as well as pollen records from Lake Urmia exhibit similar fluctuations of climate changes on a supraregional scale. A chronostratigraphic correlation of loess and palaeosols at Toshan with the aforementioned archives requires resilient age control by means of luminescence dating study. Nevertheless, the high-resolution record provided new insight into the timing and the dynamics of late Quaternary climate change in NE-Iran.

2.6 Conclusions

During the late Pleistocene changes from dry and cold to moister and warmer climatic conditions modulated the development of loess deposits and intercalated palaeosols in Northern Iran. The loess-soil sequence at Toshan gives evidence for at least nine major intervals of pedogenesis most likely during the last interglacial to glacial cycle interrupted by accumulation of dust and syngenetically altered sediments testifying to incipient soil formation. Pedogenesis most likely occurred during interglacials and interstadials, while the accumulation of dust and the formation of syngenetic soils tentatively correspond with stadials. The most typical loess within the Toshan section is found in unit 4 and was possibly formed during MIS 4.

The boundaries from palaeosols to the overlying strata constitute either an abrupt change or a gradual transition, recognizable by means of our color data and granulometric parameters. The palaeosols of units 5 and 6 exhibit abrupt transitions, suggesting a phase of morphodynamic activity causing truncation of the topsoil at the end of the interstadial during which the respective palaeosol is believed to have formed. In contrast, the upper boundaries of the palaeosols of unit 3 and 2 are gradual in nature, implying a step by step fluctuation between the dominance of soil formation and dust accumulation in relation to changes in moisture regime. Thus, associated palaeosols are seemingly the result of syngenetic soil formation. These gradual changes likely occurred during MIS 3.

The loess-soil sequence at Toshan represents an excellent terrestrial geoarchive allowing for the identification of climatic and environmental change during the late Quaternary in Northern Iran in high resolution.

2.7 Acknowledgements

The authors are grateful to the Gorgan University of Agricultural Science and Natural Resources for generous logistic support. We thank Sonja Riemenschneider for the performance of grain-size analysis. This is part of an ongoing study funded by the German Research Foundation (Deutsche Forschungsgemeinschaft, DFG-Gz.)

Chapter 3

The Agh Band loess-palaeosol sequence –

A terrestrial archive for climatic shifts during the last and penultimate glacial-interglacial cycles in a semiarid region in northern Iran

Lauer, T.^{a,d}, Vlamincik, S.^b, Frechen, M.^a, Rolf, C.^a, Kehl, M.^b, Sharifi, J.^c, Lehndorff, E.^e, Khormali, F.^c

^a Leibniz Institute for Applied Geophysics (LIAG), Stilleweg 2, 30655, Hannover, Germany

^b Institute of Geography, University of Cologne, Albertus Magnus Platz, 50923, Cologne, Germany

^c Department of Soil Sciences, Faculty of Water and Soil Engineering, Gorgan University of Agricultural Sciences and Natural Resources Gorgan, 49138-15739, Iran

^d Department of Human Evolution, Max Planck Institute for Evolutionary Anthropology, Deutscher Platz 6, D-04103, Leipzig, Germany

^e Institute of Crop Science and Resource Conservation, Soil Science and Soil Ecology, University of Bonn, Nussallee 13, D-53115, Bonn, Germany

Quaternary International (2016, in press)

doi:10.1016/j.quaint.2016.01.062

-Formatting and orthography of the publication are adapted to the dissertation style-

Abstract

The northern Iranian loess profiles host important information on Quaternary climate and palaeoenvironmental changes in the region. They build an important link within the Eurasian loess belt to correlate European and Central Asian archives. Due to a climatic gradient with decreasing precipitation from the west to the east and from the south to the north, loess-palaeosol sequences formed synchronously under different climatic conditions can be studied over short distance in the Iranian Caspian Lowland. The Agh Band profile is located in the so called Iranian “Loess Plateau”, a semi-arid region with 200-350 mm annual precipitation. The loess deposits at Agh Band reach a thickness of > 60 meters. An about 50 m thick step-profile was prepared and the litho/pedostratigraphy was investigated. Samples for laser-diffractometry grain-size measurements were taken every 2 cm. The magnetic susceptibility was measured in 4 cm intervals and the CaCO₃-content in 8 cm intervals. To establish a chronological framework a pIRIR₂₉₀ luminescence dating approach was applied to the 4-11 µm polymineral fraction.

The results show that the Agh Band profile yields a climate archive reaching from MIS 7 to MIS 2. Several chronological hiatuses of some 10 ka show that periods of intense loess accumulation were interrupted by phases of only minor loess sedimentation and/or erosion. The Agh Band profile is subdivided by several shifts in grain-size distribution. The coarsening- and fining up trends correlate with increasing and decreasing wind- velocity, respectively. In the central part of the Agh Band loess sequence a weakly developed palaeosol is preserved which was developed at around 80 ka. Furthermore, the loess deposits formed from about 100 ka to 60 ka ago show banded structures. A pedocomplex including two well-developed palaeosols consisting of Bw(y) horizons and a CB-horizon as well as intercalated loess can be found in the lower part of the sequence also evidenced by the increased values of magnetic susceptibility. The corresponding luminescence age estimates indicate that the palaeosols represent a period of increased humidity and landscape stability during late MIS 7 and MIS 6. Hence, in the Agh Band loess, various changes in the palaeo-sedimentary system, triggered by changes in climate can be observed. This yields important information on the sensitive response of sedimentary systems and landscapes within semi-arid regions to shifts in moisture and possibly temperature.

Keywords: Northern Iran; Agh Band; loess; grain-size; luminescence dating; palaeosols

3.1 Introduction

Loess-deposits react sensitively to changes in climate. Thus loess-palaeosol sequences often yield detailed archives for Quaternary palaeoenvironmental reconstruction (e.g. Pecsí, 1990; Frechen et al., 1997; Boenigk and Frechen, 2001; Marković et al., 2008; Wacha et al., 2011). Accordingly, the northern Iranian loess palaeosol-sequences are valuable archives to study palaeoenvironmental changes in the region. Furthermore, they build a link to better correlate European and Central Asian loess-palaeosol sequences. Hence, these archives

deliver important information to obtain a more comprehensive understanding of the response of sedimentary and ecological systems to changes in climate in different parts of the Eurasian Loess Belt.

Loess in Northern Iran was deposited along the northern foothills of the Alborz Mountains where up to 30 m thick loess deposits can be found. Even thicker loess-sediments are preserved in the so called Northern Iranian loess-plateau with > 60 m thick loess deposits. Northern Iranian loess profiles have already been studied in detail by Kehl et al. (2005), Frechen et al. (2009), Kehl (2010), Karimi et al. (2009; 2013) or recently by Vlamincx et al. (2016) or Lauer et al. (2017a). Fig. 3.1 gives an overview on the distribution of major loess deposits in Northern Iran and shows the location of sections investigated by the authors mentioned above. These mentioned loess-sections were focusing on mainly loess-palaeosol sequences mainly correlating to the last glacial-interglacial cycle.



Fig. 3.1: Study area; map showing the distribution of loess in northern Iran and the locations of loess sections studied before on the foothills of the Alborz Mountains and in the so-called loess-plateau of Northern Iran. The new section at Agh Band presented here, is located at less than 100 m distance from locations studied by Kehl et al. (2005) and Frechen et al. (2009).

A new study on last glacial Iranian loess deposits from the Northern Iranian loess plateau dealing with grain-size fluctuations, aeolian transport mechanisms and potential source areas of the dust is published by Wang et al. (2016a). In a recent paper, Wang et al. (2016) investigated early Pleistocene loess in the northeastern Iranian Golestan Province (Northern Iranian loess plateau) and demonstrated the deposition and preservation of loess being ~2.4–1.8 Ma old.

It was demonstrated that several climatic shifts from more humid and warmer climate conditions including soil formation and only minor dust accumulation to more arid and cooler climate-phases with increased dust accumulation are documented in the archives. The recently published studies by Vlamincx et al. (2016) and Lauer et al. (2015) on the Toshan loess section near to Gorgan City (Fig. 3.1) have illustrated that especially for the last glacial-interglacial cycle, several climatic shifts are recorded and also several interstadials could be documented beyond the last interglacial (MIS 5e). Palaeosols of different development degrees ranging from strongly developed ones indicated by Bt to weakly developed



Fig. 3.2: Picture of the northern Iranian loess “plateau” with > 60 thick m loess deposits (left), characterized by steep hillslopes. Head cut of one of the frequent gullies (right). Sheep trails mark the present day land surface and the intensive usage of the loess-hills accelerates erosion. The recent landscape has no plateau-character and it is debated when the incision of the valleys started and if land surfaces of the past had been plateau-like.

represent by CB(k) horizons correlate with several periods of higher morphodynamic stability and corresponding soil formation. More arid climate led to increased dust accumulation.

Especially from about 60 ka on, increased loess sedimentation rates were documented for the Toshan loess section.

The modern gradient in precipitation in Northern Iran with decreasing precipitation from the west to the east and also from the south to the north (e.g. Khormali et al., 2012; Khormali and Kehl, 2011) allows studying loess and palaeosols which were probably formed isochronously under different palaeoclimatic conditions. Whereas e.g. in Neka, the annual precipitation is at around 750 mm, the precipitation in the semi-arid loess plateau is at only 200-350 mm/ year. Especially in the semi-arid loess plateau, past changes in moisture most likely led to sensible changes in the palaeoenvironmental system. A decrease in precipitation might have caused a reduction of the vegetation cover and led to increased morphodynamic activity. Hence, the loess-palaeosol sequences in the Northern Iranian loess plateau are especially valuable archives to study the response of the sedimentological and palaeoecological system to aridification.

The aim of this study was to establish a litho- and pedostratigraphy for the Agh Band loess sequence located in the Northern Iranian loess plateau. A chronological framework for periods of loess deposition, soil formation and probably erosion was established by luminescence dating applied to polymineral fine-grains. Furthermore, highly resolved grain-size analyses intend to obtain detailed information on changes in the palaeo-sedimentary system and the palaeo-wind activity. In addition, magnetic susceptibility was used to obtain information on soil-formation in the study area.

It was also intended to correlate the Agh Band loess palaeosol sequence with other sediment-archives in the region and to discuss especially the dating-results with previous findings obtained by Frechen et al. (2009) or Kehl et al. (2005), also from the Agh Band area and with the luminescence dating results obtained by Lauer et al. (2017a) for the Toshan loess section (Fig. 3.1). These information can further complete the knowledge on palaeoenvironmental changes in Northern Iran and will contribute to better correlate the Northern Iranian loess sequences with archives in Eastern Europe and Central Asia.

3.2 Geographical setting

The Agh Band profile (Fig. 3.1) is located at N 37°37′06 °N and E 055°09′27. The top part of the sequence is at 183 m a.s.l. Hence, it is located > 200 m above the recent sea level of the Caspian Sea (- 26 m). The geological basement is formed by conglomerates of the Pliocene

Akchagyl formation. This formation consists of limestones, marl and mudstones with thicknesses reaching from 3 meter up to more than 100 meter in the Kopeh Dagh sedimentary basin. These Tertiary deposits are covered by reddish-brown sediments of the so-called red-series (Wang et al., 2015) which show a strong overprint by soil formation. Gypsum infillings between large soil prisms and in post-depositional fissures reflect diagenetic alteration. The exact age of the red series is unclear but an Upper Pliocene to Lower Quaternary age is assumed. The red series is characterized by an erosional upper boundary. The overlying loess (Fig. 3.2) is up to > 60 m thick and subdivided by several palaeosols.

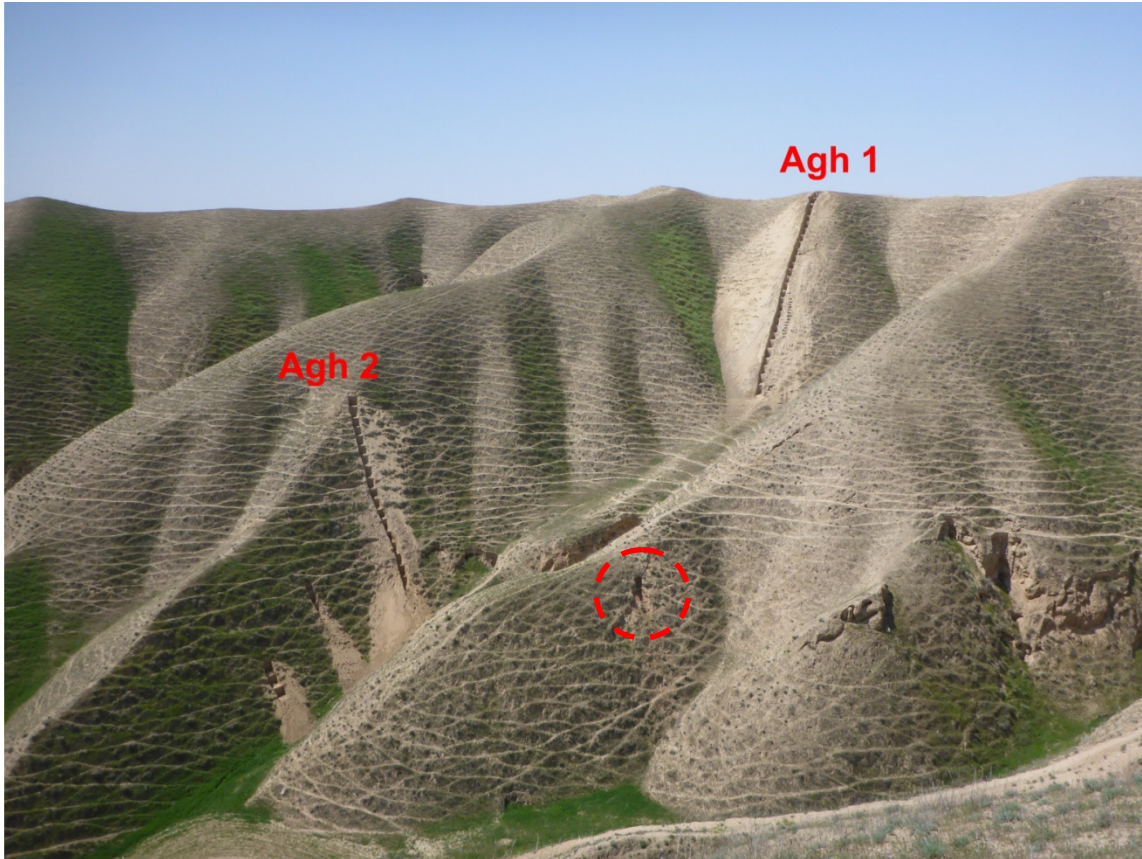


Fig. 3.3: Agh Band loess-palaeosol sequence with the 2 sub-profiles Agh 1 and Agh 2. Profile Agh 1 describes an about 30 m thick loess succession, profile Agh 2 an about 20 m thick sequence. The location of the lower part of profile Agh Band as studied by Kehl et al. (2005) and Frechen et al. (2009) is marked with a circle.

3.3 Methods

3.3.1 Preparation of the profile and sampling

The Agh Band loess was already studied by Kehl et al. (2005) and first luminescence age estimated had been provided by Frechen et al. (2009) for the loess at the Agh Band area indicating a last-glacial age for most of the Agh Band loess. Nevertheless, at that time the preparation of a step-wise profile for the whole loess-palaeosol succession in the Agh Band area including a high resolution sampling for multi-proxy-analyses could not be realized. In two field campaigns in spring 2014, a stepwise profile of about 54 m was prepared and the loess -palaeosol sequence was described in the field by lithostratigraphy and by pedogenic

patterns. The denomination of palaeosol horizons widely follows criteria for soil horizon description of WRB (2007). Due to the technical reasons, the Agh Band profile had to be split up into two subprofiles (Agh 1 and Agh 2). The two profiles are shown in Fig. 3.3.

The top part of Agh 2 was chosen in a way that there is no gap between the bottom part of Agh 1 and the upper part of Agh 2 with the intention to sample the whole loess sequence without missing any sediment-unit. Furthermore, the same lithological features (layered loess) could be found at the lower part of profile Agh 1 and the top part of profile Agh 2. Hence, it can be assumed that the lower part of Agh 1 and the upper part of Agh 2 correspond to the same lithostratigraphical unit (unit 3-1, see chapter 4.1.2). As there is no well-developed soil neither at the bottom part of Agh 1 nor at the top part of Agh 2 that could have been used for correlation, an exact determination of the overlapping between the two profiles is not possible. Therefore the two profiles are not shown in a single profile-sketch.

The whole loess-palaeosol sequence was sampled in 2 cm intervals for multi-proxy analyses. Further 45 samples were collected for luminescence dating. The profiles Agh 1 and Agh 2 are closely located to the sampling location of profile Agh Band a investigated by Kehl et al. (2005) and Frechen et al. (2009).

3.3.2 Luminescence dating

To obtain a chronological framework for periods of loess deposition, soil formation but probably also erosion and reworking of the loess, luminescence dating was applied. Luminescence dating is a method to determine the time elapsed since the last sunlight exposure of sediment grains and it is based on the storage of trap charge in minerals such as quartz or feldspar (Aitken, 1998).

For loess-sediments it has many times been demonstrated that luminescence dating is a suitable approach to obtain resilient chronologies for aeolian deposits (e.g. Li and Li, 2012; Stevens et al., 2013; Schmidt et al., 2013; Lauer et al., 2014, 2015) and such chronologies are mandatory for palaeoenvironmental reconstruction. All luminescence samples were collected from the Agh Band profile using light-tight plastic and steel-tubes.

Further material was taken from the luminescence-sample surrounding for gamma-spectrometry and hence, to determine concentrations of uranium, thorium and potassium (K^{40}). Nuclide concentrations were measured with a high purity Germanium N-type detector and the dose rates of each sample are listed in Table 1. The averaged dose rate of the Agh Band loess is at 3.9 Gy/ka, values range from 3.12 ± 0.22 Gy/ka to 4.61 ± 0.25 Gy/ka. To account for alpha efficiency an a-value of 0.11 ± 0.02 was used. Previously, a-values of 0.08 ± 0.02 , based on Rees-Jones (1995) had been used for pIRIR₂₉₀ fine-grain studies (Thiel et al., 2011; Murray et al., 2014; Schmidt et al., 2014), but Biswas et al. (2013) and Kreutzer et al. (2014) stressed that for pIRIR signals a-values are higher if compared to IRSL signals. Hence, a higher a-value was used in this study equal to Lauer et al. (2015).

For luminescence measurements, the fine grain-material (4-11 μ m) was prepared under subdued red light in the luminescence laboratory in Hannover. The common steps of chemical treatment with HCl (10 %) to remove carbonates, sodium oxalate to dissolve aggregates and H₂O₂ (30 %) to destroy any organic matter were applied. Finally, several

runs of centrifugation were conducted to get the preferred grain size fraction (Frechen, 1996). All luminescence measurements were conducted on a Risø TL/OSL reader. For irradiation a $^{90}\text{Sr}/^{90}\text{Y}$ source with a dose rate of about 6.2 Gy/min was used. The luminescence signal of feldspars among the polymineral subsample was stimulated by IR-LEDs transmitting at 870 nm. The luminescence signal was recorded through a filter combination of Schott BG-39 and Corning 7-59 passing between 320 and 460 nm to detect the blue-violet wavelength.

Table 3.1:

Results from gamma spectroscopy and luminescence dating including non-fading corrected pIRIR₂₀₉ ages. Abbreviations: DR = dose rate; De = equivalent dose. The right column shows the number of measured aliquots and the amount of accepted aliquots. As acceptance criteria, aliquots showing recycling ratios deviating > 10% from unity were rejected.

Sample Code	Depth (m)	U (ppm)	Th (ppm)	K (%)	Cosmic DR	Total DR	De IR50	De pIRIR290	pIRIR290 age	meas./acc. AI
					(mGy/a)	(mGy/a)				
Agh S1 b	0.9	1.9 ± 0.1	7.0 ± 0.4	1.6 ± 0.1	0.19	3.35 ± 0.22	33.2 ± 0.8	56.1 ± 0.6	17 ± 1	10/7
Agh S2c	2.5	2.3 ± 0.1	8.8 ± 0.5	1.6 ± 0.1	0.16	3.64 ± 0.23	74.6 ± 1.2	125.5 ± 1.2	34 ± 2	15/15
Agh S4b	4.5	2.1 ± 0.1	6.9 ± 0.4	1.9 ± 0.1	0.14	3.62 ± 0.22	105.0 ± 3.2	185.0 ± 2.2	51 ± 3	10/10
Agh S5b	5.9	2.3 ± 0.1	7.9 ± 0.4	2.7 ± 0.2	0.12	4.57 ± 0.25	110.9 ± 1.8	193.9 ± 2.9	42 ± 2	10/10
Agh S6b	7	2.6 ± 0.1	9.0 ± 0.5	1.6 ± 0.1	0.11	3.78 ± 0.24	116.1 ± 2.0	205.6 ± 3.6	55 ± 4	10/10
Agh S7b	8.2	2.7 ± 0.1	9.4 ± 0.5	1.7 ± 0.1	0.1	3.89 ± 0.24	129.4 ± 3.0	223.8 ± 2.7	58 ± 4	10/10
Agh S8 b	9.4	2.0 ± 0.1	8.0 ± 0.4	2.7 ± 0.2	0.09	4.37 ± 0.24	134.6 ± 8.3	221.9 ± 7.1	51 ± 3	7/7
Agh S10b	11.8	2.6 ± 0.1	9.6 ± 0.5	1.7 ± 0.1	0.08	3.89 ± 0.24	133.8 ± 4.5	241.1 ± 4.4	62 ± 4	10/10
Agh S11b	13	2.1 ± 0.1	8.0 ± 0.4	1.8 ± 0.1	0.07	3.60 ± 0.23	124.4 ± 5.5	218.5 ± 6.7	61 ± 4	10/10
Agh S12b	14.3	2.7 ± 0.1	10.4 ± 0.5	1.7 ± 0.1	0.06	4.04 ± 0.25	135.2 ± 2.2	234.7 ± 3.6	58 ± 4	10/10
Agh S13b	15.1	2.2 ± 0.1	8.3 ± 0.5	1.8 ± 0.1	0.06	3.64 ± 0.23	131.5 ± 3.8	247.1 ± 3.5	68 ± 4	10/10
Agh S14b	16.3	2.2 ± 0.1	2.3 ± 0.1	2.3 ± 0.1	0.06	3.29 ± 0.22	134.6 ± 1.6	252.9 ± 2.5	77 ± 5	10/10
Agh S15b	17.5	2.2 ± 0.1	9.2 ± 0.5	1.8 ± 0.1	0.05	3.77 ± 0.24	130.2 ± 3.2	243.6 ± 6.3	65 ± 4	8/8
Agh S16b	18.8	2.2 ± 0.1	9.1 ± 0.5	2.0 ± 0.1	0.05	3.96 ± 0.23	160.7 ± 10.6	278.2 ± 4.2	70 ± 4	10/9
Agh S17b	19.6	2.3 ± 0.1	9.0 ± 0.5	2.3 ± 0.1	0.05	4.23 ± 0.24	138.3 ± 3.1	273.0 ± 3.5	65 ± 4	10/10
Agh S18b	21	2.4 ± 0.1	9.7 ± 0.5	1.8 ± 0.1	0.04	3.91 ± 0.24	157.5 ± 4.4	282.0 ± 3.2	72 ± 5	9/9
Agh S19b	21.9	2.4 ± 0.1	10.0 ± 0.5	2.6 ± 0.1	0.04	4.67 ± 0.25	144.9 ± 2.6	271.0 ± 3.7	58 ± 3	12/12
Agh S 20 b	23	2.4 ± 0.1	9.1 ± 0.5	1.7 ± 0.1	0.04	3.73 ± 0.24	154.7 ± 5.9	284.9 ± 5.3	76 ± 5	10/10
Agh S21b	24.1	2.1 ± 0.1	8.3 ± 0.4	2.4 ± 0.1	0.04	4.12 ± 0.24	142.7 ± 3.5	253.3 ± 2.3	61 ± 4	10/10
Agh S22b	25.1	2.0 ± 0.1	7.4 ± 0.4	1.9 ± 0.1	0.03	3.52 ± 0.22	147.8 ± 3.3	265.1 ± 4.3	75 ± 5	8/8
Agh S23b	26.2	2.1 ± 0.1	8.1 ± 0.4	2.5 ± 0.1	0.03	4.18 ± 0.24	139.3 ± 3.8	271.3 ± 3.5	65 ± 4	10/10
Agh S24b	27.5	2.0 ± 0.1	7.7 ± 0.4	1.8 ± 0.1	0.03	3.44 ± 0.22	155.3 ± 4.9	291.2 ± 3.3	85 ± 6	10/10
Agh S25b	28.8	2.1 ± 0.1	8.0 ± 0.4	2.1 ± 0.1	0.03	3.84 ± 0.23	167.7 ± 6.5	314.3 ± 7.1	82 ± 5	10/10
Agh S26b	29.9	2.2 ± 0.1	8.6 ± 0.5	2.2 ± 0.1	0.03	4.07 ± 0.24	156.5 ± 10.6	315.7 ± 9.3	78 ± 5	10/10
Agh S 27 b	31	2.2 ± 0.1	8.5 ± 0.4	1.6 ± 0.1	0.03	3.47 ± 0.23	182.9 ± 11.5	334.8 ± 9.3	96 ± 7	14/10
Agh S28b	32.4	2.2 ± 0.1	9.3 ± 0.5	2.7 ± 0.2	0.02	4.61 ± 0.25	178.4 ± 3.3	348.6 ± 4.4	76 ± 4	8/8
Agh II S1 a	32.7	2.6 ± 0.1	10.3 ± 0.6	1.8 ± 0.1	0.02	4.02 ± 0.25	143.5 ± 2.0	259.2 ± 3.7	65 ± 4	10/10
Agh II S1 b	33.5	2.8 ± 0.1	11.3 ± 0.6	1.7 ± 0.1	0.02	4.15 ± 0.25	134.2 ± 4.5	257.5 ± 4.2	62 ± 4	8/8
Agh II S2 a	34.6	2.8 ± 0.2	11.0 ± 0.6	1.8 ± 0.1	0.02	4.13 ± 0.25	137.6 ± 3.2	264.6 ± 3.5	64 ± 4	8/7
Agh II S3 a	35.9	2.8 ± 0.2	11.5 ± 0.6	1.7 ± 0.1	0.02	4.16 ± 0.26	151.5 ± 2.3	299.4 ± 3.9	72 ± 5	10/10
Agh II S5 a	37.8	3 ± 0.2	11.8 ± 0.6	1.6 ± 0.1	0.02	4.18 ± 0.26	151.1 ± 2.5	297.6 ± 3.1	71 ± 5	10/10
Agh II S5 b	38.5	3.3 ± 0.2	12.7 ± 0.7	1.6 ± 0.1	0.02	4.43 ± 0.27	153.5 ± 3.1	295.2 ± 4.8	67 ± 4	11/11
Agh II S6 a	38.8	2.8 ± 0.2	9.4 ± 0.5	1.6 ± 0.1	0.02	3.76 ± 0.24	142.8 ± 3.1	259.9 ± 3.4	69 ± 5	11/11
Agh II S6 b	39.3	2.9 ± 0.2	10.4 ± 0.6	1.5 ± 0.1	0.02	3.88 ± 0.25	171.8 ± 10.4	288.8 ± 6.7	75 ± 5	10/10
Agh II S7 a	39.9	3.0 ± 0.2	10.1 ± 0.5	1.5 ± 0.1	0.02	3.85 ± 0.25	202.3 ± 4.4	372.5 ± 11.8	97 ± 7	11/11
Agh II S8a	41.2	3.5 ± 0.2	10.1 ± 0.5	1.7 ± 0.1	0.02	4.3 ± 0.3	290.2 ± 5.8	754.9 ± 18.7	177 ± 12	10/10
Agh II S8 b	42.1	3.2 ± 0.2	10.0 ± 0.5	1.7 ± 0.1	0.02	4.06 ± 0.25	270.5 ± 6.5	693.8 ± 20.2	171 ± 12	10/10
Agh II S9 a	43.1	2.9 ± 0.2	10.4 ± 0.6	1.8 ± 0.1	0.02	4.14 ± 0.25	284.9 ± 4.6	757.1 ± 17.8	183 ± 12	10/10
Agh II S10 a	44.2	2.7 ± 0.1	10.0 ± 0.5	1.7 ± 0.1	0.02	3.94 ± 0.24	307.2 ± 5.3	615.2 ± 10.7	156 ± 10	10/10
Agh II S11a	45	2.4 ± 0.1	8.9 ± 0.5	1.7 ± 0.1	0.01	3.6 ± 0.2	291.5 ± 6.0	639.7 ± 15.2	175 ± 12	10/10
Agh II S12 b	46	2.5 ± 0.1	9.3 ± 0.5	1.7 ± 0.1	0.01	3.70 ± 0.24	283.5 ± 4.5	674.3 ± 11.7	182 ± 12	10/10
Agh II S13 b	48	2.5 ± 0.1	10.1 ± 0.5	1.6 ± 0.1	0.01	3.82 ± 0.24	273.2 ± 6.5	698.3 ± 11.7	183 ± 12	10/10
Agh II S15 a	50	1.8 ± 0.1	7.2 ± 0.4	1.6 ± 0.1	0.01	3.12 ± 0.22	279.8 ± 5.9	604.0 ± 6.8	194 ± 14	7/7
Agh II S 17	53.3	1.9 ± 0.1	7.7 ± 0.4	2.4 ± 0.1	0.01	3.97 ± 0.23	297.9 ± 4.4	678.6 ± 7.7	171 ± 10	10/10
Agh II S 18	53.9	2.2 ± 0.1	9.1 ± 0.5	2.0 ± 0.1	0.01	3.86 ± 0.24	339.7 ± 11.4	797.0 ± 24.8	206 ± 14	15/15

For equivalent dose (De) measurements, the pIRIR₂₉₀ -dating approach (Thiel, 2011) was applied to the polymineral fine-grain fraction. The same dating approach was recently chosen by Lauer et al. (2017a) for the Toshan loess section ensuring a reliable comparison of the chronological data of the two profiles. Prior to De-measurements, the dating protocol was tested for reproducibility by applying dose recovery tests to selected samples. Therefore, 6 aliquots of the material were bleached by a solar simulator for 5 hrs to reset the luminescence signal. After that bleaching-step, the remaining dose residuals were measured on 3 aliquots. The other 3 aliquots were irradiated with a known dose which was selected to be close to the expected natural one. Subsequently, this dose was treated as unknown and it was tested how precise the pIRIR₂₉₀-dating approach can recover this given dose.

If measuring feldspar, also the amount of anomalous fading has to be quantified (Wintle, 1973) as fading leads to age underestimation if not corrected properly. It was several times demonstrated that the IR-stimulated feldspar signal measured at high temperatures after depleting the IR₅₀ signal shows only little fading (e.g. Thiel et al., 2011; Buylaert et al., 2012; Lauer et al., 2015). Nevertheless, fading measurements are recommended also for the pIRIR₂₉₀ signal to quantify the signal loss. For 10 samples, the g-values were therefore determined following the procedure after Huntley and Lamothe (2001).

3.3.3 Determination of carbonate content – Mid-infrared spectroscopic measurements

Dried and homogenized sample material was given to a micro plate and compacted by means of a plunger in order to create a plain and dense surface for measuring its diffuse reflectance. Altogether 660 samples (8 cm intervals) with 3 aliquots each were measured from the section at Agh Band. Their diffuse reflectance spectra were recorded using a Bruker Tensor 27. This mid-infrared spectrometer is fitted with a liquid N₂-cooled mercury-cadmium telluride (MCT) detector and a broadband KBr splitter, providing a measurable spectral range from 8000-600 cm⁻¹ (1250-16.700 nm). Within a single run spectra were recorded in 4 cm⁻¹ increments.

Mid-infrared spectroscopy (MIRS) is based on laboratory-analysis “ground-truth” data and the reflectance of a sample, combined to predict the concentrations of e.g. carbonate and organic matter.

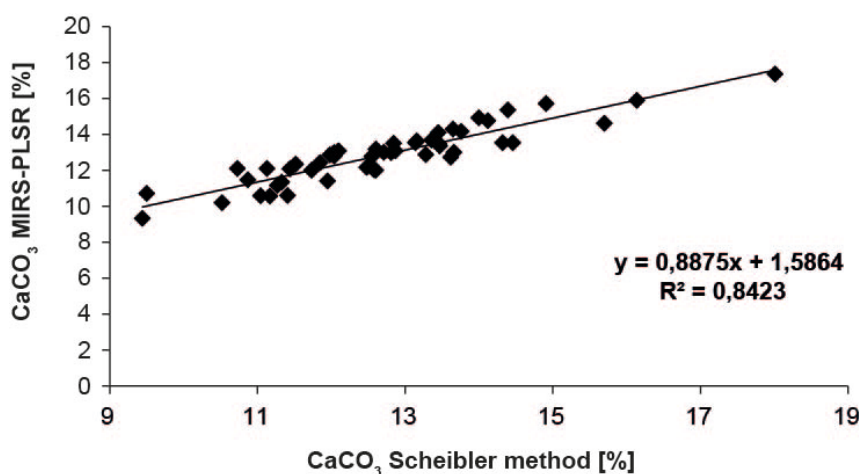


Fig. 3.4: Prediction of CaCO₃ from MIRS analyses and partial least square regression, compared to the CaCO₃ content obtained by the Scheibler method.

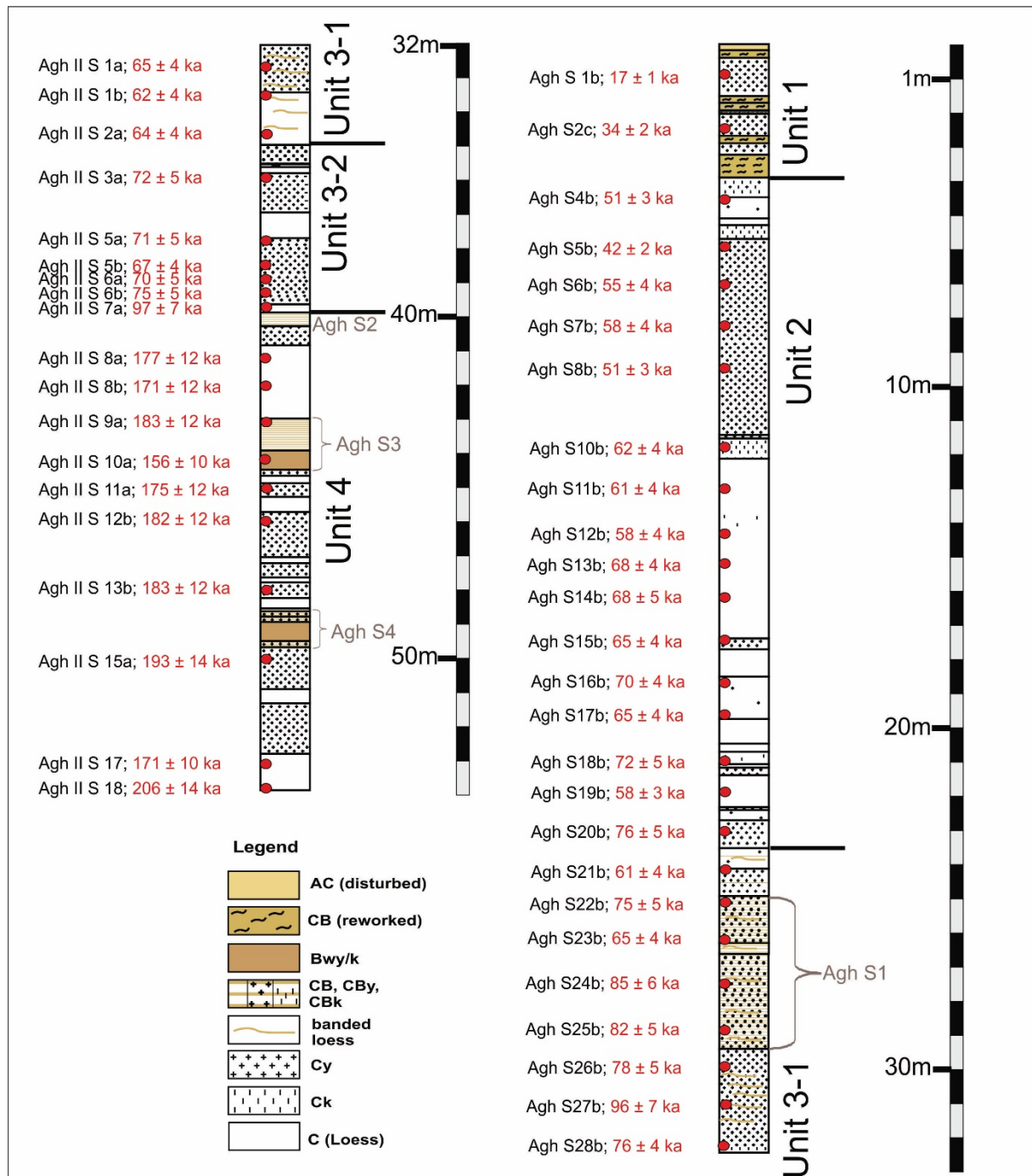


Fig. 3.5: Litho/ pedostratigraphic column and pIRIR₂₉₀ luminescence age estimates of the Agh Band profile.

A set of 83 samples of Northern Iranian loess and palaeosols (Kehl, 2010) was used to calibrate a statistical model for predicting the amount of CaCO_3 . For ground truth measurements of CaCO_3 the Scheibler method was applied. Hence, the samples were treated with HCl to determine their carbonate content according to the volumetric release of CO_2 . The predictive power of the applied model is supported by the CaCO_3 within loess and palaeosol horizons that were sampled across a climosequence in previous studies (Kehl, 2010). The quantification was conducted by means of OPUS QUANT software (©Bruker, 2006), applying partial least square regression (PLSR). The OPUS QUANT software provides an automated routine, testing combinations of diverse spectral ranges and data

treatment for the best possible prediction power of the model (Bornemann et al., 2008). Thus the spectral ranges from 1997.8 to 1216.8 cm^{-1} and 6853.6 to 2653.5 cm^{-1} were suggested. A manual adjustment of the spectral range was not performed. The measurement protocol, the spectral pretreatment and the statistical analysis followed the routine of Bornemann et al. (2008). The high accuracy of this prediction is reflected by a close correlation between measured and predicted values (Fig. 3.4). The same statistical model was successfully applied to unravel the CaCO_3 -content of the Toshan loess-soil sequence (Vlaminck et al., 2016). For model parameters the reader is referred to Vlaminck et al. (2016).

3.3.4 Grain-size measurements

Grain-size measurements were conducted on every sample (2 cm interval), applying the same measurement-procedure as described by Vlaminck et al. (2016) for the Toshan loess palaeosol sequence. For granulometric analyses a Beckman-Coulter LS 13320 PIDS laser diffractometer was used and a spectrum ranging from 0.4 to 2000 μm diameter was detected. Laser diffractometry offers the possibility of measuring high quantities of samples and only a small amount of sample material is needed. The reproducibility of measurement is high but the detection of clay-sized particles might lead to underestimates due to the flat morphology of clay-particles (Beuselinck et al., 1998). Hence, particles with $< 5.5 \mu\text{m}$ diameter were defined as clay-sized components.

The grain-size distribution was measured by using the standard measurement protocol as described by Machalett et al. (2008) based on Fraunhofer theory for determining the grain-size spectrum. Prior to measurements the sample material was dispersed for a minimum of 12 hrs with 1 % ammonium hydroxide (NH_4OH) in overhead tube rotators. Sample preparation included no further chemical treatment, hence no removal of organic matter or CaCO_3 . Test measurements were then conducted on samples of each stratigraphical layer to achieve the best sample dispersion. Every sample was then measured five times and depending on the reproducibility of the measurements 5 to 3 grain size distributions were averaged to obtain the final grain-size cluster. As quality criteria, the accepted standard deviation for all grain-size spectra was below 5%, otherwise measurements were repeated.

3.3.5 Magnetic susceptibility

Samples for rock and palaeomagnetic investigations were taken, using a sophisticated technique (Schnepp et al., 2008) to collect oriented samples in soft rocks. The palaeomagnetic investigations, their results and interpretation will be described and published elsewhere. Complementary to the oriented samples scratched sediment material was taken at the profiles to increase the frequency of taken samples for rock magnetic proxies (low field susceptibility K_{lf} and frequency dependent susceptibility K_{fd}). In the rock and palaeomagnetic laboratory of LIAG this material was dried, homogenised and pressed into plastic cubes (8 cm^3). In this way we were able to collect more than 600 oriented and more than 1000 not oriented samples. In the frame of the present publication we only present the susceptibility measurements.

These non-destructive measurements react sensitively on concentration and grain size variability of magnetic minerals. K_{lf} -intensity reacts sensitive on the variation of ferro(i)-magnetic mineral concentrations while frequency dependent magnetic susceptibility (K_{fd}) allows identifying very small so called superparamagnetic (SP) grains. After Dearing et al. (1996) in samples which are dominated by frequency independent stable single (SD) and multi domain grains (MD) the frequency dependence is $< 3 \%$. Therefore, values above 3% proof SP grains. After the model of magnetic enhancement in loess-palaeosol sequences SP grains reflect soil forming processes due to the neoformation of magnetic minerals with grain sizes of SP character ($< 0.03 \mu\text{m}$ for magnetite) as well as with SD and MD character. All this leads to increased values in K_{lf} and K_{fd} , and therefore allows distinguishing soils and highly weathered loess from unweathered loess after the method introduced by Heller and Liu (1982) on samples from the Chinese loess plateau (CLP). In this light, the magnetic property variations are mainly climatically controlled. Since climatic fluctuations produce changes in sedimentary and soil-forming environments, the changing magnetic properties may reflect alternating cold/dry or warm/humid climates during the Quaternary (Evans and Heller, 2003; Maher, 2011; Rolf et al., 2014).

K_{lf} of all samples was measured using a frequency and field variable Magnon VSM Susceptibility Bridge (Magnon; Dassel Germany) which was also used measuring K_{fd} (at 505 and 5050 Hz).

3.4 Results and discussion

3.4.1 Lithological/pedological field-description

The Agh Band loess sequence consists of sandy-loess, in most parts enriched by gypsum, and is subdivided by several palaeosols exhibiting different degrees of soil formation. The most strongly developed buried soil horizons are situated at the bottom part of sub-profile Agh2 where a pedocomplex consisting of two palaeosols showing a sequence of Bw(y) horizons and CB horizons can be found pointing to periods with increased humidity, landscape stability and corresponding pedogenesis at that time. In sub-profile Agh1 only moderately developed palaeosol horizons were found (CBy-horizons) while most parts of Agh 1 consist of loess. These loess layers give a high percentage of fine-sand, slight variations in color and several shifts in grain-size including various coarsening and fining-up trends. At the bottom part of Agh 1 and also at the top part of Agh 2 the loess hosts banded structures which occur as wavy laminates and are characterized by a brownish color and an increased clay-content.

The Agh Band loess-profile was subdivided into 5 units (units 4, 3-2, 3-1, 2 and 1) as defined by litho-/pedological features (Fig. 3.5). The following chapters give a lithological/ pedological description of the single units. The Appendix-Table gives a detailed overview about the thickness of the single sediment units and palaeosols also including additional information on lithological- and pedological characteristics. The outlined profile-depths refer to the total profile depth, pretending a continuous connection of Agh 1 and Agh 2. The related difficulties were outlined in chapter 3.3.1. The sequence hosts 4 in-situ palaeosol-horizons which were named as Agh S 4 – Agh S 1 (Fig. 3.5).

Unit 4

Unit 4 (53.04 – 39.88 m total profile depth) consists of the basal loess of the Agh Band profile and the capping pedocomplex, formed by two palaeosols (Bwy- and CBy-horizons) and intercalated loess.

The basal sandy loess deposits (54.04 - 50.08) show banded features between 53.2 - 53.4 m depth. The loess layers from the bottom part of the Agh Band profile are partly enriched in gypsum as based on visual detection, mainly at around 52.4 m depth where coarse crystals of gypsum have precipitated. At around 51.5 m profile depth, small black stains of manganese hydroxide concretions reflect weak redoximorphic alteration.

The basal loess is partly disturbed by bioturbation as evidenced by krotovina. Post-depositional biogenic mixing of the loess deposits might play an important role for the whole loess-sequence at Agh Band, and may have caused contamination of sampled layers by younger sediment from overlying deposits. This mixing may also have levelled out diachronic changes in granulometric composition and rock magnetism.

At around 49.9 m profile depth the pure loess merges into a CBy(k) horizon, defined by a weak pedogenic overprinting of the loess and characterized by gypsum and an enrichment of secondary carbonates.

A Bwy(k) horizon (Fig. 3.6) is preserved in between 49.9 - 49.36 m, showing a dark-brownish color and a subangular – angular blocky structure. The lower boundary of the Bwy(k) is well defined. This palaeosol horizon is weakly enriched in secondary carbonates in the form of pseudomycelia and shows embedded crystals of gypsum.

Above 49.4 m the Bwy(k)-horizon gradually merges into a weakly developed palaeosol horizon (CBy/ CB) extending to about 48.9 m (Fig. 3.6). This horizon exhibits minor aggregation and a subangular-coherent structure. The Bwy(k)- and CBy/CB-horizons were named together as soil Agh S4 (Fig. 3.5).

The overlying stratum (Cy and C; 48.94 - 44.88 m) is characterized by an alternating sequence of layers hosting visually detectable gypsum crystals and sandy loess. At around 46.8 m small (< 1mm) Mn-concretions can be found. The loess shows weak variations in color and the slightly brownish color in between 48.94-48.66 m might indicate initial pedogenesis.

A second soil within unit 4 is preserved between 44.88 - 43.38 m (Fig. 3.7). Between 44.88 - 44.32 m a strongly brownish Bwy-horizon, enriched in gypsum is found. This buried soil horizon has subangular blocky aggregates embedded in a coherent matrix.

The Bwy-horizon gradually merges into several CB(y)-horizons in between 44.32 - 43.38 m with decreasing soil-forming intensity upwards. The CB-horizon preserved in between 44.1-43.78 m is characterized by a minor content of humic material probably indicating the preservation of a buried humic horizon. The Bwy- and CB(y)-horizons were together named as soil Agh S3 (Fig. 3.5).

The capping loess (43.38 - 40.04 m) can be subdivided by its lithology and sedimentological characteristics. Between 41.24 - 40.68 m the loess is enriched in gypsum. A noticeable thin silt-band appears in between 43.28 - 43.16 m probably indicating reworking of the loess. The upper part of unit 4 is defined by a weakly developed palaeosol horizon (CBy) showing concretions of gypsum, a weak brownish color and a coherent soil structure (soil Agh S2; Fig. 3.5).

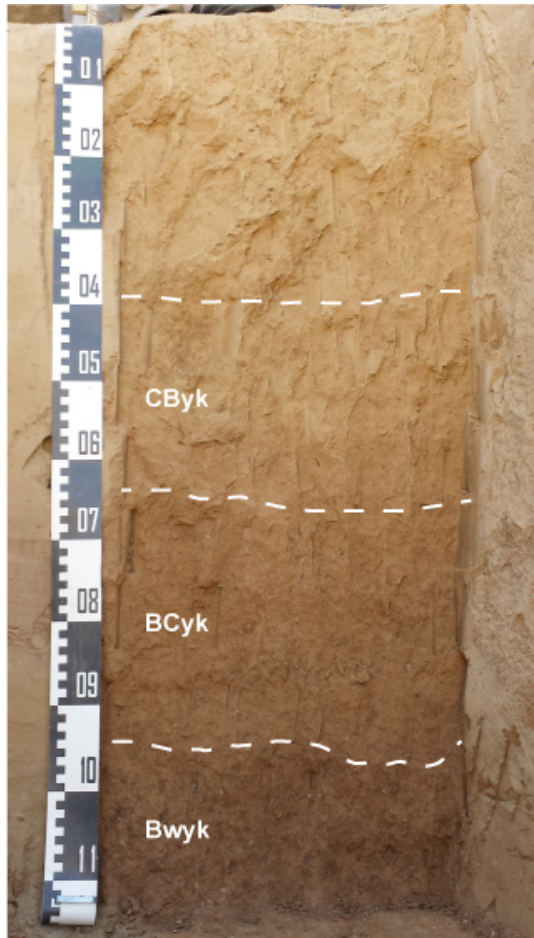


Fig. 3.6: Lowermost soil of the Agh Band loess sequence (subprofile Agh 2; soil Agh 4). The Bwyk-horizon grades into a CByk-horizon. The smooth transition marks climatic shift towards most likely increased aridity and dust accumulation.

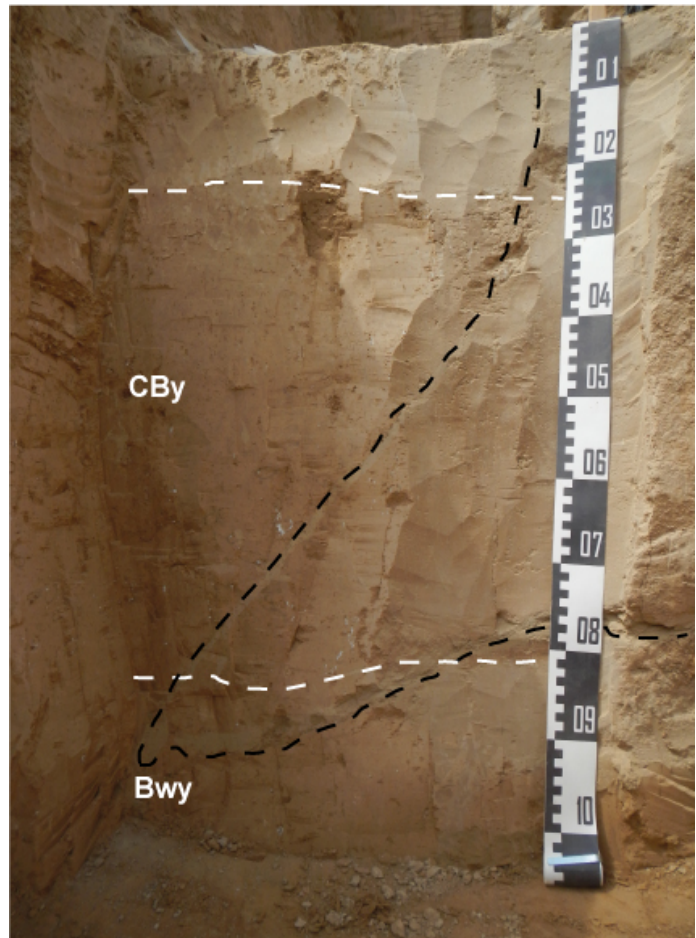


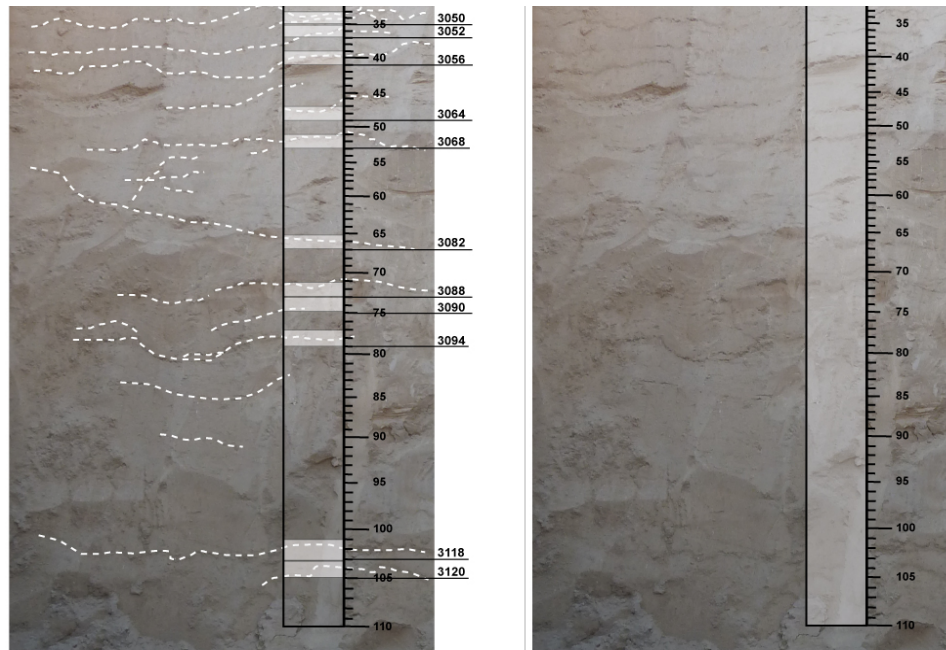
Fig. 3.7: Palaeosol Agh S3 (See Figure 5). The Bwy-horizon grades into a CBy-horizon indicating a climatic shift towards less soil-forming intensity and most likely dryer climate conditions. There is no sharp boundary between the soil horizons and the transition towards the overlying loess. The dashed black line marks tectonic disturbance of the soil pointing to tectonic activity after the soil had been formed.

Units 3-2 and 3-1

Unit 3-2 (39.88 - 36.02m) is characterized by sandy loess without any indication for soil formation. The loess deposits are subdivided by their varying content of gypsum and exhibit variations in grain-size patterns with various fining- and coarsening-up trends.

Unit 3-1 builds the top part of subprofile Agh 2 and the bottom part of Agh 1. Unit 3-1 is characterized by banded features within the loess-sediments what distinguishes unit 3-1 from unit 3-2. The some millimeters thin bands are defined by a wavy, horizontally structure and by an increased clay-content as compared to the over- and underlying loess strata. Fig. 3.8 shows the banded loess at around 30 - 31 m depth.

Fig. 3.8: Banded loess-deposits (Unit 3-1); 30.18-31.20 m depth. The dashed lines (left) mark the orientation of the banded features. The black numbers (e.g. 3120) mark the total profile depth within sub-profile Agh 1. The genesis of the bands is still under debate but might be linked to former biogenetic crusts preserved at that part of the Agh Band profile. The horizontal orientation of the bands with only a minor inclination represents the palaeosurface and shows that the steep slope, characterizing the present day landscape, was not developed while unit 3-1 was formed.



Moreover, unit 3-1 is characterized by a weakly developed palaeosol horizon (CB/ CBy) preserved at the bottom part of Agh 1 between 29.44 - 24.94 m. This horizon exhibits both the properties of sandy loess such as a coherent structure and a faint brownish soil color indicating incipient pedogenesis. Thus the CB/CBy horizon represents a transitional stage between C and B horizons in which the features of loess as parent material prevail.

Unit 2

Unit 2 is characterized by almost pure sandy loess. Banded features only appear at about 19.4 m depth. The almost complete absence of the banded loess is the main difference if compared to the loess of unit 3-1. Unit 2 shows no stronger pedogenic features but can be subdivided by subtle variations in sediment color and several shifts in grain-size. Only between 22.72 - 22.4 m, Mn-concretions can be found. In that layer, a weak reddish color is preserved probably indicating initial pedogenic overprinting.

Most parts of unit 2 are enriched in gypsum to various amounts as indicated by layers showing an increased appearance of crystals of gypsum. At some parts, e.g. around 12 m and 5.5 m depth, the loess is slightly enriched in secondary carbonates.

Unit 1

Unit 1 builds the partly disturbed upper part of the Agh Band loess palaeosol sequence. The unit is characterized by erosional features as evidenced by short-scaled changes in sedimentology including erosional contact to the underlying strata. Furthermore, unit 1

contains reworked soil material (CBy) at its bottom part (3.9 – 1.52 m). The reworked Cby is defined by loosely packed sediment of brownish color (10 YR 6/4 – 10 YR 7/4) with concretions of gypsum. The redeposited soil is mixed with sandy loess material and the loose and unstructured appearance of the layer indicates a pedosedimentary origin such as a soil sediment. A well sorted fine-sand layer is intercalated into the Cby horizon between 2.04 – 1.94 m depth. The relatively well sorted sand-layer might indicate an aquatic transport of the material or could even point to a storm event being able to transport the sand-sized material. The inclination of the reworked Cby-horizon is almost parallel to the recent hill-slope (contrary to the banded features of unit 3-1) and indicates that the palaeo-landscape was already characterized by steep slopes at time of deposition.

The uppermost part of the Agh Band loess section is built by partly disturbed loess without any pedogenetic features (1.52 – 0.18 m). The modern soil is almost fully missing and only a very initial disturbed humic horizon with low degree of compaction is preserved at the top. That illustrates that the present day landscape is strongly affected by erosion as the current climate conditions should at least allow the genesis of a weak soil (CB-horizon).

3.4.2 Luminescence dating results

Dose recovery and fading

The results of dose recovery tests are shown in Fig. 3.9. The quoted measured-given dose ratios are residual-subtracted.

It is shown that generally, the measured-given dose ratios overestimate the given dose, especially for the older samples. But the results can be improved by excluding the hotbleach at 325° at the end of the SAR cycle. The same was observed for the loess from Toshan (Lauer et al., 2017a).

Hence, for the pIRIR₂₉₀ measurements of the Agh Band loess, the hotbleach was excluded from equivalent dose measurements.

Fig. 10 shows the dose residuals after the 5hrs bleach under solar lamp for the pIRIR₂₉₀-signal. The residuals were plotted against corresponding equivalent doses (see also Buylaert et al., 2012; Lauer et al. 2017a). It is highlighted, that dose residuals decrease with decreasing equivalent dose (see also Lauer et al., 2017a). The estimated intercept value of about 15 Gy indicates that dose residuals, defining the unbleached trap charge at time of deposition were higher than those obtained by Lauer et al. (2017a) for the Toshan-loess section where a dose-residual intercept value of only 5 Gy was estimated. That points to a relatively short sunlight exposure and therefore a shorter transport-distance for the Agh Band loess if compared to the Toshan loess sediments. That is also indicated by the coarser median-grain-size of the Agh Band loess with a high content of fine-sand (see chapter 4.3).

Nevertheless, dose residuals of about 15 Gy at time of deposition do not substantially influence the final luminescence age if sediments are some 10 ka old. But for the youngest sediments of the Agh Band loess sequence, dose residuals might lead to a slight age-overestimation of about 4 ka by considering the averaged dose rate of 3.9 Gy/ka.

The fading-results are shown in Fig.3.11. The pIRIR₂₉₀ g-values are generally lower than the corresponding g-values of the IR₅₀ signal (except for sample Agh S 8b) and are mostly below

2. Only sample Agh S 8b gives a high outlier with a significant error-bar. Hence, the g-value of the sample should be treated with care as they are not representative.

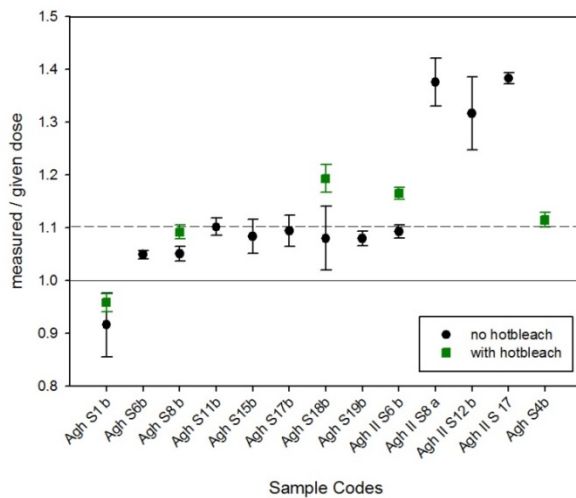


Fig. 3.9: Results of dose recovery tests.

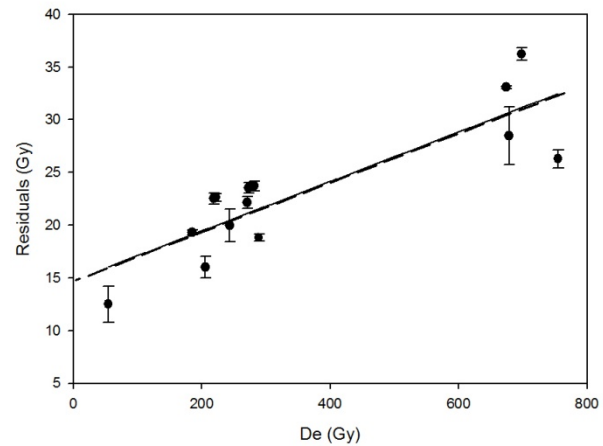


Fig. 3.10: pIRIR₂₉₀-dose residuals plotted against the corresponding equivalent doses. The intercept dose residual of about 15 Gy should be similar to dose residuals at time of deposition.

The averaged pIRIR₂₉₀ g-value of the Agh Band loess is at 2 ± 0.3 . If excluding the outlier of sample Agh S8b, a mean g-value of 1.7 ± 0.1 is obtained. The latter is similar to the mean pIRIR₂₉₀-g-value of loess from Toshan which is at 1.6 ± 0.1 (Lauer et al., 2017a).

The fading-tests show, that, also for the pIRIR₂₉₀ signal, there is some detectable fading for the loess from Agh Band. Nevertheless, fading test for aliquots beyond the linear range of the dose response curve should be discussed carefully. Furthermore, e.g. Buylaert et al. (2012) evidenced the high stability of the pIRIR₂₉₀-signal. Hence, for the Agh Band loess, fading of the pIRIR₂₉₀ signal might lead to some age underestimation but the amount of age-underestimation might not change the broad chronostratigraphic framework.

Chronological framework of the sediment units

Table 1 gives a detailed overview about all luminescence dating results. The luminescence age estimates used for interpretation and discussion are non-fading corrected pIRIR₂₉₀-ages (see also Fig. 3.5). As outlined in chapter 4.2.1, fading-rates are relatively low but as there was still some fading measured, also for the pIRIR₂₉₀-signal, ages might be slightly underestimated. Table 2 also shows the fading corrected pIRIR₂₉₀-luminescence ages of those samples for which g-values were measured. But as fading-corrections for samples showing non-linear dose response curves are problematic, it might be useful to base the chronostratigraphic classification on the non-fading corrected pIRIR₂₉₀ ages. Furthermore, Buylaert et al. (2012) also outline that low measured fading rates might be regarded as artifacts explained by the measurement procedure.

Residuals were not subtracted equal to the dating-study by Lauer et al. (2017a) for the Toshan loess-section.

The pIRIR₂₉₀-luminescence age estimates show that unit 4 was formed during MIS 7 and 6 as the luminescence ages range from 206 ± 14 to 156 ± 10 ka (Fig. 3.5, Table 1). But as previously mentioned, bioturbation might have sometimes affected the luminescence-dating results and the age of 156 ± 10 (sample Agh2 S 10a) can therefore be interpreted as underestimated. This could partly explain that it is reverse to the ages of samples Agh2 S 9a and Agh 2 S 8b taken from above. Hence, unit 4 most likely represents a time span ranging from about 210 ka – 170 ka. It is assumed that the upper soil of unit 4 (Agh S 2) was also formed during that time period but this cannot be evidenced by the dating results as no luminescence age directly from below that soil is available. But it is possible, that soil Agh S2 builds the upper part of a pedocomplex (Agh S4 – Agh S2) from the penultimate glacial-interglacial period. Probably soil Agh S2 was partly eroded and defines the lower boundary of a substantial erosional unconformity as the age obtained directly from above soil Agh S2 is at 96.8 ± 6.9 ka, but there is no sedimentological field evidence for that hypotheses. Based on the luminescence age estimates it is not possible to chronologically distinguish units 3-2 and 3-1. The ages of the units range from 96.8 ± 6.9 (sample Agh2 S 7a; lower part of unit 3-2) to 61.4 ± 3.6 (sample Agh S21b; upper part of unit 3-1). Hence, both units were formed during MIS 5 and 4.

Table 3.2:

IR₅₀ and pIRIR₂₉₀ g-values and corresponding luminescence ages (fading-uncorrected and fading-corrected). For the calculation of fading corrected luminescence ages, the R-luminescence package was used (Dietze et al., 2013). For sample Agh S8 b, the fading corrected age was not calculated due to significant scatter among obtained g-values (see Figure 3.11).

Sample ID	Sample Code	g IR ₅₀	g pIRIR ₂₉₀	g IR ₂₉₀ / g IR ₅₀	Uncorr. pIRIR ₂₉₀ age (ka)	Corr. pIRIR ₂₉₀ age (ka)
3118	Agh S11b	1.76 ± 0.4	1.67 ± 0.1	0.95	60.6 ± 4.2	70.5 ± 4.5
3122	Agh S15b	1.42 ± 0.3	1.23 ± 0.1	0.87	64.7 ± 4.4	72.7 ± 5.1
3124	Agh S17b	2.41 ± 0.3	1.80 ± 0.1	0.74	64.6 ± 3.8	76.9 ± 5.3
3125	Agh S18b	2.08 ± 0.5	1.75 ± 0.2	0.84	72.1 ± 4.5	84.8 ± 5.2
3126	Agh S19b	1.70 ± 0.4	1.51 ± 0.1	0.89	58 ± 3.2	66.7 ± 3.6
3103	Agh S 27 b	1.39 ± 0.4	1.54 ± 0.1	1.11	96.4 ± 6.9	112 ± 8
3104	Agh II S15 a	2.00 ± 0.1	1.89 ± 0.1	0.95	194 ± 14	233 ± 17
3105	Agh II S 17	3.18 ± 0.3	1.95 ± 0.2	0.61	171 ± 10	208 ± 16

The luminescence age estimates obtained for unit 2 range from 76 ± 5.0 ka (sample Agh S 20b) to 42.4 ± 2.4 ka (sample Agh S5 b). The latter age might be underestimated as sample Agh S4b, taken from above yielded an age of 51.1 ± 3.2 ka.

Hence, unit 2 represents a time-range of about 30 ka during which about 20 m of loess were deposited. That points to very high dust accumulation rates of $> 60\text{cm/ka}$ especially during MIS 4 (ranging from 71 – 57 ka following Lisiecki and Raymo, 2005).

The luminescence ages obtained from unit 1 are at 34.4 ± 2.2 ka for the reworked layer (sample Agh S2c) and the loess from the very top of the profile was dated to 16.7 ± 1.1 ka indicating dust deposition during late MIS 2. The youngest ages might be overestimated for probably 4 ka due to the dose residuals of the pIRIR₂₉₀-signal, as illustrated in Fig. 3.10.

The pIRIR₂₉₀ ages show that the Agh Band loess covers a time range spanning from MIS 7 to MIS 2, including chronological gaps. Frechen et al. (2009) also applied luminescence dating to the loess from Agh Band using IR-light at 50°C for stimulation without correcting for fading. The age estimates presented by Frechen et al. (2009) yielded ages ranging from about 10 ka – 150 ka. These ages gave a hint that the Bw-horizon at the bottom part of the profile might correlate to the last interglacial. A similar chronological interpretation was already presented by Kehl et al. (2005). Nevertheless, the here presented new age estimates which are based on the detection of a more stable feldspar signal indicate that a correlation of the bottom soil to MIS 5e has to be questioned and a correlation to an older isotope stage is more likely.

Furthermore, the new findings show that the Agh Band loess sequence hosts two separate paleosols represented by Bw-horizons at the bottom part of the sequence, whereas the previous studies (Kehl et al., 2005; Frechen et al., 2009) only illustrated one paleosol with Bw-horizon.

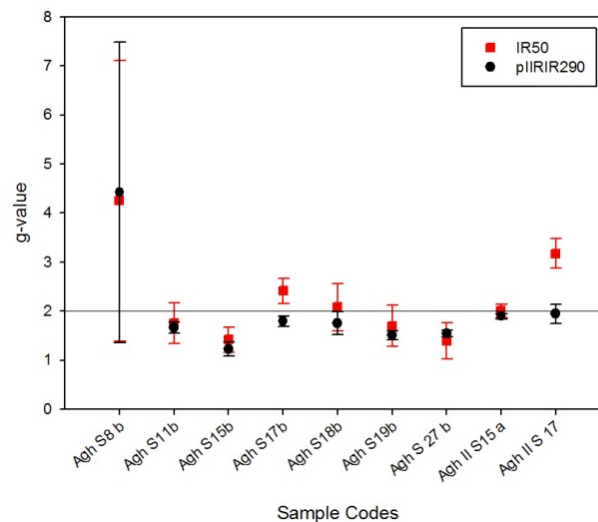


Fig. 3.11: IR₅₀ and pIRIR₂₉₀ g-values.

3.4.3 Carbonate content

The results of CaCO₃-measurements are presented in Fig. 3.12 and 3.13. The median carbonate content of both profiles, Agh 1 and Agh 2 is at around 12 % CaCO₃. That fits well to the median CaCO₃-contents presented by Frechen et al. (2009) who also quoted a median CaCO₃-content of 12 % for the Agh Band loess sediments.

The maximum carbonate content was found in subprofile Agh 2 at around 50.5 m profile depth (unit 4) yielding CaCO₃ amounts of 21 %. This culmination in CaCO₃-content corresponds with decalcification during the formation of the capping Bwy-horizon resulting in the precipitation of secondary carbonates (soil Agh S4; see Figure 5). Soil Agh S4 was surely fully decalcified and carbonate-values found in that soil-horizon decrease to < 1 %. The minor carbonate content might be explained by a slight re-calcification after pedogenesis.

In the unweathered loess (e.g. in between 5 – 23 m profile depth; Agh 1; unit 2) the carbonate content ranges between 8 and 15% (see Fig. 3.12 and 3.13).

In between 0 – 4.5 m profile depth, CaCO_3 -contents vary in between 3 – 17 %. The clear scatter in CaCO_3 -contents in the upper part of Agh 1 (unit 1; see Fig. 3.13) indicates the disturbance of those sediments and the reworking of soil-material partly mixed with loess.

Overall, the carbonate data support the litho/ pedomorphology, presented in Fig. 3.5, and reflect the removal and vertical translocation of CaCO_3 during soil formation including leaching of primary carbonate and precipitation of secondary carbonate affecting the palaeosols and the loess layers below the soil horizons, respectively.

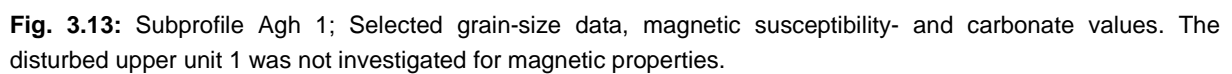
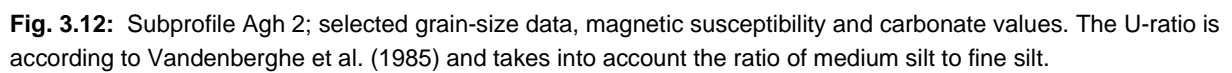
If compared with loess sections located on the foothills of the Alborz, the median CaCO_3 -contents (12 %) obtained at Agh Band are lower. Vlamincx et al. (2016) determined CaCO_3 -contents of mostly > 15 % for the unweathered loess at Toshan. Also Frechen et al. (2009) show median CaCO_3 -contents of 17 % for the Neka loess section and 16 % for the Now Deh section (see Fig. 3.1 for locations). Those variations might be explained by differences within the dust source areas of the loess formed at the Iranian loess-plateau as compared to the aeolian dust deposited on the foot-hills of the Alborz.

3.4.4 Patterns of high resolution grain size analyses

The loess in Agh Band is defined by a high content of fine sand. The averaged median grain size of the Agh Band loess is at around 33 microns for Agh 1 (Fig. 3.14) and 27 microns for Agh 2. Previous studies defined a median grain-size of 29 microns (Kehl, 2010) at Agh Band as based on grain size analyses using the pipette method.

The grain size of the loess deposited on the foothills of the Alborz-mountains is substantially finer. Vlamincx et al. (2016) defined an averaged modal grain-size of 10 microns for the Toshan-loess based on the same measurement procedure as applied for Agh Band. Kehl (2010) found a median grain-size of 9 microns at the Neka loess and of 11 microns at Now Deh based on sieve and pipette method (see Fig. 3.1 for locations).

The lowermost part of the Agh Band profile is characterized by a high content of fine-sand with maximum values > 30%. Also the U-ratio shows values larger than 12 whereas the clay-fraction is reduced to about 5 %. After that peak towards coarse grain-sizes a fining-up trend can be observed and the grain-size patterns within unit 4 clearly reflect the transitions between the pure loess deposits and the intercalated palaeosols (Fig. 3.12). The palaeosols are characterized by a shift towards finer grain sizes and for the lowermost BWy-horizon, the clay content increases to values > 35 % whereas the content of fine-sand decreases to values < 5 %.



In unit 3-1 (Figure 3.12) the grain-size data reflects the interplay between loess- and the banded features and the layering of the loess is indicated by short-scale shifts within the grain-size fractions. This might reflect rapid changes within the sedimentological system with short, intense dust accumulation periods and increasing- and decreasing wind-speed causing shifts towards coarser and finer grain-size distributions.

63

at least 2 longer-term coarsening- trends, probably pointing to an increase in wind speed, respectively.

Also in unit 2, characterized by high dust accumulation rates if considering the sediment thickness and corresponding luminescence ages, the fine-sand content points to several coarsening/ fining trends (Fig. 3.13) illustrating fluctuations in wind velocity during MIS 4 and the MIS 4-3 transition. Furthermore, changes of dust deflation areas and either more proximal or distal loess transport might explain the cyclicity reflected by the grain-size data. The clay content within unit 2 shows a smooth increase from the bottom to the top part of unit 2 and reaches values of about 17% at the upper part whereas the clay content is around 14 % at the bottom part of unit 2.

The grain-size data of unit 1 should be treated with care as intense reworking of the material surely affected the grain-size distribution of the loess. But the peak within the U-ratio illustrates the sorting of the material towards coarser grain-sizes, as also seen by a shift to low clay contents within the reworked material. Hence, due to that coarsening/fining-up pattern a reworking and sorting of the material by water is likely.

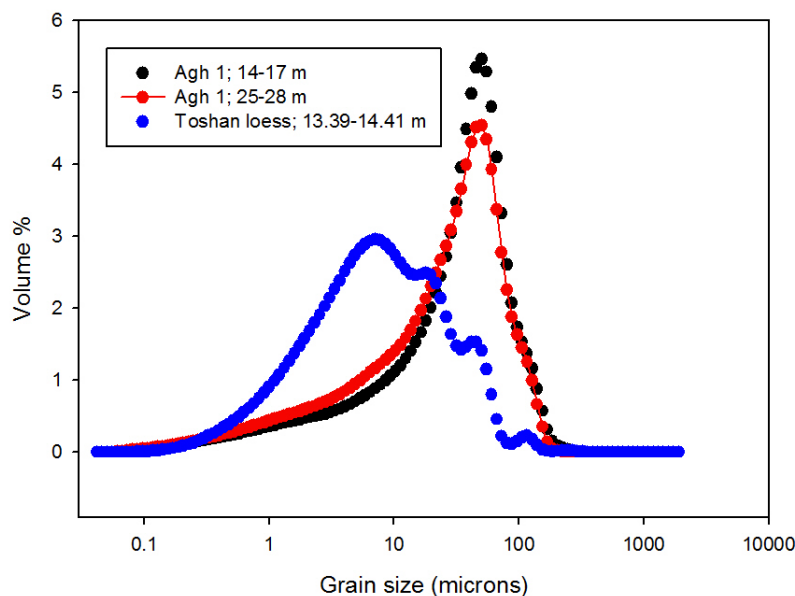


Fig. 3.14: Averaged mean grain-size curves from Agh 1 (14-17 m and 25 - 28 m profile depth) in comparison with loess from Toshan (see Vlamincx et al. 2016). The Agh Band loess shows, in contrast to the Toshan loess, a uni-modal distribution and is substantially coarser than the Toshan loess.

3.4.5 Interpretation of magnetic susceptibility data

The results of magnetic susceptibility data (K_{if} and K_{fd}) are shown together as a function of the profile depth (Fig. 3.12 and 3.13). The upper and middle parts of the Agh Band loess profile are characterized by low variability in both parameters and K_{fd} values < 3 indicate stable environmental conditions with limited weathering and soil formation. The bulk susceptibility mean value K_{if} of $338 \cdot 10^{-6}$ SI ($\triangleq 21 \cdot 10^{-8}$ m³/kg as specific susceptibility) fits well to data from the Chinese loess Plateau (CLP; Heller and Liu, 1991), where unweathered loess characterized by K_{fd} values below 3 (hardly super paramagnetic (SP) grains) show

bulk susceptibility mean values of $400 \cdot 10^{-6}$ SI. Only the bulk susceptibility data from the Bwy-horizons at the bottom part of the sequence (Agh Band 2) show characteristic peaks in both parameters indicating the enrichment/ neoformation of ferromagnetic particles in the course of pedogenesis after the “Chinese” model of magnetic enhancement (Heller et al., 1991).

A graphic display with whole rock K_{fd} values versus K_{lf} data, as suggested by Heller et al. (1991), for the Agh Band profile is shown in Fig. 3.15 in comparison with the data set from Baichaoyuan in the Western part of the Chinese Loess Plateau (Heller et al., 1991). The susceptibility data bear similarity. For both profiles most K_{fd} values lay below 3% with an overwhelming majority of bulk susceptibility data between 30 and $40 \cdot 10^{-5}$ SI. Frequency dependent data $>3\%$ with concurrent slightly higher values in bulk susceptibility in the Agh Band plot could be clearly assigned to the Bwy-horizon at the bottom part of Agh Band II profile.

After Heller et al. (1991) Baichayuan in the Western part of the Chinese LP is characterized by semi- arid climate with very low natural moisture content in the loess sediments and weakly developed soils. At Agh Band similar climatic conditions prevail. The resembling susceptibility data sets from both regions confirm the climatic analogy.

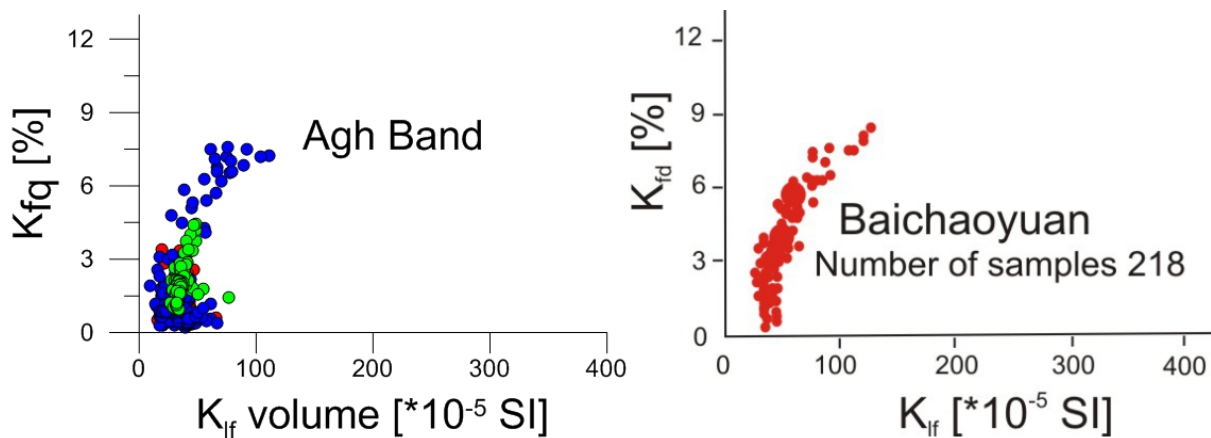


Fig. 3.15: Frequency depended susceptibility (K_{fd}) against low field susceptibility (K_{lf}) after the idea of Heller et al. (1991) for data from Agh Band in comparison to data from the western part of the CLP (Baichaoyuan). Both locations are characterized by semi-arid climate and the susceptibility data confirm climatic analogy.

3.4.6 Hiatuses within the Agh Band profile

The luminescence age estimates show that the Agh Band loess sequence covers the time range from MIS 7 to late MIS 2 (or MIS 2 – MIS 1 transition). The profile can be subdivided into several chronostratigraphical periods. These periods were obviously characterized by high dust accumulation rates and hence intense aeolian activity. A more detailed chronological subdivision of these units based on the pIRIR₂₉₀ ages is not possible due to the error-marks and the scattering among luminescence ages. The fact that the pIRIR₂₉₀ age estimates are in some cases reverse to each other might be explained by the intense bioturbation of the sandy loess deposits which most likely caused the incorporation of

younger and even recent grains into the in-situ loess. Hence, young grains mixed into the older loess might have caused age underestimation in some cases.

The pIRIR₂₉₀ ages also highlight several chronological gaps within the Agh Band loess-palaeosol sequence. The most significant hiatus occurs in Agh 2 (Fig. 3.16) where sediments from about 170 – 100 ka are missing.

Further chronological gaps occur in the upper part of Agh 1 where sediments corresponding to the period ~ 50-35 ka are most likely missing. Also the MIS 2 loess seems to be almost fully absent. Only at the top part of the profile loess from the transition of the late MIS 2 to the Holocene period is preserved. These chronological gaps represent periods of erosion, only minor loess-accumulation or a combination of both factors. Erosion most likely controlled the sediment budget significantly at Agh Band. Intensive rain falls causing extensive denudation of the silty-sandy material might have occurred after periods of aridity causing a minimization of the vegetation cover.

Minor loess accumulation might be explained by a more dense vegetation cover in the potential dust deflation areas causing landscape stability and a fixation of the silty-material.

For the sediment budget, also the significant sea-level changes of the Caspian Sea (Yanina, 2014) might have played an important role as sea-level high stands should have reduced the potential areas of dust deflation.

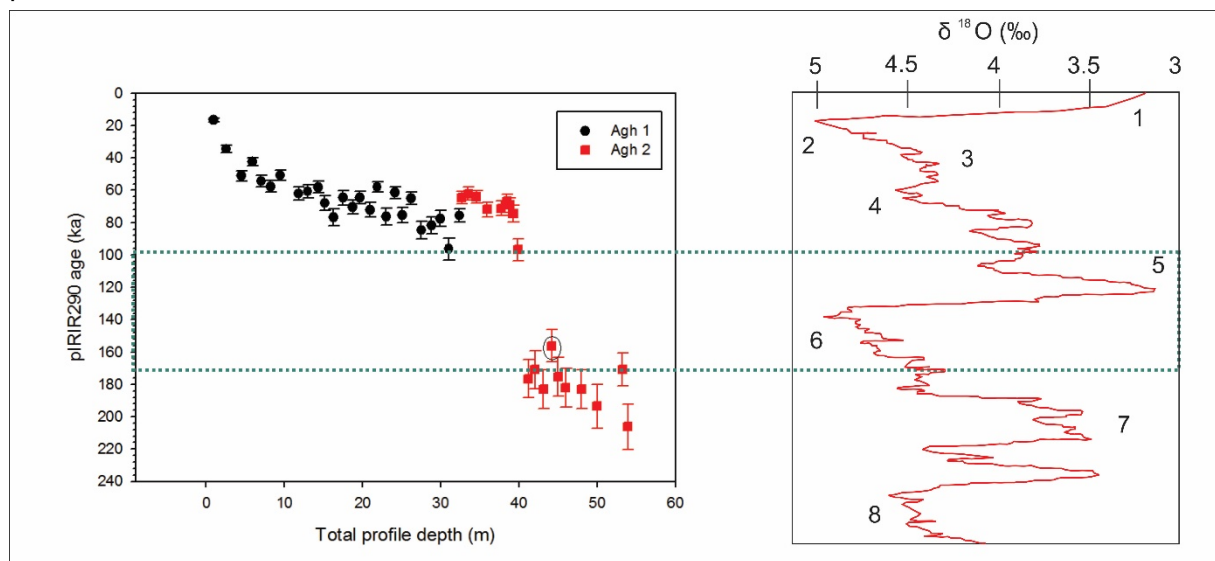


Fig. 3.16: Left; pIRIR₂₉₀-luminescence age estimates plotted against profile-depth. The green box indicates the chronological gap found in subprofile Agh 2. The age framed by the black circle is interpreted as underestimated. Right: Benthic δ¹⁸O record including marine isotope stages modified after Lisiecki (2005).

Nevertheless, Fig. 3.16 illustrates that in between 170 – 100 ka the global climate had undergone cooling and warming. Hence, it is unlikely that the absence of the about 170 – 100 ka deposits can be explained by a climate-controlled reduction of loess deflation in the source areas and limited loess-sedimentation at Agh Band. The hiatus can most likely be explained by an intensive erosion period probably occurring slightly before 100 ka, maybe at the climate shift from the last interglacial to glacial period.

3.4.7 Relation of the Agh Band loess-palaeosol sequence to other loess profiles in Northern Iran

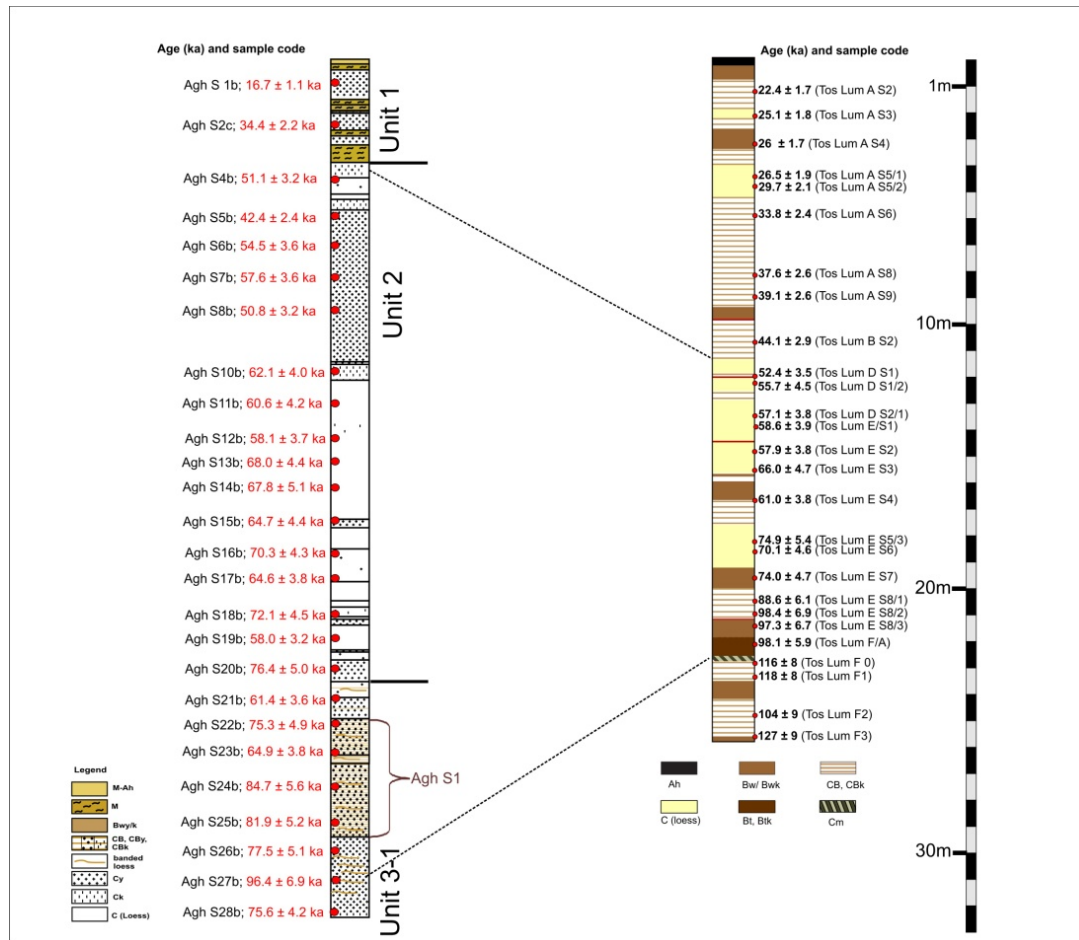


Fig. 3.17: Attempt of a correlation between the loess-sequences Agh Band (loess-plateau) and Toshan (foothills of the Alborz-mountains) based on pIRIR₂₉₀-luminescence age estimates. It is illustrated, that in periods during which the Toshan loess was strongly affected by soil-formation, the Agh Band area was most likely too dry and hence characterized by intense dust accumulation and almost no soil-formation.

The hitherto investigated loess sequences located at the foothills of the Alborz mountains (e.g. Kehl et al., 2005; Kehl, 2010; Frechen et al., 2009; Vlamincx et al., 2015; Lauer et al., 2017a) host a relatively good temporal resolution for the last glacial-interglacial cycle and are defined by several interstadial soils corresponding to the last interglacial period and a pedo-complex at the bottom parts of the sequences including well developed Bt-horizons most likely correlating to the last interglacial (Eemian, MIS 5e) period.

On the other hand, the pedocomplex at the bottom part of Agh Band is not correlating to the last glacial-interglacial cycle and the luminescence age estimates point to a formation of these soils during MIS 7 – MIS 6. The upper and middle part of the Agh Band loess is defined by only weak pedogenic overprinting in terms of changes in soil color in some profile parts and the CB-horizon in unit 3-1.

Based on the different lithological, pedogenetic and chronological characterization of the Agh Band loess in the loess plateau, if compared to profiles such as Toshan, Neka or Now Deh, a correlation is difficult.

Fig. 3.17 shows the pIRIR₂₉₀-luminescence ages of Agh 1 and the Toshan loess profile. The profiles are roughly correlated for the time period 100 ka – 50 ka. The fact that just one in-situ CB-horizon corresponding to the last glacial-interglacial cycle is preserved at Agh Band is explained on the one hand by erosion of parts of the sequence, as detected by luminescence ages. On the other hand high aridity and dust accumulation rates during MIS 5 and 4 may have impeded soil formation. Pedogenetic processes such as accumulation of organic matter, formation of structure or leaching of carbonate are only possible if there is sufficient edaphic moisture available. That was obviously the case on the foothills of the Alborz (more humidity and less dust accumulation), but not in the Agh Band area.

It is of importance, that soils correlating to the penultimate glacial-interglacial cycle are preserved at Agh Band indicating relatively humid climate conditions at around 190 – 170 ka (stage 7 to 6). Humidity should be regarded as the key factor controlling soil formation at Agh Band. During periods while last-glacial, interstadial soils were formed on the foothills of the Alborz, it was mostly too dry at the Iranian loess plateau.

3.5 Summary and conclusions

The Agh Band loess-palaeosol sequence hosts information about climatic shifts and changes in sedimentological regime in periods between MIS 7 to late MIS 2. Most likely, palaeo-precipitation rates played a key-role for the arrangement of the sedimentological system in the present-day semi-arid region. Climate and especially precipitation was most likely triggered by global-climate changes and e.g. shifts of the polar-front, but also sea-level changes of the Caspian Sea may have affected dust deflation thus accumulation rates too.

The pedocomplex at the bottom part of the profile yields luminescence ages indicating soil formation and hence increased humidity in between about 190 – 170 ka. In dryer periods with high dust accumulation rates, thick loess deposits were accumulated but these loess-sediments show almost no indication for soil formation, also reflected by low bulk magnetic susceptibility and frequency dependent susceptibility values. The significant chronological gap covering a time-span from about 170-100 ka indicates that an intensive erosion-period caused this hiatus. But also limited dust deflation and accumulation might have played a role. Due to the luminescence ages, the Eemian-interglacial soil is missing, and was probably eroded. The Agh Band loess sequence shows a good temporal resolution for parts of MIS 5 and MIS 4. The shifts in grain-size with several coarsening- and fining-up trends point to several changes in wind-speed.

The erosional layer and reworked soil material at the upper part of the Agh Band profile also illustrates that in the region periods of intense loess sedimentation were interrupted by erosion. The luminescence age of about 34 ka points to a more humid and erosional period during MIS 3. The top part of the profile represents a late period of MIS 2. Loess from the last glacial maximum is not found at Agh Band. The recent soil is almost fully missing and long-time human activity and farming in combination with semi-arid climate conditions and temporal intense rain-falls make the present day landscape very susceptible for erosion as seen by the dissection of the loess-landscape by gullies.

3.6 Acknowledgements

We are grateful to the technicians from the Leibniz Institute for Applied Geophysics (LIAG) Hannover (Germany) for work in the field and laboratory responsibilities. In detail we thank: Kathrin Worm for collecting samples in the field, Sonja Riemenschneider, Astrid Jäckel and Gudrun Drewes for grain-size measurements. Furthermore, we want to thank Sonja Riemenschneider and Ragna Bergmann for preparation of luminescence samples, Petra Posimowski for gamma spectrometry measurements and Lena Wallbrecht and Kathrin Worm for sample preparation and laboratory work (rock magnetic measurements).

The project “Northern Iranian loess and its palaeoclimatic implication” is founded by the German Research Foundation (DFG; project-number FR877/26-1, KE818/5-1).

The field work in Iran was only possible with the great help and hospitality of Iranian colleagues from Gorgan University.

Appendix

Table app. 3.1:

Stratigraphy of the Agh Band loess-palaeosol sequence. The table gives an overview about the thickness of the sedimentological layer and intercalated palaeosols. Please note that a more specific classification of the pedogenetic processes based on results of micromorphological studies colorimetric and MIRS analysis will be published elsewhere.

Unit	Profile depth (m)	Lithological/ pedological classification	Description/ characteristics
1	Subprofile Agh 1		
1	0-0.18	AC	Modern soil almost fully missing, only a very weakly developed, disturbed humic horizon can be found; low degree of compaction
1	0.18-0.4	CB	Disturbed, partly reworked sandy loess with thin rooting
1	0.4-1.52	Cy	Sandy loess with gypsum
1	1.52-1.94	CBy	Reworked soil material with gypsum, brownish color; in the upper part of the reworked soil substrate (1.5 m -1.7 m) loose structure
1	1.94-2.04	Sand-layer	Mainly fine-sand material; 2.5 YR 7/2
1	2.04-3.9	C(B)y	Reworked sandy loess and partly embedded reworked soil material; Slightly varying in color (10 YR 6/4 and 10 YR 7/4); Concretions of gypsum
2	3.9-4.48	Cky	Sandy loess with brighter color due to enrichment of secondary carbonate and gypsum
2	4.48-5.1	C(y)	Sandy loess with only minor content of (primary/ secondary?) gypsum
2	5.1-5.3	Cy	Sandy loess with gypsum
2	5.3-5.7	Cky	Sandy loess with precipitation of secondary carbonate and gypsum
2	5.7-11.44	Cy	Sand loess with gypsum, smooth variations in sediment-color (10 YR 7/2 – 10 YR 6/4)
2	11.44-11.54	Cy	Change in color to 10 YR 6/3
2	11.54-12.14	Ck	Sandy loess, weakly enriched in secondary carbonate
2	12.14-17.4	C	Sandy loess with smooth variations in color (10 YR 5/4 – 10 YR 6/4); reworking features (?), loess snail at 16.8 m
2	17.4–17.72	Cy	Sandy loess with gypsum
2	17.2-21.18	C	Sandy loess; first occurrence of brownish horizontal/ wavy laminates at about 19.4 m depth
2	21.18-21.4	Cy	Increased content of gypsum if compared to the capping strata
2	21.4-22.34	C	Sandy loess
2	22.34-22.42	Cy	Sandy loess with gypsum
2	22.4-22.72	C	Minor Mn-concretions; loess snail at 22.54 m depth; in parts weakly reddish color (hematite?). Wavy laminates (banded loess)
2	22.72-23.54	C(y)	Sandy loess with minor content of gypsum
3-1	23.54-24.92	C(By)	Weak pedogenetic overprinting, - in parts weakly developed reddish/ brownish color
3-1	24.94-29.44	CBy/CB	Slightly more intensive pedogenic overprinting if compared to the overlying loess, especially from 28.28 m depth on; variations in content of gypsum; partly banded loess with clear brownish, clay-enriched wavy layers.
3-1	29.44-32.46	Cy	Sandy loess with gypsum; characteristic layering (banded loess)

Subprofile Agh 2			
3-1	32.46-33.84	Cy	Banded loess, see bottom part of Agh 1; the banded loess was used as marker for the correlation of the bottom part of Agh 1 and the upper part of Agh 2
3-1	33.84-35.38	C	Sandy loess with banded structures
3-1	35.4-35.94	Cy	Sandy loess, partly banded; no banded structures between 35.4-35.54 m depth
3-1	35.96-36.02	C(M)	Sandy loess; partly layered (indicator for reworking ?)
3-2	36.02-36.2	C	Sandy loess
3-2	36.2-36.88	Cy	Sandy loess with gypsum; banded structures
3-2	36.88-37.34	Cy	No layering or banded structures
3-2	37.34-38.1	C	Loess, partly banded; less fine-sand content if compared to the overlying loess
3-2	38.1-39.76	Cy	Loess with gypsum
3-2	39.76-39.88	C	Increased silt content as compared to overlying loess; no gypsum
4	39.88-40.4	CBy	Concretions of gypsum; weak brownish color; coherent structure. The CB-horizon defines the upper boundary of unit 5
4	40.4-40.68	C	Highly compacted sandy loess
4	40.68-41.24	Cy	Increased content of gypsum; root channels; coherent soil structure
4	41.24-43.38	C	Sandy loess with only minor content of gypsum (only single concretions of gypsum); partly disturbed by krotovina; at 43.16-43.28 m depth silt bands (reworking-features ?)
4	43.38-43.78	CB	Pedogenic overprinting; Mn-concretions; some subangular blocky aggregates in a coherent matrix
4	43.78-44.1	CB	Pedogenic overprinting; minor content of humic material probably indicating the preservation of a fossil humic horizon. Coherent structure; partly disturbed by bioturbation
4	44.1-44.32	CBy	Stronger pedogenic overprinting as compared to the overlying material; less bioturbation; enhanced content of gypsum
4	44.32-44.88	Bwy	Palaeosol, enriched with gypsum; clear brownish color; subangular blocky aggregates in coherent matrix
4	44.88-48.94	Cy and C	Sandy loess; coherent structure; alterations of layers with and without gypsum; at around 46.78 m depth Mn-precipitations; loess partly disturbed by bioturbation. Smooth variations in color with probably initial pedogenesis between 48.66-48.94 m depth
4	48.94-49.02	CB	Transition to a weakly developed CB-horizon
4	49.02-49.18	CBy	Loess overprinted by weak pedogenesis; aggregates; subangular-coherent; gypsum
4	49.18-49.34	BCy	More intensive pedogenic overprinting; dominance of subangular blocky soil structure
4	49.36-49.9	Bwy(k)	Dark-brownish color; strongly developed; subangular locky structure; soil of interglacial character; increased clay content but no clay-coatings; well defined lower boundary of the Bwy
4	49.9-50.08	CBy(k)	Sandy loess with pedogenic overprinting; precipitation of secondary carbonate
4	50.08-53.2	C and Cy	Sandy loess; coherent structure; alterations of layers with and without gypsum; at around 50.8 m depth disturbance of the loess by bioturbation (probably also reworking of the unconsolidated material); Mn-concretions at 51.4 m depth; at 52.42 m depth coarse crystals of gypsum
4	53.22-53.4	C	Banded loess
4	53.4-54.04	C	Sandy loess

Chapter 4

130.000 years of loess and palaeosol formation:

Geochemical and rock magnetic properties of the
Toshan loess-soil sequence (NE Iran)

Vlaminck, S.^a, Rolf, C.^b, Franz, S.O.^c, Lauer, T.^d, Kehl, M.^a, Lehndorff, E.^e, Frechen, M.^b,
Khormali, F.^f

^a Institute of Geography, University of Cologne, Albertus Magnus Platz, 50923, Cologne, Germany

^b Leibniz Institute for Applied Geophysics (LIAG), Stilleweg 2, 30655, Hannover, Germany

^c Steinmann-Institute of geology, Mineralogy and Palaeontology, Nussallee 8, 53115, Bonn, Germany

^d Department of Human Evolution, Max Planck Institute for Evolutionary Anthropology, deutscher Platz 6,
D-04103, Leipzig, Germany

^e Institute of Crop Science and Resource Conservation, Soil Science and Soil Ecology, University of Bonn,
Nussallee 13, D-53115, Bonn, Germany

^f Department of Soil Sciences, Gorgan University of Agricultural sciences and Natural resources, Gorgan, Iran

-Formatting and orthography of the manuscript are adapted to the dissertation style-

Abstract

High dust accumulation rates during the late Pleistocene left extensive loess deposits in southern Eurasia. Northern Iran apparently formed a dust hotspot as indicated by thick late Pleistocene loess deposits located along the Alborz Mountains and the so-called Iranian Loess Plateau. These deposits are intercalated by a series of differently developed palaeosols, representing excellent terrestrial archives of climate change. In order to understand the dust and soil formation dynamics of the past, dust source areas and weathering intensities have to be known. Among the hitherto known section, the Toshan loess-soil sequence represents a key site. The inorganic geochemical inventory and rock magnetic properties of loess at Toshan might help to elucidate these dynamics for much of the past 130.000 years. We here put emphasis also on the relative sensitivity of our methods to palaeoclimate change as recorded in the Toshan section.

We present bulk mineralogical and geochemical data supplemented by a high resolution magnetic susceptibility record of the Toshan section. Our results suggest that loess in north-eastern Iran is derived from sediments that have undergone at least one phase of upper crustal recycling. Its immobile major elements composition ($\text{TiO}_2/\text{Al}_2\text{O}_3$) reveals a different provenance of loess along the Alborz Mountains as compared to loess in the Iranian Loess Plateau. Strongly developed palaeosols at Toshan are well recorded by ratios of Fe/Mg, Ti/Mg, Ti/Sr and Ba/Sr. However, these geochemical proxies are insensitive to weak pedogenic alterations attributed to MIS 3, whereas the latter were clearly identified by means of mass and frequency dependent magnetic susceptibilities. These records yield a saw tooth pattern during MIS 3, corresponding with a rapid development of moister soil environmental conditions favouring soil formation, followed by a gradual aridization promoting the formation of comparatively unweathered loess. It is therefore likely that these palaeosols formed during ongoing (syngenetic) dust accumulation. The discrepancy between the magnetic susceptibility record and the geochemical weathering proxies reflect the differential timing in the formation of magnetic minerals such as magnetite and maghemite as compared to the depletion in silicate minerals.

Keywords: Late Pleistocene, dust accumulation, soil formation, provenance

4.1 Introduction

In north-eastern (NE) Iran loess deposits with thicknesses of up to 70 m have developed from extensive dust accumulation during the Late Pleistocene (Kehl, 2010). Up to 9 periods of soil formation were observed for the last 130.000 years (Kehl et al., 2005), confirming the ongoing deposition of loess in NE Iran. However the source regions of these loesses were not yet identified.

As a clastic terrestrial sediment loess covers ca. 10% of the earth's land surface (Muhs and Budahn, 2006; Kehl, 2010). It may originate from different source regions (Hao et al., 2010) Its formation involves the production of mainly silt-sized particles as the result of physical

weathering of the exposed crust such as volcanic rocks by e.g. glacial grinding, fluvial comminution or salt weathering (e.g. Yaalon and Dan, 1974; McTainsh, 1987; Smalley and Derbyshire, 1990; Pye, 1995; Wright et al., 1998). However, numerous studies investigating the composition of immobile elements in loess such as e.g. the pattern of rare earth elements (REE) found a remarkable similarity as compared to the REE pattern of the upper continental crust (UCC) (Taylor et al., 1983; Taylor and McLennan, 1995; Gallet et al., 1996, 1998; Jahn et al., 2001; Hao et al., 2010). This homogeneity implies that loess is derived from well-mixed sedimentary protoliths being subject to several processes of upper crustal recycling (Gallet et al., 1996). Due to extensive silt producing mechanisms combined with its aeolian transport, loess provides a sediment approximating the average geochemical composition of the UCC (Taylor, 1983; Taylor and McLennan, 1995; Ujvári et al., 2008). Hitherto, it is not clear whether north-eastern (NE) Iranian loess represents originates from well-mixed sediments and/or sedimentary rocks. Frechen et al. (2009) state that the spatial extent of loess deposits in north eastern Iran is closely related to the vicinity of rivers in Golestan Province, suggesting that the floodplains of the rivers might at least represent the proximal dust source of the loess deposits at the sections Neka, Toshan, Now Deh and Agh Band. The inventory of major and trace elements might bear significant information on the geochemical assemblage of NE Iranian loess and thus offer valuable implications about its dust source.

Climate change is recorded by the degree of loess weathering. The granulometric, mineralogical and geochemical properties of loess on a global scale form similar physico-chemical starting conditions as parent material for the development of intercalated palaeosols (Ujvári et al., 2008). Palaeosols represent past land surfaces, which have formed on loess during interglacials and interstadials. Climatic conditions during interstadials are considered more humid than during stadials, promoting decalcification, mineral weathering and thus soil formation (Smykatz-Kloss, 2003; Buggle et al., 2011). The nature and degree of soil formation also depends on mineral assemblage of the parent material, hosting differential amounts of major and trace elements (McLennan, 1989). Chemical weathering including hydrolysis and protolysis and leaching, cause depletion of soluble mobile elements in soil horizons. Conversely, less soluble and immobile elements are enriched in palaeosols, implying a reduction in the amount of easily weatherable minerals such as e.g. plagioclase (McLennan, 1989; Buggle et al., 2011). Geochemical ratios allowing for the quantification of pedogenesis are therefore based on the selective removal of mobile elements and the enrichment of immobile elements as compared to the parental loess (Smykatz-Kloss, 2003; Buggle et al., 2011). However, the concept of loess deposition during intervals of cold and arid glacial climate alternating with post sedimentary palaeosol formation might reflect only part of the late Pleistocene dust dynamics in NE Iran, since dust deposition might have continued at reduced rates in the form of syngenetic soil formation during interstadials and interglacials (Vlaminck et al., 2016). In order to thoroughly characterize and determine different weathering conditions in strongly to weakly developed palaeosols throughout the late Pleistocene of NE Iran, sensitive and resilient geochemical proxies are needed. The results of this study might thus be of interest to loess research in other subhumid and semiarid regions on the globe.

The magnetic susceptibility has proven to be sensitive to even weak pedogenic alterations allowing for the distinction between highly weathered loess from relatively “unweathered” loess (Maher, 1998). Secondary minerals such as e.g. superparamagnetic iron oxides

affecting the rock magnetic properties of a weathering profile may be formed in situ as a function of moisture availability (Mullins, 1977; Maher, 1998; Cornell and Schwertmann, 2003; Maher et al., 2009). K_{lf} -intensity (low field magnetic susceptibility) reacts sensitively on the variation of ferro(i)-magnetic mineral concentrations whilst frequency dependent magnetic susceptibility (K_{fd}) allows to identify very small so called superparamagnetic (SP) grains. According to Dearing et al. (1996) the frequency dependence accounts for < 3 % in samples which are dominated by frequency independent stable single (SD) and multi domain grains (MD) whilst values above 3% indicate the presence of SP grains. Considering the Chinese model of magnetic enhancement in loess-palaeosol sequences introduced by Heller and Liu (1982), SP grains reflect soil forming processes due to the neoformation of magnetic minerals with grain sizes of SP character (< 0.03 μm for magnetite) as well as with SD and MD character. As a result values in K_{lf} and K_{fd} are found increased and thus allow distinguishing soils and highly weathered loess from relatively “unweathered” loess. Hence, variations in magnetic properties are mainly climatically controlled. As climatic fluctuations produce changes in sedimentary and soil-forming environments the changing magnetic properties may reflect alternating cold/dry or warm/humid climates during the Quaternary (e.g Mullins, 1977; Heller and Liu, 1982; An et al., 1991; Heller and Evans, 1995; Maher, 1998, 2009; Maher and Thompson, 1995; Evans and Heller, 2003; Rolf et al., 2014). Jahn et al. (2001) state that a comparison of the rock magnetic and geochemical proxies in palaeosols is complicated, since the rate of susceptibility enhancement might differ from the rate of mineral transformation and chemical alteration. Conversely, Bokhorst et al. (2009) successfully correlated the magnetic susceptibility signature of loess from Serbia and Ukraine with alkaline element ratios from bulk chemical analyses of the respective profiles. It is therefore important to test whether geochemical proxies in relation to rock magnetic properties yield comparable results in NE Iranian loess.

Scientific contributions to the geochemical composition of northern Iranian loess and palaeosols are scarce. A first comparison of the mineralogical and chemical inventory of the loess-soil sequences at Neka, Now Deh and Agh Band, was provided by Kehl (2010). This investigation was based on X-ray diffraction (XRD) analysis offering semi-quantitative estimates of general mineral assemblages and X-ray fluorescence measurements (XRF) for determination of the geochemical composition. Accordingly, the relative proportions of minerals such as quartz and feldspar suggest a petrologic homogeneity between loess and/or palaeosols. Strongly developed Bt-horizons exhibit a tendency of reduced plagioclase content as compared to parental loess (Kehl, 2010). The major element composition indicates a similarity within Northern Iranian loess and to the geochemical composition of other loess on the globe. In contrast, trace elements considerably scatter in loess and palaeosols from the sections at Neka, Now Deh and Agh Band (Kehl, 2010).

Asadi et al. (2013) combined mineralogical and geochemical investigations on bulk samples of loess in Golestan Province (NE Iran). Accordingly, the geochemical composition of loess deposits in the region is controlled by phyllosilicates such as muscovite, chlorite, illite and by heavy minerals e.g. zircon and tourmaline. The Golestan loess deposits exhibit uniform chemical characteristics, implying similar alteration processes (Asadi et al., 2013).

Frechen et al. (2009) provided, although fragmentary, the first rock magnetic investigations on Neka section, inferring the magnitude of weathering as based on the mass susceptibility of loess and palaeosols. Recently, Lauer et al. (2017b) presented a high resolution magnetic

susceptibility record of the 54 m thick loess-sequence at Agh Band located in the Iranian loess Plateau. Ghafarpour et al. (2016) investigated the rock magnetic properties of Mobarakabad section, situated in the vicinity of Now Deh section (Fig. 4.1).

Vlaminck et al. (2016) and Lauer et al. (2017a) introduced the loess-soil sequence of Toshan presenting high-resolution records of grain-size, colour and CaCO_3 , as well as a detailed chronostratigraphic framework based on luminescence dating. The Toshan sequence complements the known sections at Neka, Now Deh and Agh Band to establish a pedostratigraphic record of the north-eastern Caspian Lowland (Vlaminck et al., 2016). Estimations of relative intensities of soil formation were basically inferred from the contents of clay-sized particles ($< 5.5 \mu\text{m}$), the content of CaCO_3 and the Redness Index (RI) by Barrón and Torrent (1986). The contents of clay and the RI values are increased in palaeosols as compared to loess, likely due to the neoformation of siliceous clay and the pigmenting effect of hematite respectively. Most palaeosols are depleted in CaCO_3 , while precipitation of secondary calcite caused recalcification, particularly in the palaeosols attributed to marine isotope stage 3 (MIS 3) (Vlaminck et al., 2016; Lauer et al., 2017a).

Toshan site includes 26 m of loess in which at least 9 palaeosols are intercalated (Vlaminck et al., 2016) showing differential degrees of soil development. Thus, the Toshan section gives an excellent opportunity to study different weathering conditions in loess and palaeosols during the late Pleistocene in NE Iran. Results of mineralogical and geochemical analysis on 33 samples of unweathered loess and palaeosols extracted from the loess-soil sequences at Neka, Now Deh and Agh Band (Kehl, 2010) are considered for comparison. The mineralogical, geochemical and rock magnetic inventory of loess and palaeosols bear information about i) the comparative sensitivity of geochemical climate proxies with the high resolution magnetic susceptibility record towards differentially developed palaeosols ii) variations in loess and dust source composition in NE Iran and its relation to the UCC.

4.2 Study area

In the southern part of Golestan Province loess is found along the northern foothills of the Alborz Mountains (Fig. 4.1). In the north eastern part of Golestan Province loess deposits cover the westernmost part of the Kopet Dagh Mountains, forming the so called Iranian loess plateau (Fig. 4.1). In both mountain ranges loess is unconformably overlying the respective bedrock. Along the Alborz Mountains the bedrock is mainly composed of Jurassic limestone and metamorphic rocks such as the Gorgan schists, whilst in the Iranian loess plateau the bedrock largely consists of Cretaceous shales and limestones (Fig. 4.1).

These loess-soil sequences are located along a modern precipitation gradient spanning the range from subhumid conditions in the west near Neka to semiarid conditions towards the north and north-east at Agh Band. The profiles represent a climosequence including climatophytomorphic modern soils, which show differential degrees of soil formation, expressed by their respective morphology, clay mineralogy and their physicochemical properties corresponding to decreasing humidity from W to E (Khormali and Kehl, 2011). The majority of precipitation is associated with the months from September to March (Molanejad et al., 2015). The main driving force of precipitation along the southern coast of the Caspian Sea during these months is attributed to westerly cyclones which originate primarily from the

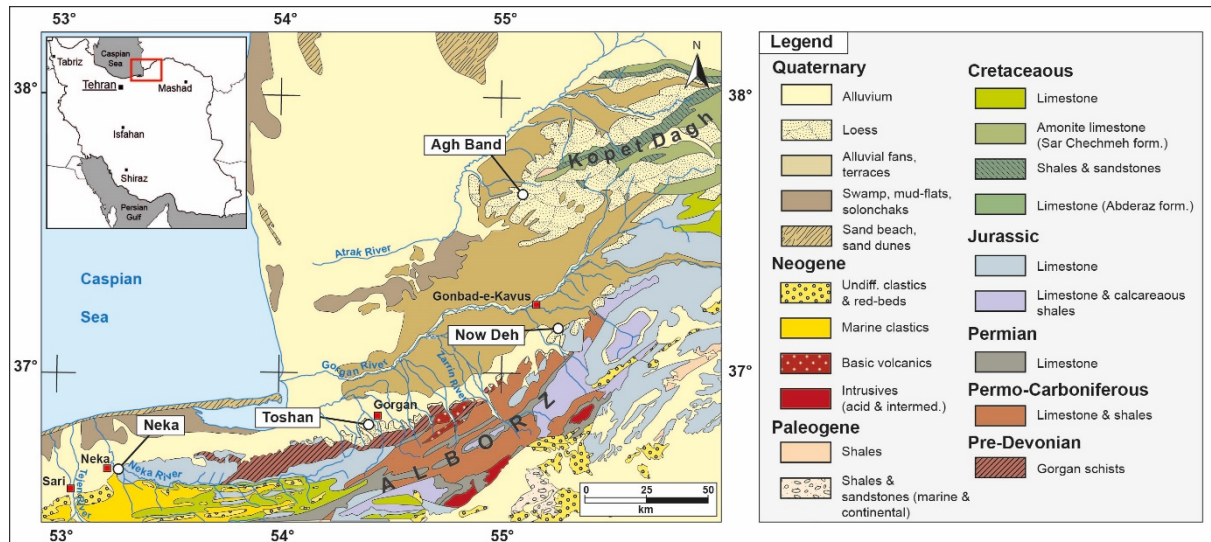


Fig. 4.1: Simplified geological map 1:1000000 of North-eastern Iran, displaying the different lithologies in the vicinity of the loess-soils sequences at Neka, Toshan, Now Deh and Agh Band (modified from Geological Survey of Iran, 1991).

Eastern Mediterranean Sea intruding into the southern Caspian Lowland (Molanejad et al., 2015; Molavi-Arabshahi et al., 2016). In contrast to these meso-scale climatic patterns upon the precipitation along the southern coast of the Caspian Sea also local influences from the Caspian Sea itself have to be taken into account. Nouri et al. (2013) have shown that cloud formation over the Caspian Sea is strongly related to its sea surface Temperature (SST), causing orographic precipitation along the Alborz Mountains. This effect is diminished from West to East (Molavi-Arabshahi et al., 2016).

4.2.1 The loess-soil sequence at Toshan

The Toshan loess-soil sequence is located on the Northern foot slopes of the Alborz Mountain range, in immediate vicinity to the City of Gorgan (Fig. 4.1). In this region the Alborz Mountains are drained basically by tributaries of the Gorgan River. Loess deposits in the region attain thicknesses of up to 30 m, whilst the Toshan section itself has an overall thickness of 25.75 m. An abbreviated description of the palaeosol found at the Toshan loess-soil sequence is given in table 4.1. The Toshan section hosts a strongly developed reddish-brown argillic palaeosol (Bt), as well as eight moderately to weakly developed brownish palaeosols (Bw/Bwk), covering at least the past 130 ka (Lauer et al., 2017a). For a thorough profile description of the loess-soil sequence at Toshan the reader is referred to Vlaminc et al. (2016).

These deposits disconformably overlay metamorphic rocks known as the Gorgan Schists (Geological Survey of Iran, 1991; Allen et al., 2003). The Gorgan Schists are considered to be metamorphic relicts of the Palaeo-Tethyan collision in the Late Triassic (Allen et al., 2003). To the south and south-east of Toshan Jurassic and Permo-Carboniferous limestones basically define the rock assemblage of the Alborz Mountain range (Fig. 4.1). These limestones host intercalated layers of carbonaceous shales, sandstones and conglomerates (National Geological Survey of Iran, 1991). To the east of the Toshan section Neogene basic

volcanics are located. According to Castro et al. (2013) these rocks mostly consist of trachybasalt and basaltic trachyandesite exhibiting shoshonitic (potassium-rich) signatures.

Table 4.1:

Brief description of palaeosols (3-1 to 6-2) and the modern soil (1-1). The soil horizons were denominated according to WRB (2007). The palaeosols were numbered depending on their allocated stratigraphic unit and their position within this unit. Hence, the first palaeosol of unit 3 is referred to as soil 3-1. Structure, pedofeatures and the estimated degree of soil development are based on field findings and micromorphological analyses (Vlaminck et al., 2016). Loess strata (L1 to L4) were excluded from this description due to their homogeneous characteristics in terms of color, CaCO_3 -content and structure. This holds true also for CBk-horizons. These horizons are characterized by partial decalcification, coherent to subangular blocky structure, thus representing a transitional stage between C and B horizons in which features of the parental loess still prevail. For a thorough description of the Toshan loess-soil sequence the reader is referred to Vlaminck et al. 2016.

(soil) no.	horizon	color	structure	features	estimated degree of soil development	soil type
1-1	Bwk	dark brownish	angular to subangular blocky	weakly recalcified (powdery lime), krotovina	strongly developed	<i>calcic</i> Kastanozem
3-1	Bwk	light brownish	subangular blocky	weakly recalcified (powdery lime), krotovina	weakly developed	palaeosol
3-2	Bwk	light brownish	subangular blocky	weakly recalcified (powdery lime)	weakly developed	palaeosol
5-1	Bwk	moderately brownish	subangular blocky	strongly recalcified (pseudomycelia), overlying charcoal layer	moderately developed	palaeosol
5-2	Bwk and ABwk	dark brownish	angular to subangular blocky	weakly recalcified, Mn-mottling	strongly developed	palaeosol
5-3a	Bwk	reddish brown	angular to subangular blocky	weakly recalcified, Mn-mottling	moderately developed	palaeosol
5-3b	Bt	reddish brown	angular blocky to prismatic	weakly recalcified, Mn-mottling, clay coatings	strongly developed	palaeosol
6-1	Bwk	moderately brownish	subangular blocky	moderately recalcified (pseudomycelia), Mn-mottling	moderately/weakly developed	palaeosol
6-2	Bwk	moderately brownish	subangular blocky	moderately recalcified (pseudomycelia), Mn-mottling	moderately/weakly developed	palaeosol

4.3 Materials and methods

4.3.1 Magnetic susceptibility

Scratched sediment material was taken at the Toshan profile for investigation of rock magnetic proxies (low field susceptibility K_{lf} and frequency dependent susceptibility K_{fd}). This material was dried, homogenised and pressed into plastic cubes (8 cm³) in the rock and palaeomagnetic laboratory of the Leibniz Institute for Applied Geophysics (LIAG). Thus, we were able to collect 695 non-oriented samples allowing for a highly resolved record of K_{lf} and K_{fd} in 4 cm increments.

X_{lf} of all samples was measured using a frequency and field variable Magnon VSM Susceptibility Bridge (Magnon; Dassel Germany) which was also used for determining K_{fd} (at 505 and 5050 Hz).

4.3.2 Geochemical and mineralogical analysis

Bulk samples were dried at 105 °C for 24 h and homogenized with a vibratory disk mill (tungsten carbide grinding set) for mineralogical and geochemical analyses. Powdered press pills were analysed for trace elements (Sc, V, Cr, Co, Ni, Zn, Ga, As, Rb, Sr, Y, Zr, Nb, Cs, Ba, La, Ce, Nd, Sm, Hf, W, Pb, Th, U) and fused discs for major and minor (Na₂O, MgO, Al₂O₃, P₂O₅, SO₃, K₂O, CaO, TiO₂, MnO, Fe₂O₃) elements by a wavelength dispersive X-ray fluorescence (Axios, 3kW, PANalytical GmbH). The loss on ignition (LOI) was determined after heating to 1100 °C for 2 h.

Qualitative mineralogical data was obtained by X-ray diffraction (XRD) of powdered bulk samples using a Bruker AXS D8 Advance. Operation conditions were: voltage (kV): 30, current (mA): 40, scan range (°2 θ): 4-70, step size (°2 θ): 0.04, counting time (s): 2, divergence slit: V20, anti-scatter slit: V20, detector slit: 0.2 mm. The raw data was evaluated using MacDiff software (version 4.2.5). Our analytical data showed an enrichment of tungsten and copper caused by the tungsten carbide grinding set. These trace elements were therefore excluded from discussion. As, La, Pb, U showed slightly higher values, whilst Hf and Sm exhibited lower values. In order to present a reliable data set As, La, Pb, U, Hf and Sm were excluded as well. Mineral identifications were based on evaluations of prominent intensity peaks. Conversely, the nature of heavy minerals was determined microscopically on three samples belonging to L4 and samples from a depth of 18.5 to 19 m.

4.3.3 Geochemical parameters and ratios

Canonical ratios such as e.g. K/Na, K/Rb were calculated for each sample as based on the entire data set of the selected major and/or trace elements. The data set comprises sample numbers TOS-1 to TOS 52 given in tables 4.2 and 4.3. In order to study the elemental behavior within a vertical succession these ratios were plotted as depth profile in comparison with our physical stratigraphy being based on field findings, micromorphological, granulometric and colorimetric results (Vlaminck et al., 2016). Biplots of selected major and

trace elements are based on the entire data set of the Toshan loess-soil sequence as well as selected samples from the section Neka, Now Deh and Agh Band considered for comparison. These biplots are supplemented by fields representing the composition of the upper continental crust and shales taken from Taylor and McLennan (1985) and Condie (1993). This supplementary data serves for a graphical comparison of elemental abundances in relation to the UCC and shales.

Spidergrams shown in Fig. 4.5 display the abundances of trace (Sc, Mn, Cu, Zn, Ga, Rb, Sr, Y, Zr, Nb, Ba, Ce, Nd, Th, V, Cr, Ni and Cs) and major (Na, Mg, Al, Si, P, K, Ca, Ti, and Fe) elements normalized to the average composition of the UCC being based on data from McLennan (2001). The number of interfering spidergrams in Fig. 5 A to D is limited to a maximum of 4 to maintain readability. Each spidergram represents an arithmetic mean of the respective strata put in relation to the UCC.

The degree of weathering was quantified using the Chemical Proxy of Alteration (CPA) (Buggle et al., 2011; Buggle et al., 2013) and the Chemical Index of Alteration (CIA) (Nesbitt and Young, 1982). The CPA basically relies on Na as mobile element and Al as its immobile counterpart and may be considered as proxy of silicate weathering e.g. of Na-rich plagioclase applicable to loess and palaeosol sequences without notable contents of soluble salts (Buggle et al., 2011).

The CPA was calculated according to $CPA = 100 \times Al_2O_3 / [Al_2O_3 + Na_2O]$. Buggle et al. (2011) suggest to divide by the Al_2O_3 content and to multiply with 100 in order to restrict the CPA to values between 0 and 100, thus avoiding out-of-scale variations when Na contents is low. The molar proportions of Al_2O_3 and Na_2O are used for calculation. Furthermore, this index excludes Ca as mobile element, whose amount is mainly governed by the presence of $CaCO_3$ in the loess-palaeosol sequences at Toshan.

The CIA represents a widely used index of subaerial weathering (e.g. Fedo et al., 1995; Gallet et al., 1998; Jahn et al., 2001; Ujvári et al., 2008; Galovic et al., 2011; Asadi et al., 2013; Kühn et al., 2013). It takes into account the molar proportions of Al as immobile element as well as Na, K and Ca as mobile elements. The latter ones are thought to represent elements bound to silica. Therefore, the Ca-values were corrected according to the procedure described by McLennan (1993), assuming that the ratio of Na/Ca does not exceed 1. The corrected data was also used for the A-C-NK diagram shown in Fig. 8.

The determination of quantitative alteration of major elements in palaeosols with respect to loess is shown in a gain-and-loss calculation (Fig. 4.4). The calculation was done by dividing the content of a given oxide from palaeosol by the content of the same oxide from loess ($[oxide\ palaeosol / oxide\ loess] \times 100$) (Garrels and Mackenzie, 1971; Gallet et al., 1996; Jahn et al., 2001; Kehl, 2010). However, such a gain-loss determination is based upon the following requirements: 1) All palaeosols have formed on airborne dust (loess) being deposited during cold/arid palaeoclimate prior to a climatic interval favoring pedogenesis. This assumption excludes the syngenetic formation of palaeosols. 2) The existence of (parental) loess subjacent to each pedomember. 3) The oxide composition of this loess reflects the geochemical composition of the parental material at the onset of palaeosol formation.

4.4 Results

4.4.1 Mineral assemblage

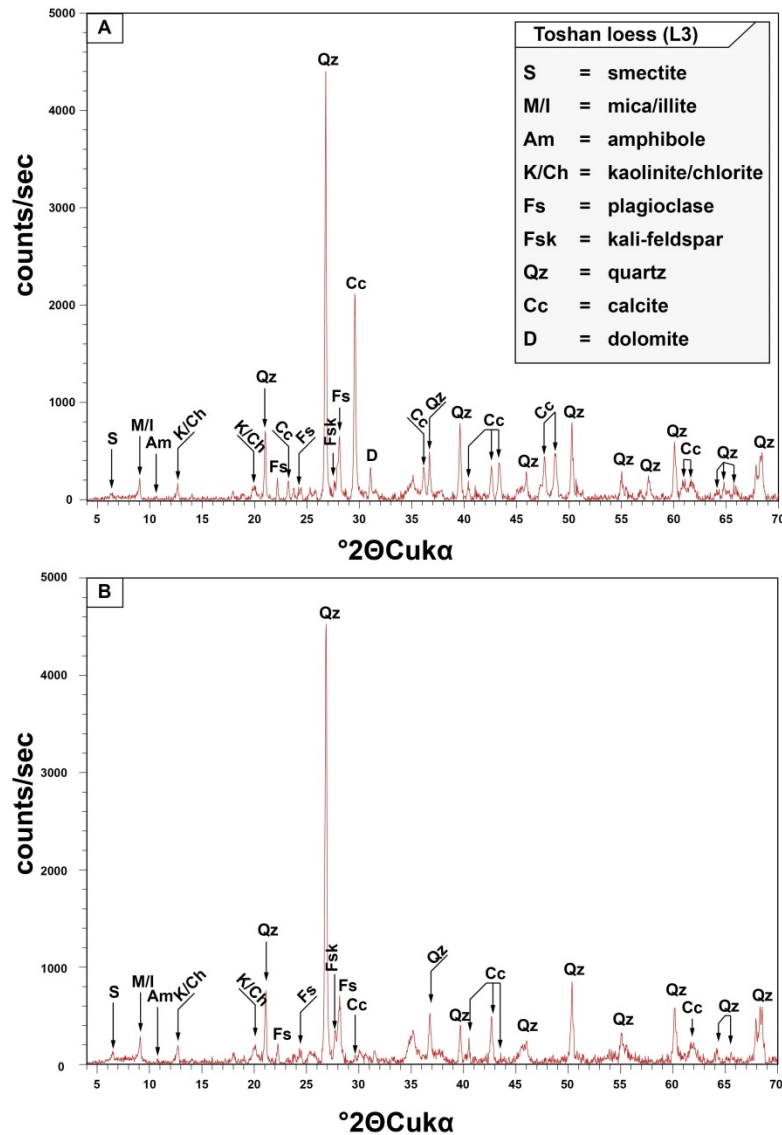


Fig. 4.2 A: X-ray diffractogram showing the main mineral assemblage in loess at Toshan as parent material for soil formation. This sediment at a depth of 13.19 m is attributed to MIS 4 and represents the most “typical” loess at Toshan (Vlaminck et al. 2015, Lauer et al. 2016). **B:** X-ray diffractogram indicating the assemblage of main minerals within soil 5-3b. This Bt-horizon is believed to be the most strongly weathered soil of the entire loess-soil sequence at Toshan and possibly formed during MIS 5e (Vlaminck et al., 2016, Lauer et al. 2017a). The X-ray diffractograms were evaluated using MacDiff 4.2.5 software. The primary peaks in this diffractogram are labeled with an abbreviation of the minerals identified. The abbreviation used for labeling is referred only to the mineral exhibiting the highest intensity within the respective 2Theta interval. In order to maintain visual clarity interfering minerals were excluded from labeling

Figure 4.2 shows two X-ray diffractograms from the most “typical” loess L4 (Fig. 4.2 A) and palaeosol 5-3b (Fig. 4.2 B) which represent the most strongly developed palaeosol found at Toshan section (Vlaminck et al., 2016). The loess strata in Fig. 4.2 A is attributed to MIS 4, whilst correlation of palaeosol 5-3b with MIS 5e is not certain (Vlaminck et al., 2016; Lauer et al., 2017a). The diffractogram shown in Fig. 4.2 A does not represent the parent material of

palaeosol 5-3b. Thus, a comparison of both strata bears on the assumption of mineralogical homogeneity of the parent material both in nature and abundance of the primary minerals. Based on X-ray diffraction analysis loess as parent material for soil formation at the Toshan section contains quartz (Qz)>calcite (Cc)>plagioclase (Fs)> dolomite (D)> mica/illite (M/I)> potassium-feldspar (Fsk)> kaolinite/chlorite (K/C)> smectite (S)> amphibole (Am) (in a sequence of decreasing abundance). Additionally, the nature of heavy minerals was determined microscopically. The composition of these minerals comprises zircon, apatite, rutile, anatase, brookite, epidote, amphibole, pyroxene and pyrite. According to Fig. 4.2B soil 5-3b exhibits a comparable mineralogical inventory. The most distinct difference within this diffractogram as compared to loess (Fig. 4.2 A) is the decrease in calcite (Cc) and dolomite (D).

4.4.2 Composition of major elements

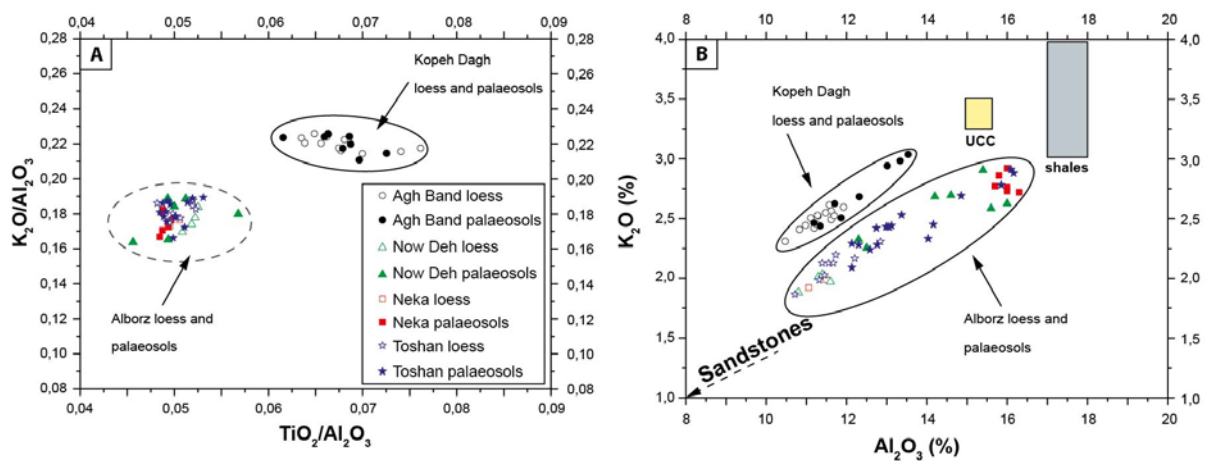


Fig. 4.3: Biplots comparing the K_2O/Al_2O_3 vs. TiO_2/Al_2O_3 ; K_2O/Al_2O_3 ratios of loess and palaeosols from the sections at Neka, Now Deh, Agh Band and Toshan with respect to the composition of the upper continental crust (UCC) and shales. The major elements composition of Neka and Now Deh loess and palaeosols was taken from Kehl (2010) and the data for UCC and shales was taken from McLennan (2001). Palaeosols are illustrated by geometric forms being entirely filled with one color, whereas the fill color of symbols indicating loess is white.

The bulk composition of major elements is given in table app. 4.2. Loss on ignition (LOI) spans a range from 5.26 to 21.24 wt%. LOI and CaO-content yield a positive correlation of $r=0.97$ ($n=52$), being significant at confidence level of $>99.9\%$. Hence, LOI and CaO-content encompass the primary and secondary $CaCO_3$ content of loess and palaeosols, respectively. Clay minerals and organic matter, being destructured during heating to $1100^\circ C$, as well as the release of hygroscopic water may slightly affect the mass balance of LOI. SiO_2 contents of the entire data set comprising both loess and palaeosols samples amounts for 43.49 to 63.93 wt%. The range of Al_2O_3 content spans 10.55 to 16.16 wt% whilst K_2O amounts attain 1.85 to 2.91 wt%. Na_2O content ranges from 0.63 to 2.04 wt% and the weight-percentage of Fe_2O_3 comprises 4.11 to 7.83 wt%.

Al_2O_3 and SiO_2 show a strong statistical relationship in loess and palaeosols ($r=0.91$; $p>99.9\%$) reflecting the presence of aluminosilicates such as mica and feldspar (Újvári et al.,

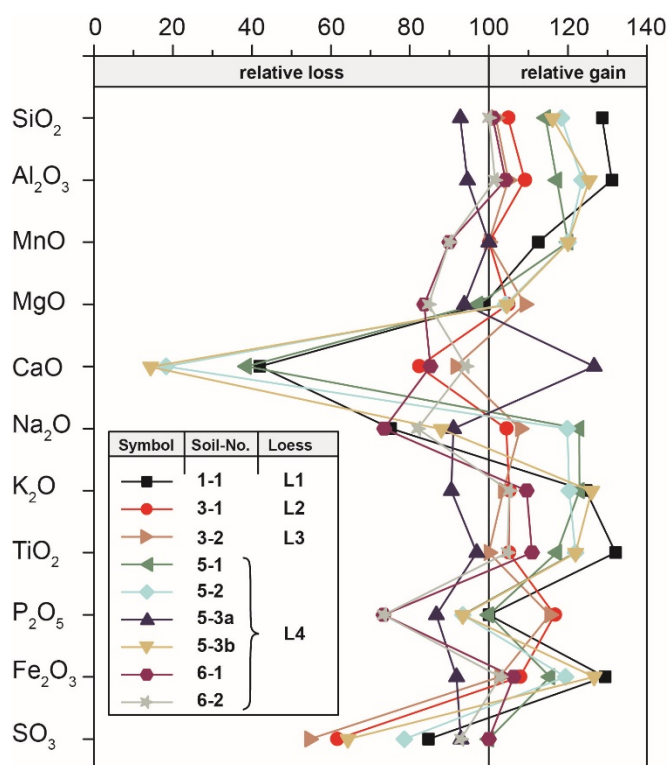


Fig. 4.4: Determination of quantitative alteration of major elements in palaeosols with respect to loess as based on Garrels and Mackenzie (1971). The calculation was done by dividing the content of a given element from altered material (palaeosol) by the respective content from the relatively unaltered sediment (loess) ([oxide palaeosol/oxide loess] * 100).

likely represents a relative enrichment due to the dilution effect of CaCO_3 being dissolved by meteoric water (Gallet et al., 1996). The gain and loss (Fig. 4.4) calculation confirms the results shown in Fig. 4.3. Most palaeosols have experienced a substantial loss in CaO , P_2O_5 , MgO and SO_3 contents which have resulted in the relative enrichment of insoluble/immobile elements such as SiO_2 , Al_2O_3 , K_2O and TiO_2 . Thus the major effect may be attributed to the dissolution of CaCO_3 .

2008). The strong correlation of K_2O and Al_2O_3 ($r = 0.94$; $p > 99.9\%$) confirms the presence of mica and may identify feldspar in the samples as K-feldspar. Conversely, Na_2O and SiO_2 exhibit a weaker statistical relationship ($r = 0.65$; $p > 95\%$) likely indicating the existence of Na-rich plagioclase, which is part of the mineral assemblage of loess at Toshan as shown in Fig. 4.2A. TiO_2 is highly correlated with MnO ($r = 0.95$; $p > 99.9\%$) and Fe_2O_3 ($r = 0.92$; $p > 99.9\%$), suggesting that TiO_2 is primarily associated with rutile-type minerals in which both Mn^{3+} and Fe^{3+} may be incorporated (Farges, 1999).

Biplots in Fig. 4.3 give a graphical comparison of the geochemical behavior of TiO_2 , K_2O and Al_2O_3 in loess and palaeosols. Generally, palaeosols exhibit higher proportions of TiO_2 , K_2O and Al_2O_3 approaching the average composition of shales and the upper continental crust. This increase most

4.4.3 Trace elements and UCC-normalized spidergrams

The trace element assemblage in loess and palaeosols is given in table app. 4.3. As shown in Fig. 4.5A most trace elements (Sc, Mn, Cu, Ga, Rb, Sr, Y, Zr, Nb, Ba, Ce, Nd, V, Cr, Ni) in loess are confined between 0.5 and 1.5 of upper crustal abundances. This pattern holds true also for the major elements Mg, Al, Si, P, K, Ti, and Fe. Spidergrams referring to loess 1 to loess 4 (Fig. 5 A) exhibit a homogeneous pattern with minor variations. Loess at Toshan sequence is slightly depleted in high field strength elements (HFSE) such as Th, Zr, Nb, Y and P, whilst Ti is enriched relative to UCC. Large-ion lithophile elements (LILE) K, Rb, Sr and Ba exhibit lower abundances than those of the UCC except for Cs, being considerably enriched. Ferromagnesian transition elements Fe, V, Cr, Ni and the light rare earth (LREE)

elements such as Ce and Nd attain values of nearly 1 in relation to upper crustal abundances. Among the ferromagnesian transition elements, Sc exhibits the largest variation, spanning the range from 0.5 to nearly 1 relative to UCC.

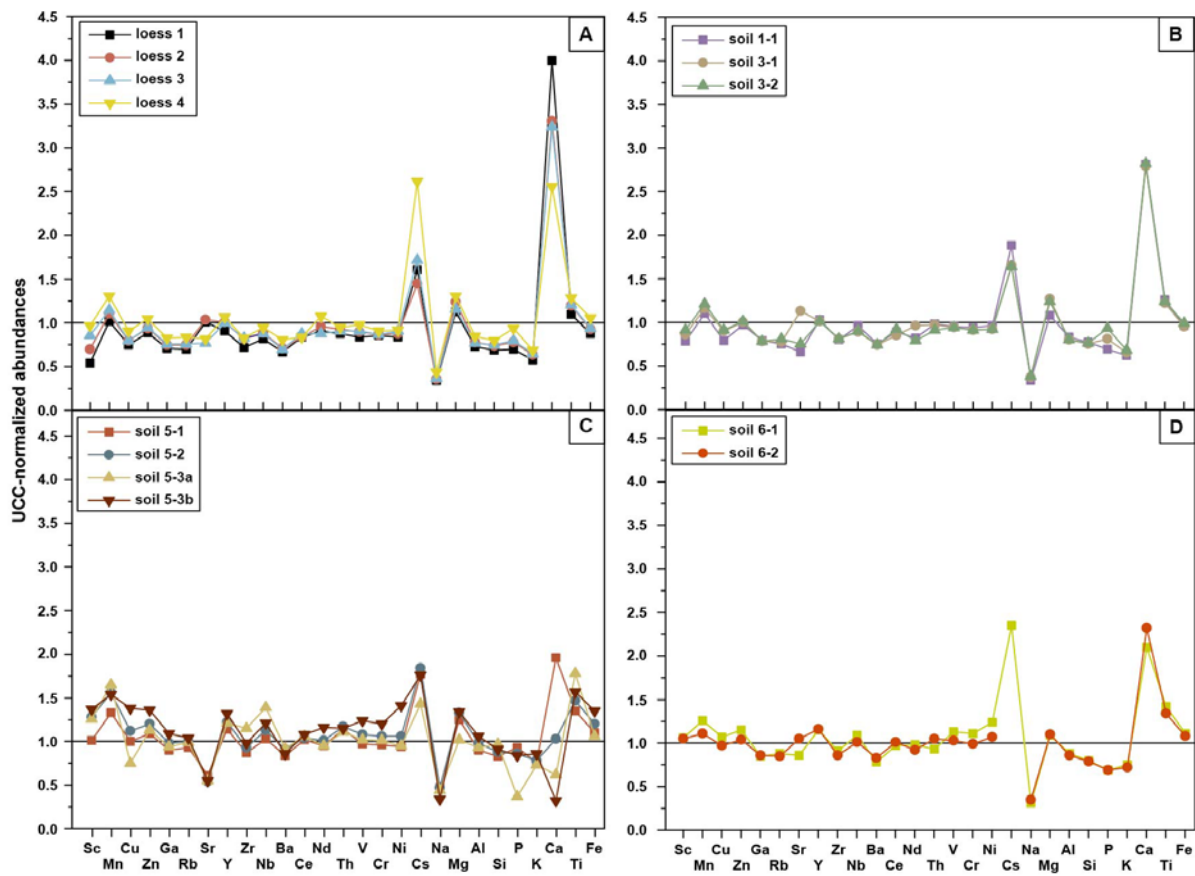


Fig. 4.5: Spidergrams showing the composition of major and trace elements in loess (A) and palaeosols (B to D) normalized to the average geochemical composition of the upper continental crust. The element abundances of UCC used for normalization were taken from McLennan (2001). The number of interfering curves was restricted to a number of 4 in order to maintain readability. Each curve represents an arithmetic mean of the data set of the respective strata. Conversely, the data referring to palaeosols 6-1 and 6-2 (D) were converted directly, since there was merely one sample analyzed for each of both palaeosols. Please note that, Cs-value for palaeosol 6-2 (D) was beyond detection limit and is hence missing in this spidergram.

Both trace and major element abundances in palaeosols (Fig. 4.5B to C) basically range between 0.5 and 1.5. Within this range pronounced differences exist as compared to UCC-normalized patterns in loess (Fig. 4.5C). Spidergrams shown in Fig. 4.5B and C exhibit merely small differences and seem to parallel the trace and major element signature of loess. However, HFSE and ferromagnesian transition elements tend to be enriched relative to UCC and loess (Fig. 4.5A). These trends are most pronounced in Fig. 4.5C comprising spidergrams of the most strongly developed palaeosols found at Toshan loess-soil sequence. Accordingly, the HFSE Th, Zr, Nb, Ti, Y and the ferromagnesian trace elements V, Cr, Sc, Ni exhibit a distinct enrichment. The LILE K, Rb, Ba behave similarly and are systematically found enriched in palaeosols. Furthermore, these elements show a range of high correlation with Al_2O_3 , reaching from $r = 0.83$ to $r = 0.95$ ($p > 99.9\%$), suggesting that their geochemical behavior might be governed by adsorption onto clay minerals and thus monitor

palaeo-weathering (e.g. Ujvári et al., 2008; Galovic et al., 2011). Sr^{2+} is known to be closely associated with CaCO_3 , since its ionic radius comparable to that of Ca^{2+} thus allowing for isomorphic substitution in CaCO_3 (Bokhorst et al., 2009). Sr weakly correlates with Ca ($r=0.61$; $p>99.9\%$), likely corresponding with leaching and reprecipitation of carbonates.

Cs is the most volatile of the ferromagnesian elements and it is commonly hosted by K-feldspar, biotite or amphibole (Mittlefehldt, 1999). It tends to be enriched in loess as compared to palaeosols except for palaeosol 6-1 (Fig. 4.5), although its geochemical behavior appears not as systematic as that of other ferromagnesian transition elements. The enrichment of Cs relative to upper crustal values suggests high abundances of K-feldspar, biotite and amphibole. However, in such a case Cs abundance should be followed by considerably higher K or Rb values and/or clear correlation coefficients. Therefore, the identification of the mineral phase hosting Cs remains difficult.

4.4.4 Mass and frequency dependent susceptibility

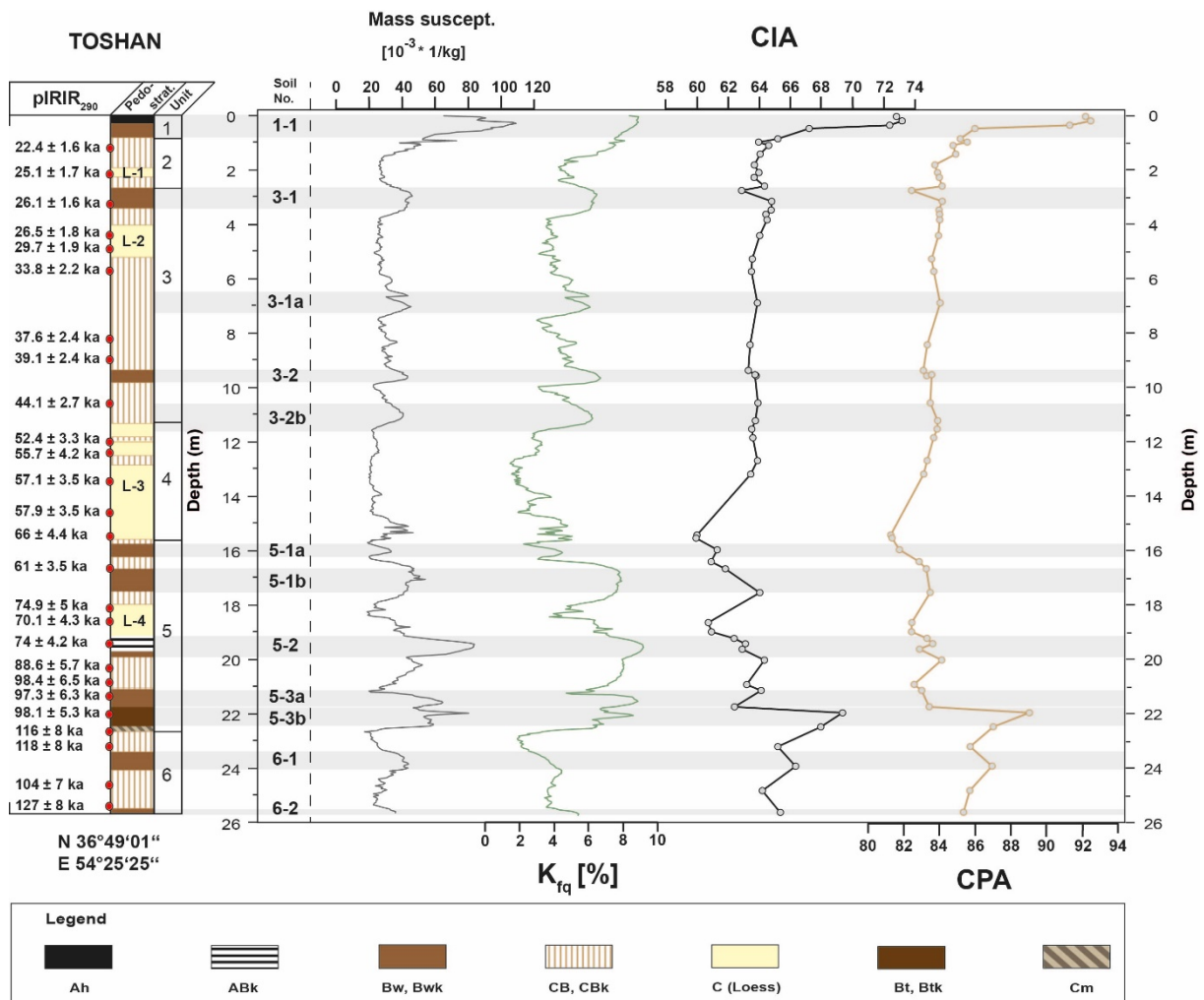


Fig. 4.6: Stratigraphy of the Toshan loess-soils sequence supplemented by records of magnetic susceptibility, the chemical proxy of alteration (CPA), the chemical index of alteration (CIA). The chronological framework was taken from Lauer et al. (2017a).

The results of magnetic susceptibility data (K_{lf} and K_{fd}) are shown as a function of profile depth (Fig. 4.6). Mass (K_{lf}) and frequency dependent susceptibility (K_{fq}) are in good accordance with our physical stratigraphy (Fig. 4.6), showing a systematical enhancement of both magnetic parameters in palaeosols and a decrease in loess layers. Bwk-horizons estimated to be weakly developed as based on field findings (3-1, 3-2, 5-1a table 4.1) exhibit mass susceptibility values between 30 and $55 \times 10^{-3} \text{ kg}^{-1}$ and a frequency dependence of 4.5 to 6.5% (Fig. 4.6). Conversely, the moderately developed palaeosols (5-1b, 5-3b, 6-1 and 6-2) span a larger range of K_{lf} and K_{fq} . Accordingly, mass susceptibility encompasses values from 40 to $70 \times 10^{-3} \text{ kg}^{-1}$, whilst the determination of K_{fq} yields values of 4.5 to 8.8% . Palaeosols 5-2, 5-3a, and the modern soil (1-1) attain mass susceptibilities of 85 to $110 \times 10^{-3} \text{ kg}^{-1}$. Frequency dependent susceptibility are confined between 8.6 to 9% (Fig. 4.6).

At Toshan section CBk-horizons are found subjacent to Bwk-horizons. These CBk-horizons are characterized by partial decalcification, coherent to subangular blocky structure, thus representing a transitional stage between C (loess) and B horizons in which features of the parental loess still prevail. This transitional character is also observed in relation to mass and frequency dependent susceptibility showing fluctuations particularly in CBk-horizons attributed to unit 3 (Fig. 4.6). K_{lf} attains values of 23 up to $45 \times 10^{-3} \text{ kg}^{-1}$ and K_{fq} ranges between 4 to 7.5% .

Loess layers are generally characterized by mass susceptibility values of 23 to 30 and frequency dependence of 2 to 3% . However, a pronounced shift towards elevated values of both parameters is recorded in the bottom part of L-3 (14.65-15.50 m).

4.5 Discussion

4.5.1 Loess composition and provenance in NE Iran deduced from major and trace element abundances

The trace element composition of loess layers (L1 to L4) show mostly analogous UCC-normalized patterns. This holds particularly true for elements known to have low concentrations in natural waters such as the REE (here only Nd and Ce), Y, Zr, Nb and Th (McLennan and Taylor, 1991). Loess layers L1 to L4 are found in different chronostratigraphic positions, representing different intervals of loess accumulation as based on the chronological framework provided by Lauer et al. (2017a). The analogous UCC-normalized trace element patterns of Toshan loess (Fig. 4.5A) imply that the geochemical composition of the sediment source/sources has not substantially changed through time. As a result airborne dust forming loess at Toshan (L1 to L4) might originate from the same sediment source/sources being reactivated during intervals of loess accumulation or active at different rates as compared to rates of present dust accumulation.

Numerous studies investigating the chemical composition of loess have shown that based on the comparatively homogenous assemblage of trace and major elements most loess deposits on a worldwide basis originate from sediments and/or sedimentary rocks, which have undergone at least one phase of upper crustal recycling (e.g. McLennan, 1989; Gallet et al., 1996, 1998; Jahn et al., 2001; Smykatz-Kloss, 2003; Muhs and Budahn, 2006; Ujvári et al., 2008; Buggle et al., 2008; Hao et al., 2010). This concept of upper crustal recycling or

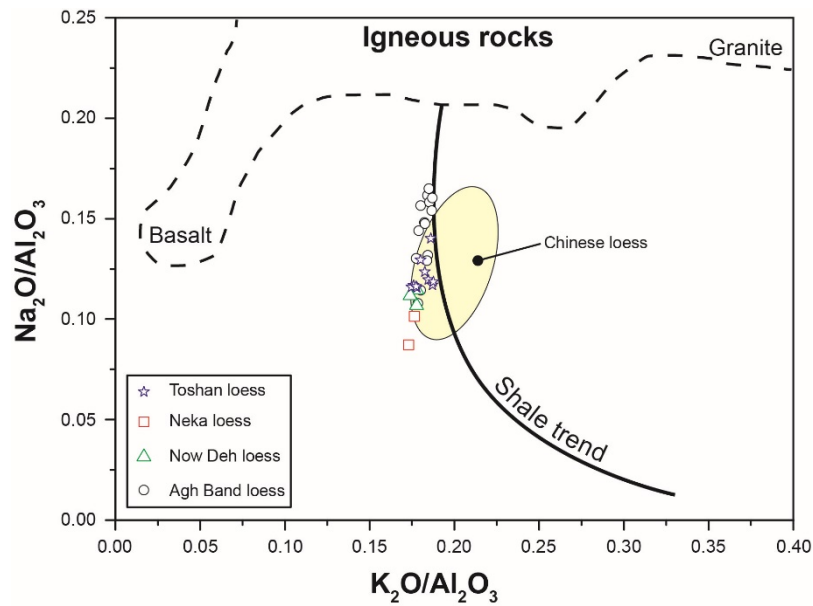


Fig. 4.7: Biplot of $\text{Na}_2\text{O}/\text{Al}_2\text{O}_3$ vs. $\text{K}_2\text{O}/\text{Al}_2\text{O}_3$ indicating the geochemical maturity of bulk loess in NE Iran. Particularly the $\text{Na}_2\text{O}/\text{Al}_2\text{O}_3$ ratio displays a gradient showing increasing Na_2O depletion from the semi-arid climate in the Iranian loess plateau (Agh Band) towards subhumid climatic conditions at Neka. The positions of igneous rocks, Chinese loess and the shale trend were taken from Muhs & Budahn (2006). NE Iranian loess thereafter group close to Chinese loess and the shale trend testifying to a degree of enhanced chemical maturity in relation to igneous rocks.

“preweathering” prior to loess formation runs contrary to the notion of loess as a first-cycle sediment being derived from glacial grinding of igneous rocks (Muhs and Budahn, 2006). NE Iranian loess groups close to shales and the Chinese loess (Fig. 4.7). This is primarily due to lower Na_2O contents relative to the composition of igneous rocks, likely attributed to the loss of Na-plagioclase within the source rocks or sediments. Neka loess exhibits the lowest $\text{Na}_2\text{O}/\text{Al}_2\text{O}_3$ -ratio of the entire loess samples analyzed, while loess at Toshan and Now Deh have slightly higher $\text{Na}_2\text{O}/\text{Al}_2\text{O}_3$ -ratios. In contrast Agh Band loess possesses the highest $\text{Na}_2\text{O}/\text{Al}_2\text{O}_3$ ratio suggesting a lower degree of mineralogical maturity of the sediment source as compared to Neka, Now Deh and Toshan (Fig. 4.7). In this context maturity is considered to represent the depletion in major elements relative to the initial composition of those elements in volcanic rocks. As a result the ratio of $\text{Na}_2\text{O}/\text{Al}_2\text{O}_3$ gives evidence of a gradient from Neka, Toshan and Now Deh to Agh Band, which seems to correspond with the modern precipitation gradient spanning the range from subhumid conditions in the western Caspian Lowland near Neka merging into a semi-arid climate to the north at Agh Band, located in the Turkmen steppe. This observation suggests that the different degrees of mineralogical maturity in NE Iranian loess, in the form of Na-depletion are primarily governed by the local climatic conditions in the respective source areas. Possibly, the protoliths were affected by depletion in Na-plagioclase prior to their aeolian entrainment from the source area. However such interpretation bears on the assumptions of 1) a pre-existing precipitation gradient during intervals of Pleistocene loess formation and that 2) loess in the Caspian Lowland originates basically from local sources, which is hitherto not clear since the dust sources are unknown. The distinct $\text{Na}_2\text{O}/\text{Al}_2\text{O}_3$ signatures might also be the result of post-sedimentary depletion in Na, driven by the local climatic conditions of

the respective sections and thus explaining an apparent atmospheric influence. Analogous to the $\text{Na}_2\text{O}/\text{Al}_2\text{O}_3$ -ratio the proportions of $\text{K}_2\text{O}/\text{Al}_2\text{O}_3$ exhibit a sequence of gradually decreasing K_2O -values from Agh Band loess towards Now Deh, Toshan and Neka loess (Fig. 4.3B, Fig. 4.7). Loess at Agh Band section plots closest to the shale trend, probably indicating the presence of more illitic particles as compared to the other sections (Muhs and Budahn, 2006).

Based on our geochemical data we observe that the major element properties of loess in the Caspian Lowland are distinct from the composition of igneous rocks, resembling those of shales and the Chinese loess. The trace elements assemblage of the Toshan section shown in Fig. 4.5A encompasses a range of 0.5 to 1.5 of upper crustal abundances, indicating geochemical analogy to the UCC. Hence, loess at Toshan likely originates from protoliths that have undergone at least one phase of upper crustal recycling. Moreover the ratios in Fig. 4.7 suggest that dust forming loess at Neka, Now Deh and Agh Band does not represent a first cycle sediment. We therefore assume that loess at Neka, Now Deh and Agh Band might also be derived from protoliths that have experienced at least one cycle of sedimentary mixing.

The ratios presented in Fig. 4.7 may primarily serve as maturity indicator instead of giving evidence to different source areas for the respective loess-soil sequences. Conversely, the $\text{TiO}_2/\text{Al}_2\text{O}_3$ -ratio (Fig. 4.5) was successfully used in provenance studies in the Chinese Loess Plateau (Hao et al., 2010). Both Al and Ti have the lowest solubility of all major elements in natural waters (Hao et al., 2010). Ti-contents may show considerable variations among different rock types, which qualify this element as provenance indicator. According to Fig. 4.5 the loess deposits at Neka, Toshan, Now Deh have similar bulk $\text{K}_2\text{O}/\text{Al}_2\text{O}_3$ and $\text{TiO}_2/\text{Al}_2\text{O}_3$ ratios constituting a consistent geochemical entity located along the northern foot slopes of the Alborz Mountain range. In contrast Agh Band loess situated in the Iranian Loess Plateau, belonging to the Kopet Dagh Mountains, exhibits both increased $\text{K}_2\text{O}/\text{Al}_2\text{O}_3$ and considerably higher amounts of TiO_2 relative to the other loess sequences as reflected in the $\text{TiO}_2/\text{Al}_2\text{O}_3$ signature.

Our results suggest that loess at Neka, Toshan and Now Deh originate from geochemically similar source rocks, whilst loess at Agh Band might be derived from a distinct source area. Frechen et al. (2009) state that the location of loess deposits in the Caspian Lowland is closely related to the vicinity of rivers. Hence, we assume that loess at Neka, Toshan and Now Deh might be derived from the floodplains of the rivers draining the Alborz Mountains, thus creating comparable bulk $\text{TiO}_2/\text{Al}_2\text{O}_3$ ratios. Conversely, the larger variety in the $\text{TiO}_2/\text{Al}_2\text{O}_3$ ratio observed in Agh Band loess might correspond with dust being derived from multiple source areas, than merely from the floodplains of the Atrak River. Loess in the Caspian Lowland hosts a variety of different grain size fractions from clay reaching to fine sand-sized particles (Frechen et al., 2009; Kehl, 2010; Vlamincx et al., 2016; Lauer et al., 2017b). As especially the finer particles such as the fraction $<20\ \mu\text{m}$ may be transported over larger, or even interhemispheric distances than coarse silt or sand-sized particles (Machalett et al., 2008), it is likely that NE Iranian loess is derived from both proximal and distant source areas (Vlamincx et al., 2016). Although the bulk composition of major elements in NE Iranian loess seems to be governed by local geological sources a common source of fine particles

(e.g. $<20\ \mu\text{m}$) cannot be excluded, since the trace and major element abundances in relation to particle-size are beyond the scope of this article. In general, possible dust source areas for the formation of loess in the Caspian Lowland other than river floodplains encompass the Karakoum Desert in Turkmenistan, river floodplains and subaerially exposed shelves of the Caspian Sea during the Pleistocene (e.g. Frechen et al., 2009; Kehl, 2010; Yanina, 2012; Asadi et al., 2013; Svitoch, 2013). Yet, particularly the exact timing of palaeo-hydrological changes of the Caspian Sea level is still a matter of debate (Forte and Cowgill, 2013).

4.5.2 Weathering and soil formation in loess

The nature and abundance of major- and trace-elements is primarily governed by the assemblage of the respective host minerals being found in loess (e.g. Buggle et al., 2011; Muhs and Budahn, 2006). Knowledge of the mineral assemblage described in chapter 4.1 constitutes the basis for understanding the geochemical behavior of major and trace elements in terms of element mobility/immobility in low temperature aqueous solutions responsible for mineral weathering in the pedosphere. Hence, ratios of palaeo-weathering may be formed based on mobile and immobile elements, both hosted by the same mineral (Buggle et al., 2011).

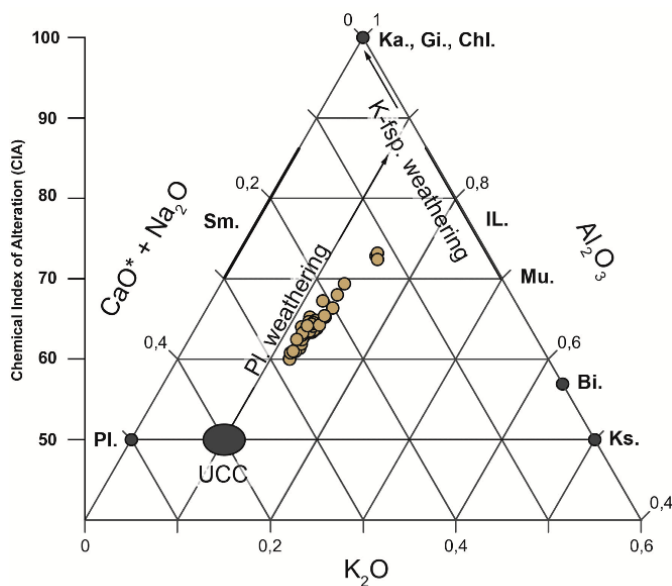


Fig. 4.8: A-CN-K diagram according to Nesbitt and Young (1984) of the loess-soil sequence at Toshihan (n=52). CaO^* represents Ca bound to silica such as feldspars. This ternary diagram reveals overall CIA-values of 60 to 73. Accordingly, data points plot close to the plagioclase weathering trend, suggesting that element mobility is governed by plagioclase depletion.

In Fig. 4.2 the mineralogical composition of loess (L4) and a strongly developed palaeosol (5-3b) are compared revealing clear differences in soluble minerals such as calcite and dolomite. These minerals are strongly depleted in palaeosol 5-3b. The absence of calcite and dolomite is likely due to carbonate leaching during pedogenesis. Both minerals are responsible for buffering soil pH-value. The dissolution of calcite and dolomite represents a precondition for the preferential chemical weathering of primary minerals such as e.g. plagioclase. Generally, weathering of plagioclase such as Na-bearing (albite) and Ca-bearing (anorthite) feldspar is considered one source of neoformation of siliceous clay such as e.g. vermiculite and smectite (Hao et al.,

2010; Galovic et al., 2011). Fig. 4.2A and B exhibit similar proportions in plagioclase, although plagioclase content in strongly developed soils is expected to decrease with respect to the parental loess. The negligible difference in plagioclase content may be masked by the

dilution effect of calcite, since the depletion of one mineral species will lead to the relative enrichment of the other minerals.

Compared to loess (Fig. 4.2A) palaeosol 5-3b (Fig. 4.2B) exhibits merely a minor increase in the contents of mica/illite (M/I) and kaolinite/chlorite (K/Ch). Illite is a 2:1 clay mineral that may originate both from physical weathering and the transformation of mica due to the removal of interlayer K^+ (Khormali et al., 2011; Asadi et al., 2013). The relative abundance of mica and illite cannot be determined based on our XRD-analysis owing to the interference of those minerals in the X-ray pattern. Possibly, the Bt-horizon (palaeosol 5-3b) inherited most of its M/I and K/C content from loess (Khormali et al., 2011). Furthermore, the Bt-horizon at the Toshan section hosts a distinct amount of smectite. The formation of smectite requires comparatively high edaphic moisture to mobilize interlayer K^+ from illite and micaceous minerals (Khormali et al., 2011). Thus, the transformation of illite and mica to smectite might be primarily the result of a moister palaeo-climate instead of being inherited by the parent material.

Potential inhomogeneities in the feldspar composition of loess can be tested by using the A-CN-K ternary diagram presented in Fig. 4.8. This is important, since an increase in the K-feldspar/albite ratio of the parental loess would result in too high or low CPA and CIA values (Buggle et al., 2011). In the case of varying amounts of both minerals, our data should plot parallel to the CN-K axis (Fedo et al., 1995). According to Fig. 4.8 our data points plot close to the plagioclase weathering trend, revealing comparatively stable K-feldspar/albite ratios in loess. This circumstance also bears the important corollary that the alteration of Na and Al are not due to sorting effects such as the selective enrichment of finer (more clayey) or coarser (more feldspar-like) particles. Grain-size sorting would effect a vertical scattering of the data points towards the Al-apex as shown for the Ukrainian loess-soil sequence Stary Kaydaky (Buggle et al., 2011). Thus, the CPA and the CIA are thought to reflect weathering intensity of the palaeosols at Toshan section.

The CIA-values of the bulk sample composition range between 60 and 73 (Fig. 4.8), whilst the CPA attains ratios of 82 to 92. The down-profile variations of both proxies in relation to the mass and frequency dependent susceptibility are presented in Fig. 4.6. Accordingly, lowest CPA and CIA values are attributed to loess layers, whereas these ratios are found increased in palaeosols of units 6 and 5 and the modern soil (Fig. 4.6). These palaeosols, particularly the modern soil and the Bt-horizon (5-3b) have experienced depletion in feldspars such as plagioclase. Comparing the modern (Holocene) soil with palaeosol 5-3b reveals a slightly higher degree of plagioclase depletion in the modern soil, indicating moister palaeo-climatic conditions during the Holocene. Generally, CIA-values of the Bt-horizon (5-3b) may be biased by K^+ being adsorbed onto clay minerals; however, the CPA exhibits a similar relationship with the modern soil. These results are in good accordance with K_{lf} and K_{fq} testifying to a higher amount of magnetizable minerals and superparamagnetic particles in the modern soil (Fig. 4.6). The lowest CIA and CPA ratios of 60 and 82 respectively, fall in a profile segment above palaeosol 5-1a. Conversely, this segment is characterized by peaks of K_{lf} and K_{fq} . During sample extraction and profile description in the field a charcoal layer was found in this stratigraphic position (15.05-15.45 m below surface). Hence, this discrepancy is likely due to wildfires, resulting in an enhancement of the rock magnetic signal (LeBorgne, 1955). The weakly developed palaeosols (3-2 and 3-1) allocated to unit 3 are well recorded in the K_{lf} and K_{fq} . In contrast CPA and CIA show merely small increases

suggesting that palaeosols 3-1 and 3-2 are characterized by very low degrees of feldspar weathering. Correlation of the CIA and CPA with mass susceptibility (K_f) yields only a moderate statistical relationship of $r = 0.61$, being valid on a confidence level of 99.9% (Fig. 4.6). This moderate correlation-coefficient is primarily due to differential sensitivity of the proxies applied with respect to weak pedogenic alterations such as those found in the palaeosols of Unit 3. Similar to the CIA and the CPA, Ba/Sr-ratios may be considered to mimic feldspar weathering. The most important carrier-minerals of Ba^{2+} are K-feldspars and micas in which Ba may be incorporated by substitution for K^+ . During weathering Ba may be retained through adsorption onto clay minerals, while Sr is depleted. However, a pronounced secondary carbonate metabolism as present in unit 3 may disturb this signal. The relationship between Ba/Sr and the mass susceptibility yields a correlation-coefficient ($r = 0.66$; $p > 99.9\%$) that is comparable to those of the CIA and CPA (Fig. 4.6 and 4.9). Thus, Ba/Sr-ratios are merely found increased in palaeosols that have undergone substantial feldspar depletion such as palaeosols 5-1a, 5-1b, 5-2, 5-3a, 5-3b and the modern soils (1-1), while this ratio seems insensitive to weakly developed palaeosols (3-1 and 3-2). The Fe/Mg ($r = 0.76$; $p > 99.9\%$), and Ti/Sr-ratios ($r = 0.74$; $p > 99.9\%$) yield the strongest correlation with the mass susceptibility record (Fig. 4.9). Fe and Mg both occur in mafic minerals such as pyroxene, amphibole, olivin and biotite, whereas Mg represents also a primary component of dolomite (Cornell and Schwertmann, 2003). Weathering proxies relying on Fe as immobile element are subject to problems, since Fe may be depleted in palaeosols, which are affected by redoximorphic conditions (Buggle et al., 2011). However, the palaeosols of the Toshan section are characterized by Fe-enrichment owing to the absence of redoximorphic features in the entire sequence (Vlaminck et al., 2016). The palaeosols allocated to units 6 and 5 as well as the modern soil (1-1) and the interstadial palaeosol 3-2 are well recorded by the Fe/Mg-ratio. Correspondingly, the highest degree in the depletion of mafic minerals is found in the modern soil. The palaeosols of unit 5 exhibit a lower degree of mineral weathering, suggesting that these soils have formed under more arid palaeoclimatic conditions, probably during MIS 5 (Lauer et al., 2017a).

The overall weak correlation of the mineral weathering proxies (Fig. 4.6 and 4.9) with the mass susceptibility is likely due to weakly developed interstadial palaeosols (unit 3), that have not experienced substantial depletion in feldspars and mafic minerals. Magnetite ($Fe^II Fe^III_2 O_4$) differs from most other iron oxides due to the incorporation of both Fe in the divalent and in the trivalent state (Cornell and Schwertmann, 2003). Cornell and Schwertmann (2003) state that magnetite may form through the interaction of Fe^{II} with amorphous iron hydroxides such as ferrihydrite. This interaction takes place before decalcification in the early stages of weathering at pH levels of >7 . Conversely, feldspar weathering is preferentially associated with pH 7-6 thus occurring at a later time (Cornell and Schwertmann, 2003). We therefore assume, that the discrepancy between rock magnetic and geochemical weathering indices is primarily due to the differential timing of magnetite formation and silicate mineral depletion in the course of pedogenesis.

4.5.3 Interstadial pedogenesis during MIS 3 inferred from the rock magnetic properties of the loess-soil sequence at Toshan

The entire loess-soil sequence at Toshan is characterized by a pronounced variability in K_{fd} and K_{lf} . K_{fd} -values $<3\%$, exclusively found in loess indicate dry and dusty environmental conditions favoring loess accumulation at the expense of soil formation. The bulk susceptibility mean value K_{lf} of $75.2 \cdot 10^{-5}$ SI ($\pm 21 \cdot 10^{-8}$ m³/kg as specific susceptibility) fits data from the Chinese loess Plateau (CLP; Heller et al., 1991), where unweathered loess characterized by K_{fd} values below 3% (hardly super paramagnetic (SP) grains) shows bulk susceptibility mean values of ca. $40 \cdot 10^{-5}$ SI.

A comparison of the rock magnetic properties of the Toshan section with the data set from Xifeng, located in the central part of the CLP (Fig. 4.10) reveals similarities. For both profiles the majority of K_{fd} values are above 3% with a considerable amount of bulk susceptibility data between 100 and $200 \cdot 10^{-5}$ SI. Xifeng is characterized by sub-humid climatic conditions with annual precipitation amounts of 561 mm (Jahn et al., 2001), corresponding with those found

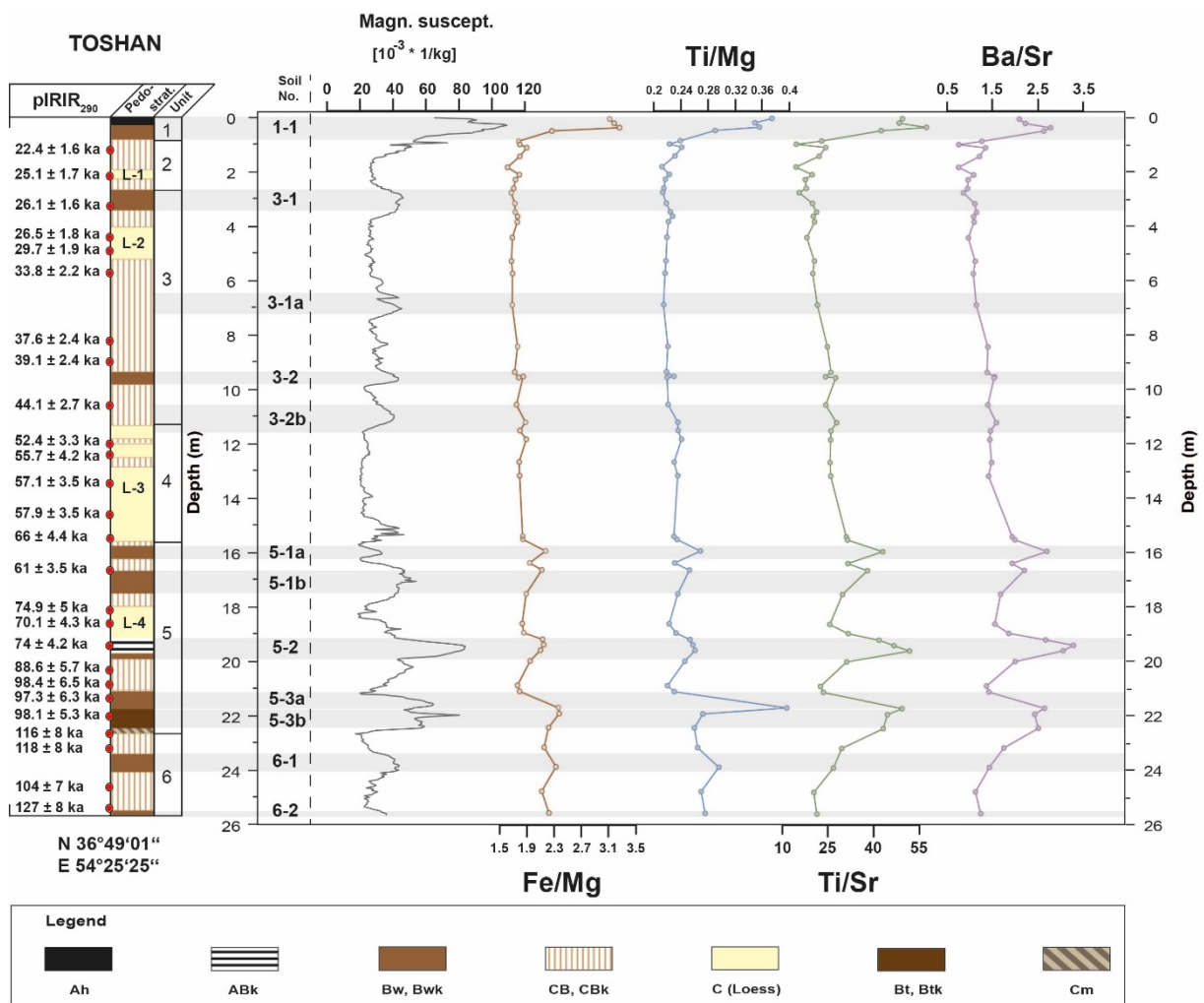


Fig. 4.9: Stratigraphy of the Toshan loess-soil sequence supplemented by the record of magnetic susceptibility, ratios of Fe/Mg, Ti/Mg, Ti/Sr and Ba/Sr.

Toshan (550 mm). Thus the similar susceptibility data sets from both regions confirm climatic analogy.

Frequency dependent data $<3\%$ with equally low values in bulk susceptibility in the Toshan plot could be clearly assigned to loess layer L3 (unit 4). Conversely L1, L2 and L4 exhibit K_{fd} -

values slightly >3% testifying to the formation of super paramagnetic particles during or after loess accumulation. These results confirm the findings of Vlaminck et al. (2016) and Lauer et al. (2017a) that the most “typical” loess found at Toshan was accumulated during MIS 4 L3) implying that it represents the driest stage. All other loess layers were affected by weathering to a larger extent.

The down-profile variations of K_{fd} and K_{lf} (Fig. 4.6) reveal recurrent intervals of pedogenesis during MIS 3 (60-25 ka before present). According to Fig. 4.6 and the chronological framework of the Toshan section provided by Lauer et al. (2017a), at least 4 characteristic enhancements in the rock magnetic properties are found between 52–44 ka, 44–39 ka, 37–33 ka and 26–25 ka. The stratigraphic positions of palaeosols 3-1 (26–25 ka) and 3-2 (44–39 ka) coincide with increases in both K_{lf} and K_{fd} . The remaining peaks in K_{lf} and K_{fd} chronologically assigned to 52–44 ka (3-2b) and 37–33 (3-1a) ka coincide with layers denominated as CBK-horizons (Vlaminck et al., 2016). The latter exhibit similar magnitudes in both rock magnetic parameters as compared to the weakly developed interstadial palaeosols 3-1 and 3-2. It is therefore likely, that unit 3 hosts at least 2 more palaeosols distinct from a CBK-horizon that were not recognized during field work (Vlaminck et al., 2016). Thus the total number of palaeosols found at Toshan section formed during the last glacial-interglacial cycle is increased from 9 to (at least) 11. The mass susceptibility and frequency dependent susceptibility records of MIS 3 at Toshan constitute a saw tooth-like pattern suggesting a relatively rapid increase in soil moisture, thereby favoring the formation of ferromagnetic minerals such as magnetite and maghemite (Heller et al., 1991; Cornell and Schwertmann, 2003). Subsequent to culminating concentrations of magnetizable minerals and super paramagnetic particles K_{lf} and K_{fd} decrease gradually. Based on high-resolution colorimetric analysis (VIS-spectroscopy) Vlaminck et al. (2016) were able to infer gradual upper and lower boundaries separating MIS 3 palaeosols from subjacent and overlying strata. Correspondingly, these palaeosols are the result of fluctuating moisture availability in relation to changes in the accumulation of calcareous dust. Assuming constant or decreasing moisture availability relative to gradually increasing dust accumulation rates may cause a shift in the weathering regime from incipient pedogenesis to the formation of comparatively unaltered loess. The neoformation of ferromagnetic minerals and super paramagnetic particles would be inhibited by constant dust supply in relation to decreasing moisture availability and thus cause a decline in K_{lf} and K_{fd} (Fig. 4.6). As a result it is likely that MIS 3 palaeosols are the result of syngenetic soil formation during interstadials (Vlaminck et al., 2016).

Recently, Lauer et al. (2017b) provided high-resolution records of the rock-magnetic and granulometric properties of the Agh Band loess-soil sequence supplemented by a chronological framework as based on a luminescence dating study. Agh Band is located in the Iranian Loess Plateau (ILP) ca. 110 km to the North of the Toshan section (Fig. 4.1). As opposed to the climatic conditions prevailing along the foot slopes of the Alborz Mountains, the loess Plateau is characterized by a semi-arid climate. A stratigraphic correlation of MIS 3 palaeosols found in the Toshan sequence with the Agh Band section is difficult, since soil forming intervals in the ILP are likely referred to the penultimate interglacial (Lauer et al., 2017b). According to the magnetic susceptibility results of Lauer et al. (2017b) the climatic conditions in the ILP during MIS 3 were characterized by pronouncedly higher aridity thus inhibiting pedogenesis. The rock magnetic properties of the Toshan and Agh Band sections

suggest, that NE Iran was affected by different climatic conditions being active over a comparatively small distance (ca. 110 km).

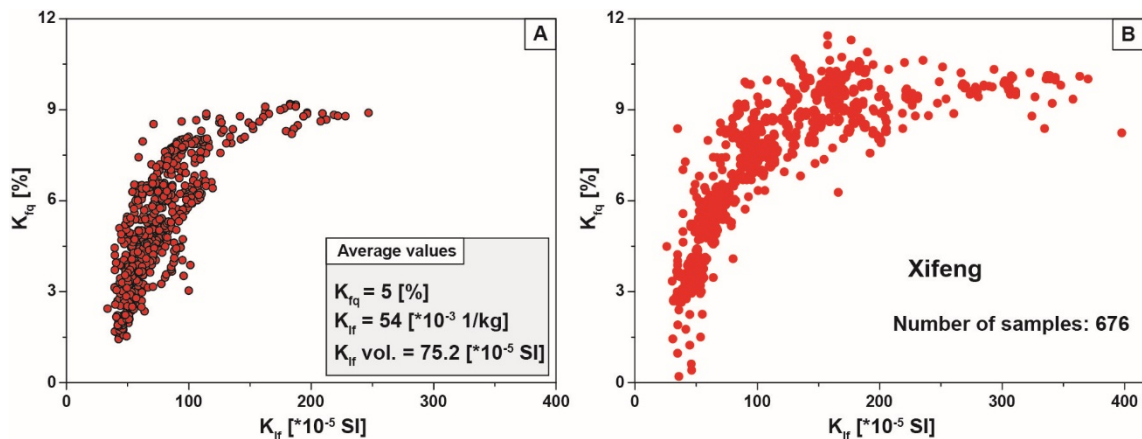


Fig. 4.10: Frequency dependent susceptibility (K_{fd}) against low field susceptibility (K_{lf}) according to the idea of Heller et al. (1991). Rock magnetic properties of the loess soil-sequence at Toshan (A) as compared to those of the Xifeng loess and palaeosol sequence (B) located in the central part of the Chinese Loess Plateau. Both locations are characterized by mean annual precipitation amounts of approx. 550 mm. Our susceptibility data confirm climatic analogy.

Çağatay et al. (2014) analyzed the oxygen isotope signature in a sediment core from Lake Van on the east Anatolian Plateau (Turkey), revealing excursions in the $\delta^{18}\text{O}$ content on a millennial scale during 57, 53, 46, 34 ka as well as a rise in lake level 25 ka before present. These fluctuations are related to warmer and moister interstadial climatic conditions governing the enrichment of ^{18}O in the lake water and causing lake level transgressions (Çağatay et al., 2014; Stockhecke et al., 2016; Rowe et al., 2012). The timing of these isotopic events falls in the range of soil forming intervals at the Toshan section (Fig. 4.6) from 52-44 ka, 44-39 ka, 37-33 ka and 26-25 ka (Lauer et al., 2017a). A common feature governing the climatic conditions at Lake Van as well as those along the southern Coast of the Caspian Sea are i.e. westerly cyclones originating from the eastern Mediterranean Sea. These cyclones represent a tentative explanation for the consistent timing of moister palaeoclimatic intervals on the east Anatolian Plateau as compared to the southern Caspian Lowland suggesting that palaeoclimate in Northern Iran was governed by large scale climatic fluctuations.

4.6 Conclusions

Loess at Toshan has a polymineral assemblage. The UCC-normalized trace element patterns in Toshan loess (L1 to L4) exhibit homogenous abundances of HFSE, LILE, REE and ferromagnesian elements, implying that the dust source/sources of this airborne sediment have not substantially changed during the last glacial-interglacial cycle. Nevertheless, loess layers L1 to L4 each represent differentially weathered strata as evidenced by K_{fd} and K_{lf} . Correspondingly, L3 shows the lowest degree of weathering representing the most “typical” loess found at Toshan section. This loess layer formed during MIS 4.

UCC-normalized trace elements comprise a narrow range of 0.5 to 1.5 implying that Toshan loess is derived from sediments that have undergone at least one phase of upper crustal recycling. From similar geochemical signatures we assume that not only Toshan loess, but also loess at Neka, Now Deh and Agh Band are derived from well mixed sedimentary protoliths. Ratios of immobile major elements give evidence for a common sediment source for the sections along the northern foot slopes of the Alborz Mountains (Neka, Toshan and Now Deh), whilst Agh Band loess contains a larger quantity and variation in TiO_2 contents, suggesting different/multiple dust sources.

In most palaeosols the enrichment in relatively immobile major elements is due to the dilution effect caused by CaCO_3 . However, in strongly developed soils such as 5-3b, 5-2, 5-1b and 1-1 a substantial loss in plagioclase is likely, as shown by the down-profile variations of weathering proxies such as the CIA, CPA, Ba/Sr. Soils 6-2, 6-1, 5-3b, 5-3a, 5-2, 5-1b and 1-1 are enriched in HFSE, LILE and the ferromagnesian trace elements. Yet, the correlation of geochemical weathering proxies (CIA, CPA, Ba/Sr, Fe/Mg, Ti/Mg and Ti/Sr) with the magnetic susceptibility has met only partial success, since the weakly developed interstadial palaeosols of MIS 3 are not well recorded in these ratios. We assume that the discrepancy between the magnetic susceptibility record and the geochemical weathering proxies is due to the differential timing in the formation of magnetic minerals such as magnetite and maghemite as compared to the depletion in i.e. plagioclase. According, to the high resolution records of mass and frequency dependent susceptibility at least two further palaeosols were found to have formed during MIS 3. The total amount of soil forming intervals in the Toshan section is hence increased from 9 to 11 as compared to field observations. The weakly developed MIS 3 palaeosols are likely the result of syngenetic soil formation as previously assumed.

4.7 Acknowledgements

The authors are grateful to the Gorgan University of Agricultural Science and Natural Resources for generous logistic support. We thank Kathrin Worm for the performance of magnetic susceptibility analysis. This is part of an ongoing study funded by the German Research Foundation (Deutsche Forschungsgemeinschaft, DFG-Gz.) (KE 818/6-1, FR 877/26-1, LE 1812/6-1).

Appendix

Table app. 4.2:

Composition of major elements given in wt% supplemented by lithological information. LOI = Loss on Ignition at 1100°C.

<i>Lithology</i>	<i>Sample</i>	<i>Na2O</i>	<i>MgO</i>	<i>Al2O3</i>	<i>SiO2</i>	<i>P2O5</i>	<i>SO3</i>	<i>K2O</i>	<i>CaO</i>	<i>TiO2</i>	<i>MnO</i>	<i>Fe2O3</i>	<i>LOI</i>	<i>Σ</i>
Ap	TOS-1	0.6	2.4	12.4	44.5	0.2	0.1	2.4	14.7	0.9	0.2	7.5	13.8	99.7
Ap	TOS-2	0.6	2.5	12.7	45.4	0.2	0.1	2.4	14.2	0.9	0.1	7.8	12.8	99.8
Ap	TOS-3	0.8	2.6	13.8	50.4	0.1	0.1	2.7	9.8	0.9	0.2	8.5	9.8	99.7
Bw	TOS-4	1.4	2.4	14	56	0.1	0.1	2.3	7.2	0.7	0.1	5.5	9.5	99.5
Bw	TOS-5	1.2	2.3	11.3	45.1	0.1	0.1	1.9	16.5	0.6	0.1	4.2	16.7	100.1
CBk	TOS-6	1	2.2	9.5	38.1	0.1	0.2	1.6	21.7	0.5	0.1	3.9	21.2	100
CBk	TOS-7	1.2	2.3	11.1	45	0.1	0.1	1.9	16.6	0.6	0.1	4.4	16.7	100.2
CBk	TOS-8	1.1	2.3	10.6	42.5	0.1	0.2	1.9	18.8	0.5	0.1	4.1	18.3	100.5
CBk	TOS-9	1.3	2.6	10.9	44.5	0.1	0.1	1.9	17.2	0.6	0.1	4.2	17.1	100.7
loess	TOS-10	1.3	2.5	11.3	45.8	0.1	0.2	2	15.2	0.6	0.1	4.5	15.7	99.3
loess	TOS-11	1.2	2.4	10.7	43.5	0.1	0.1	1.9	17.2	0.5	0.1	4.2	17.3	99.4
CBk	TOS-12	1.4	2.7	11.8	48.3	0.1	0.1	2.1	14	0.6	0.1	4.7	14.7	100.7
Bwk	TOS-13	1.5	2.7	11.2	46.3	0.1	0.1	2	14	0.6	0.1	4.5	15	98.2
Bwk	TOS-14	1.4	2.9	12.6	51	0.1	0.1	2.2	10.4	0.6	0.1	5	12.2	98.8
Bwk	TOS-15	1.5	2.9	12.8	51.9	0.1	0.1	2.3	10.7	0.6	0.1	4.9	12.2	100.2
CBk	TOS-16	1.4	2.7	12.1	49.5	0.1	0.1	2.2	12.1	0.6	0.1	4.8	13.4	99.1
loess	TOS-17	1.4	2.8	12.2	49.6	0.1	0.1	2.2	12.5	0.6	0.1	4.8	13.6	100.2
loess	TOS-18	1.3	2.6	11.4	47	0.1	0.2	2	14.9	0.6	0.1	4.5	15.4	100.3
loess	TOS-19	1.4	2.8	11.5	48.7	0.1	0.1	2.1	12.7	0.6	0.1	4.6	13.8	98.7
CBk	TOS-20	1.4	2.7	11.4	47.9	0.1	0.1	2.1	13.7	0.6	0.1	4.6	14.4	99.2
CBk	TOS-21	1.4	2.8	11.8	49.1	0.1	0.1	2.2	13.1	0.6	0.1	4.8	14.4	100.6
CBk	TOS-22	1.4	2.8	11.8	49.7	0.1	0.2	2.2	11.8	0.6	0.1	4.9	12.9	98.6
CBk	TOS-23	1.5	2.7	11.8	49	0.1	0.1	2.2	13.4	0.6	0.1	4.7	13.9	100.3
Bwk	TOS-24	1.5	2.8	12.3	50	0.2	0.1	2.3	11.9	0.6	0.1	4.9	13.3	100.1
Bwk	TOS-25	1.5	2.7	12.1	50.6	0.2	0.2	2.3	11.8	0.6	0.1	5	13.1	100.3
CBk	TOS-26	1.5	2.7	12.1	48.5	0.1	0.1	2.2	13.5	0.6	0.1	4.7	14.5	100.8
CBk	TOS-27	1.4	2.6	12	49.9	0.2	0.2	2.3	12	0.6	0.1	4.9	13.5	99.8
loess	TOS-28	1.3	2.5	11.4	47.9	0.1	0.1	2.1	14	0.6	0.1	4.5	14.9	99.7
loess	TOS-29	1.4	2.5	11.7	49.2	0.1	0.2	2.2	13	0.6	0.1	4.8	14.1	100
CBk	TOS-30	1.5	2.7	11.9	50.5	0.1	0.1	2.1	11.8	0.6	0.1	4.7	13.4	99.7
loess	TOS-31	1.4	2.6	11.7	50	0.1	0.1	2.1	12.2	0.6	0.1	4.6	13.4	99.1
loess	TOS-32	1.8	2.7	13.1	53.4	0.2	0.2	2.4	9.6	0.6	0.1	5	10.6	99.9
Bwk	TOS-33	1.8	2.7	13	52.5	0.2	0.1	2.4	10	0.6	0.1	5	10.8	99.5
Bwk	TOS-34	2	2.8	15	59.7	0.2	0.1	2.8	4	0.8	0.1	6.1	11.2	105
Bwk	TOS-35	1.7	2.8	13.1	51	0.1	0.2	2.4	10.8	0.6	0.1	5.4	11.9	100.3
CBk	TOS-36	1.7	2.8	14.2	56.7	0.1	0.1	2.7	6.2	0.7	0.1	6	8.5	99.9
CBk	TOS-37	1.5	2.6	12.2	48.6	0.2	0.2	2.2	13.1	0.6	0.1	4.9	14.1	100.3
loess	TOS-38	1.7	2.9	12.8	52.2	0.2	0.1	2.3	10.3	0.6	0.1	5.3	11.7	100.4
Abk	TOS-39	1.7	2.9	13.3	54.4	0.2	0.1	2.4	8.3	0.7	0.1	5.4	10.1	99.8
ABk	TOS-40	1.8	2.9	14.9	57.4	0.1	0.1	2.7	4.3	0.7	0.1	6.1	6.8	98.2
ABk	TOS-41	1.8	2.9	15.4	59.3	0.1	0.1	2.7	2.9	0.8	0.1	6.2	5.9	98.4
Bw	TOS-42	2	3	15.9	61.8	0.1	0.1	2.8	1.9	0.8	0.1	6.3	5.3	100.2
CBk	TOS-43	1.3	2.4	11.7	45.9	0.1	0.2	2.1	15.4	0.6	0.1	4.7	15.7	100.4
CBk	TOS-44	1.4	2.5	11.2	44.5	0.1	0.2	1.9	16.3	0.6	0.1	4.5	16.4	99.9
Bw	TOS-45	1.5	2.7	12.1	48.4	0.1	0.1	2.1	13.1	0.6	0.1	4.8	13.9	99.8
Bw	TOS-46	1.7	2.3	14.2	63.9	0.1	0.1	2.5	2.6	0.9	0.2	5.3	5.3	99.1
Bt	TOS-47	1.2	2.9	16.2	60	0.1	0.1	2.9	1.3	0.8	0.1	6.9	6.9	99.5
Bt	TOS-48	1.5	3	16.1	60.6	0.1	0.1	2.9	1.5	0.8	0.1	6.7	6.3	99.9
CBk	TOS-49	1.3	2.4	12.5	48.8	0.1	0.1	2.4	11.8	0.6	0.1	5.1	13.9	99.2
Bw	TOS-50	1.2	2.4	13.4	52.7	0.1	0.1	2.5	8.8	0.7	0.1	5.6	12.1	100
CBk	TOS-51	1.1	2.2	11	44.3	0.1	0.1	2.1	16.7	0.6	0.1	4.6	17.3	100.4
Bw	TOS-52	1.4	2.4	13	52.2	0.1	0.1	2.4	9.7	0.7	0.1	5.4	12.2	100

Table app. 4.3:

Composition of trace elements given in ppm. BDL = beyond detection limit.

<i>Sample</i>	<i>Sc</i>	<i>V</i>	<i>Cr</i>	<i>Ni</i>	<i>Cu</i>	<i>Zn</i>	<i>Ga</i>	<i>Rb</i>	<i>Sr</i>	<i>Y</i>	<i>Zr</i>	<i>Nb</i>	<i>Cs</i>	<i>Ba</i>	<i>Ce</i>	<i>Nd</i>	<i>Th</i>
TOS-1	13	105	81	44	20	72	13	85	195	23	156	11	6	408	61	22	10
TOS-2	11	105	83	45	23	72	14	87	189	23	159	11	9	421	60	23	10
TOS-3	15	115	88	49	23	77	15	92	169	24	173	12	1	471	57	24	12
TOS-4	15	113	87	47	23	77	15	93	177	25	171	12	11	467	60	23	11
TOS-5	7	90	69	37	17	61	12	74	282	20	133	10	6	358	54	20	10
TOS-6	BDL	79	63	32	17	53	10	62	420	17	111	8	10	320	46	11	8
TOS-7	5	89	70	37	17	61	12	74	264	19	130	9	11	357	56	23	9
TOS-8	3	85	64	34	16	57	11	73	279	19	123	9	5	340	48	17	9
TOS-9	6	86	68	36	18	60	12	76	484	19	131	9	2	366	55	16	10
TOS-10	8	92	69	37	18	64	12	80	336	21	140	10	3	367	54	20	9
TOS-11	7	85	73	36	19	61	12	76	367	19	130	9	11	354	52	19	9
TOS-12	9	96	70	37	22	67	13	83	400	21	144	10	8	382	46	18	11
TOS-13	11	95	73	37	22	67	12	82	460	21	140	10	14	398	54	26	10
TOS-14	12	106	76	42	22	73	14	90	375	23	160	11	7	418	49	25	11
TOS-15	12	102	78	43	23	73	14	89	353	23	162	11	2	407	61	24	10
TOS-16	10	98	77	40	21	69	13	86	364	22	154	10	5	395	63	21	10
TOS-17	9	99	74	40	20	67	13	85	349	22	156	11	9	383	58	23	11
TOS-18	6	91	69	37	19	64	13	80	388	22	151	10	8	378	53	20	9
TOS-19	10	95	73	38	20	67	13	83	344	22	157	10	3	386	49	20	10
TOS-20	9	95	72	38	19	66	13	82	349	21	149	10	4	378	49	21	10
TOS-21	7	97	76	40	23	69	13	83	331	22	151	10	6	381	54	22	9
TOS-22	9	100	84	40	24	70	13	86	281	22	159	10	3	394	41	18	10
TOS-23	10	96	73	39	22	69	13	84	284	22	147	10	3	394	48	19	10
TOS-24	12	101	75	41	23	71	13	86	266	22	153	10	8	409	59	22	9
TOS-25	13	100	76	41	22	72	14	945	258	23	155	11	8	401	58	19	10
TOS-26	10	97	72	39	22	69	13	84	283	21	146	10	5	397	44	14	10
TOS-27	8	99	75	41	23	72	13	87	251	22	156	10	6	398	56	25	9
TOS-28	7	97	71	38	20	66	12	82	258	21	150	10	2	376	58	16	10
TOS-29	10	98	72	40	21	67	13	85	268	22	154	10	9	387	54	18	9
TOS-30	11	98	75	42	21	69	12	85	270	22	159	10	7	401	58	26	10
TOS-31	11	95	71	40	19	67	13	84	268	22	162	10	13	380	54	24	10
TOS-32	13	95	76	37	21	69	15	100	225	24	174	12	10	437	61	19	12
TOS-33	12	95	74	37	22	71	14	100	225	24	165	11	5	450	65	24	13
TOS-34	17	115	87	46	28	86	17	116	188	28	184	14	9	507	77	25	14
TOS-35	13	100	79	40	24	76	15	98	225	23	146	11	10	436	52	25	11
TOS-36	16	111	85	46	30	86	16	109	203	26	167	12	12	448	57	19	13
TOS-37	9	98	73	39	23	69	13	86	229	22	150	10	14	385	57	22	9
TOS-38	13	103	75	40	23	74	14	92	284	23	157	11	12	442	53	24	10
TOS-39	15	106	80	41	25	79	15	99	238	24	169	12	11	443	55	25	12
TOS-40	17	116	89	48	26	88	17	118	188	27	167	13	7	504	71	19	13
TOS-41	18	120	89	49	32	89	18	116	172	28	179	13	10	564	77	30	12
TOS-42	20	121	92	49	30	86	17	114	160	28	190	14	7	488	63	30	13
TOS-43	8	89	71	36	21	65	13	82	210	21	142	11	18	420	57	25	10
TOS-44	7	87	66	34	19	61	13	79	288	20	136	10	8	396	47	20	10
TOS-45	9	96	70	37	20	66	13	86	304	22	148	11	4	433	63	24	11
TOS-46	17	109	84	42	19	80	16	111	192	27	219	16	7	509	68	25	12
TOS-47	19	135	100	62	33	97	19	115	190	30	193	14	9	463	69	31	13
TOS-48	19	130	100	63	36	96	18	117	194	29	181	14	7	488	69	30	12
TOS-49	13	106	80	45	22	75	14	93	238	22	145	11	5	418	62	22	10
TOS-50	14	121	92	55	27	82	15	98	299	25	173	13	11	429	62	26	10
TOS-51	6	92	73	41	21	67	12	83	337	20	133	10	4	380	53	26	9
TOS-52	14	110	82	47	24	74	15	95	367	26	163	12	BDL	457	65	24	11

Chapter 5

The loess-soil sequence at Neka-Abelou and its palaeoclimatic implications: towards a pedo-stratigraphic model of northeastern Iran

Vlaminck, S.^a, Kehl, M.^a, Köhler, T.^b, Frechen, M.^b, Lehndorff, E.^c, Khormali, F.^d

^a *Institute of Geography, University of Cologne, Albertus Magnus Platz, 50923, Cologne, Germany*

^b *Leibniz Institute for Applied Geophysics (LIAG), Stilleweg 2, 30655, Hannover, Germany*

^c *Institute of Crop Science and Resource Conservation, Soil Science and Soil Ecology, University of Bonn, Nussallee 13, D-53115, Bonn, Germany*

^d *Department of Soil Sciences, Gorgan University of Agricultural sciences and Natural resources, Gorgan, Iran*

-Formatting and orthography of the manuscript are adapted to the dissertation style-

Abstract

During the last Interglacial-glacial cycle recurrent phases of aridization, alternating with moister climatic conditions promoted the analogous extension and retreat of dust sources in the southern Caspian Lowland. Located in a distal position to these deflation areas the Neka-Abelou loess palaeosol sequence (LPSS) is composed of finely textured loess, which is structured by at least ten differently developed palaeosol (PS) horizons. Moreover, a tephra layer, separating approx. early glacial from last pleniglacial loess deposits was detected and might serve as an additional stratigraphic marker. In order to understand the dust and soil formation dynamics of the late Pleistocene we have elaborated high resolution records on grain-size and calcium carbonate (CaCO_3). The clay-rich polygenetic palaeosols assigned to the last interglacial and the early glacial interstadials are composed of strongly developed Bt, ABk and Bw horizons, which were completely decalcified and are underlain by a distinct carbonate enrichment horizon. This palaeosol-triple has likely formed in a postsedimentary manner, i.e. under strongly reduced or absent dust accumulation. It constitutes an excellent pedostratigraphic marker that can be recognized in numerous exposures along the northern declivity of the Alborz Mountains. In contrast, the transitions to the following stadial loess deposits are marked by gradually increasing texture and decreasing degrees of pedogenesis, suggesting enhanced dust deposition and reduced moisture availability, favouring the formation of weakly developed synsedimentary palaeosols (CBk). Similar phases of soil formation under ongoing dust deposition coincide with presumably short-lived interstadials of the last pleniglacial and were also identified in the Toshan and Now Deh sections. Thus, the manifold palaeosols structuring the LPSS of the Neka-Abelou, Toshan and Now Deh sections document differential soil forming intensities depending on the relation between dust accumulation and moisture availability in the context of late Pleistocene climate change.

Key words: Palaeoclimate, dust accumulation, polygenesis, synsedimentary soil formation, post sedimentary soil formation

5.1 Introduction

During the Quaternary global climate has experienced manifold changes which differed in magnitude, period and their spatial extent. The reconstruction of this dynamics by means of sedimentary geoarchives requires signals to be recorded in the form of e.g. alternating physical and/or chemical properties in response to fluctuations of climatic parameters such as precipitation, temperature and wind strength. Ideally, those palaeoclimatic signals are preserved over long time intervals thus offering the opportunity to study coherent records of environmental dynamics related to a given period within the Quaternary. Depending on the geoarchive under consideration inferences about past climates may be drawn for different spatial scales. While e.g. the signature of $\delta^{18}\text{O}$ from Greenland ice cores reflects global ice volume effect (Rasmussen et al., 2014; Bradley, 2015) loess-palaeosol sequences host

evidence of past climatic fluctuations on regional and local scales. The large number of different organic and inorganic proxies applicable to decipher past climatic and environmental information from loess (see chapter 1.5) fosters a detailed view on the nature of late Pleistocene palaeoclimates. Due to the, in most cases, regional significance of loess-palaeosol sequences the combination of several sequences is necessary to elaborate a pedostratigraphic model of a given region and to gain insights into its palaeoclimatic evolution.

In northeastern Iran loess-palaeosol sequences are found along a modern precipitation gradient (Kehl, 2010; Vlamincx et al., 2016) from the comparatively moist area near the city of Neka in the west towards the dry areas of the Iranian loess plateau in the east. The recently studied Toshan and Now Deh sections are located on the subhumid northern foothills of the Alborz Mountain range (Kehl, 2010; Vlamincx et al., 2016, Lauer et al., 2017a), whereas the Agh Band profile is found in the semi-arid Iranian loess plateau to the north. Along the northern foot slopes of the Alborz Mountain range loess deposits unconformably cover carbonate rocks mostly consisting of Jurassic limestones as exemplified in Fig. 2. Due to the economic interest in these geological units as construction materials, loess and limestones are exploited in numerous quarries in the region. Thus, just as many artificial exposures exist along the Alborz Mountain range, in which the successions of loess layers and palaeosols of the region may be studied. The newly discovered Neka-Abelou section gives evidence of late Pleistocene climate fluctuations in the moistest part of the study area, which was missing so far. Located in the western part of the Caspian Lowland, the Neka-Abelou section completes the south-west/north-east transect of hitherto known sections at Toshan, Now Deh and Agh Band.

As the numbering of the sequence designation suggests, Neka-Abelou represents the third profile of its kind being prepared in this part of the Alborz Mountains. The first profile simply denominated as “Neka” in the scientific literature, was the first in the line of these profiles to be sampled and described systematically by Kehl et al. (2005) and Kehl (2010). These publications provide results of micromorphological investigations, low-resolution records of grain-size, free (Fe_d), active (Fe_o) and total iron, and CaCO_3 . Furthermore a detailed framework based on a luminescence dating study was presented in Frechen et al. (2009). The Neka section described by Kehl et al. (2005) had a total thickness of 16 m hosting moderately to strongly developed Bwk, Bt or AhBt horizons, which were chronostratigraphically attributed to MIS 5a, 5c and the last interglacial period 5e (Kehl et al., 2005; Frechen et al., 2009). Shahriari et al. (2017) studied the Neka2 section, which was exposed in a large limestone quarry. This sequence hosted strongly to moderately developed Bw, Bt and ABt horizons. This section was partly destroyed by collapse of the loess exposure and was no longer safe for any further investigations. Hence, an alternative sequence was found in a neighbouring quarry. In contrast to the previous profiles, the Neka-Abelou section has a total thickness of 22.25 m and the exposure offers to trace palaeosols over large lateral distances. Hitherto, analyses of the section yielded highly resolved grain-size records supplemented by a preliminary CaCO_3 -record. Detrital carbonates in loess greatly affect its ability to buffer incoming acids such as e.g. carbonic acid (H_2CO_3) and thus to protract silicate weathering. Silicate weathering leads to differentiation of distinct soil horizons in the course of pedogenesis. The dissolution of carbonate is considered a prerequisite for

preferential weathering of silicates and therefore relative amounts of CaCO_3 may serve as proxy for pedogenesis.

The objectives of the present chapter are to i) to provide a thorough description of the profile under study, ii) to estimate the relative degrees of soil formation, iii) to stratigraphically correlate our findings with the other known sections in northeastern Iran, iv) to propose a regional pedostratigraphy for the area.

5.2 The Neka-Abelou exposure

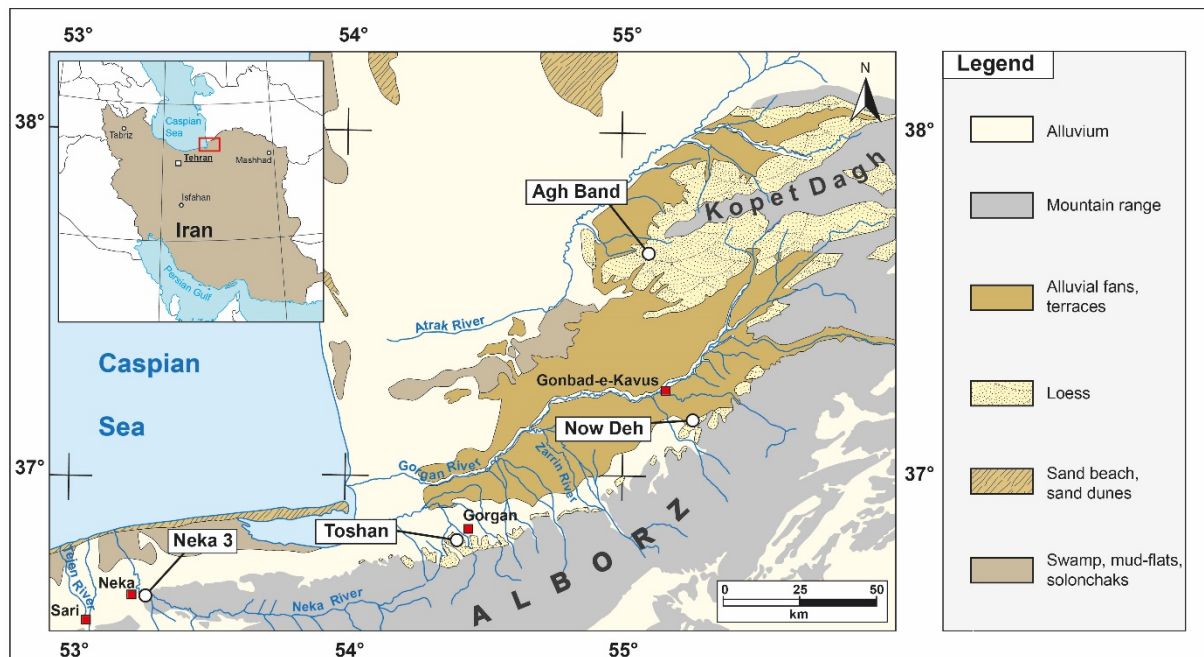


Fig. 5.1: Map of northeastern Iran showing the locations of the hitherto known loess-soil sequences and the occurrence of loess deposits supplemented by other geomorphological features in the region (based on National Iranian Oil Company, 1978). The location of loess deposits in the southwestern part of the study area have not been mapped yet and are therefore missing.

The Neka-Abelou profile (N 36°38'43"/ E 53°19'15') was investigated in a large loess quarry, located in the southern vicinity of the town of Neka and east of Sari (Fig. 5.1), where loess deposits attain a thickness of around 25 m. The quarry has the shape of an amphitheatre with a diameter of about 130 m. Towards the south the highest wall reaches 23 m above the present mining floor. To the west the quarry is bound by a large loess wall, left from previous loess mining in the past. Many of these loess walls, several hundred meters long, up to about 10 m high and more than 5 m thick, can be found near the town of Neka, testifying to intense loess mining in the past. The profile is located on a watershed position in the northwest facing part of the quarry, 105 m above sea level. The artificial exposure in the quarry of Neka-Abelou (Fig. 5.2 and 5.3) reveals numerous loess layers and palaeosols. Particularly the palaeosols as past land surfaces show a change of convex and concave forms and thus reflect the palaeorelief.

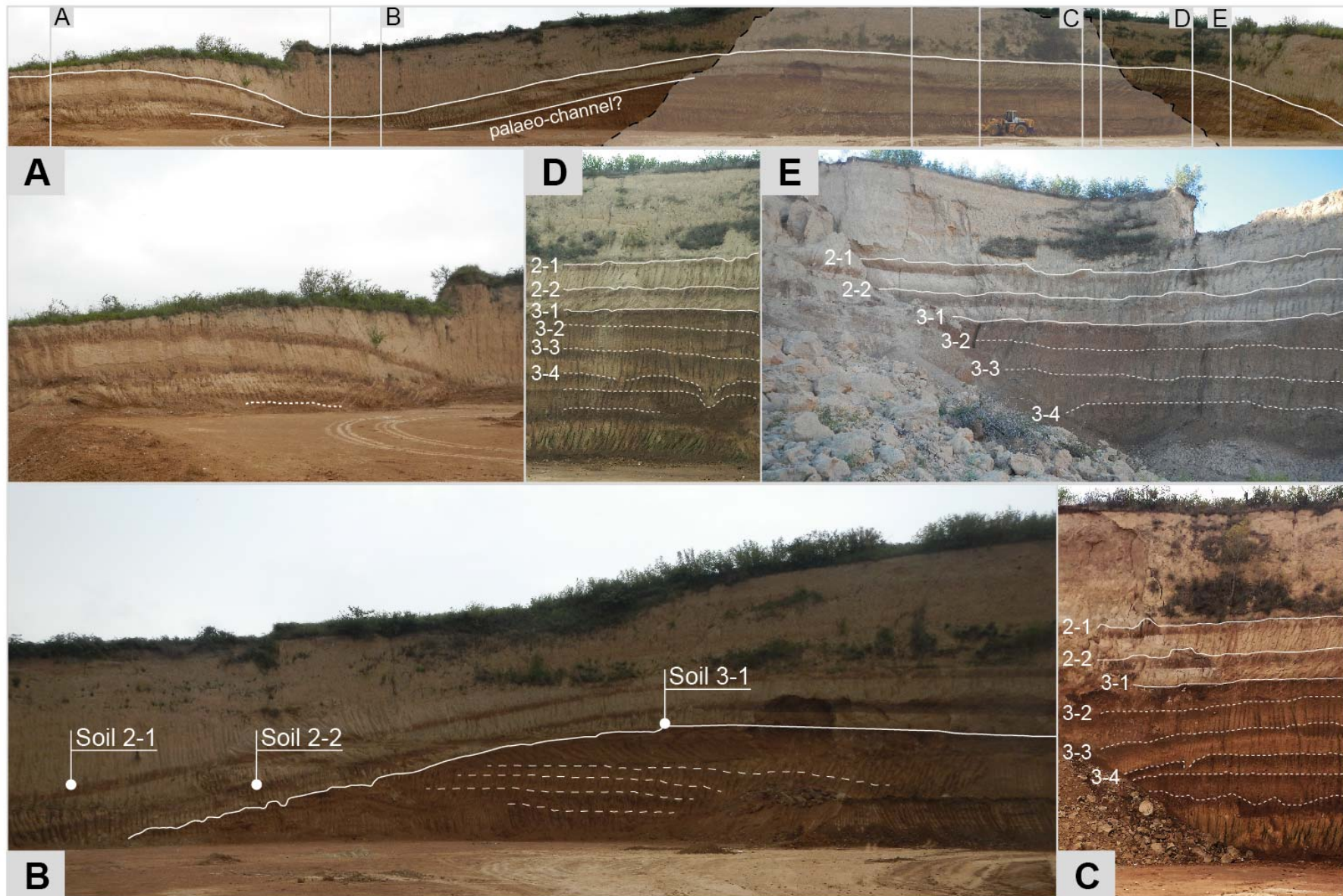


Fig. 5.2 Top: Panoramic picture displaying the palaeo-morphology of the Neka-Abelou loess-soil sequence. The lower concave line might be a hint at the formation of a palaeo-channel, which truncated palaeosols underneath soil 3-1. Picture **B** illustrates the unconformable contact of the MIS 5 pedo-complex (soils 2-1, 2-2 and 3-1) with underlying palaeosol horizons which are indicated by dashed lines. Pictures **C**, **D** and **E** show the location of sample extraction (panoramic picture and pictures **A** and **B** were taken by Martin Kehl in 2014; Pictures **C** and **D** were taken by Stefan Vlaminc in 2014; Picture **E** was taken by Stefan Vlaminc in 2015).

The thick white line in the panoramic picture of Fig. 5.2 coincides with a former land surface formed by palaeosol 2-1. This palaeosol suggests the presence of two hills (Fig. 5.2A, B), which are separated by a channel-like structure. Within these hills horizontally running palaeosols are apparent as indicated by dashed lines in Fig. 5.2A and B. These dashed lines are abruptly interrupted by the former land surface belonging to palaeosols 3-1 (Fig. 5.2B), giving potential evidence for morphodynamic activity. Similar features, however, at a considerably smaller magnitude, may be observed by in palaeosols 3-4 and 3-3, whose irregular upper boundaries seem to be additionally dissected by several small channels. Today the amphitheatre-like exposure of the Neka-Abelou exposure has collapsed (Fig. 5.2E). Subsequently, large parts of the loess wall are covered by a heap and no longer accessible.

5.3 Materials and methods

5.3.1 Field sampling

For field sampling the loess walls shown in Fig. 5.2E were selected, because this accessible part of the sequence is close to the watershed position. Moreover, the heap (in the foreground of Fig. 5.3A) gives access to the entire loess sequence.

In order to sample the whole succession of loess and palaeosols at Neka-Abelou seven discrete and trench-like profiles were prepared, penetrating into the steep loess walls in the quarry (Fig. 5.3). During the preparation of each profile care was taken to remove recently displaced material that had accumulated on these walls. Thus, pristine sediment samples could be extracted in 2 cm increments from Profiles M (modern soil), A, B, C and half of profile D. The remaining part of profile D and the profiles E and F were sampled in 10 cm intervals. These discrete profiles were aggregated along the sharp lower boundaries of palaeosols found in the Neka-Abelou section, thus forming a quasi-continuous pedostratigraphy. Additionally, 23 samples for micromorphology and 15 samples for optically stimulated luminescence dating were taken. Luminescence dating of these samples is still in progress, but age results measured on two pilot samples extracted in April 2014 from the east wall of the quarry will be included in this paper.

During field description the emphasis was placed on soil structure, mottling, precipitation of secondary carbonate, soil color and the nature of upper and lower boundaries of the respective strata. The different soil horizons were classified according to the WRB (IUSS Working Group WRB, 2007) whilst the visual color estimates are based on the Munsell soil color chart. Granulometric properties of each sample were determined by means of laser-diffractometric analysis resulting in 864 measurements. Mid-infrared spectroscopy (MIRS) was applied to predict the CaCO_3 -content of 100 samples and to create a preliminary record of calcium carbonate. These samples are evenly distributed over the Neka-Abelou -profile. Laser-diffractometric as well as MIRS measurements follow the same routines as those applied to the analyses of the Toshan and Agh Band sections. Hence, for a description of sample pretreatments and measurement procedures the reader is referred to chapters 2.

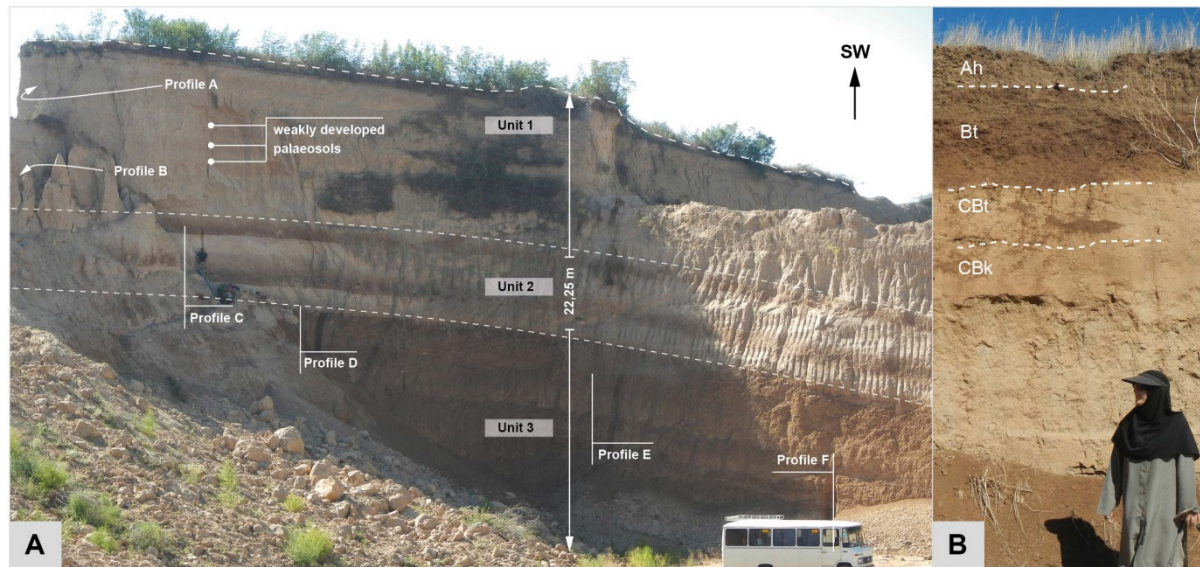


Fig. 5.3 A: Photograph of the Neka-Abelou section, showing the arrangement of profiles C, D, E and F penetrating in a northeastern facing wall within the partly collapsed quarry. Profile B is hidden behind collapsed blocks, while profile A was prepared on the reverse side of the quarry. **B:** The undisturbed modern soil (profile M) was found around 30 m to the east of the area displayed on the present photograph (photos taken by Martin Kehl, 2015).

5.4 Results

Fig. 5.4 shows the pedostratigraphic column of Neka-Abelou supplemented by granulometric and CaCO_3 -records. The stratigraphic sequence was subdivided into three units (Fig. 5.3), each of which is characterized by pronounced differences in sediment and soil colour. This subdivision also serves to structure the following descriptions. Additionally, palaeosol horizons are numbered depending on the allocated pedostratigraphic unit and their respective position within that unit. For example the second palaeosol in unit two is numbered soil 2-2.

Hitherto, age control independent from the dating results from Frechen et al. (2009) is restricted to two pIRIR_{290} age estimates being determined by Dr. Tobias Lauer in 2015, prior to Neka-Abelou field campaign. These results are given in Fig. 5.4.

5.4.1 Field description

Unit 3 (22.25-13.38 m below surface)

Unit 3 represents a succession of strongly developed Btk- and Bwtk-horizons as indicated by their structural, colorimetric and granulometric properties (Fig. 5.4). In the following descriptions only the strongly developed Bt, Btk and Btgk-horizon were numbered. These strata are bracketed by relatively less strongly developed layers denominated as Bwtk-horizons.

22.25-21.15 m: The basal stratum of the sequence is formed by a reddish-brown Bwtk-horizon hosting large angular blocky to prismatic soil aggregates (peds) with clay coatings on

their faces. Weak redoximorphic mottling is indicated by the presence of small bleaching spots and iron hydroxide and manganese oxide concretions. Between 21.75 and 22.00 m a dense network of horizontal carbonate crusts was detected. Moreover, carbonate nodules of spherical to ellipsoidal shape were found whose longitudinal axis may reach up to 22 cm. The Bwtk-horizon gradually merges into a reddish-brown Btk-horizon (3-5).

21.15- 20.15 m: The Btk-horizon (3-5) exhibits a clearly developed prismatic structure and clay coatings. Redoximorphic features similar to those of the subjacent layer are found. Furthermore, carbonate nodules of up to 4 cm in diameter were found.

20.15- 19.05 m: A reddish-brown Bwtk-horizon was detected whose lower boundary is defined by a 3 cm thick horizontal carbonate crust. This Bwtk-horizon differs from the underlying horizon by its angular blocky structure, which disintegrates into coarse blocky aggregates. The aggregate surfaces are strongly coated by manganese (Mn) and small bleaching zones. Carbonate nodules of spherical to ellipsoidal shape are found until 19.85 m. The diameter or the longitudinal axis of these nodules ranges between 4 to 7 cm. The Bwtk-horizon gradually merges into a stratum denominated as Btgk-horizon (3-4).

19.05-18.35 m: The diffuse lower boundary of the Btgk (3-4) was macroscopically identified by means of a gradual increase in prismatic structure elements and an evenly increasing reddish soil colour resulting in a reddish-brown horizon. Moreover, clear and comparatively large bleaching zones were found within soil aggregates. Several horizontal carbonate crusts (18.50-18.28 m) delimit the present Btgk from an overlying Bwtk-horizon.

18.35-17.5 m: This Bwtk-horizon is characterized by a reddish-brown soil colour and an increasingly blocky structure, which is strongly coated by Mn-oxides. The stratum was apparently affected by clay illuviation as evidenced by clay coatings. In the upper part of the Bwtk-horizon small horizontal carbonate crusts were found. Additionally, the structure merges into a more prismatic soil structure towards the overlying Bt-horizon (3-3).

17.5-16.9 m: The large prismatic aggregates of this reddish-brown Bt-horizon (3-3) are subject to strong Mn-mottling and include common clay coatings. Towards the top the Bt-horizon merges into a Bwtk-horizon.

16.90-16.25 m: The Bwtk-horizon is characterized by a gradual transition from a prismatic to a more angular blocky structure and exhibits less clay coatings than the subjacent stratum.

16.25-15.20 m: Another Btk-horizon (3-2) was detected by means of abundant clay coatings, a clearly developed prismatic structure and a reddish-brown soil colour. The large aggregates are densely coated by Mn-oxides. Between 16.05 and 15.20 m frequent spherical carbonate nodules were found whose diameter range from 2.0 to 3.5 cm. The stratum gradually merges into a moderately reddish-brown Bwtk-horizon

15.20-14.35: In the Bwtk-horizon less clay coatings were observed. The angular blocky to prismatic aggregates are covered by Mn-mottles. Between these aggregates spherical carbonate nodules are abundant, which are of analogous diameter as those found in the subjacent stratum.

14.35-13.90 m: A comparatively sharp colour boundary defines the transition into a overlying Btk-horizon (3-1). The Btk-horizon is reddish-brown and has an angular blocky to prismatic structure and common clay coatings. Analogous to the underlying strata in unit 1 a dense network of Mn-mottles was observed. Thick carbonate nodules (ca. 3 cm in diameter) were detected in the entire horizon. Towards the top the influence of reddish pigments upon the

soil colour seems to decrease gradually. Hence, from 13.90 to 13.38 m a horizon denominated as Bw(t)k was found. The horizon is characterized by a weakly reddish-brown soil colour and an angular blocky structure disintegrating into markedly finer aggregates than in the underlying strata. Conversely, the presence of clay coatings is not clear and has to be verified with micromorphological analyses. A pronounced secondary carbonate metabolism was identified by means of abundant pseudomycelia in the void zones between the aggregates. Additionally, spherical carbonate nodules could be found, however less than in the underlying horizons described above. These nodules are slightly smaller, reaching diameters of 1.5 to 2.5 cm.

Unit 2 (13.38-6.14 m below surface)

13.38-12.88 m: A brownish BCK-horizon forms the basal segment. This denomination was chosen, since the stratum is basically dominated by structural properties testifying to soil formation such as a fine subangular blocky structure. Conversely, the present horizon hosts merely a minor portion of elements associated with loess as parent material such as its coherent soil structure. Furthermore, the present BCK-horizon is strongly recalcified by a dense network of pseudomycelia filling particularly the secondary pores. It is delimited by a sharp boundary, separating the BCK from the overlying stratum.

12.88-12.63 m: Whitish Bkkm-horizon hosting three distinct horizontally orientated carbonate crusts, each being separated by strongly recalcified layers of angular blocky soil aggregates. These crusts and the recalcified layers form a petrocalcic horizon, defining the sharp lower boundary of an overlying horizon.

12.63-12.18 m: Brownish Bw-horizon (2-2). The Bw-horizon comprises small aggregates forming a strongly developed angular blocky structure. In its upper part the soil colour of the Bw-horizon is increasingly dominated by blackish pigments.

12.18-11.78 m: A blackish ABwk-horizon was identified, exhibiting analogous structural properties as the subjacent Bw-horizon. In addition, the ABwk-horizon shows abundant pseudomycelia. The influence of blackish pigments upon the soil colour markedly decreases up to a depth of 11.78 m.

11.78-11.48 m: Gradual transition into a light brownish BCK-horizon. The soil structure exhibits an evenly gradual shift towards a subangular blocky structure. Analogous to its counterpart in the basal segment of unit 2, the BCK-horizon shows abundant pseudomycelia and a minor portion of coherent structure elements.

11.48-11.38 m: The amount of coherent structure elements increases with decreasing depth, forming a CBk-horizon. In contrast to the subjacent horizon, the coherent structure associated with loess as parent material prevails in the CBk-horizon and subangular blocky aggregates show decreasing abundance. Thus, the succession of BCK- as well as CBk-horizon represents a continuum, which is indicative of a gradually decreasing degree of pedogenesis.

11.48-10.93: A layer of dull yellowish loess (C-horizon; L5) is found, which is characterized by a coherent structure. The loess stratum is delimited by a sharp boundary from an overlying horizon.

10.93-10.53 m: Whitish-yellow Ck-horizon. The Ck-horizon has a coherent structure, which is coated by soft powdery carbonate. The upper boundary of this horizon is gradual in nature.

10.53-10.18 m: A whitish-brown CBk-horizon was found. The CBk-horizon was subject to a pronounced secondary carbonate metabolism as indicated by abundant pseudomycelia refilling the void zones of the macro aggregates.

10.18-9.98 m: A sharp transition defines the lower boundary of a whitish Bkkm-horizon. Analogous to the first Bkkm-horizon (12.88-12.63 m) in unit 2, the present petrocalcic horizon comprises several carbonate crusts, being separated by strongly recalcified layers comprising small subangular aggregates.

9.98-9.44 m: Dark brownish Bw-horizon (2-2), which is delimited along a sharp boundary from the subjacent petrocalcic horizon. The Bw-horizon exhibits a clearly developed angular blocky structure, disintegrating into comparatively small aggregates. In contrast to the underlying horizons, the present Bw appears to be completely decalcified. It shows a diffuse upper boundary.

9.44-8.74 m: Light brownish BCK-horizon, dissected by a dense network of pseudomycelia. The BCK-horizon comprises subangular aggregates but also coherent parts, thus forming a transitional stratum between B and C horizon.

8.74-8.29 m: Gradual transition into a light yellowish-brown CBk-horizon. Its soil structure is dominated by a coherent structure comprising a minor portion of small subangular aggregates. The entire horizon is subject to an intense secondary carbonate dynamics as shown by abundant pseudomycelia. Interestingly, the CBk-horizon hosts thick charcoal pieces of hitherto undetermined plant taxa found between 8.50 and 8.47 m. These charcoal pieces are cubically shaped and their lengths range from 0.75 to 1.5 cm.

8.29-8.19 m: Dull yellowish loess, defining the completion of unit 2. Interestingly, this loess stratum hosts a thin tephra layer (8.25 to 8.21 m), which was characterized by a coherent structure and a greyish colour.

Unit 1 (0.00-8.19 m below surface)

8.19-5.86 m: Analogous to the underlying, however considerably thinner loess layers within the profile this thick loess stratum (L4) has a coherent structure. Undetermined mollusc taxa were macroscopically observed which are sparsely distributed over this loess layer.

5.86-5.32 m: Transition into a CBk-horizon (1-4). This horizon differs from loess by its light brownish-yellow soil color. The structure of this CBk comprises a minor portion of subangular blocky aggregates, being embedded in a coherent matrix. The CBk-horizon is sparsely covered by pseudomycelia. Furthermore, mollusc shells of unknown taxa were detected. Its upper and lower boundaries are gradual in nature.

5.32-3.89 m: Layer of dull yellowish loess (L3) with a coherent structure. Shell fragments of undetermined mollusc taxa were found within this layer. Towards the top a gradual transition into an overlying soil horizon is apparent.

3.89-3.40 m: Another weakly developed C(B)k-horizon (1-3) which was identified merely by its light brownish-yellow colour forming a subtle and gradual upper and lower boundary. The macroscopic investigation of the soil structure revealed the absence of any aggregation. The C(B)k-horizon shows signs of powdery lime and fragments of mollusc shells.

3.40-2.86 m: Layer of dull yellowish loess (L2), showing a coherent structure. Analogous to underlying strata, L2 hosts fragments of mollusc shells.

2.86-2.26 m: The present light brownish-yellow C(B)k-horizon (1-2) shows a coherent soil structure and gradual upper and lower boundaries. The soil structure is partly disturbed by bioturbation features in the form of krotovina and former root channels. Moreover, fragments of mollusc shells were found.

2.26-1.64 m: Layer of dull yellowish loess (L1). This loess layer has a coherent structure which is also marked by root channels and krotovina. Towards the top a relatively sharp boundary was observed.

1.64-1.34 m: Brownish-yellow CBk-horizon. The CBk is largely composed of a coherent soil structure with minor portions of initially subangular blocky aggregates. Pseudomycelia are particularly found within inter aggregate zone. The pseudomycelia are partly disrupted by krotovina. This CBk-horizon is believed to belong to the modern soil.

1.34-0.00 m: The upper boundary of this CBk was attributed to a depth of 1.26 below surface, where it gradually merges into a moderately strong reddish-yellow CB(t)-horizon (1.26-0.90 m). The CB(t) represents an admixture of clearly developed angular blocky aggregates and structurally coherent parts. The blocky aggregates show sparse clay-coatings and the entire stratum appears devoid of carbonate. From 0.90 to 0.44 m a strongly developed reddish-brown Bt-horizon (1-1) was detected, comprising large angular blocky to prismatic aggregates. Towards its upper part the colour of the Bt-horizon is increasingly affected by blackish pigments, which mark the gradual transition into the overlying Ah-horizon (0.44-0.00 m). The Ah-horizon has an angular blocky structure. Clay coatings were detected only in its lower part. In summary the modern soil consists of a succession of Ah-Bt-CB(t)-CBk-C horizons. According to the WRB (2014) the diagnostic argillic (Bt-horizon) may qualify this soil as Luvisol if it is found in a depth of 0.5 to 1.0 m below surface. Additionally, this soil classification requires the argillic horizon to have a high cation exchange capacity (CEC) as inferred by pH 6. The present argillic horizon reached pH values of 6.2 to 6.5. Thus, the modern soil at Neka-Abelou is classified as Luvisol (WRB 2014).

5.4.2 Carbonate content

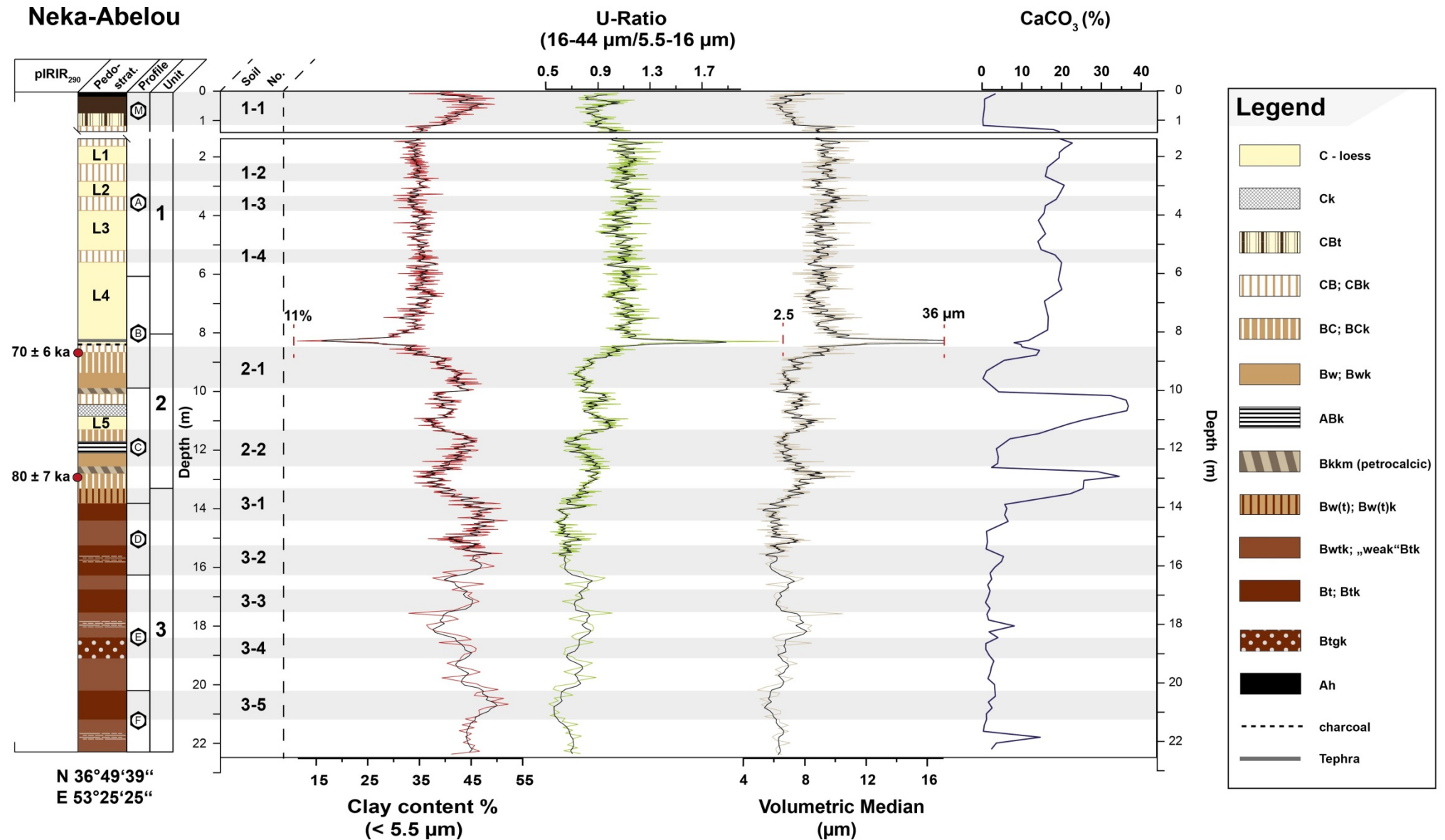
The amount of calcium carbonate in relatively unweathered loess layers of the Neka-Abelou section ranges from 14 to 19%, while average values attain 15.7% (Fig. 5.4). Generally, the CaCO_3 -content reflects the threefold division of the section into units. Carbonate content in unit 3 is equally low both in Bwtk and Btk-horizons, reaching ca. 3.5%. Conversely, carbonate enrichment zones in the form of horizontal carbonate crusts cause peaks in carbonate content (up to 40%), which are centered at depths of 22, 18 and 15.5 m (Fig. 5.4). The overlying unit 2 shows the highest amplitude of the entire sequence. CaCO_3 amounts in soils 2-2 and 2-1 approach ca. 2%, while culminations in carbonate content are referred to the position of a Ck- and Bkkm-horizons attaining 35%. Further carbonate enriched parts within unit 2 such as CBk-horizons exhibit values of ca. 16%. In contrast intermediate contents of carbonate were received for unit 1. The modern soil (1-1) seems largely

decalcified, whereas carbonate content in weakly developed palaeosols 1-2 to 1-4 amounts to ca.16.5% (Fig. 5.4).

5.4.3 Grain-size

The granulometric properties of the Neka-Abelou loess-palaeosol sequence (Fig. 5.4) indicate a fining downward trend from unit 1 to unit 3. The strongly developed Bt-, Btk and Btgk-horizons in unit 3 (soils 3-5 to 3-1) exhibit clay ($<5.5\ \mu\text{m}$) proportions between 47.5 and 53%. Clay contents of less strongly developed Bwtgk-horizons span the range from 35 to 47%. Conversely, these strata are characterized by highest U-ratios ($16\text{-}44/5.5\text{-}16\ \mu\text{m}$) within unit 3, attaining values of ca. 0.9 and median particle sizes between 7 and $10\ \mu\text{m}$. Soils 3-5 to 3-1 are composed of a finer texture as evidenced by U-ratios of ca. 0.5 and volumetric median of around $6\ \mu\text{m}$ (Fig. 5.4).

Palaeosols 2-1 and 2-2 comprise analogous textural patterns. Maximum clay proportions are found in Bw and ABk-horizons ranging from 38 to 46.5%. Consequently, U-ratios and median particle-sizes reach minimum values of 0.5 and ca. $6\ \mu\text{m}$. The amount of clay-sized particles in soil 2-2 gradually decreases towards the overlying loess (11.48-10.93 m) reaching up to 37%. U-ratios and median grain-size indicate an inverse trend, gradually increasing to values of 1.1 and $10.5\ \mu\text{m}$, respectively. Clay contents of palaeosol 2-1 decrease in a corresponding manner as compared to palaeosol 2-2 attaining ca. 35%. However, the gradual transition seems to be interrupted by recurrent cascade-like increases in clay-sized particles (Fig. 5.4). This trend is also reflected by records of U-ratio and median grain-size, indicating a cascade-like coarsening upwards and corresponding values of up to 1.1 and $10.5\ \mu\text{m}$. Obviously, the transition from unit 2 into unit 1 is marked by an abrupt culmination in U-ratios and volumetric median, which attain 2.5 and $36\ \mu\text{m}$, respectively. As opposed to its underlying counterparts, unit 1 represents the coarsest segment of the Neka-Abelou section. It hosts loess, which is relatively unaltered by soil forming processes and weakly developed intercalated palaeosols. The consistent behavior of recorded U-ratios, clay proportions and median particle-sizes suggest minor textural differences between both types of strata with only little variation. Clay contents reach 33 to 36%. Moreover, U-ratios and medians span the range from 1.0 to 1.3 and 9 to $12\ \mu\text{m}$, respectively (Fig. 5.4). Considering particularly the running means of these records reveals frequently recurring coarsening and fining trends. However, the granulometric properties of soils 1-4 and 1-2 do not differ from those of the loess layers bracketing them. Conversely, soil 1-3 is characterized by slightly decreasing clay contents (33%) and corresponding increases in U-ratio (1.3) and median grain-size ($12\ \mu\text{m}$). The modern soil (1-1) is finely textured as indicated by clay contents of up to 50% and median grain-size of $5.5\ \mu\text{m}$. The relationship between medium and fine silt as expressed by U-ratios, are centered at 0.9 (Fig. 5.4).



5.5 Discussion

5.5.1 Relative changes in wind velocity and dust source area deduced from textural composition of loess

The textural composition of loess depends on wind strength and intensity, the distance from the source of clastic sediments, susceptible to aeolian entrainment, the number of dust sources and their particle-size characteristics (Tsoar and Pye, 1987; Sun 2002).

Loess layers at Neka-Abelou section exhibit a relatively coarse grained habitus as compared to palaeosol horizons (Fig. 5.4) which is reflected by higher U-ratios and volumetric median values and lower clay contents. The conjunction of these proxies implies higher wind energy during the formation of L1 to L5, since middle to coarse silt provide higher weight and are thought to be transported in short suspension cascades operating on low altitudinal levels and over relatively short horizontal distances (Tsoar and Pye, 1987; Pye 1995). Higher portions of coarser particles may also be translated into the extension of dust source areas as continuous aridification during stadials is believed to result in a retreat of vegetated land surfaces promoting the formation of deflation areas and hence phases of morphodynamic activity (Kehl, 2010; Vlamincx et al., 2016). Conversely, high amounts in clay particles primarily reflect reduced wind velocities. The deposition of sediments rich in clay and fine silt may suggest moister interstadial climatic conditions favouring the extension of vegetation cover thus causing a retreat in potential deflation areas. Such intervals are associated with morphodynamic stability promoting soil formation. It was shown, that the syngenetical palaeosols of the Toshan section have not experienced notable depletion in feldspar minerals. Thus, high clay amounts in these soils likely constitute a primary feature due to reduced wind velocity and/or distal sediment supply. In contrast post-genetical palaeosols are characterized by the secondary formation of siliceous clay (see chapter 3). Reduced U-ratios are therefore the result of chemical weathering and subsequent textural alteration of the parent material.

Loess at Neka-Abelou has a median grain size of 9.12 μm , and hosts considerable amounts of clay which may indicate a predominantly distal sediment supply. However, Fig. 5.5A reveals a polymodal particle-size distribution of loess in the Neka-Abelou loess-palaeosol sequence. This polymodality encompasses a variety of coarse grain-size fractions such as middle and coarse silt, and fine sand, which indicate sediment supply from proximal dust source areas and/or higher wind strength. Thus, airborne dust, forming loess at Neka-Abelou most likely originates from proximal as well as distal dust sources.

The textural compositions of L1 to L4 are remarkably consistent with the average particle-size distribution of loess (Fig. 5.5A) suggesting that loess at Neka-Abelou formed under comparable wind and moisture regimes. In contrast to these loess strata, L5 exhibits higher clay and fine silt contents at the expense of the middle to coarse silt and the fine sand fractions. These compositional differences might reflect less dynamic atmospheric conditions and/or post-sedimentary alteration by weathering processes. The down-profile variations of the granulometric proxies (Fig. 5.5) show that loess formation associated especially with unit 1 (L1 to L4) is characterized by recurrent phases of coarsening and fining as expressed by high-frequent fluctuations in clay contents, U-ratio and median. These fluctuations suggest highly dynamic atmospheric conditions. The transition from unit 1 to unit 2 is marked by a

culmination in U-ratio and median values, which coincide with a tephra layer. A similar peak was detected in a comparable stratigraphic position within the Toshan section. It is therefore, likely that this feature represents a regional rather than a local phenomenon. However, the magnitude of this culmination is twice as high in the Neka-Abelou section than in the Toshan loess-palaeosol sequence.

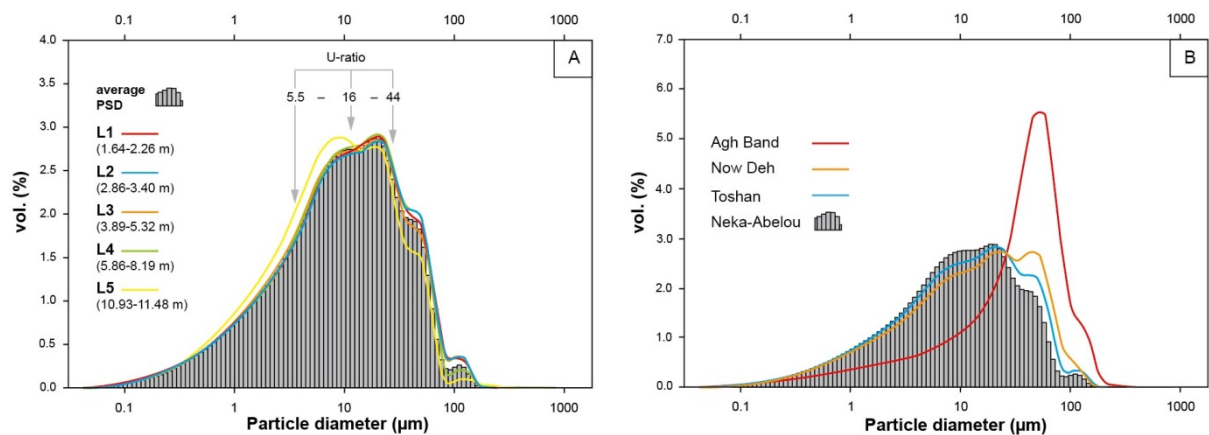


Fig. 5.5 A: Histogram showing the average particle size distribution (PSD) of loess at the Neka-Abelou loess-palaeosol sequence. This average distribution is superimposed by PSD of distinct loess layers (L1 to L5) in order to illustrate compositional differences. **B:** Histogram displaying the average particle-size distribution of loess deposits in the Neka-Abelou section, superimposed by granulometric composition of the Toshan, Now Deh and Agh Band sections.

5.5.2 Palaeosols at Neka-Abelou: implications for polygenesis and differential soil formation

“Polygenetic soils are those that record multiple morphological, mineralogical and chemical imprints as the geographical pattern of climates shifts spatially and new boundaries are established.” (Chadwick et al., 1995). The detection of polygenesis is crucial because in palaeopedology palaeoclimatic information is deduced from comparison of palaeosols with the modern soil, having formed under known climatic conditions. For instance the comparison of strongly weathered polygenetic palaeosols with the modern soil might therefore yield misleading results. However, the distinction between single phases of polygenesis might be very subtle. This is particularly the case if a given palaeosol records multiple climatic intervals, which have promoted strong weathering and thereby obliterated the original climatic signal or previous palaeoclimatic influences on the formation of the respective soil.

Unit 3 forms a succession of strongly developed polygenetic palaeosol horizons (soils 3-5 to 3-2) which are apparently intercalated in less strongly developed Bt or Bwtk horizons (Fig. 5.2 and 5.4). Differences in the degree of pedogenesis of these palaeosols may be addressed by means of combined macroscopic observations and analytical data from MIRS and laser-diffractometry. The polygenesis of these palaeosols is exemplified by soil 3-2. This palaeosol hosts horizontal carbonate crusts, which separate this stratum into an upper and a lower part. The incrustated horizon might indicate the former leaching front of loess overlying soil 3-2, which was decalcified in response to a subsequent palaeoclimatic episode. The

descendant translocation and final precipitation of dissolved Ca^{2+} formed the present carbonate crust found in a depth of 15.80 m. This incrustation formed in an already well developed palaeosol horizon. Thus the upper part of soil 3-2 has experienced at least two cycles of chemical weathering, affecting its pedogenic properties. Such incrustated strata were also found in two Bwtk-horizons at around 18 and 22 m below surface and might be indicative of a likewise polygenesis. Moreover, the palaeosols of unit 3 suggest comparable degrees of soil formation, since they all comprise a coarse prismatic structure and comparable clay amounts. It is very likely that this complex of reddish soil horizons was affected by a multitude of palaeoclimatic intervals thus obliterating monogenetic soil properties. The comparison of palaeosols 3-5 to 3-2 with the modern soil is obsolete owing to the strong polygenetic overprint.

Palaeosol 3-1 holds the uppermost position in the line of strongly developed Bt-horizons attributed to unit 3. Fig. 5.2B shows that this soil cuts subjacent and horizontally orientated palaeosols, forming a convex shaped erosional unconformity. Conversely, Fig. 5.2C to E illustrates the sampling location within the quarry, where palaeosols 3-1 to 3-4 run parallel. Possibly, the land surface was truncated by one or several erosional events, prior to the formation of soil 3-1 thus exhuming the former surface. It is most likely, that soil 3-1 did not form on unweathered loess deposits, but rather on material that was affected by soil formation during previous palaeoclimatic intervals. Based on field observations, soil 3-1 exhibits a comparable degree of pedogenesis as its subjacent counterparts (see chapter 4.1.1). We conclude that the formation of this soil comprises several climatic stages and at least one phase of morphodynamic activity.

Thus, soil 3-1 is considered a polygenetic soil. From a pedostratigraphic point of view soil 3-1 could be tentatively attributed to the last interglacial (MIS 5e), as it is the third strongly developed palaeosol based on “counting from the top”. Moreover, preliminary results from OSL-dating yields an age estimate of >80ka (Fig. 5.4). This assumption is, however, afflicted with severe restrictions since i) there is currently no age control available from underneath this palaeosol, ii) consequently the timing of morphodynamic activity phases cannot be limited iii) and it cannot be excluded that the last interglacial soil was completely eroded and is therefore missing.

Other “red series” of strongly weathered loess deposits and palaeosols that might compare to unit 3 of the Neka-Abelou section are found in the Iranian loess Plateau. There, reddish loess deposits are structured by strongly reddish palaeosols (Wang et al., 2016a). This sequence of early to middle Pleistocene age is overlain by late Pleistocene loess deposits. Although Wang et al. (2016a) do not provide a thorough profile description a similar pattern is observed in unit 3, where weathered horizons are structured by strongly developed palaeosols, which are unconformably overlain by late Pleistocene loess deposits. We therefore hypothesize that the sequence of unit 3 may be allocated to the middle Pleistocene.

Soils attributed to unit 2 form a complex of strongly and weakly developed palaeosol horizons. Palaeosol 2-2 hosts a thick ABk-horizon (Fig. 7.1), which compares to soil 5-2 found in the Toshan section, in which also an ABk-horizon was detected (Vlaminck et al., 2016). The thickness of the ABk-horizon of the Neka-Abelou section suggests that soil development was affected by accumulation of biomass. In contrast to the modern soil, no

clay coatings could be detected in the field, suggesting that this soil formed under more arid conditions than the present climate. Hence, we assume steppe-like environmental conditions. However,



Fig. 5.6: Palaeosols 2-2 and 2-1 allocated to unit 2. Both palaeosols are characterized by gradual upper boundaries. To the top of palaeosol 2-1 thick charcoal pieces were found (A). B: decalcified Bw-horizon belonging to pedo-complex (PC) 2-2. C: relatively unweathered loess, separating PC 2-2 from 2-1. D: recalcified ABk-horizon belonging to PC 2-2.

the genesis of this ABk-horizon as well as its genetic relation to the underlying Bw-horizon has to be verified by means of micromorphological analyses, because both soil horizons might potentially be the result of independent palaeoclimatic episodes.

Towards the top, the ABk-horizon gradually merges into a BCk-horizon (Fig. 5.4 and Fig. 5.6). This transition is also verified by equally decreasing clay contents (Fig. 5.7). According to results from Vlamincx et al. (2016) such gradual boundaries may be considered as syngenetic soil formation. Generally, deposition of calcareous dust and soil formation are two competing processes and the presence of palaeosol horizons indicates the predominance of pedogenesis (Guo et al., 1996). Thus, we hypothesize that the formation of the BCk-horizon indicates a gradual aridization leading to the accumulation of unweathered loess (L5), when dust supply and moisture availability reached a threshold value. Pseudomycelia within the void zones of the ABk-horizon testify not only to a pronounced secondary carbonate metabolism (Fig. 7), but also indicate leaching from the overlying BCk-horizon causing polygenetic alteration.

While palaeosol 2-1 is characterized by similar structural and textural properties as compared to soil 2-2, there was no macroscopic evidence of any fossil top-soil horizon.

Possibly, this humic horizon was truncated during a phase of morphodynamic activity. Alternatively it might have been mineralized, preserving merely its microstructure.

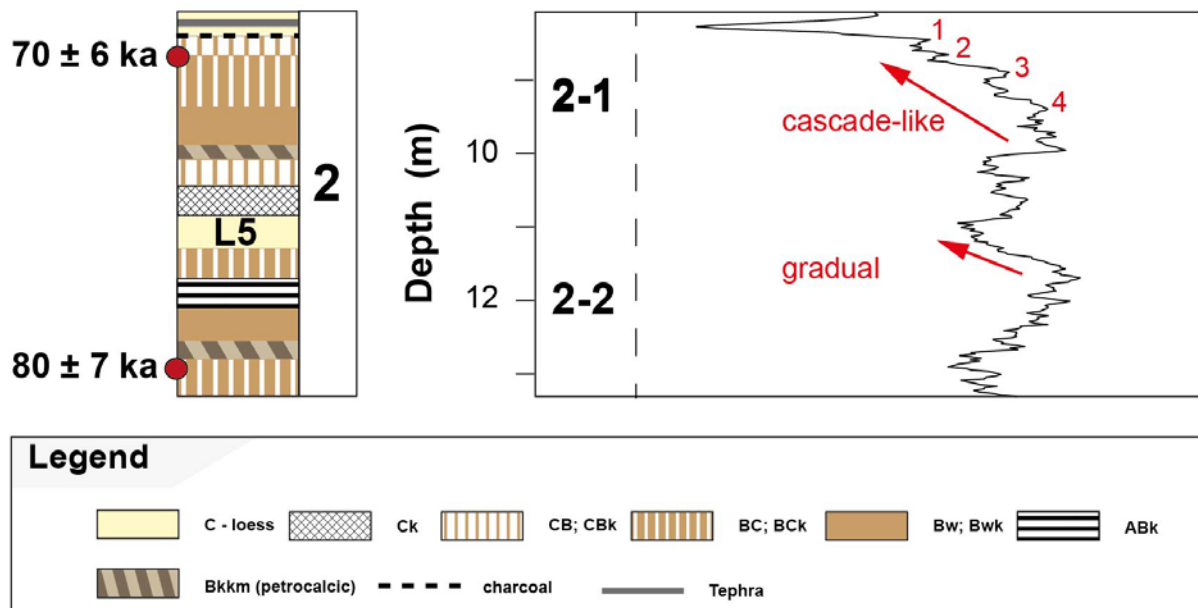


Fig. 5.7: Shape of upper boundaries of soils 2-2 and 2-1. The present curve was extracted from the running mean of the clay-contents graph shown in Fig. 5.4. While the transition from soil 2-2 into the overlying loess is gradual in nature, the upper boundary of soil 2-1 exhibits a gradual decrease, interrupted by 4 clay “pulses”.

Analogous to the underlying complex of palaeosols, soil 2-1 lacks macroscopically detectable clay coatings which might correspond with more arid conditions than the present climate. Palaeosol 2-1 merges into a BCK, followed by a CBk and relatively unweathered loess, indicating a weathering gradient. The overall gradually decreasing weathering trend towards the overlying loess is shown in Fig. 5.7. This trend is, however, interrupted by four clay pulses, which may testify to decreasing wind energy if these fluctuations are considered a sedimentary feature. Alternatively, these slight increases in clay contents might be the result of secondary clay mineral formation and thus indicate a gradual aridization, which was interrupted by four phases of moister climate (Fig. 5.7). Due to the intermittent decrease in clay contents, which superimposes the generally gradual trend, the upper boundary of soil 2-1 is denominated as cascade-like. In a Chronostratigraphic respect, palaeosols 2-2 and 2-1 might be tentatively allocated to interstadials of MIS 5c and 5a. This is not clear, since the age estimates are preliminary in nature and suggest somewhat younger ages in relation to the respective climatic stages defined within the marine and oxygen isotope stratigraphy (Rasmussen et al., 2014). Based on pedostratigraphic reasoning we hypothesize that the clay “pulses” presented in Fig. 5.7 indicate distinct climatic intervals such as e.g. interstadial substages.

The C(B)k-horizons detected in the deposits of unit 1 (soils 1-2 to 1-4) stand out from those of unit 3 and 2 by their weak degree of pedogenesis. In the field these soils were basically observed as layers of loess-like structure. Their light brownish color is likely based on the pigmenting effect of amorphous iron hydroxides such as ferrihydrite. Thus soils 1-4 to 1-2 were primarily detectable as weakly brownish layers bracketed by unweathered loess

deposits. These weakly developed soils neither exhibit a systematic increase in clay contents due to neoformation of siliceous clay minerals nor a subsequent decrease in volumetric median or U-ratio (Fig. 5.4). The carbonate contents are also close to those of unweathered loess, hence, an increased soil forming intensity due to leaching cannot be attested. Consequently, the analytical distinction of these weakly developed palaeosols from unweathered loess by means of grain-size analysis is difficult. Thus, the textural composition of these soils likely constitutes a primary feature. Possibly the particle-size distribution of soils 1-4 to 1-2 found in the Neka-Abelou loess-palaeosol sequence was not significantly altered by soil forming processes. If these palaeosols are considered the result of postgenetic soil formation the palaeosols would have inherited their granulometric properties from loess indicating wind energy prior to the onset of pedogenesis. In case of a syngenetic soil formation the grain-size distribution of these soils would reflect atmospheric conditions during the time of formation of soils 1-4 to 1-2.

More analytical data is required for an enhanced characterization of the palaeosols of the Neka-Abelou section such as the magnetic susceptibility, micromorphology and soil color determined by spectrophotometry.

5.5.3 Pedostratigraphy of northern Iranian loess along the northern declivity of the Alborz Mountains

After first sedimentological and palaeo-pedological works carried out by Kehl et al. (2008), improved stratigraphic investigations of the loess-palaeosol sequences at Now Deh, Toshan (Vlaminck et al., 2016), and Neka-Abelou as well as additional luminescence dating results (Lauer et al., 2017a) yielded further insight into the pedostratigraphic division of the MIS 5 pedo-complex and pleniglacial loess deposits.

The MIS 5 pedo-complex is composed of three strongly developed palaeosols, which were classified as Bt(k)-, ABk- and Bw(k)-horizons (Fig. 5.8). The uppermost horizon of this palaeosol triple is overlain by weakly weathered (typical) loess which is comparatively easy to recognize in numerous exposures in northeastern Iran. Thus, this loess layer and the pedo-complex combined constitute an excellent stratigraphic marker. In contrast to the MIS 5 pedo-complex, last pleniglacial loess hosts several syngenetical palaeosols such as CB and Bw-horizons (Fig. 5.8). The visual detection of these weakly developed palaeosol in the field is subtle, particularly if these are bracketed by pedogenically altered loess deposits. Conversely, analytical results yielded distinct signals in colour and magnetic susceptibility. Most of the syngenetical palaeosols are also characterized by minima in U-ratio and volumetric median and subsequent maxima in clay sized particles. As discussed in the previous chapter, grain-size fluctuations are not necessarily the result of chemical weathering, causing formation of secondary clay minerals but those may be primarily inherited from the parent material.

The lowermost palaeosol within the MIS 5 pedo-complex shows the highest degree of pedogenic maturity as compared to overlying palaeosols. At the Toshan and Now Deh loess-soil sequences for instance the lowermost soil is expressed as a double palaeosol being composed of one basal Bt-horizon overlain by a Bw-horizon (Fig. 5.8). Both palaeosols are genetically not related to one another (Vlaminck et al., 2016). The palaeosol allocated to this

pedostratigraphic position is similar to the modern soil of the respective loess-soil sequence. We therefore assume that these palaeosol horizons formed isochronously during a palaeoclimatic interval that resembled the present climatic conditions. However, at the Neka-Abelou section the palaeosol found in the respective stratigraphic position possibly formed during a previous palaeoclimatic interval and was potentially subject to considerable polygenesis, thus impeding a direct pedostratigraphic correlation (see previous chapter).

The last interglacial as chronostratigraphic unit is the most recent climatic interval being characterized by somewhat warmer climate conditions than those of the Holocene (Kukla, 2002). The timing of the last interglacial was determined by means of raised coral reefs, since eustatic sea-level changes represent a proxy that is globally in phase (Müller, 2009). The radioactive series of U-Th yielded ages of 127 ka to 115 ka (Muhs, 2002). In contrast, OSL-dating of the Toshan section yielded a time frame of 116 ± 8 ka to 98 ± 5 ka for the formation of the tentatively last interglacial palaeosol (soil 5-3b). The maximum age of this palaeosol is slightly younger considering the standard deviation of the age estimate. The chronological discrepancy is, however, higher in relation to the minimum age of 98 ± 5 ka. The results suggest that the palaeoclimatic interval promoting the development of this palaeosol lasted longer than the upper boundary of the last interglacial period, determined by U-Th dating. Despite the above mentioned restrictions we assume that palaeosols at the Neka-Abelou and Now Deh sections, equivalent to soil 5-3b of the Toshan loess-palaeosol sequence are associated with the last interglacial period. Currently, the analysis of recently extracted luminescence dating samples from the Neka-Abelou section is under progress, while the samples from the Now Deh sequence discussed by Frechen et al. (2009) will be reanalyzed by applying the pIRIR₂₉₀-protocol.

It appears that the MIS 5 pedo-complex is covered by poorly weathered loess. At Neka-Abelou this loess includes a thin tephra layer, which is particularly apparent with respect to the amount of clay-sized particles (Fig. 5.8). Preliminary results from OSL-dating within the present study yielded ages centered at ca. 70 ka, suggesting that this relatively coarse grained Tephra layer might have formed at the onset of MIS 4 or afterwards (Fig. 5.8). A comparable grain-size excursion was found in the Toshan section as well, which was sampled and analyzed independently from the Neka-Abelou section. It is therefore likely that the tephra layer may be found in Toshan after selective mineralogical investigations of our sample material.

The magnitude of the grain-size signal tends to decrease from the Neka-Abelou towards the Toshan section, while it seems to be missing in the Now Deh loess sequence (Fig. 5.8). We assume that this tephra might be associated with a volcanic eruption located in a western direction to our study area. Hitherto, it is not known which volcanic eruption the tephra may be allocated to. Nevertheless, such a layer represents an occasion for independent age control in a significant position just above the MIS 5 pedo-complex. It may therefore serve as a stratigraphic marker for the western and southwestern loess-palaeosol sequences, correlating with the formation of relatively unweathered loess (Fig. 5.8). At the Toshan section this phase of loess formation basically encompasses MIS 4, while MIS 3 is characterized by the development of weakly developed syngenetical palaeosols during interstadial climatic intervals (Vlaminck et al., 2016).

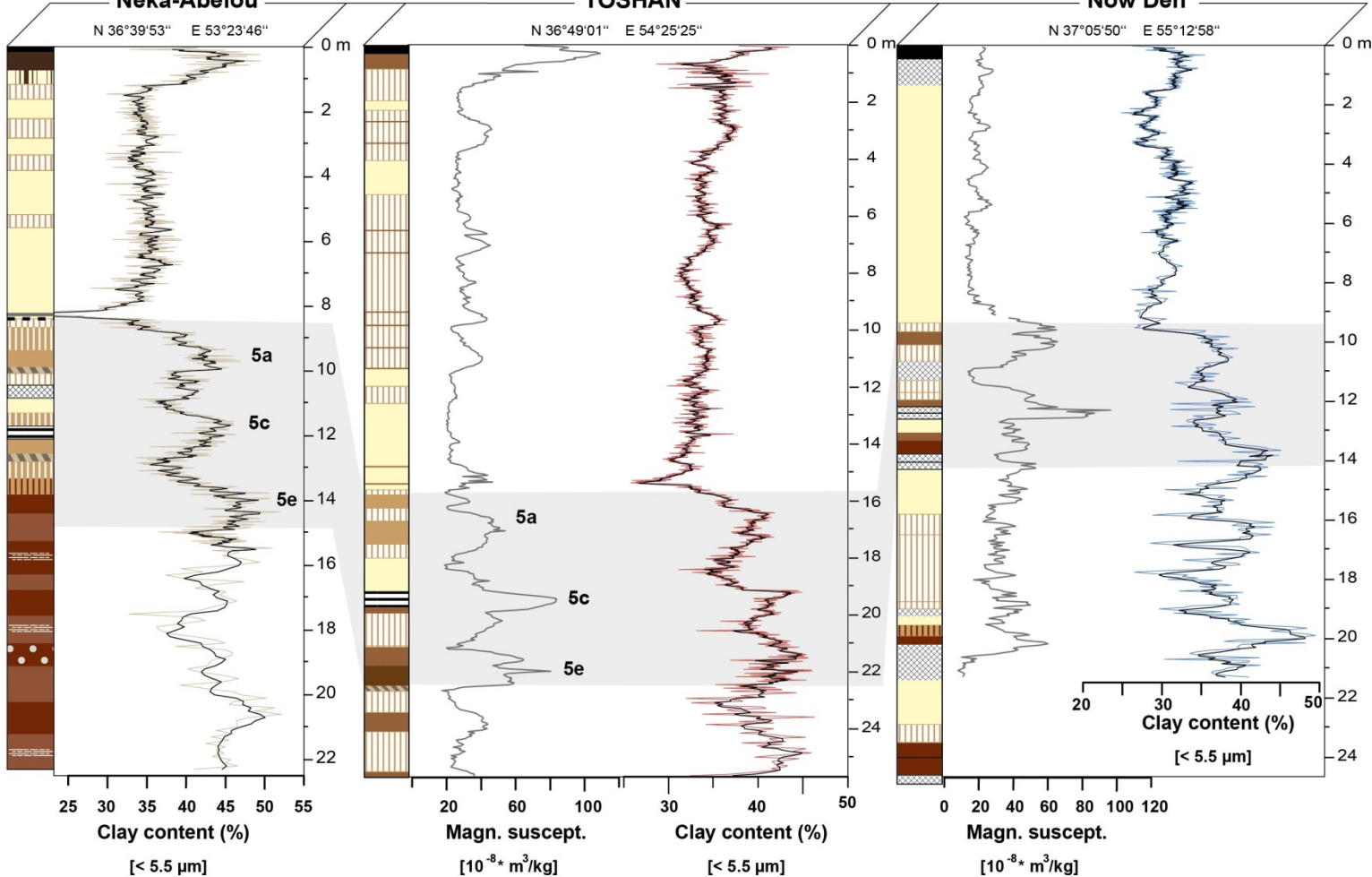


Fig. 5.8: Pedostratigraphy of northern Iranian loess sequences along the northern declivity of the Alborz Mountains. The MIS 5 pedo-complex is indicated by the greyish zone. This pedo-complex and the overlying layer of relatively unweathered loess combined constitute an excellent stratigraphic marker. Last pleniglacial loess hosts at least 3 weakly developed interstadial palaeosols. Due to large uncertainties in geochronological dating the intercorrelation of these fossil soil horizons as well as their allocation to distinct Greenland Interstadials (GI) remain unclear.

Such palaeosols were also found in the Neka-Abelou section. Although not given in the pedomorphology of the Now Deh loess-palaeosol sequence (Fig. 5.8), its rock magnetic signature suggests the presence of at least four weakly developed palaeosols intercalated in pleniglacial loess deposits. At the Neka-Abelou section three of these palaeosols were visually detected. Further analyses such as e.g. magnetic susceptibility might reveal more palaeosols and thus foster the development of a more differentiated pedomorphology. Thus, the different numbers of interstadial palaeosols recognized in northeastern Iranian loess deposits may be the result of hitherto lacking analytical results. Notwithstanding this deficit, such strata might be lost due to phases of morphodynamic activity, causing the complete or partial truncation of soil horizons. Differences in dust accumulation and edaphic moisture availability may also be responsible for a different number of these palaeosols. For instance low sedimentation rates in relation to high precipitation rates might cause polygenetic overprint of the previously developed palaeosol. Thus, one fossil soil horizon could represent several palaeoclimatic intervals. Conversely, high sedimentation rates of calcareous dust in relation to low precipitation rates might inhibit silicate weathering. Subsequently, relatively moist climatic intervals would not be recorded in the form of differentiated palaeosol horizons.

Generally, the presence of these interstadial soil formations in the present loess deposits is indicative of a palaeoclimatic phenomenon of regional magnitude. In global palaeoclimatology fluctuations of climate allocated to interstadials of MIS 3 are thought to operate on millennial or even centennial time scales (Dansgaard et al., 1993; Voelker, 2002). In this context potential millennial or sub-millennial scale fluctuations are difficult to define, since standard deviation of OSL-dating techniques amounts for ca. 10% of the average age estimate. The palaeoclimatic intervals of interest recorded during MIS 3 fall within the range of standard deviation. Hence, the intercorrelation of interstadial palaeosols in northeastern Iranian loess is afflicted with considerable uncertainty.

The textural composition of these loess deposits exhibits a coarsening trend in a northwestern direction as shown in Fig. 5.9. Coarser particles are likely to be transported by stronger winds and may also indicate proximal sediment transport. Thus, the strong statistical relationship between average volumetric median values and the geographical latitude (Fig. 5.9) suggests dust transport by north to northeasterly winds. Since the statistics in Fig. 5.9 relies merely on four values it is to be verified by further sampling sites in order to close the gaps along the regression line. North to northeasterly winds are most frequent during late autumn and winter as the influence of the Siberian anticyclone intensifies (see chapter 1.2). Assuming that the synoptic climate during modern winter might roughly serve as analogue for stadial air mass movements, we hypothesize that the activity of the Siberian anticyclone is one of the primary drivers of dust transport.

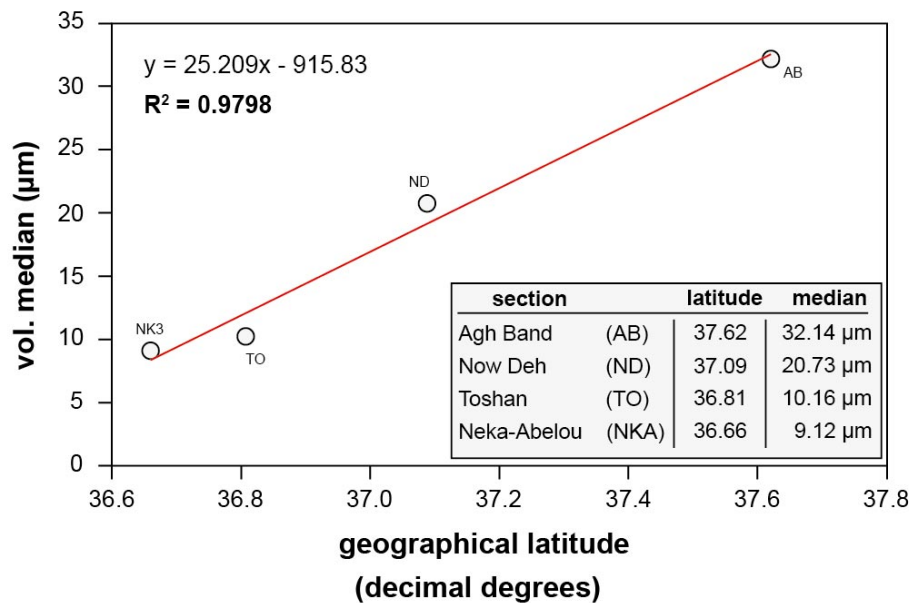


Fig. 5.9: Statistical relationship between the volumetric median and the geographical latitude of the loess-soil sequences located along the northern foot slopes of the Alborz Mountain range supplemented by data from the Agh Band section in the Iranian Loess Plateau. The volumetric median given in the present figure represents an arithmetic mean of all volumetric median values from all layers denominated as loess (C) in the respective loess section. The strong coefficient of determination is valid on a confidence interval of >0.95.

5.6 Conclusions

During the last interglacial-glacial cycle recurrent intervals of aridization alternating with moister climatic conditions promoted the analogous extension and retreat of dust sources in the Caspian Lowland. Located in a distal position to these deflation areas, the Neka-Abelou section is composed of finely textured (clayey) loess deposits in which at least ten palaeosols are intercalated. In addition a tephra layer was found in early glacial loess deposits of the section, which may provide independent age control and thus contribute to a resilient chronostratigraphy.

Repeated phases of morphodynamic activity have caused the truncation and exhumation of former land surfaces found in Unit 3 which were pedogenically altered by subsequent palaeoclimatic intervals. The succession of strongly weathered palaeosols in Unit 3 may potentially give insights into early to middle Pleistocene. In this context the base of the MIS 5 pedo-complex, the tentatively last interglacial palaeosol, possibly formed on preweathered soil material and therefore records multiple palaeoclimatic changes.

During the following interstadials of the early glacial period two polygenetic palaeosol complexes formed, encompassing ABk, Bw(k), BCK and CBk-horizons that may be correlated with the MIS 5 pedo-complexes found in the Toshan and the Now Deh section. This palaeosol triple is overlain by relatively unweathered loess and thus constitutes an excellent stratigraphic marker.

Spatial trends deduced from the textural composition of pleniglacial loess deposits of the region suggest that airborne dust was transported by north to northeasterly air mass flows whose intensity and/or strength seem to have decreased towards the Neka-Abelou section.

The pleniglacial loess strata along the northern declivity of the Alborz Mountains host at least four syngenetical palaeosol horizons that formed in response to ongoing dust deposition competing with edaphic moisture availability. The occurrence of these weakly developed interstadial soil horizons is therefore a supraregional phenomenon. Due to large uncertainties in geochronological dating the allocation of these fossil soil horizons to a specific Greenland Interstadial (GI) and their intercorrelation remain unclear.

Chapter 6

Comprehensive discussion

„Loess is not just the accumulation of dust“

M. Pécsi (1990)



As part of this doctoral thesis three new loess-palaeosol sequences were described, sampled and investigated by means of a multi-proxy approach. Records of soil colour, magnetic susceptibility, grain-size and CaCO_3 -content were elaborated, standing out from other western and central Asian loess sections by their highly resolved character.

The present dissertation, thus, provides differentiated insights into the palaeopedological and sedimentological properties of the Neka-Abelou, Toshan and Agh Band sections. During the thorough investigation of these sequences considerable attention was attributed to the palaeoclimatic implications of the respective findings and their spatial relevance for northeastern Iranian as a loess region. The presented results, however, are not only of high regional relevance but may be placed into a broader spatial context and thus contribute to improve the global palaeoclimatic record. In the following chapter key findings of the work on northeastern Iranian loess and its palaeoclimatic implications are discussed.

6.1 Pedostratigraphic improvements based on high-resolution proxy records of loess and palaeosols

In chapters 2 to 5 highly resolved proxy-records of the Toshan, Agh Band and Neka-Abelou section were presented. These records helped identifying particularly weakly developed interstadial palaeosols which are intercalated in last pleniglacial loess deposits of the Neka-Abelou, Toshan and Now Deh section. To date, such interstadial palaeosols were known only from the Saravan loess sequence in northwestern Iran. The visual detection of these palaeosols in the field is subtle, particularly if these are bracketed by pedogenically altered loess deposits. In this context the application of magnetic susceptibility and colorimetric analyses has proven to be most sensitive in detecting weak pedogenic alterations. Interstadial palaeosols in northeastern Iran are characterized by distinct peaks in rock magnetic, colorimetric and granulometric proxies as exemplified in chapter 4. Although such soils were not described in the field at Now Deh (Kehl et al., 2005), its magnetic susceptibility record suggests the presence of four palaeosols that have formed during interstadials of the last pleniglacial. Additionally, four weakly developed palaeosols were found in the Neka-Abelou section, which will be corroborated by future rock magnetic measurements. In contrast, rock magnetic signature of the Agh Band section reflects the absence of such palaeosols. Hence, interstadial palaeosols that formed during the last pleniglacial seem to be restricted to the loess deposits of the northern declivity of the Alborz Mountain range. Possibly, the relief position played a crucial role in intercepting moisture laden air masses and causing orographic precipitation. In contrast the Iranian loess Plateau is located at a considerable distance from the Kopet Dag Mountains as an orographic obstacle, which might have favoured aridity.

In addition to interstadial palaeosols of the last pleniglacial, the application of highly resolved proxy records fosters a thorough characterization and definition of the MIS 5 palaeosol triple, which is clearly identifiable in various exposures of the region and thus serves as primary marker horizon (chapter 5.3).

Moreover, field findings, micromorphology and high-resolution grain-size analysis provide evidence of a tephra layer, which is intercalated in loess of the Neka-Abelou section. This

tephra is found in a transitional position between the last interstadial palaeosol belonging to the early glacial period (~MIS 5a) and MIS 4. Independent dating results of this layer by means of e.g. $^{40}\text{Ar}/^{39}\text{Ar}$ -dating could improve the definition of this boundary within the pedostratigraphy of northeastern Iran. This is important, because the palaeosol triple forming MIS 5-pedocomplex is the major pedostratigraphic marker in the region (chapter 5.3) and the tephra layer may thus serve as additional chronological tie point for an entire region. To date, the tephra layer was merely found in the Neka-Abelou section. The Neka-Abelou tephra is a coarse grained sedimentary layer, whose particle-size distribution clearly differs from the fine texture of loess at the Neka-Abelou section (Fig. 6.1A). Consequently, in the down profile variations of grain-size proxies the tephra layer is reflected by peaks in U-ratio and median grain-size. The particle-size records of the Toshan section exhibit a comparable peak, however at a considerably smaller magnitude. In contrast to the particle-size characteristics of the Neka-Abelou tephra, the grain-size distribution of a potential tephra in the Toshan section exhibits only a somewhat finer texture than Toshan loess (Fig. 6.1A).

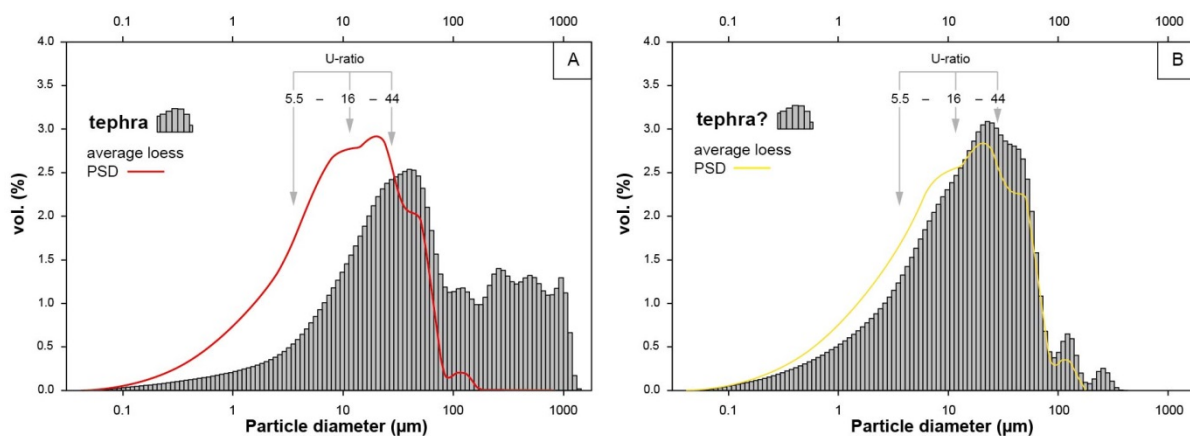


Fig. 6.1: Multimodal particle-size distribution of **A:** the Neka-Abelou tephra in relation to the average grain-size distribution of loess from the Neka-Abelou section. **B:** Multimodal particle-size distribution of a potential tephra at the Toshan loess-palaeosol sequence in relation to the average granulometric composition of Toshan loess.

The tentative fining trend from Neka to Toshan (Fig. 6.1) might indicate a volcanic eruption located to the west of the study area. Although at the current state of research any correlations of the Neka-Abelou tephra with volcanic eruptions are highly hypothetical, the Damavand volcano (Fig. 6.2) might represent the most proximal known tephra source in the region. It is located ~135 km to the southwest of the Neka-Abelou section and ~250 km from the Toshan section. Davidson et al. (2004) have documented an eruptive phase of the so-called young Damavand, which was dated to ~66 ka, i.e. the early MIS 4.

Among the Iranian loess-palaeosol sequences, the Toshan section represents the hitherto most thoroughly analysed succession of loess and palaeosols offering differentiated and well constrained insights into the dynamics of late Pleistocene palaeoclimate in the region. Within the present dissertation it was shown that the palaeoclimatic fluctuations recorded in the Toshan loess deposits may be correlated with those from Neka-Abelou and Now Deh sections. The pedostratigraphical results inferred from Toshan may hence be considered representative of those along the northern declivity of the Alborz Mountains. In this capacity

Toshan loess profile is selected as northeastern Iranian key sequence to be placed within a supraregional context.



Fig. 6.2: Photograph taken from the Neka-Abelou section in a south-western direction. The buildings in the foreground belong to the town of Neka. In the background the 5600 m high Damavand volcano is in visual range. It is located at a distance of ~135 km to the southwest of the Neka-Abelou section (photo was taken by Martin Kehl 2015).

6.2 The nature of upper and lower boundaries of palaeosols and their implications for morphodynamics, differential soil formation and palaeoclimate

Based on field findings, granulometric, rock magnetic and colorimetric proxies the transitions between palaeosols and loess (and vice versa) are defined as i) abrupt, ii) gradual or iii) cascade-like.

Generally, the abrupt change in soil colour, magnetic susceptibility and grain-size might indicate a phase of morphodynamic activity, corresponding with the partial or complete truncation of palaeosols (Fig. 6.3A). In this context, former topsoil-horizons are rarely preserved in loess-palaeosol sequences, because they are prone to e.g. fluvial and/or aeolian erosion owing to their structural weakness. The absence of macroscopically detectable blackish pigments, indicating fossil topsoils might also be caused by the mineralisation of organic matter. Thus, colorimetric properties are no longer visible, whereas the former soil structure might be preserved. In a palaeoclimatic respect abrupt upper boundaries might indicate a moist interval, favouring soil formation on loess, which has been deposited during a previous cold and arid climatic interval. Subsequent to this postgenetic soil formation another phase of loess formation would cause an abrupt boundary between loess and the buried palaeosol. This static model of formation, however, implies that palaeoclimate alternates abruptly between pedogenesis and dust accumulation.

Conversely, most upper transitions between palaeosols and loess within the MIS 5 pedo-complex of Neka-Abelou (Fig. 6.3B), Toshan and Now Deh are gradual in nature as indicated by likewise decreases in magnetic susceptibility, colour or clay contents. This holds also true

for palaeosol Agh S4 from the Agh Band section (Fig. 6.3C), which likely formed during MIS 7. Magnetic susceptibility was used as proxy of palaeo-precipitation, whereas clay contents mirror either pedogenesis in the form of neoformation of siliceous clay or reduced wind energy and/or distal sediment supply. In the context of gradual boundaries these proxies may be translated into gradually increasing atmospheric dynamics, promoting the deposition of relatively coarse grained calcareous sediments and/or reduced soil moisture availability. This chain of processes corresponds with decreasing weathering intensity, which is observed by means of a gradually decreasing amount of brownish soil pigments (Fig. 6.3B, C). In the case of palaeosols 5-1 from the Toshan section and palaeosol 2-1 from the Neka-Abelou section, grain-size records reveal a cascade-like upper boundary, which may testify to accumulation of increasingly coarse sediments, interrupted by several pulses of fine sediments. Macroscopically, soil 2-1 shown in Fig. 6.3B exhibits a gradual decrease in brownish soil pigments. The cascade-like upper boundary is, therefore, deduced from high-resolution grain-size analysis.

Considering pedogenesis and dust supply to represent two competing processes (Liu, 1985; Kemp, 2001), the palaeosols of MIS 5 might have formed during phases of considerably reduced dust deposition.

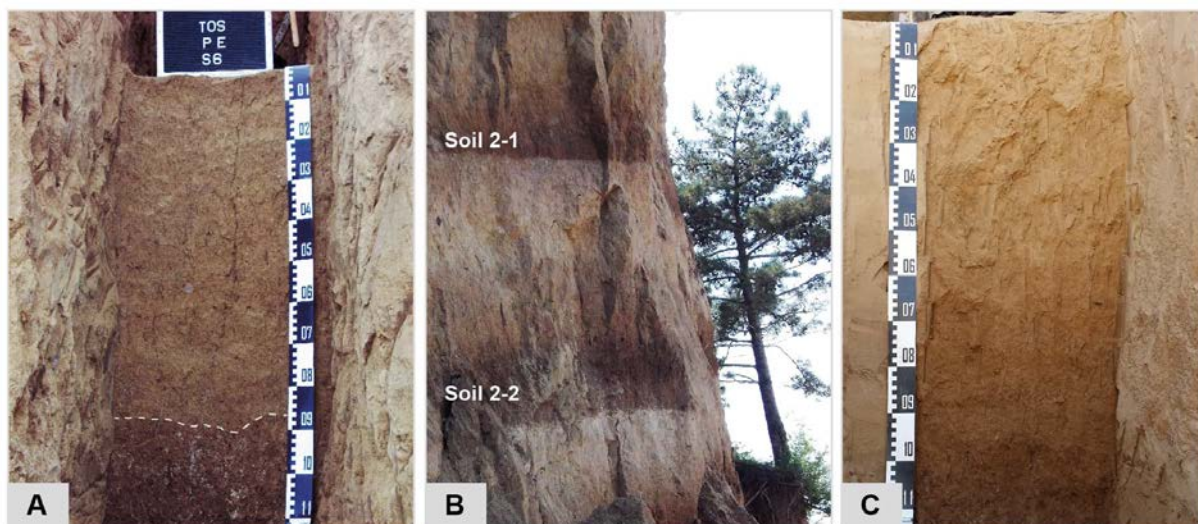


Fig. 6.3: Photographs from **A:** Erosional contact of the ABk-horizon belonging to palaeosol 5-2 and the overlying loess strata at the Toshan section, as indicated by the irregularly shaped boundary between the two strata. **B:** Palaeosols 2-1 and 2-2 from the Neka section, characterized by a gradual upper boundary. **C:** Soil Agh S4 from the Agh Band section exhibits a gradual upper boundary (all photos were taken by Stefan Vlaminc, A and B in 2013 and C in 2014).

This is e.g. reflected by increased CIA-values and clay contents (Fig. 6.1), indicating neoformation of clay at the expense of feldspars. Overall these palaeosols are composed of strongly developed mineral subsoil horizons (Bt[k] and Bwk[k]-horizons) overlying a carbonate enrichment horizon. The latter forms a sharp lower boundary, testifying to vertical leaching of the palaeosols (Fig. 6.3B). Moreover a subangular blocky, angular blocky or prismatic structure is apparent which points to the presence of swellable clay minerals. It is therefore likely that these palaeosols formed (basically) in a postgenetic manner (table 6.1), whereas the transition from the last interglacial and the interstadials of MIS 5 into the respective early glacial stadials was characterized by a phase of syngenetic soil formation.

Analogous phases of syngeneses at an interstadial-stadial transition are known from the Tagidjar section in Tajikistan, where accretionary Serozems have formed (Mestagh et al., 1999).

In contrast to palaeosols of the MIS 5 pedo-complex, weakly developed interstadial palaeosols (CBk and Bwk-horizons) attributed to the last pleniglacial (MIS 3 to MIS 2) exhibit a gradual lower boundary as well as a gradual upper boundary. Although these palaeosols lack carbonate enrichment horizons in the form of e.g. distinct Ck-horizons, most Pleniglacial soils are affected by a pronounced secondary carbonate metabolism. Currently unpublished micromorphological investigations reveal the presence of primary detrital carbonates. These soils are, hence, not decalcified but exhibit a somewhat finer texture than underlying and overlying loess strata. Conversely, the CIA-values are comparable to those recorded in relatively unweathered loess, which suggests that the texture of these interstadial palaeosols is inherited from the parent material and thus constitutes a sedimentary instead of a pedogenic feature. The soil structure is basically coherent and shows evidence of initial aggregation. Low RI-values point to low amounts of hematite, which underlines the immaturity of these soils. Their weak brownish colour is likely the result of amorphous iron hydroxides such as ferrihydrite, which may even form at elevated soil pH >7 (Cornell and Schwertmann, 2003).

Table 6.1:

Summary of major differences between postgenetic and syngenetic soils in Northern Iranian loess.

	Upper boundary	Lower boundary	Carbonate	Primary silicate minerals	clay content	soil structure	Iron oxide/hydroxide
postgenetic	gradual/ abrupt	abrupt	decalcified	depleted	secondary clay mineral neo-formation	prismatic, angular blocky, subangular blocky	rel. high amounts of hematite and goethite
syngenetic	gradual	gradual	partial depletion	not/initially depleted	inherited from parent material	coherent, initial aggregation	dominated by ferrihydrite

The lower boundary of syngenetic palaeosols is characterized by enhanced magnetic susceptibility and increasing clay contents indicating gradually increasing moisture availability corresponding with decreasing wind velocities and/or distal sediment supply. Magnetic susceptibility tends to decrease towards the top, while the amount of coarser particles exhibits an opposite trend. The end of such an interstadial is, therefore, marked by gradual aridization and increasing wind energy and/or proximal sediment supply. Hence, assume that these interstadial palaeosols are the result of syngenetic soil formation, leading to the accretion of soils as opposed to “top-down pedogenesis” deduced from MIS 5-palaeosols.

The similarity of last pleniglacial loess and respective interstadial palaeosols suggests overall dusty environmental conditions in which syngenetic soil formation documents phases of intermittent reduction in dust deposition and increasing moisture availability.

6.3 Granulometric properties of northeastern Iranian loess: Implications for relative wind energy

Due to pedogenic alteration of its original texture within the postgenetic palaeosols of MIS 5, the granulometric signature of these soils basically reflects soil formation. U-ratio is believed to circumvent this issue by disregarding the potential pedogenic clay fraction (Vandenberghe et al., 1997). This assumption implies a general syngenetic formation of the palaeosols under consideration. In the previous section this concept was challenged by arguing for a largely postgenetic formation of the MIS 5 palaeosols under considerably reduced dust deposition rates. Thus, relative wind energy may not be inferred directly from the granulometric properties of these palaeosols, since they likely developed on loess that has formed during a previous stadial. However, the assumption of weakened or even absent dust deposition suggests an extension of vegetated land surfaces, thus reducing the area of potential dust sources and/or reduced wind energy.

Within the last interglacial-glacial cycle, MIS 4 to 2 in northeastern Iran was marked by the most dynamic atmospheric conditions as documented by relatively coarse-grained loess at Neka-Abelou, Toshan, Now Deh. This coarsening may also reflect an aridization trend leading to the retreat of vegetated land surface and the subsequent extension of potential dust source areas. Within the last pleniglacial, MIS 3 was likely the major phase of loess accumulation. In this context last pleniglacial interstadials, coinciding with the syngenetic soil formation represent phases of comparatively distal sediment supply and/or reduction in wind energy.

Conversely, at the Agh Band section, interstadials may not be detected in the form of incipient palaeosols. Moreover, the allocation of chronostratigraphic stages to distinct parts of the Agh Band pedostratigraphy is considerably complicated by contradicting dating results. Overall, U-ratios of the Agh Band section reveal pronouncedly higher wind velocities in the ILP than along the northern declivity of the Alborz Mountain range suggesting higher wind speed and/or proximal dust supply.

6.4 Geochemical characteristics of the dust source

Bulk geochemical characterization of these deposits bears a high resemblance with the average composition of the upper continental crust (see chapter 5.1). This relationship suggests that loess in northeastern Iran is derived from source rocks/sediments that have undergone at least one cycle of upper crustal recycling, encompassing clastic reworking, aeolian transportation as dust and final deposition to form loess. The comparison of the major elements composition of loess with the major elements assemblage of igneous rocks is useful to derive relative maturity of the substrate. The $\text{Na}_2\text{O}/\text{Al}_2\text{O}_3$ is thought to reflect plagioclase content in relation to residual clays, where a higher portion of the latter signals depletion in Na-feldspar and enhanced geochemical maturity. Accordingly, loess deposits in northeastern Iran exhibit a trend of decreasing maturity from Neka-Abelou, over Toshan and Now Deh to Band. This maturity gradient might indicate that loess deposits along the

northern declivity of the Alborz Mountains originate from sediments that are “preweathered” to a higher degree than those of the Iranian loess Plateau (ILP).

The $\text{TiO}_2/\text{Al}_2\text{O}_3$ -ratio serves as “real” provenance indicator, since Al and Ti have the lowest solubility of all major elements in natural waters and are hence resistant to alterations by chemical weathering (Hao et al., 2010). Additionally, titanium may exhibit pronounced variations among different rock types. $\text{TiO}_2/\text{Al}_2\text{O}_3$ -ratios of Neka, Toshan and Now Deh are grouped closely together, while loess at Agh Band indicates a considerable scatter. The results indicate that Neka, Toshan and Now Deh loess originate from geochemically similar source rocks. In contrast, Agh Band loess is marked by distinctively higher Ti-values. Hence, loess in the ILP likely derives from different source rocks. In a geochemical respect loess in the ILP seems to be derived from several dust sources. Alternatively, dust sources might have changed over the course of the late Pleistocene, thus causing highly varying $\text{TiO}_2/\text{Al}_2\text{O}_3$ -ratios in loess of the ILP. In contrast, the geochemical composition of loess deposits on the northern declivity of the Alborz Mountains indicates relative geological homogeneity and/or constant dust sources. Possibly, loess at Neka, Toshan and Now Deh is derived from local sources, such as the alluvial plains of the Gorgan River and its tributaries, draining the Alborz Mountains, whereas loess of the ILP might be associated with the Atrek River. The concept of local dust sources inferred from geochemistry may be considered contradictory in relation to the finely textured loess deposits along the northern declivity of the Alborz Mountains which suggest rather distal dust supply. However, it has to be taken into account that i) low current speeds of the Gorgan River might result in the preferential deposition of finely textured on its alluvial plains and/or ii) overall lower wind energy might cause the preferential entrainment of finer particles.

6.5 Loess deposits along the northern declivity of the Alborz Mountains and in the Iranian Loess Plateau – is there a pedostratigraphic connection?

As part of previous findings the Agh Band profile described by Kehl et al. (2005) hosts one strongly developed palaeosol that consists of a Bw(t) and an overlying Bw horizon. First age estimates of this palaeosol provided by Frechen et al. (2009) suggested a last interglacial formation of this palaeosol. In contrast, the highly detailed profile Agh Band (Agh1/2) studied within the present dissertation revealed the presence of three palaeosols which were denominated as Bwy(k) and CBy. Recent dating results, however, suggest that the lower soils (Agh S4 and Agh S3) have formed during MIS 7.

The MIS 5 pedo-complex represents an excellent pedostratigraphic marker and has proven to be suited for the correlation of the Neka-Abelou, Toshan and Now Deh sections (see chapter 5.5.3). The preservation of this palaeosol triple is based on morphodynamic stability, which is documented in a relatively consistent age increase of the Toshan loess deposits (Fig. 6.4B). In contrast, the Agh Band loess-palaeosol sequence is characterized by heterogeneous age increase with depth as indicated by numerous inverse age estimates (Fig. 6.4A, C). Moreover, dramatic age increases between 74, 96 and 171 ka document phases of considerable morphodynamic activity, covering large parts of the MIS 5 pedo-complex as constrained by means of luminescence dating along the northern declivity of the

Alborz Mountain range. Thus, merely a remnant of a fossil soil horizon (Agh S2) was preserved in a depth of ca. 40 m that has likely formed during MIS 5 (see chapter 3). To date it is not clear whether this truncated palaeosol represents a part of the last interglacial soil or whether it is to be allocated to a subsequent interstadial. Statements concerning palaeoclimate in the ILP and its chronological relation to the Neka-Abelou, Toshan and Now Deh sections are therefore hypothetical.

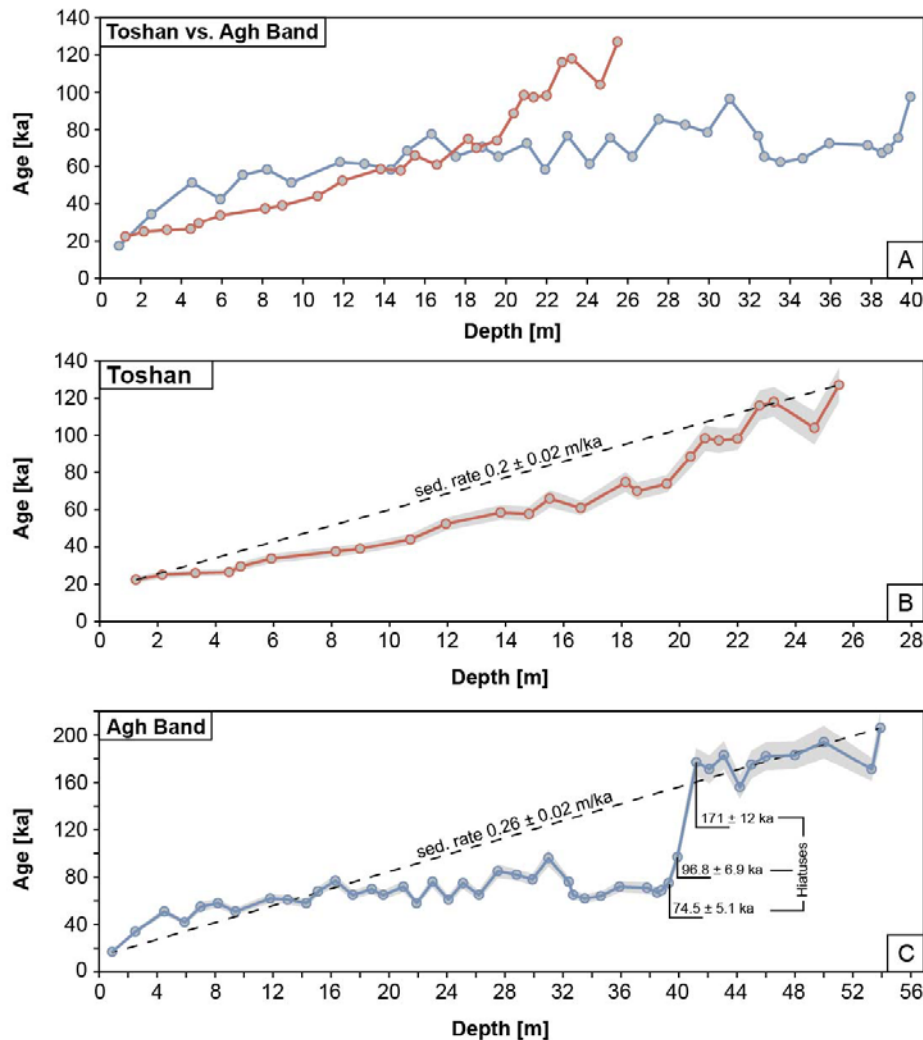


Fig. 6.4 A: Comparison of age increase of Agh Band and Toshan loess. **B:** at Toshan age increase with depth shows a consistent trend, whilst **C:** the age increase curve belonging to the Agh Band section is characterized by numerous inversions. OSL age estimates given were determined by Lauer et al. (2017b) and clearly illustrate the hiatuses in the sequence. The grey shaded area indicates the standard deviation of luminescence ages.

Moreover, it has to be investigated whether these hiatuses (Fig. 6.4C) represent a general stratigraphic feature of the ILP or whether these high magnitude erosional events are confined to a local spatial scale. In contrast to Neka-Abelou, Toshan and Now Deh loess sequences, neither field observations nor analytical results indicate the presence of interstadial palaeosols intercalated in loess of the Agh Band loess. We hypothesize that soil formation might have been inhibited by a lack of edaphic moisture availability and/or high sedimentation rates. The latter are given in Fig. 6.4 for the Toshan and the Agh Band loess sections. Due to the above mentioned hiatuses in Agh Band loess, sedimentation rates in the ILP have to be understood as minimum rates of dust accumulation.

Since palaeosols Agh S4 and Agh S3 attributed were allocated to MIS 7, they might serve as a potential pedostratigraphic linkage to the loess deposits along the Alborz Mountains. Underneath the MIS 5 pedo-complex of the Neka-Abelou, Toshan and Now Deh sections more palaeosols were observed and analyzed. In chapter 5 it was assumed that the palaeosols of unit 3 at Neka-Abelou are of early to middle Pleistocene age and might thus have formed significantly earlier than MIS 7. Irrespective of hitherto missing age control, a correlation based on pedostratigraphical reasoning is afflicted with severe uncertainties.

Luminescence dating result of soils 6-1 and 6-2 in the Toshan section indicate ages (116 ± 8 to 127 ± 8 ka), which are younger than MIS 7. Chronological results for the Now Deh sections provided by Frechen et al. (2009) yielded a basal age of the lowermost Bt-horizon of 159 ± 15 ka. Based on its bare age this palaeosol may be correlated with palaeosol Agh S3 of the Agh Band section. However, age control of the Agh Band section was determined by means of the post IRIR₂₉₀-protocol, whilst chronology of Now Deh loess is based on IRSL age estimates. For resilient comparisons it is recommendable to apply the same measurement protocol. Therefore, the entire OSL-sample set of the Now Deh section will be reanalyzed in the future.

The Agh Band section in the Iranian Loess Plateau (ILP) and the Toshan loess sequence on the northern foot hills of the Alborz Mountains are characterized by different present climatic conditions and constitute distinct geomorphological entities. Morphodynamics as well as palaeoclimatic conditions over the course of the late Pleistocene significantly affect our ability to elaborate a clear correlation of both regions.

6.6 Northeastern Iranian loess in a supraregional context

A thorough supraregional correlation requires chronologically well constrained and highly resolved archives of Quaternary climate change, which are regrettably scarce in western and central Asia. In central Asia the most extensively investigated loess deposits are those from Tajikistan and Kazakhstan and the associated key sections at Tagidjar and Remisowka. In a western direction the most promising loess deposits are found in Armenia in the form of the BL profile. Besides loess as an archive of palaeoclimate change several thoroughly investigated lacustrine pollen sequences may be found in northern Iran and its western vicinity. Such archives often provide continuous sedimentary successions, which may offer highly resolved insights into the climate dynamics of the last interglacial-glacial cycle. Among these deposits the Lake Urmia (northwestern Iran) and Lake Van (eastern Turkey) pollen records are of particular interest, because they are located closest to the study area in northeastern Iran. Although the pollen record from Tenaghi Philippon is situated farthest from the study area, it provides a highly resolved palaeoclimatic record of the late Quaternary.

Loess areas in central Asia are located e.g. between the southeastern margins of the Karakum, Kyzylkum and Muyunkum deserts and adjacent mountain ranges, close to the Syr Darya and Amu Darya Rivers and their tributaries (Dodonov, 1991; Dodonov and Baiguzina, 1995). Deserts as well as river floodplains served as sources of deflation for considerable amounts of silt-sized particles which subsequently accumulated on topographic obstacles

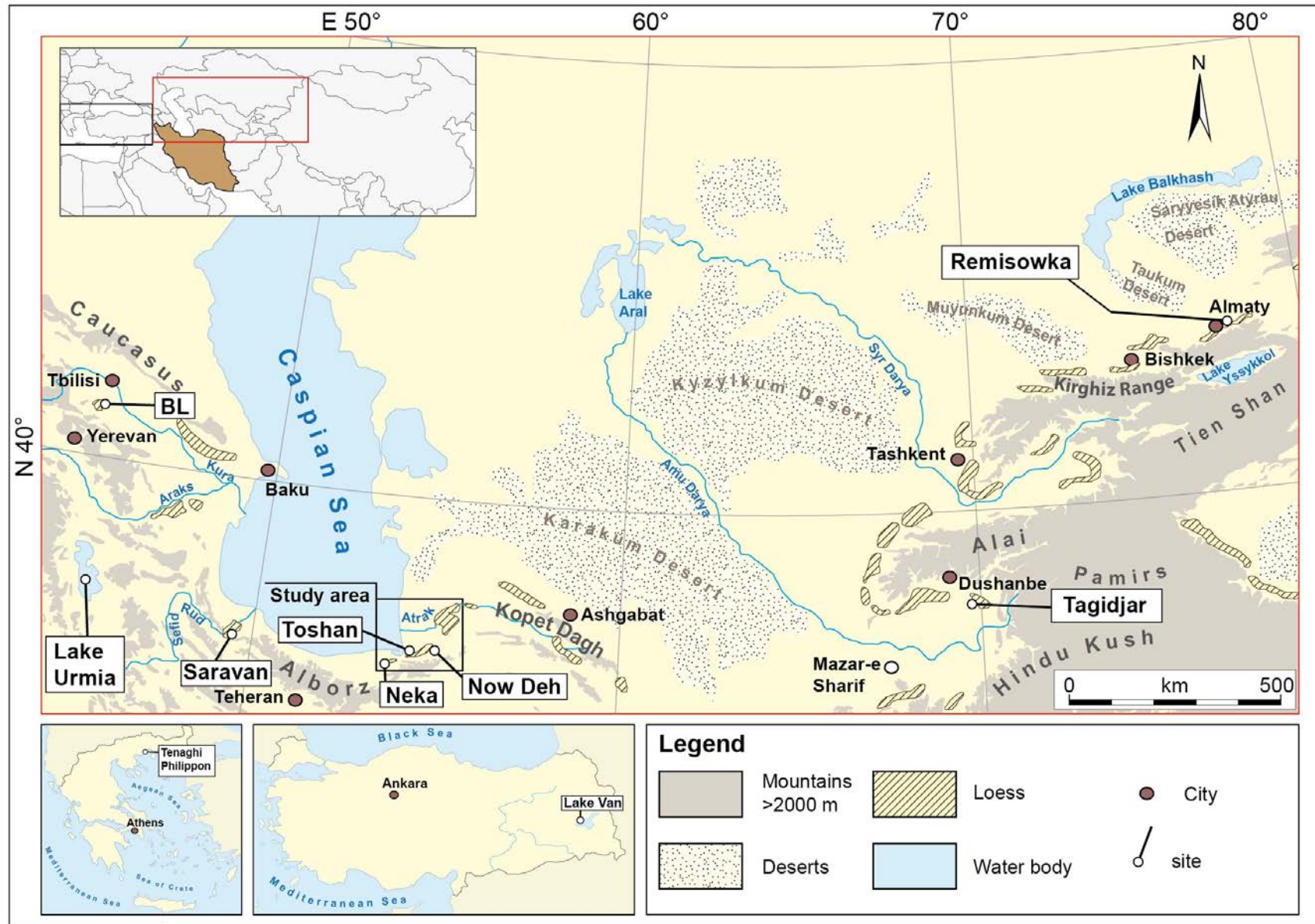


Fig. 6.5: Loess distribution map of central Asia and parts of western Asia according to Machalet et al. (2008), supplemented by the location of pollen sequences and by data from Lateef (1988) for loess deposits in northwestern Iran, Kehl (2010) and own field observations and Wolf et al. (2016) for loess in Armenia.

such as the piedmonts of the Alai, Kirghiz, Pamirs and Hindu Kush (Mestdagħ et al., 1999; Dodonov et al., 2006; Machalett et al., 2008; Schroder et al., 2011; Feng et al., 2011). Due to the interaction of distal and proximal source areas, the granulometric composition of central Asian loess contains both a fine-grained and a comparatively coarse-grained component (Machalett et al., 2008). The lateral extents and the thicknesses of the central Asian loess deposits decrease with increasing altitude. While the most significant loess mantles are hypsometrically located below 2000 and 2500 m respectively, only fragmentary loess strata are found above 2500 m (Dodonov and Baiguzina, 1995; Fig. 6.5).

In southern Tajikistan next to Dushanbe and to the west of the Pamirs, Dodonov et al. (2006) report on loess thicknesses of 100 to 200 m. In the Darai Kalon and Tagidjar loess-palaeosol sequences 176 m and ca. 140 m of Tajik loess were analyzed. Palaeomagnetic studies revealed ages of more than 1.000.000 years for both sections reaching back until MIS 35 (Mestdagħ et al., 1999; Dodonov et al., 2006). Mestdagħ et al. (1999) assume, that the high-mountain nival zone of the Pamirs and the Tien Shan represented areas of increased physical weathering, which provided silt-sized particles. This sediment was reworked by fluvial systems and deposited in the piedmonts from where it was deflated and subsequently formed loess of Darai Kalon and Tagidjar.

Machalett et al. (2006) introduced the loess-palaeosol sequence of Remisowka, located in southern Kazakhstan in the vicinity of Almaty. In this region ca. 80 to 100 m thick loess deposits mantle the perimontane foothill zone of the Tien Shan mountain range. Analogous to the Tajik model of loess formation, the floodplains of regional river systems, draining the Tien Shan served as deflation area. The neighboring Muyunkum and Taukum Deserts are considered as additional distal dust sources providing fine-grained sediment (Machalett et al., 2006). The Remisowka loess-palaeosol sequence is structured by six pedocomplexes. However, luminescence age estimates show only little increase with depth, resulting in ages of around 83.000 years in the bottom part of the sequence underneath the sixth pedocomplex. Based on pedostratigraphical correlation with other central Asian sections such as Darai Kalon, these ages are likely subject to considerable underestimation (Machalett et al., 2008).

In western Asia loess deposits are found e.g. in Iran and Armenia. In Armenia the presence of loess deposits is associated with the vicinity of Rivers such as the Kura River, draining the Caucasus Mountains (Wolf et al., 2016; Fig. 6.5). The Armenian loess profile BL is located in a tectonic depression within the catchment of the Aghstev River, which is a tributary of the Kura River. The BL profile is structured by at least 5 palaeosols belonging to the last interglacial-glacial cycle.

Last interglacial and interstadials of the early glacial period

The threefold MIS 5 pedo-complex, which serves as primary pedostratigraphic marker for the Alborz loess sections may be tentatively correlated with pedo-complex P1 of the BL section in Armenia (Wolf et al., 2016), S1 soil of the Tagidjar profile in Tajikistan (Mestdagħ et al., 1999) and the 5a, 5c, 5e palaeosol triple in Remisowka, Kazakhstan (Machalett et al., 2008; Fig. 6.6). The Armenian pedo-complex is composed of three strongly developed palaeosols, which formed between 109 ± 23 ka and 62 ± 9 ka. For further chronostratigraphic differentiation of P1 more age estimates are required (Wolf et al., 2016). The bare luminescence ages,

however, suggest that P1 represents a coeval formation with respect to the Iranian MIS 5 pedo-complex. In contrast, the chronostratigraphical scheme of the 5a, 5c and 5e palaeosol triple from Remisowka is based on amino acid racemization whose dating limits may reach up to 40 ka (Machalett et al., 2008). The allocation of these palaeosols to MIS 5a, 5c and 5e is hence based on pedostratigraphical reasoning and lacks resilient age control, whereas the S1 soil from Tagidjar most likely correlates with MIS 5 as evidenced by palaeomagnetic results. Due to the lack of highly resolved age control it is difficult to exactly confine the actual extent of the last interglacial palaeosol for the western and central Asian loess sequences. We therefore assume that the formation of the lowermost palaeosol within the respective MIS 5 pedo-complexes coincides with the last interglacial period. In Toshan, Remisowka and Tagidjar last interglacial climate promoted the formation of subsurface soil horizons in which clay illuviation features could be detected (Mestdagh et al., 1999; Machalett et al., 2008; Vlamincx et al., 2016). The neoformation of siliceous clay, its peptization and translocation indicate relatively moist climatic conditions (Stephan, 2000). Comparing the modern soils of Toshan (calcic Kastanozem), Remisowka (weakly developed Kastanozem) and Tagidjar (Cinnamon soil) with the potentially last interglacial soil therefore indicates moister palaeoclimatic conditions during last interglacial. Mestdagh et al. (1999) hypothesize that an intensification of the zonal westerlies might have caused increased moisture transport to central Asia, which was intercepted by the western flanks of the Tien Shan and Alai Mountains, thus favouring enhanced precipitation. Based on the pollen taxa recorded in sediments from Lake Urmia, the last interglacial climate was characterized by *Zelkova carpinifolia*, which is not a common tree species throughout the Holocene in northern Iran. Hence, Djamali et al. (2008) suggest that last interglacial (Sahand interglacial) climate provided milder winters and periods of more spring or summer rainfall as compared to the modern climate which is dominated by autumn to winter precipitation and summer drought (Alijani and Harman, 1985). According to ^{230}Th dating results of Stevens et al. (2012) Sahand interglacial peaked around 123 ± 6 ka (Fig. 6.6). The formation of high relative amounts of hematite in soil 5-3b of the Toshan section (Vlamincx et al., 2016) likely document pronounced seasonal differences, which suggest hot and dry summers and precipitation peaks during winter time.

Generally, the correlation of the following strata within the Tagidjar, BL and Remisowka sections with marine isotope stages is based on pedostratigraphical considerations. The subsequent stadial (MIS 5d), denominated as “Espir Stadial I” by Djamali et al. (2008) corresponds with a CBk-horizon in the Toshan section, which was likely formed in response to surface leaching during the following interstadial period (MIS 5c). Luminescence age estimates, however, suggest that this stratum formed between 97 ± 6 and 88 ± 6 ka, thus representing an age underestimation of ca. 10 ka (Lauer et al., 2017a; Fig. 6.6). In Remisowka and Tagidjar sections arid and cold climatic conditions caused the formation of loess deposits, whereas in the BL profile the strongly developed palaeosols of MIS 5 are separated by relocated material (Mestdagh et al., 1999; Machalett et al., 2006, 2008; Wolf et al., 2016). The pollen record from Lake Urmia and Lake Van suggest a treeless stadial period promoting *Artemisia* and grass steppe vegetation, which are particularly adapted to colder and arid climatic conditions (Djamali et al., 2008; Litt et al., 2014; Pickarski et al., 2015).

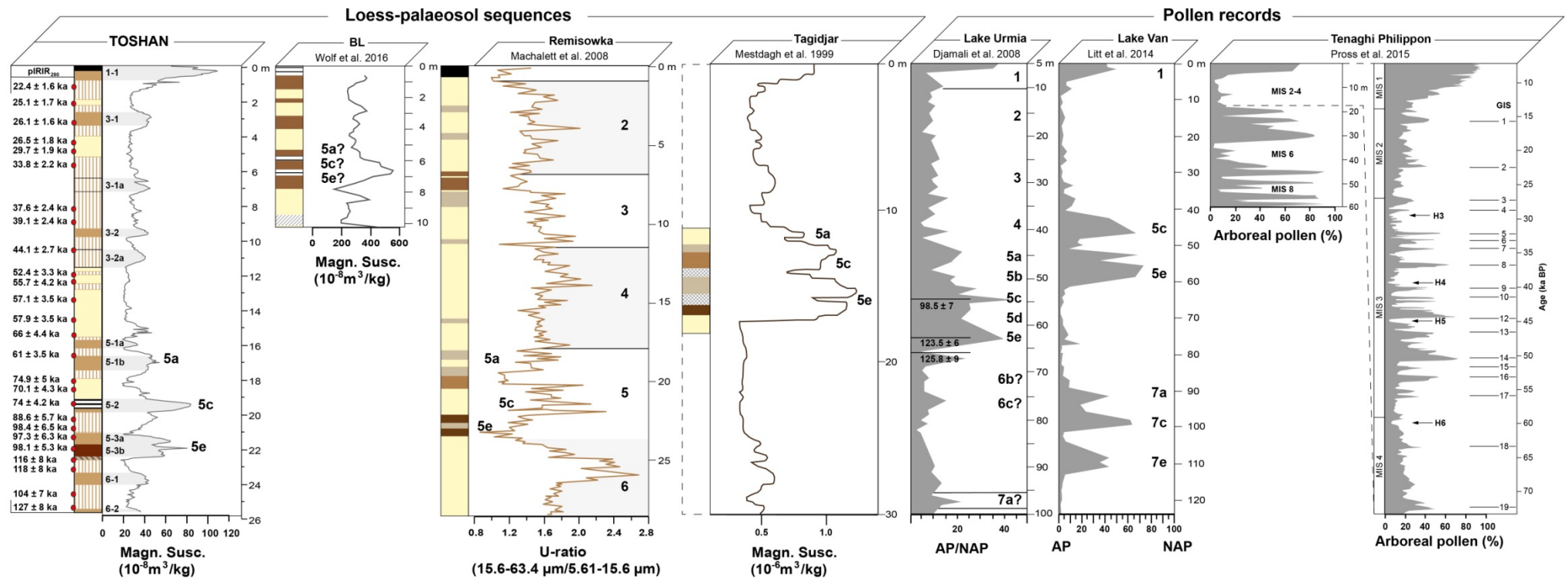


Fig. 6.6: Surpraregional correlation of northeastern Iranian loess deposits (Toshan section) with loess-palaeosol sequences from Armenia (BL), Kazakhstan (Remisowka) and Tajikistan (Tagidjar) and pollen records from Lake Urmia (Iran), Lake Van (Turkey) and Tenaghi Phillipon (Greece). For a location of the respective archives the reader is referred to Fig. 6.6. The age estimates included into the pollen record from Lake Urmia are ^{230}Th ages and were taken from Steven et al. (2012).

Soil 5-2 in the Toshan section is composed of a partly recalcified and truncated ABk and a decalcified Bw-horizon, which are indicative of a palaeosol whose formation was subject to considerable accumulation of biomass. Vlamincx et al. (2016) state that this soil has a Kastanozem-like morphology and could potentially testify to continental and semiarid/subhumid palaeoclimatic conditions. From a pedostratigraphic point of view this palaeosol might be tentatively correlated with MIS 5c, which corresponds to the Kaboudan I interstadial which peaked around 98 ± 7 ka in the pollen records from Lake Urmia (Djamali et al., 2008; Stevens et al., 2012; Fig. 6.6). The pollen assemblage allocated to the Kaboudan I interstadial is dominated by different tree taxa particularly undifferentiated *Quercus* pollen. The occurrence of the latter reinforces the argument for a continental climate in northern Iran during MIS 5c, since *Quercus* is a thermophilous tree species adapted to respective climates (Litt et al., 2014). This trend is also mentioned by Mestdagh et al. (1999), who report on a calcareous Cinnamon-like soil, which is associated with dry continental climate and sparse grassy vegetation. This soil is covered by an accretionary Serozem testifying to synchronous dust deposition and initial soil formation by the end of the interstadial period (Mestdagh et al., 1999). In contrast, the coeval palaeosol at the Toshan section (5-2) was truncated and thus exhibits a sharp upper boundary. The ending of the MIS 5c was dominated by morphodynamic activity suggesting an abrupt transition from MIS 5c to MIS 5b.

In the Lake Urmia chronostratigraphy MIS 5b is denominated as Espir Stadial II (Djamali et al., 2008). Palaeoclimatic conditions in northeastern Iran were likely cold and dry allowing for the accumulation of weakly weathered loess deposits in the Toshan loess sequence (Fig. 6.6). Loess formation is also apparent in Kazakhstan and Tajikistan, indicating likewise palaeoclimatic conditions (Mestdagh et al., 1999; Machalet et al., 2006, 2008), while MIS 5b is recorded as slope deposit in the pedostratigraphy of the BL section (Wolf et al., 2016; Fig. 6.6). The pollen signature from Lake Urmia and Lake Van exhibit decreasing tree taxa as observed for MIS 5d, corresponding with cold and dry stadial climate (Djamali et al., 2008; Litt et al., 2014; Pickarski et al., 2015).

According to Lauer et al. (2017a) palaeosol 5-1 of the Toshan section allocated to MIS 5a in Fig. 6.6 might as well have formed during early MIS 4 as based on the luminescence age estimates ranging from 75 ± 5 to 66 ± 4 ka. Soil 5-1 is composed of a moderately developed Bwk-horizon overlain by a weakly developed Bwk-horizon (Fig. 6.6). Thus, a twofold palaeosol is found in Toshan loess. Alternatively, the weakly developed upper palaeosol might also have formed during MIS 4 while the moderately developed Bwk-horizon could represent the actual MIS 5a (Kaboudan II) palaeosol. The synthesis of chronostratigraphic assumptions based on luminescence dating results (Lauer et al., 2017a) and pedostratigraphic estimations (Vlamincx et al., 2016) is hitherto ambiguous. Provided that the lower Bwk-horizon formed during the last interstadial period of MIS 5, it might be correlated with the 5a palaeosol from the BL, Remisowka and Tagidjar loess sequences. In contrast to palaeosol

5-1 at Toshan the other loess sections host a weakly developed subsoil horizon, which is believed to indicate warm and arid palaeoclimate (Mestdagh et al., 1999; Machalet et al., 2006; Wolf et al., 2016). In Tajikistan this MIS 5a palaeosol formed under ongoing dust deposition and therefore represent an accretionary soil, indicating significant dust input holding pace with the former moisture regime. Analogous to the potential MIS 5c soil of the Toshan section such environmental conditions during the formation of soil 5-1 are difficult to

deduce, since based on the present data this palaeosol was subject to a phase of morphodynamic activity (Vlaminck et al., 2016). In Lake Urmia the increase in the ratio of arboreal to non-arboreal pollen of MIS 5a is not as pronounced as for the previous interstadial, testifying to increased aridity (Djamali et al., 2008).

MIS 4 and last pleniglacial

Most “typical” loess deposits found in the Toshan section are overlying the MIS 5 pedo-complex and might therefore be allocated to MIS 4 (~77 to 61 ka). Based on our luminescence results (66 ± 4 to 57 ± 3 ka) the respective chronostratigraphic unit might extend from ca. 15 to 12 m, implying that soil 5-1a formed during an interstadial (sub)period of MIS 5. According to northeastern Iranian pedomstratigraphy (Fig. 6.6) MIS 4 represents a period of extensive loess formation, testifying to increasingly cold and arid climatic conditions. In the western Caspian region Wolf et al. (2016) described a layer of weakly weathered loess, which dates to 62 ± 9.2 ka at its base and may hence at least be partly associated with MIS 4. The argument of enhanced aridity is reinforced by Djamali et al. (2008) who report on increasing portions of herbal communities tolerant to drought and cold, which are composed of *Artemisia*, *Poaceae* and *Chenopodiaceae*. These drought conditions likely extended into Central Asia, as evidenced by thick loess deposits in Tajikistan, allocated to MIS 4 (Machalett et al., 2008). The pollen assemblage from Lake Van reveals a comparable spread of arid desert-steppe vegetation between ca. 75 to 12 ka, characterized by the absence of thermophilous and frost sensitive taxa (Pickarski et al., 2015). Interestingly, several researchers such as e.g. Kroonenberg et al. (1997); Svitoch (1997); Dolukhanov et al. (2009), Yanina et al. (2012, 2014); Tudryn et al. (2013) postulate an interval of Caspian Sea-level regression during MIS 4, the so called Atel regression. These authors suggest that Caspian Sea level, which is currently found at -26 above mean sea-level (a.m.sl.) might have dropped by at least 114 m, reaching -140 m a.m.sl (Fig. 6.7).

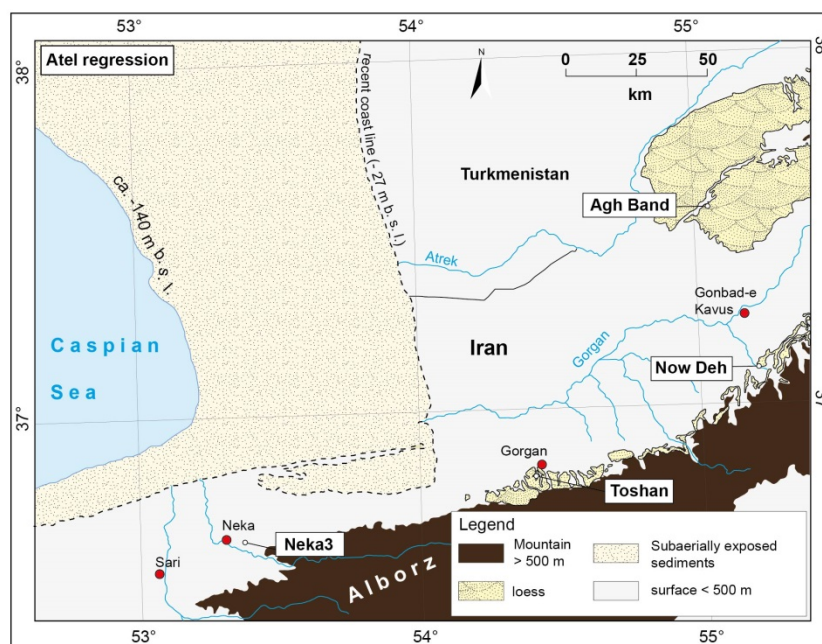


Fig. 6.7: Simplified map illustrating the extent of subaerially exposed shelf sediments in response to Atel regression as postulated by Kroonenberg et al. (1997); Svitoch (1997); Dolukhanov et al. (2009), Yanina et al. (2012, 2014); Tudryn et al. (2013). The palaeocoastline was taken from Zickel et al. (2016).

Based on theoretical reasoning a sea-level drop of the postulated order would lead to a severe decrease in sea surface and might thus favour the development of a cold continental climate. Moreover, the coastline retreat corresponding with such a high magnitude regression stage might have resulted in the subaerial exposure of former shelf sediments of the Caspian Sea, thereby representing a potential source area for airborne dust. Fig. 6.8 indirectly indicates enhanced dust fluxes, as the average time covered per 2 cm sampling increment amounts to 66 years. Consequently, decreasing dust accumulation rates would result in larger time periods per sample.

Highest rates of airborne dust accumulation, however, are associated with MIS 3 and 2 as indicated by increasing temporal resolution per sample (Fig. 6.8). Overall the Toshan loess section hosts at least four interstadial palaeosols that formed during this time interval. Periods of pedogenesis during MIS 3 and 2 were also observed by Machalet et al. (2008) and Fitzsimmons et al. (2016) at Remisowka section and description of the BL-profile in Armenia reveals 2 weakly developed interstadial palaeosols (Wolf et al., 2016; Fig. 6.8). The correlation with the latter is difficult owing to the lack of a highly resolved chronology. Both age estimates referring to the incipient palaeosol of the BL-profile date the basal part of the respective horizons and thus represent *termini post quem*. The lower palaeosol formed after 47 ± 7 ka and the upper one developed after 39 ± 5 ka, suggesting that these soils formed coeval with palaeosols 3-2a (52 ± 3 to 44 ± 3 ka) and 3-2 (44 ± 3 to 39 ± 2 ka) of the Toshan section (Fig. 6.8). According to Fitzsimmons et al. (2016) one interval of pedogenesis is found within the time slice between ca. 26 and 22 ka and is associated with the global Last Glacial Maximum (gLGM) and might thus be tentatively correlated with soil 3-1 from the Toshan section (26 ± 2 to 25 ± 2 ka). The second palaeosol is dated to ca. 34 ka by a luminescence age estimate from its top part, representing a *terminus ante quem*. Its western counterpart might be found in the Toshan section in the form of palaeosol 3-1a, which is dated to 37 ± 2 to 34 ± 2 ka (Fig. 6.8).

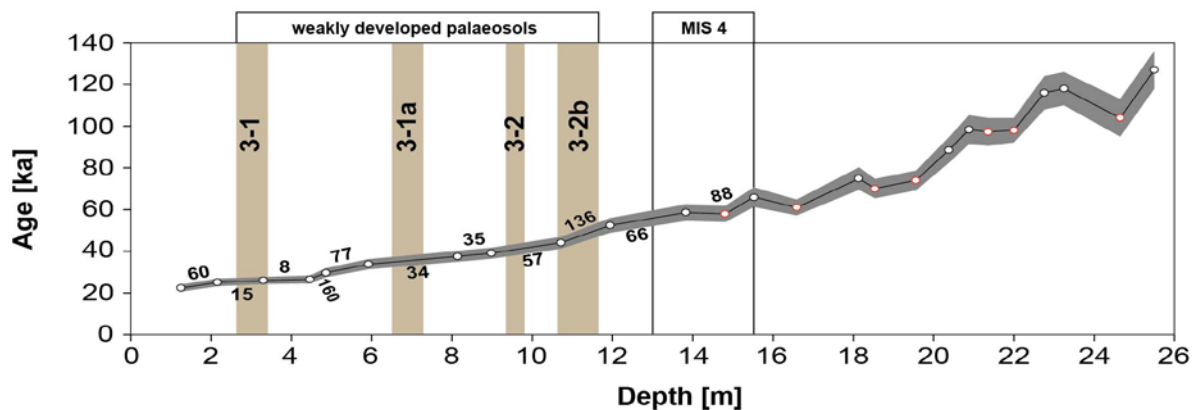


Fig. 6.8: Age increase of the Toshan section as a function of depth below surface. Luminescence dating results were taken from Lauer et al. (2017a). White dots indicate average age estimates showing consistent age increase with increasing depth, while red dots represent inversive ages. The grey surface in the background illustrates age uncertainties (Lauer et al., 2017a). The transitional zones between our luminescence results are provided with numbers representing the average age increase per 2 cm sampling increment in years. These values were inferred from linear interpolation from two succeeding average age estimates. The brownish and vertical bars crossing the age estimates indicate the position of weakly developed interstadial palaeosols 3-1, 3-1a, 3-2 and 3-2b.

Stevens et al. (2012) report on short-lived lake-level rises of Lake Urmia due to intermittently moister conditions. The timing of these fluctuations is, regrettably, not resolved by geochronological dating of the records (Djamali et al. 2008; Stevens et al. 2012). In the highly resolved pollen records from Tenaghi Philipon and Lake Van, millennial to centennial scale variations of palaeoclimate were identified (Pross et al., 2015; Pickarski et al., 2015) probably contemporaneous with Dansgaard-Oeschger (DO) stadials and interstadials. Accordingly, each DO interstadial coincides with a sharp increase in arboreal pollen such as deciduous *Quercus* percentage indicating abrupt warming. Overall nineteen of these abrupt climate changes were detected in Tenaghi Philipon and Lake Van (Pross et al., 2015; Pickarski et al., 2015) differing in magnitude. Among these nineteen DO interstadials events 8 (~37-39 ka), 12 (~44-47 ka), 14 (~50-55 ka), 16-17 (~56-60) and 19 (~70-73) were determined as the most pronounced ones (Pickarski et al., 2015).

These high-frequency oscillations are, however, difficult to correlate with climatic fluctuations emerging during MIS 3 in northeastern Iran, because of high uncertainty of geochronological dating results, which cover the duration of the interstadials of interest. Moreover, it is questionable for which reason there are merely four (pronounced) interstadials recorded in northeastern Iranian loess. To address this issue the following pedological, sedimentological and palaeoclimatic aspects have to be considered: i) since terrestrial soils form by vertical leaching, a previously developed palaeosol might be affected by polygenesis during a subsequent interval of soil formation; ii) this polygenetic overprint depends not only on palaeoprecipitation and the associated leaching depth but also on sedimentation rates. Low rates of loess accumulation may increase the likelihood of polygenesis. Thus one given palaeosol horizon detected in the field would be the result of several interstadials; iii) palaeoclimatic conditions might not have been conducive to soil formation due to high levels of dust accumulation in relation to edaphic moisture availability. The time resolution per 2 cm sample determined by linear interpolation from luminescence dating results (Fig. 6.4) indicates that temporal resolution varies between 136 to 8 years per sample. This approach may be considered crude as it implies equal sedimentation rates during loess formation and the development of syngenetic interstadial palaeosol. In contrast it is more likely that these palaeosol have formed under continuous but somewhat reduced dust accumulation (Vlaminck et al. 2016; chapter 4). Nevertheless, this linear interpolation might be a hint that temporal resolution of northeastern Iranian loess is sufficient to record single millennial scale events and that our high resolution sampling strategy matches the requirements to detect them.

6.7 High-resolution sampling and multi-proxy analysis: a review of pros and cons

The extensive loess deposits of northeastern Iran were investigated via the Neka-Abelou, Toshan and Agh Band loess-palaeosol sequences, which were sampled in high-resolution (in 2 cm increments. Depending on the thickness of the respective loess section the number of samples taken reached 1200 to 2700. These samples were analysed by means of a multitude of different methods, thereby potentizing not only the temporal resolution of the data set but also the potential hours of work invested in laboratory analysis. The workload was, therefore, distributed over several research facilities, each of which was in charge of

analyses matching their respective practical and theoretical expertise. In the following sections the pros and cons of mid-infrared spectroscopy (MIRS), visible spectroscopy (VIS), laserdiffractometry and magnetic susceptibility will be discussed before the background of high-resolution analyses.

Mid-infrared spectroscopy

MIRS was used to predict the CaCO_3 -contents within the samples. In its capacity as a primary component of loess, knowledge about CaCO_3 -contents is indispensable. From the Toshan section every second sample was analysed, resulting in an effective resolution of 4 cm. For determination of the CaCO_3 -content from the Agh Band loess sequence a resolution of 8 cm was chosen due to the high amount of samples (2700). Hitherto, the data set from Neka-Abelou is preliminary in nature as merely every tenth sample was analysed (20 cm resolution).

Pros: The record of mid-infrared spectra was done by means of an easy measurement routine, which is composed of a low number of individual operations. The analysis consumes little amounts of sample material, which are lying in the order of mg. The statistical calibration is based on ground truth measurements and may be done by using the OPUS Quant software package. Once the spectra are recorded, they are saved in a spectral library and may be used for future predictions of any component of interest. MIRS offers a particular temporal advantage if already existing data sets of multiple components (e.g. Viscarra Rossel et al. 2006) may be used for calibration. Provided that the number of these reference data permits a statistically resilient calibration, records of several components may be gained at the same time according to the number of MIR-spectra available.

Cons: Although the MIR-measurements as such are not time-consuming, the reference data (ground truth) required for the prediction model of a given component are based on standard laboratory methods. Particularly wet chemical procedures such as the Scheibler-method may be highly time-consuming. In addition, each sample has to be homogenized by grinding prior to MIR-analysis, thus significantly increasing the amount of time used for pre-treatments. As calibration of the diffuse reflectance spectra and subsequently prediction of CaCO_3 proportions rely on conventional analyses, the prediction may not be more accurate than the selected reference method. In order to establish a statistically resilient reference data base, a gradient reaching from high to low values of a given component must be created. This is important to increase the density of data point along the regression line and thus to increase the predictive power of the model. In this context the choice of the “right” samples is difficult, since the amounts of most components of interest may not be estimate macroscopically and therefore require an additional screening.

Visible spectroscopy

VIS was used for the determination of soil colour, which is crucial to field description and thus affects pedostratigraphy. Some colour changes are, however, subtle to such an extent that they are difficult to perceive for the human eye. In order to establish a reliable pedostratigraphic scheme of the northeastern Iranian loess sections, VIS was used to place

our findings on an objective base. The same samples from Toshan and Agh Band selected for MIRS were used for VIS. The colorimetric properties of the Neka-Abelou section will be investigated in the future.

Pros: VIS provides a non-destructive method enabling the investigation of colorimetric properties, which may be expressed either as $L^*a^*b^*$ -values or Munsell colour data. The analysis follows an easy routine, which allows for the rapid analysis of the samples. Moreover, this method has proven to be highly sensitive to detect even weakly developed palaeosols and was therefore very useful to support and improve our pedostratigraphy. The spectral information from VIS may be used to calibrate models in order to predict the amount of a given component. The spectral information may also be saved in a spectral library and is thus available for future investigations. In contrast to MIRS, significant information on the relative differences in soil colour may be inferred from the uncalibrated $L^*a^*b^*$ -values. This data was also used to calculate the Redness-Index according to Barrón and Torrent (1986), an empirically defined proxy for the relative amounts of hematite in sediments. The required pre-treatments for such investigations are limited to drying and rough homogenization of loess and palaeosol samples.

Cons: The prediction of absolute amounts of a given component from VIS requires additional laboratory analyses such as e.g. wet chemical analyses to create a reference data base for calibration. These analyses in turn require individual pre-treatments and routines, which may considerably affect the time spent for measurements. Analogous to MIRS, the accuracy of the prediction depends on the accuracy of the reference method.

Laser diffractometry

Laser diffractometry (Fraunhofer theory) was used to determine the particle-size distribution (PSD) of loess. The accumulation of airborne dust is one of the key processes in loess formation. Its PSD was extensively used to infer palaeoclimatic information on local as well as regional spatial scales. The PSD may be considered one of the most crucial parameters of loess. It was determined in 2 cm increments for every loess-palaeosol sequence presented and discussed in the present dissertation.

Pros: The PSD determined by laser diffractometric analyses (LS 13320 PIDS) is subdivided in 116 grain-size classes reaching from 0.04 to 2000 μm with an error of only 2% (1σ). The volume percentage of each particle-size class is multiplied by the number of samples. Thus, large data sets are created in comparatively little time, which may be used for detailed granulometric investigations and statistical methods.

Cons: The sample material has to be pre-treated in order to keep the particles dispersed. Detrital carbonates and organic matter may affect the granulometric properties of loess. If both components are to be removed, wet chemical pre-treatments have to be applied. Several fractions for clay-sized particles have been proposed, when Fraunhofer theory is applied such as e.g. $<4.8 \mu\text{m}$ (Antoine et al. 2009), $<5 \mu\text{m}$ (Obrecht et al. 2014) and $<5.5 \mu\text{m}$ (Bokhorst et al. 2009). These fractions, however, tend to overestimate the contents of clay.

Magnetic Susceptibility

Frequency dependent and mass specific magnetic susceptibility were determined in order to estimate the relative degrees of soil formation. The Toshan and Agh Band sections were analyzed in 2 cm increments. The investigation of the rock magnetic properties of the Neka-Abelou section is currently under progress.

Pros: The sample material has to be roughly homogenized by grinding soil aggregates. The resulting substrate is filled in a plastic cube. This container may be used for frequency dependent as well as mass specific susceptibility. Overall, the sampling pretreatment is comparatively fast. The measurement procedure follows an uncomplicated routine and requires around five minutes per sample for both the determination of frequency dependent and mass specific magnetic susceptibility. Analogous to VIS, magnetic susceptibility has proven to be highly sensitive to even weak pedogenic alterations, thus allowing for the detection of weakly developed palaeosols.

Cons: The results of magnetic susceptibility are temperature dependent. Increasing room temperature will lead to an increased velocity of molecular motion, which will counteract alignment of magnetic moments in a given substrate (Evans and Heller 2003). Therefore, higher temperatures will decrease magnetic susceptibility, while lower temperatures tend to increase it. The magnetic susceptibility under a given room temperature may be verified by measuring a ferromagnetic reference sample. We considered deviations of $< 0.05\%$ to be acceptable in order to create equal conditions prior to each measurement. These, conditions are, however, difficult to maintain and have to be surveyed frequently.

7. Conclusions

Within the present dissertation multi-proxy records of exceptional resolution were elaborated, allowing for detailed lithological and pedostratigraphical investigations.

The LPS of Neka-Abelou and Toshan are structured by numerous weakly to strongly developed palaeosols and thus give differentiated insights into the last interglacial-glacial cycle. Accordingly, the pedocomplex of MIS 5 is composed of three strongly developed palaeosols (Bt[k] and Bw[k]) that are covered by relatively unweathered loess deposits of MIS 4. These strata may be well identified in manifold exposures of northeastern Iran and therefore serve as primary marker horizons that have proven to be suited for the intercorrelation of the LPS along the northern declivity of the Alborz Mountain range. Moreover, a tephra layer was found at the base of MIS 4 loess of the Neka-Abelou section, which might give independent information on the age of the MIS 5 pedocomplex. In addition, at least four weakly developed palaeosols were detected that have formed during the last pleniglacial.

These palaeosols (CB[k], Bw[k]) are marked by gradual upper and lower boundaries in grain-size, magnetic susceptibility and colour, suggesting a syngenetic soil formation, which resulted only in partial decalcification. Their structural and textural similarities compared to last pleniglacial loess suggests overall dusty environmental conditions in which syngenetic soil formation documents phases of intermittent reduction in dust deposition, wind energy and increasing moisture availability. It is assumed, that these soils formed in response to millennial scale fluctuations. However, a direct correlation with Greenland interstadials is impeded by high standard deviations of luminescence dating, covering the temporal extent of the respective interstadial.

The palaeosols of the MIS 5 pedocomplex have formed postgenetically under reduced or absent dust deposition during relatively moist interglacial and interstadial climate, favouring complete decalcification and the formation of distinct soil structure. In contrast, transitions into subsequent stadials are characterized by phases of syngenetic soil formation indicating reduced edaphic moisture availability and increased dust deposition. From MIS 4 to 2 a distinct coarsening trend in loess texture indicates increasingly dynamic atmospheric conditions and/or proximal dust supply. These conditions have possibly favoured a major phase of dust deposition during MIS 3.

Immobile major elements document different dust sources of loess along the northern declivity of the Alborz Mountains as compared to loess in the ILP. It is assumed that dust, forming loess at Neka, Toshan and Now Deh originates from the alluvial plains of the Gorgan River, while loess formation at Agh Band is associated with dust deflation from the alluvial plains of the Atrek River.

At the Agh Band section (Agh 1/2) two strongly developed palaeosols (Bwyk-horizons) were found that have likely formed during MIS 7. A major phase of morphodynamic activity has caused the erosion of a potential MIS 5 palaeosols at Agh Band. Thus, a correlation by means of MIS 5 pedocomplex with the loess deposits of the ILP is hitherto not possible. Furthermore, no weakly developed interstadial palaeosols were found in the profiles Agh 1/2 of the Agh Band section.

The Toshan LPS was selected to be the northeastern Iranian key section, due to its highly detailed stratigraphy and exceptional amount of available proxy data.

The MIS 5 pedo-complex may be well correlated with loess sections from southern Europe, Armenia and central Asia. This palaeosol triple also reflects palaeoclimatic fluctuations of MIS which are recorded in other climatic archives from (e.g.) the Mediterranean, Lake Van and Lake Urmia. Furthermore, northern Iranian loess and its six interstadial palaeosols seem to offer more differentiated insights into the last glacial, than the loess deposits from the other above mentioned regions.

8. References (Chapters 1-6)

- Aitken, M.J. (Ed.), 1998. An Introduction to optical Dating – The dating of Quaternary Sediments by the Use of Photon-stimulated Luminescence. Oxford University Press, Oxford.
- Aitkenhead, M.J., Coull, M., Towers, W., Black, H.I.J., 2013. Prediction of soil characteristics and colour using data from the National Soils Inventory of Scotland. *Geoderma*, 200-201, 99-107.
- Alijani, B. and Harman, R., 1985. Synoptic Climatology of Precipitation in Iran. *Annals of the Association of American Geographers* 75(3), 404-416.
- Allen, M.B., Ghassemi, M.R., Shahrabi, M., Qorashi, M., 2003. Accomodation of late Cenozoic oblique shortening in the Alborz range, northern Iran. *Journal of Structural Geology* 25, 659-672.
- An, Z., Kukla, G., Porter, S.C., Xiao, J., 1991: Magnetic Susceptibility Evidence of Monsoon Variation on the Loess Plateau of Central China during the Last 130,000 Years. *Quaternary Research* 36, 29-36.
- Antoine, P., Rousseau, D.D., Zöller, L., Lang, A., Munaut, A.V., Hatté, C., Fontugne, M., 2001. High-resolution record of the last interglacial-glacial cycle in the Nussloch loess-palaeosol sequences, Upper Rhine Area, Germany. *Quaternary International* 76(77), 211-229.
- Antoine, P., Rousseau, D.-D., Fuchs, M., Hatté, C., Gauthier, C., Marković, S. B., Jovanović, M., Gaudenyi, T., Moine, O., Rossignol, J., 2009. High-resolution record of the last climatic cycle in the southern Carpathian Basin (Surduk, Vojvodina, Serbia). *Quaternary International* 198 (1-2), 19-36.
- Asadi, S., Moore, F., Keshavarzi, B., 2013. The nature and provenance of Golestan loess deposits in northeastern Iran. *Geological Journal* 48, 646-660.
- Assallay, A.M., Rogers, C.D.F., Smalley, I.J., 1997. Formation and collapse of metastable particle packings and open structure in loess deposits. *Engineering Geology* 48, 101-115.
- Barron, V., Torrent, J., 1986. Use of the Kubelka-Munk theory to study the influence of iron oxides on soil colour. *Journal of Soil Science* 37, 499-510.
- Bazylinski, D.A., Moskowitz, B.M., 1997. Microbial biomineralization of magnetic iron minerals: microbiology, magnetism and environmental significance. In: Banfield, J.F., Nealson, K.H. (Eds.). *Geomicrobiology: Interaction between Microbes and Minerals*. Reviews in Mineralogy, 35, 181-223.
- Berg, L.S., 1916. The origin of loess. *Communications Russian Geographical Foundation* 11, 579-646 (in Russian).
- Berger, A., 2009. Astronomical Theory of Climate Change In: Gornitz, V. (Ed.), 2009. *Encyclopedia of Palaeoclimatology*, Springer, 51-57.

Beuselinck, L., Govers, G., Poesen, J., Degraer, G., Froyen, L., 1998. Grain-size analysis by laser diffractometry: comparison with the sieve pipette method. *Catena* 32 (3-4), 193-208.

Biswas, R.H., Williams, M.A.J., Raj, R., Juyal, N., Singhvi, A.K., 2013. Methodological studies on luminescence dating of volcanic ashes. *Quaternary Geochronology* 17, 14-25.

Bobek, H., 1937. Die Rolle der Eiszeit in Nordwestiran. *Zeitschrift für Gletscherkunde* 25, 130-183.

Boenigk, W. & Frechen, M. (2001): The loess record in sections at Koblenz- Metternich and Tonchesberg in the Middle Rhine Area. – *Quaternary International*, 76/77: 201–209.

Bokhorst, M.P., Beets, C.J., Marković, S.B., Gerasimenko, N.P., Matviishina, Z.N., Frechen, M., 2009. Pedo-chemical climate proxies in Late Pleistocene Serbian-Ukrainian loess sequences. *Quaternary International* 198, 113-123.

Bond, G., Heinrich, H., Broecker, W., Labeyrie, L., McManus, J., Andrews, J., Huon, S., Jantschik, R., Clasen, S., Simet, C., Tedesco, K., Klas, M., Bonani, G., Ivy, S., 1992. Evidence for massive discharges of icebergs into the North Atlantic ocean during the last glacial period. *Nature* 360, 245-249.

Bond, G., Broecker, W., Johnsen, S., McManus, J., Labeyrie, L., Jouzel, J., Bonani, G., 1993. Correlations between climate records from North Atlantic sediments and Greenland ice. *Nature* 365, 143-147.

Bornemann, L., Welp, G., Brodowski, A., Rodionov, A., Amelung, W., 2008. Rapid assessment of black carbon in soil organic matter using mid-infrared spectroscopy. *Organic Geochemistry* 39, 1537-1544

Bradley, R., 2015. *Palaeoclimatology – Reconstructing Climates of the Quaternary*. Academic Press, Amherst, Massachusetts.

Bronger, A., Bruhn-Lobin, N., Heinkele, T., 1994. Micromorphology of paleosols – genetic and paleoenvironmental deductions: Case studies from central China, south India, NW Morocco and the Great Plains of the USA. *Developments in Soil Science* 22, 187-206.

Bronger, A., Winter, R., Sedov, S., 1998. Weathering and clay mineral formation in two Holocene soils and buried palaeosols in Tadjikistan: towards a Quaternary palaeoclimatic record in Central Asia. *Catena* 34, 19-34.

Brunet, M.-F., Korotaev, M.V., Ershov, A.V., Nikishin, A.M., 2003. The South Caspian Basin: a review of its evolution from subsidence modelling. *Sedimentary Geology* 156, 119-148.

Buggle, B., Hambach, U., Glaser, B., Gerasimenko, N., Marković, S. B., Glaser, I., Zöller, L., 2009. Stratigraphy, and spatial and temporal palaeoclimatic trends in Southeastern/Eastern European loess-paleosol sequences. *Quaternary International* 196 (1-2), 86-106.

Buggle, B., Glaser, B., Hambach, U., Gerasimenko, N., Marcović, S., 2011. An evaluation of geochemical weathering indices in loess-palaeosol studies. *Quaternary International* 240, 12-21.

Buggle, B., Hambach, U., Kehl, M., Marcović, S.B., Zöller, L., Glaser, B., 2013. The progressive evolution of a continental climate in southeast-central European lowlands during the Middle Pleistocene recorded in loess paleosol sequences. *Geology* 41, 771-774.

Buggle, B., Hambach, U., Müller, K., Zöller, L., Marković, S.B., Glaser, B., 2014. Iron mineralogical proxies and Quaternary climate change in SE-Europe loess-paleosol sequences. *Catena* 117, 4-22.

Busche, D., Grunert, J., Sarvati, R., (1990): Iran Geomorphologie. – In: Tübinger Atlas des Vorderen Orients TAVO, A III 3.

Buylaert, J.-P., Jain, M., Murray, A. S., Thomsen, K. J., Thiel, C., Sohbati, R., 2012. A robust feldspar luminescence dating method for Middle and Late Pleistocene sediments. *Boreas* 41, 435 - 451.

Çağatay, M.N., Öğretmen, N., Damci, E., Stockhecke, M., Sancar, Ü., Eris, K.K., Özeren, S., 2014. Lake level and climate records of the last 90 ka from the Northern basin of Lake Van, eastern Turkey. *Quaternary Science Reviews* 104, 97-116.

Castro, A., Aghazadeh, M., Badrzadeh, Z., Chichorro, M., 2013. Late Eocene-Oligocene post-collisional monzonitic intrusions from the Alborz magmatic belt, NW Iran. An Example of monzonite magma generation from a metasomatized mantle source. *Lithos* 180-181, 109-127.

Chadwick, O.A., Nettleton, W.D., Staidl, G.J., 1995. Soil polygenesis as a function of Quaternary climate change, northern Great Basin, USA. *Geoderma* 68, 1-26.

Cilek, V., 2001. The loess deposits of the Bohemian Massif: silt provenance, palaeometeorology and loessification processes. *Quaternary International* 76/77, 123-128.

Condie, K.C., 1993. Chemical composition and evolution of the Upper Continental Crust – contrasting results from surface samples and shales. *Chemical Geology* 104, 1-37.

Commission Internationale de l'Eclairage (CIE), 1978. Recommendations on Uniform Color Spaces, Color Differences, and Psychometric Color Terms. *Colorimetry CIE*, Paris Suppl. no. 2 to Publication no. 15.

Cornell, R. M., Schwertmann, U., 2003. The Iron Oxides – Structure, Properties, Reactions, Occurrences and Uses. Wiley-VCH, Weinheim.

Coudé-Gaussen, G., 1990. The loess and loess-like deposits along the sides of the western Mediterranean Sea: Genetic and palaeoclimatic significance. *Quaternary International* 5, 1-8.

Crouvi, O., Amit, R., Enzel, Y., Porat, N., Sandler, A., 2008. Sand dunes as a major proximal dust source for late Pleistocene loess in the Negev desert, Israel. *Quaternary Research* 70, 275-282.

Crouvi, O., Amit, R., Enzel, Y., Gillespie, A.R., 2010. Active sand seas and the formation of desert loess. *Quaternary Science Reviews* 29, 2087-2098.

Dando, W.A., 2005. Asia, Climates of Siberia, Central and East Asia. In: Oliver, J.E. (Ed.). *Encyclopedia of World Climatology*, Springer, Dordrecht, The Netherlands, 102-115.

Dansgaard, W., Johnsen, S.J., Clausen, H.B., Dahl-Jensen, D., Gundestrup, N.S., Hammer, C.U., Hvelberg, C.S., Steffensen, J.P., Sveinbjörnsdottir, A.E., Jouzel, J., Bond, G., 1993. Evidence for general instability of past climate from a 250-kyr ice-core record. *Nature* 364, 218-220.

Davidson, J., Hassanzadeh, J., Berzins, R., Stockli, D.F., Bashukoo, B., Turrin, B., Pandamouz, A., 2004. The geology of the Damavand volcano, Alborz Mountains, northern Iran. *Geological Society of America Bulletin* 116(1-2), 16-29.

Dearing, J.A., Hay, K.L., Baban, S.M.J., Huddleston, A.S., Wellington, E.M.H., Loveland, P.J., 1996. Magnetic susceptibility of soil: an evaluation of conflicting theories using a national data set. *Geophysical Journal International* 127, 728-734.

Derbyshire, E., Meng, X., Kemp, R.A., 1998. Provenance, transport and characteristics of modern aeolian dust in western Gansu Province, China, and interpretation of the Quaternary loess record. *Journal of Arid Environments* 39, 497-516.

Dietze, M., Kreutzer, S., Fuchs, M.C., Burow, C., Fischer, M., Schmidt, C., 2013. A practical guide to the R package Luminescence. *Ancient TL* 31(1), 11-18.

Djamali, M., De Beaulieu, J.-L., Shah-Hosseini, M., Andrieu-Ponel, V., Ponel, P., Amini, A., Akhiani, H., Leroy, S.A.G., Stevens, L., Lahijani, H., Brewer, S., 2008. A late Pleistocene long pollen record from Lake Urmia, Iran. *Quaternary Research* 69, 413-420.

Dodonov, A.E., 1991. Loess of Central Asia. *GeoJournal* 24(2), 185-194.

Dodonov, A.E., Baiguzina, L.L., 1995. Loess stratigraphy of Central Asia: Palaeoclimatic and palaeoenvironmental aspects. *Quaternary Science Reviews* 14, 707-720.

Dodonov, A.E., Sadchikova, T.A., Sedov, S.N., Simakova, A.N., Zhou, L.P., 2006. Multidisciplinary approach for paleoenvironmental reconstruction in loess-paleosol studies of the Darai Kalon section, Southern Tajikistan. *Quaternary International* 152-153, 48-58.

Dolukhanov, P.M., Chepalyga, A.L., Shkativa, V.K., Lavrentiev, N.V., 2009. Late Quaternary Caspian: sea-levels, environments and human settlements. *Open Geographical Journal* 2, 1-15.

Eckmeier, E., Mavris, C., Krebs, R., Pichler, B., Egli, M., 2012. Black carbon contributes to organic matter in young soils in the Morteratsch proglacial area (Switzerland). *Biogeosciences* 10, 1265-1274.

Eckmeier, E., Egli, M., Schmidt, M.W.I., Schlumpf, N., Nötzli, M., Minikus-Stary, N., Hagedorn, F., 2013. Preservation of fire-derived carbon compounds and sorptive stabilisation promote the accumulation of organic matter in black soils of the Southern Alps. *Geoderma* 159, 147-155.

Ehlers, E., 1971. Südkaspisches Tiefland Nordiran und Kaspisches Meer. Beiträge zu ihrer Entwicklungsgeschichte im Jung und Postpleistozän. *Tübinger Geographische Studien* 44, Tübingen.

Evans, M.E., Heller, F., 2003. *Environmental Magnetism – Principles and Applications of Enviromagnetics*. Academic Press, San Diego, California.

Farges, F., 1999. Titanium: Element Geochemistry. In: Marshall, C.P., Fairbridge, C.P., Rhodes, W. (Eds.). *Encyclopedia of Geochemistry*, Springer, 636-637.

Fedo, C., Nesbitt, H.W., Young, G.M., 1995. Unravelling the effects of potassium metasomatism in sedimentary rocks and paleosols, with implications for paleoweathering conditions and provenance. *Geology* 23, 921-924.

Feng, Z.D., Ran, M., Yang, Q.L., Zhai, X.W., Wang, W., Zhang, X.S., Huang, C.Q., 2011. Stratigraphies and chronologies of late Quaternary loess-paleosol sequences in the core area of the central Asian arid zone. *Quaternary International* 240, 156-166.

Fitzsimmons, K.E., Sprafke, T., Zielhofer, C., Günter, C., Deom, J.M., Sala, R., Iovita, R., 2016 (in press). Loess accumulation in the Tian Shan piedmont: Implications for palaeoenvironmental change in arid Central Asia. *Quaternary International*. <http://dx.doi.org/10.1016/j.quaint.2016.07.041>

Forte, A.M., Cowgill, E., 2013. Late Cenozoic base-level variations of the Caspian Sea: A review of its history and proposed driving mechanisms. *Palaeogeography, Palaeoclimatology, Palaeoecology* 386, 392-407.

Frechen, M., Schweitzer, U., Zander, A., 1996. Improvements in sample preparation for the fine grain technique. *Ancient TL* 14, 15 - 17.

Frechen, M., Horváth, E., Gábris, G., 1997. Geochronology of Middle and Upper Pleistocene Loess Sections in Hungary. *Quaternary Research*, 48(3), 291-312.

Frechen, M., Dodonov, A., 1998. Loess chronology of the Middle and Upper Pleistocene in Tadjikistan. *Geologische Rundschau* 87 (1), 2-20.

Frechen, M., van Vliet Lanoë, B., van den Haute, P., 2001. The Upper Pleistocene loess record at Harmignies/Belgium – high resolution terrestrial archive of climate forcing. *Palaeogeography, Palaeoclimatology, Palaeoecology*, 173, 175-195.

Frechen, M., Kehl, M., Rolf, C., Sarvati, R., Skowronek, A., 2009. Loess chronology of the Caspian Lowland in Northern Iran. *Quaternary International* 198, 220-233.

Fuchs, M., Owen, L.A., 2008. Luminescence dating of glacial and associated sediments: review, recommendations and future directions. *Boreas* 37, 639-659.

Gallet, S., Jahn, B., Torii, M., 1996. Geochemical characterization of the Luochuan loess-palesol sequence, China, and paleoclimatic implications. *Chemical Geology* 133, 67-88.

Gallet, S., Jahn, B., Van Vliet Lanoë, Dia, A., Rossello, E., 1998. Loess geochemistry and its implications for particle origin and composition of the upper continental crust. *Earth and Planetary Science Letters* 156, 157-172.

Galović, L., Frechen, M., Peh, Z., Durn, G., Halamić, J., 2011. Loess/palaeosol section in Šarengrad, Croatia – A qualitative discussion on the correlation of the geochemical and magnetic susceptibility data. *Quaternary International* 240, 22-34.

Ganji, M.H., 1968. Climate. In: Fisher, W.B. (Ed.). *The Land of Iran*. Cambridge, 212-249.

Ganopolski, A., Rahmstorf, S., 2001. Rapid changes of glacial climate simulated in a coupled climate model. *Nature* 409, 153-158.

Garrels, R.M., Mackenzie, F.T., 1971. *Evolution of Sedimentary Rocks*. Norton & Company, New York.

Geological Survey of Iran (1991). *Geological Quadrangle Map of Iran 1:250.000 series, Sheet No. H4 Gorgan*.

Ghafarpour, A., Khromali, F., Balsam, W., Karimi, A., Ayoubi, S., 2016. Climatic interpretation of loess-paleosol sequences at Mobarakabad and Aghband, Northern Iran. *Quaternary Research* 86, 98-109.

Gottschalk, J., Skinner, L.C., Misra, S., Waelbroeck, C., Menviel, L., Timmermann, A., 2015. Abrupt changes in the southern extent of North Atlantic Deep Water during Dansgaard-Oeschger events. *Nature Geoscience* 8, 950-955.

Greeley, R., Iversen, J.D., 1987. *Wind as a geological process on Earth, Mars, Venus and Titan*. Cambridge University Press, New York.

Guo, Z., Ding, Z., Liu, D., 1996. Pedosedimentary events in loess of China and quaternary climatic cycles. *Chinese Science Bulletin* 41(14), 1189-1193.

Haase, D., Fink, J., Haase, G., Ruske, R., Pécsi, M., Richter, H., Altermann, M., Jäger, K.D., 2007. Loess in Europe – its spatial distribution based on a European Loess Map, scale 1:2,500,000. *Quaternary Science Reviews* 26, 1301-1312.

Haldorsen, S., 1981. Grain-size distribution of subglacial till and its relation to glacial crushing and abrasion. *Boreas* 10(1), 91-105.

Hall, R.D. and Anderson, A.K., 2000. Comparative soil development of Quaternary palaeosols of the central United States. *Palaeogeography, Palaeoclimatology, Palaeoecology* 158, 109-145.

Hao, Q., Guo, Z., Qiao, Y., Xu, B., Oldfield, B., 2010. Geochemical evidence for the provenance of middle Pleistocene loess deposits in southern China. *Quaternary Science Reviews*, 29, 3317-3326.

Heinrich, H., 1988. Origin and consequences of cyclic ice rafting in the northeastern Atlantic Ocean during the past 130,000 years. *Quaternary Research* 29, 142-152.

Heller, F., Liu, T.-S., 1982. Magnetostratigraphical dating of loess deposits in China. *Nature* 300, 431-433.

Heller, F., Xiuming, L., Tungsheng, L., Tongchun, X., 1991. Magnetic susceptibility of loess in China. *Earth and Planetary Science Letters* 103, 301-310.

Heller, F., Evans, M. E., 1995. Loess magnetism. *Reviews of Geophysics* 33, 211-240.

Hemming, S., 2004. Heinrich events: Massive late Pleistocene detritus layers of the North Atlantic and their global climate imprint. *Reviews of Geophysics* 42, 1-43.

Hollingsworth, J., Jackson, J., Walker, R., Gheitanchi, M.R., Bolourchi, M.J., 2006. Strike-slip faulting, rotation, and along-strike elongation in the Kopeh Dag mountains, NE Iran. *Geophysical Journal International* 166, 1161-1177.

Huntley, D.J., Lamothe, M., 2001. Ubiquity of anomalous fading in K-feldspars and the measurement and correction for it in optical dating. *Canadian Journal of Earth Sciences* 38, 1093 – 1106

IUSS Working Group WRB. 2007. World Reference Base for Soil Resources 2006, first update 2007. World Soil Resources Reports No. 103. FAO, Rome.

Jahn, B., Gallet, S., Han, J., 2001. Geochemistry of the Xining, Xifeng and Jixian sections, Loess Plateau of China: eolian dust provenance and palaeosol evolution during the last 140 ka. *Chemical Geology* 178, 71-94.

Jenny H., 1941. *Factors of Soil Formation*. McGraw-Hill, New York.

Karimi, A., Khademi, H., Kehl, M., Jalalian, A., 2009. Distribution, lithology and provenance of peridesert loess deposits in northeastern Iran. *Geoderma* 148, 241-250.

Karimi, A., Frechen, M., Khademi, H., Kehl, M., Jalalian, A., 2011. Chronostratigraphy of loess deposits in northeast Iran. *Quaternary International* 234, 124-132.

Karimi, A., Khademi, H., Ayoubi, S., 2013. Magnetic susceptibility and morphological characteristics of a loess–paleosol sequence in northeastern Iran. *Catena* 101, 56-60

- Kehl, M., Sarvati, R., Ahmadi, H., Frechen, M., Skowronek, A., 2005a. Loess paleosol-sequences along a climatic gradient in Northern Iran. *Eiszeitalter und Gegenwart* 55, 151-175.
- Kehl, M., Frechen, M., Skowronek, A., 2005b. Paleosols derived from loess and loess-like sediments in the Basin of Persepolis, Southern Iran. *Quaternary International* 140/141, 135-149.
- Kehl, M., 2009. Quaternary climate change in Iran – the state of knowledge. *Erdkunde* 63(1), 1-17.
- Kehl, M., 2010. Quaternary loesses, loess-like sediments, soils and climate change in Iran. Gebr. Borntraeger Science Publishers, Stuttgart.
- Kemp, R.A., 2001. Pedogenic modification of loess: significance for palaeoclimatic reconstructions. *Earth-Science Reviews* 54, 145-156.
- Khormali, F., Kehl, M., 2011. Micromorphology and development of loess-derived surface and buried soils along a precipitation gradient in Northern Iran. *Quaternary International* 234, 109-123.
- Khormali, F., Ghergherechi, S., Kehl, M., Ayoubi, S., 2012. Soil formation in loess-derived soils along a subhumid to humid climate gradient, Northeastern Iran. *Geoderma* 179-180, 113-112.
- Kreutzer, S., Schmidt, C., DeWitt, R., Fuchs, M., 2014. The a-value of polymineral fine grain samples measured with the post-IR IRSL protocol. *Radiation Measurements* 69, 18-29.
- Kroonenberg, S., Rusakov, G.V., Svitoch, A.A., 1997. The wandering of the Volga delta: a response to rapid Caspian Sea-level change. *Sedimentary Geology* 107, 189-209.
- Kühn, P., Techmer, A., Weidenfeller, M., 2013. Lower to middle Weichselian pedogenesis and palaeoclimate in Central Europe using combined micromorphology and geochemistry: the loess-palaeosol sequence of Alsheim (Mainz Basin, Germany). *Quaternary Science Reviews* 75, 43-58.
- Kukla, G.J., Bender, M.L., de Beaulieu, J.L., Bond, G., Broecker, W.S., Cleveringa, P., Gavin, J.E., Herbert, T.D., Imbrie, J., Jouzel, J., Keigwin, L.D., Knudsen, K.L., McManus, J.F., Merkt, J., Muhs, D.R., Müller, H., Poore, R.Z., Porter, S.C., Seret, G., Shackleton, N.J., Turner, C., Tzedakis, P.C., Winograd, I.J., 2002. Last Interglacial Climates. *Quaternary Research* 58(1), 2-13.
- Lateef, A.S.A., 1988. Distribution, provenance, age and palaeoclimatic record of the Loess in Central North Iran. In: *Loess – its distribution, geology and soils*, Eden, D.N., Furkert, R.J. (Eds.), Balkema, Rotterdam, 93-101.

Lauer, T., Suchodoletz, H. von, Vollmann, H., Meszner, S., Frechen, M., Tinapp, C., Goldmann, L., Müller, S., Zielhofer, C., 2014. Landscape aridification in Central Germany during the late Weichselian Pleniglacial – results from the Zauschwitz loess site in western Saxony. *Zeitschrift für Geomorphologie* 58, suppl.1, 27-50.

Lauer, T., Frechen, M., Vlaminc, S., Kehl, M., Lehndorff, E., Shahriari, A., (2017a). Luminescence chronology of the loess-palaeosol sequence Toshan, Northern Iran – A highly resolved climate archive for the last glacial-interglacial cycle. *Quaternary International* 429, Part B, 3-12.

Lauer, T., Vlaminc, S., Frechen, M., Rolf, C., Kehl, M., Sharifi, J., Lehndorff, E., Khormali, F., (2017b). The Agh Band loess-palaeosol sequence – A terrestrial archive for climatic shifts during the last and penultimate glacial-interglacial cycles in a semiarid region in northern Iran. *Quaternary International* 429, Part B, 13-30.

LeBorgne, E., 1955. Susceptibilité magnétique anormale du sol superficiel. *Annales de Géophysique* 11, 399-419.

Lehmkuhl, F., Schulte, P., Zhao, H., Hülle, D., Protze, J., Stauch, G., 2014. Timing and spatial distribution of loess and loess-like sediments in the mountain areas of the northeastern Tibetan Plateau. *Catena* 117, 23-33.

Lei, GL., Zhang, HC., Pu, Y., Y, MS., 2010. Biomarkers of modern plants and soils from Xinglong Mountain in the transitional area between Tibetan and Loess Plateaus. *Quaternary International* 218, 143-150.

Leroy, S.A.G., Lahijani, H.A.K., Djamali, M., Naqinezhad, A., Moghadam, M.V., Arpe, K., Shah-Hosseini, M., Hosseindoust, M., Miller, Ch.S., Tavakoli, V., Habibi, P., Naderi Beni, M., 2011. Late Little Ice Age palaeoenvironmental records from the Anzali and Amirkola Lagoons (south Caspian Sea): Vegetation and sea level changes.

Li, B., Li, S., 2012. Luminescence dating of Chinese loess beyond 130 ka using the non-fading signal from K-feldspar. *Quaternary Geochronology*, 10 24-31.

Lisiecki, L. E., Raymo, M. E., 2005. A Pliocene-Pleistocene stack of 57 globally distributed benthic records. *Paleoceanography* 20, PA 1003.

Litt, T., Pickarski, N., Heumann, G., Stockhecke, M., Tzedakis, P.C., 2014. A 600,000 year long continental pollen record from lake Van, eastern Anatolia (Turkey). *Quaternary Science Reviews*, 1-12.

Loague, K., Green, R.E., 1991. Statistical and graphical methods for evaluating solute transport models: Overview and application. *Journal of Contaminant Hydrology* 7, 51-73.

Machalett, B., Frechen, M., Hambach, U., Ochse, E.A., Zöller, L., Marković, S.B., 2006. The loess sequence from Remisowka (northern boundary of the Tien Shan Mountains, Kazakhstan) – Part I: Luminescence dating. *Quaternary International* 152-153, 192-201.

Machalett, B., Oches, E.A., Zöller, L., Hambach, U., Mavlyanova, N.G., Marković, S., 2008. Aeolian dust dynamics in central Asia during the Pleistocene: Driven by the long-term migration, seasonality, and permanency of the Asiatic polar front. *Geochemistry Geophysics Geosystems* 9 (8), 1-22.

Maher, B.A., Thompson, R., 1995. Paleorainfall reconstructions from pedogenic MS variations in the Chinese loess and paleosols. *Quaternary Research* 44, 383-391.

Maher, B.A., 1998. Magnetic properties of modern soils and loessic paleosols: implications for paleoclimate. *Palaeogeography, Palaeoclimatology, Palaeoecology* 137, 383-391.

Maher, B.A., Mutch, T.J., Cunningham, D., 2009. Magnetic and geochemical characterization of Gobi Desert surface sediments: Implications for provenance of the Chinese Loess Plateau. *Geology* 37, 279-282.

Maher, B.A., 2011. The magnetic properties of Quaternary aeolian dusts and sediments, and their palaeoclimatic significance. *Aeol. Res.* 3, 87-144.

Markle, B.R., Steig, E.J., Buizert, C., Schoenenmann, S.W., Bitz, C.M., Fudge, T.J., Pedro, J.B., Ding, Q., Jones, T.R., White, J.W.C., Sowers, T., 2017. Global atmospheric teleconnections during Dansgaard-Oeschger events. *Nature Geoscience* 10, 36-40.

Marković, S. B, Bokhorst, M. P., Vandenberghe, J., McCoy, W. D., Oches, E. A., Hambach, U., Gaudenyi, T., Jovanović, M., Zöller, L., Stevens, T., Machalett, B., 2008. Late Pleistocene loess-paleosol sequences in the Vojvodina region, north Serbia. *Journal of Quaternary Science* 23 (1), 73-84.

Marković, S. B, Hambach, U., Catto, N., Jovanović, M., Buggle, B., Machalett, B., Zöller, L., Glaser, B., Frechen, M., 2009. Middle and Late Pleistocene loess sequences at Batajnica, Vojvodina, Serbia. *Quaternary International* 198 (1-2), 255-266.

Marković, S.B., Stevens, T., Kukla, G.J., Hambach, U., Fitzsimmons, K.E., Gibbard, P., Buggle, B., Zech, M., Guo, Z., Hao, Q., Wu, H., O'Hara Dhand, K., Smalley, I.J., Újvári, G., Sümegi, P., Timar-Gabor, A., Veres, D., Sirocko, F., Vasiljević, A., Jary, Z., Svensson, A., Jović, V., Lehmkuhl, F., Kovács, J., Svirčev, Z., 2015. Danube loess stratigraphy – Towards a pan-european loess stratigraphic model. *Earth-Science Reviews* 148, 228-258.

Marshall, S.J., 2009. Glaciations, Quaternary. In: Gornitz, V. (Ed.), 2009. *Encyclopedia of Palaeoclimatology*, Springer, 389-394.

Mason, J.A., Miao, X., Hanson, P.R., Johnson, W.C., Kacobs, P.M., Goble, R.J., 2008. Loess record of the Pleistocene-Holocene transition on the northern and central Great Plains, USA. *Quaternary Science Reviews* 27, 1772-1783.

McLennan, S.M., 1989. Rare earth elements in sedimentary rocks: Influence of provenance and sedimentary processes. In: Lipin, B.R., McKay, G.A. (Eds.), *Geochemistry and Mineralogy of Rare Earth Elements*. Chelsea, Michigan. *Reviews in Mineralogy* 21, 169-200.

McLennan, S.M., Taylor, S.R., 1991. Sedimentary Rocks and Crustal Evolution: Tectonic setting and Secular Trends. *Journal of Geology* 99, 1-21.

McLennan, S.M., 1993. Weathering and Global Denudation. *The Journal of Geology*. 101, 295-303.

McLennan, S.M., 2001. Relationships between the trace element composition of sedimentary rocks and upper continental crust. *Geochemistry, Geophysics, Geosystems* 2.

McTainsh, G., 1987. Desert loess in northern Nigeria. *Z. Geomorph.* 31, 145-165.

Melville, M.D., Atkinson, G., 1985. Soil colour: its measurement and its designation in models of uniform colour space. *Journal of Soil Science* 36, 495-512.

Mestdagh, H., Haesaerts, P., Dodonov, A., Hus, J., 1999. Pedosedimentary and climatic reconstruction of the last interglacial and early glacial loess-palaeosol sequence in South Tadzhikistan. *Catena* 35, 197-218.

Mittlefehldt, D.W., 1999. Cesium. In: Marshall, C.P., Fairbridge, C.P., Rhodes, W. (Eds.). *Encyclopedia of Geochemistry*. Springer, 76.

Molavi-Arabshahi, M., Arpe, K., Leroy, S.A.G., 2016. Precipitation and temperature of the southwest Caspian Sea region during the last 55 years: their trends and teleconnections with large-scale atmospheric phenomena. *International Journal of Climatology* 36, 2156-2172.

Mogensen, I.A., 2009. Dansgaard-Oeschger Cycles. In: Gornitz, V. (Ed.), 2009. *Encyclopedia of Palaeoclimatology*, Springer, 229-233.

Molanejad, M., Soltani, M., Ranjbar SaadatAbadi, A., Babu, C.A., Sohrabi, M., Martin, M.V., 2015. Climatology of Cyclones and Their tracking over Southern Coasts of Caspian Sea. *International Journal of Environmental Research* 9(1), 117-132.

Molavi-Arabshahi, M., Arpe, K., Leroy, S.A.G., 2016. Precipitation and temperature of the southwest Caspian Sea region during the last 55 years: their trends and teleconnections with large-scale atmospheric phenomena. *International Journal of Climatology* 36, 2156–2172.

Mortazavi, M., Moussavi-Harami, R., Mahoubi, A., 2013. Detrital Mode and Geochemistry of the Shurijeh formation (Late Jurassic-Early Cretaceous) in the central and Western Parts of the Intracontinental Kopet-Dagh Basin, NE Iran: Implications for Provenance, Tectonic Setting and Weathering Processes. *Acta Geologica Sinica (English Edition)* 87(4), 1058-1080.

Müller, U.C., 2009. Eemian (Sangamonian) Interglacial. In: Gornitz, V. (Ed.), 2009. *Encyclopedia of Palaeoclimatology*, Springer, 302-307.

Muhs, D.R., 2002. Evidence for the timing and duration of the last interglacial period from high-precision Uranium-Series Ages of corals on tectonically stable coastlines. *Quaternary Research* 58, 36-40.

Muhs, D.R., Budahn, J.R., 2006. Geochemical evidence for the origin of late Quaternary loess in central Alaska. *Canadian Journal of Earth Sciences* 43, 323-337.

- Muhs, D.R., 2012. The geologic records of dust in the Quaternary. *Aeolian Research* 9, 3-48.
- Muhs, D.R., Bettis III, E., Roberts, H.M, Harlan, S.S., Paces, J.B., Reynolds, R.L., 2013. Chronology and provenance of last-glacial (Peoria) loess in western Iowa and paleoclimatic implications. *Quaternary Research* 80, 468-481.
- Mullins, C.E., 1977. Magnetic susceptibility of the soil and its significance in soil science – A review. *Journal of Soil Science* 28, 223-246.
- Murray, A.S., Schmidt, E.D., Stevens T., Buylaert, J.-P., Marković, S. B., Tsukamoto, S., Frechen, M., 2014. Dating Middle Pleistocene loess from Stari Slankamen (Vojvodina, Serbia) - Limitations imposed by the saturation behaviour of an elevated temperature IRSL signal. *Catena*, 117, 34-42.
- Nahon, D., Trompette, R., 1982. Origin of siltstones: glacial grinding versus weathering. *Sedimentology* 29, 25-35.
- Nesbitt, H.W., Young, G.M., 1982. Early Protozoic climates and plate motions inferred from major element chemistry of lutites. *Nature* 229, 715-717.
- Nouri, H., Ghayour, H., Masoodian, A., Azadi, M., Ildoromi, A., 2013. The effect of Sea Surface Temperature and 2m Air Temperature on Precipitation Events in the Southern Coasts of Caspian Sea. *Ecopersia* 4, 369-383.
- Novothny, A., Frechen, M., Horváth, E., Wacha, L., Rolf, C., 2011. Investigating the penultimate and last glacial cycles of the Süttö loess section (Hungary) using luminescence dating, high-resolution grain size, and magnetic susceptibility data. *Quaternary International* 234, 75-85.
- Obrecht, I., Buggle, B., Catto, N., Marković, S.B., Bösel, S., Vandenberghe, D.A.G., Hambach, U., Svirčev, Z., Lehmkuhl, F., Basarin, B., Gavrilov, M.B., Jović, G., 2014. The late Pleistocene Belotinac section (southern Serbia) at the southern limit of the European loess belt: environmental and climate reconstruction using grain size and stable C and N isotopes. *Quaternary International* 334-335, 10-19.
- Okhravi, R, Amini, A., 2001. Characteristics and provenance of the loess deposits of the Gharatikan watershed in Northeast Iran. *Global and Planetary Change* 28, 11-22.
- Orlovsky, L., Orlovsky, N., Durdyev, A., 2005. Dust storms in Turkmenistan. *Journal of Arid Environments* 60, 83-97.
- Pécsi, M., 1990. Loess is not just the accumulation of dust. *Quaternary International* 7/8, 1-21.
- Pécsi, M., 1995. The Role of Principles and Methods in Loess-Paleosol Investigations. *GeoJournal* 36, 117-131.

Pécsi, M., Richter, G., Löss: Herkunft – Gliederung – Landschaften. *Annals of Geomorphology*, suppl. Volume 98, Gebrüder Bornträger, Berlin, Stuttgart.

Pickarski, N., Kwiecien, O., Langgut, D., Litt, T., 2015. Abrupt climate and vegetation variability of eastern Anatolia during the last glacial. *Climate of the Past* 11, 1491-1505.

Prescott, J.R., Hutton, J.T., 1994. Cosmic ray contributions to dose rates for luminescence and ESR dating: large depths and long-term time variations. *Radiation Measurements* 23, 497 - 500.

Prins, M.A., Vriend, M., Nugteren, G., Vandenberghe, J., Lu, H., Zheng, H., Weltje, G.J., 2007. Late Quaternary aeolian dust input variability on the Chinese Loess Plateau: inferences from unmixing of loess grain-size records. *Quaternary Science Reviews* 26, 230-242.

Pross, J., Koutsodendris, A., Christianis, K., Fischer, T., Fletcher, W.J., Hardiman, M., Kalaitzidis, S., Knipping, M., Kotthoff, U., Milner, A.M., Müller, U.C., Schmiedl, G., Siavalas, G., Tzedakis, P.C., Wulf, S., 2015. *Newsletters on Stratigraphy* 48(3), 253-276.

Pye, K. (1987). *Aeolian Dust and Dust Deposits*. Academic Press, London.

Pye, K., 1995. The nature, origin and accumulation of loess. *Quaternary Science Reviews* 14, 653-667.

Rasmussen, S.O., Bigler, M., Blockley, S.P., Blunier, T., Buchardt, S.L., Clausen, H.B., Cvijanovic, I., Dahl-Jensen, D., Johnsen, S.J., Fischer, H., Gkinis, V., Guillevic, M., Hoek, W.Z., Lowe, J.J., Pedro, J.B., Popp, T., Seierstad, I.K., Steffensen, J.P., Svensson, A.M., Vellelonga, P., Vinther, B.M., Walker, M.J.C., Wheatley, J.J., Winstrup, M., 2014. A stratigraphic framework for abrupt climatic changes during the Last Glacial period based on three synchronized Greenland ice-core records: refining and extending the INTIMATE event stratigraphy. *Quaternary Science Reviews* 106, 14-28.

Richthofen, F. von, 1882. On the mode of origin of the loess. *Geological Magazine* 9, 293-305.

Rees-Jones, J., 1995. Optical dating of young sediments using fine-grain quartz. *Ancient TL* 13, 9e14.

Rieben, E.H., 1966. Geological observations on alluvial deposits in Northern Iran. Geological Survey of Iran, Report 9, Teheran

Robert, A.M.M., Letouzey, J., Kavoosi, M.A., Sherkati, S., Müller, C., Vergés, J., Aghababaei, A., 2014. Structural evolution of the Kopeh Dagh fold-and-thrust belt (NE Iran) and interactions with the South Caspian Sea Basin and Amu Darya Basin. *Marine and Petroleum Geology* 57, 68-87.

Roberts, H.M., Muhs, D.R., Wintle, A.G., Duller, G.A.T., Bettis, E.A., 2003. Unprecedented last-glacial mass accumulation rates determined by dating of loess from western Nebraska. *Quaternary Research* 59, 411-419.

Roberts, H.M., 2008. The development and application of luminescence dating to loess deposits: a perspective on the past, present and future. *Boreas* 37, 483-507.

Roberts, H.M., 2015. Luminescence Dating, Loess. In: Rink, W.J., Thompson, J.W. (Eds.). *Encyclopedia of Scientific Dating Methods*. Springer, New York, 425-430.

Rolf, C., Hambach, U., Novothny, Á., Horváth, E., Schnepf, E., 2014. Dating of a Last Glacial loess sequence by relative geomagnetic palaeointensity: A case study from the Middle Danube Basin (Süttő, Hungary). *Quaternary International* 319, 99-108.

Rowe, P.J., Mason, J.E., Andrews, J.E., Marca, A.D., Thomas, L., van Calsteren, P., Jex, C.N., Vonhof, H.B., Al-Omari, S., 2012. Speleothem isotopic evidence of winter rainfall variability in northeast Turkey between 77 and 6 ka. *Quaternary Science Reviews* 45, 60-72.

Schatz, A.K., Zech, M., Buggle, B., Guylás, S., Hambach, U., Marković, S.B., Sümegid, P., Scholten, T., 2011. The late quaternary loess record of Tokaj, Hungary: reconstructing palaeoenvironment, palaeovegetation and palaeoclimate using stable C and N isotopes and biomarkers. *Quaternary International* 240 (1-2), 52-61.

Scheffer, F., Schachtschabel, P. (Eds.) 2009. *Lehrbuch der Bodenkunde*. Spektrum Akademischer Verlag, Heidelberg.

Schmidt, E. D., Tsukamoto S., Frechen M., Murray A.S., 2014. Elevated temperature IRSL dating of loess sections in the East Eifel region of Germany. *Quaternary International*, 334-335, 141-154.

Schnepf, E., Worm, K., Scholger, R., 2008. Improved sampling techniques for baked clay and soft sediments. *Physics and Chemistry of the Earth, Parts A/B/C* 33, 407-413.

Schroder, J.F., Jensen Schettler, M., Weihs, B.J., 2011. Loess failure in northeast Afghanistan. *Physics and Chemistry of the Earth* 36, 1287-1293.

Shahriari, A., Khormali, F., Bläsing, B., Vlamincx, S., Kehl, M., Frechen, M., Karimi, A., Lehdorff, E., 2017. Biomarkers in modern and buried soils of semi-desert and forest ecosystems of northern Iran. *Quaternary International*, 1-12. [dx.doi.org/10.1016/j.quaint.2016.02.048](https://doi.org/10.1016/j.quaint.2016.02.048)

Smalley, I.J., Krinsley, D.H., 1978. Loess deposits associated with deserts. *Catena* 5(1), 56-66.

Smalley, I.J., Derbyshire, E., 1990. The definition of ice-sheet and mountain loess. *Area* 22, 300-301.

Smalley, I.J., Jefferson, I.F., Dijkstra, T.A., Derbyshire, E., 2001. Some major events in the development of the scientific study of loess. *Earth-Science Reviews* 54, 5-18.

Smalley, I.J., Kumar, R., O'Hara-Dhand, K., Jefferson, I.F., Evans, R.D., 2005. The formation of silt material for terrestrial sediments: Particularly loess and dust. *Sedimentary Geology* 179, 321-328.

Smalley, I.J., O'Hara-Dhand, K., Wint, J., Machalett, B., Jary, Z., Jefferson, I., 2009. Rivers and loess: The significance of long river transportations in the complex event-sequence approach to loess deposit formation. *Quaternary International* 198, 7-18.

Smalley, I.J., Marković, S.B., Svirčev, Z., 2011. Loess is [almost totally formed by] the accumulation of dust. *Quaternary International* 240, 4-11.

Smalley, I.J., Marković, S.B., 2014. Loessification and hydroconsolidation: There is a connection. *Catena* 117, 94-99.

Smith, B.J., Wright, J.S., Whalley, W.B., 2002. Sources of non-glacial, loess-size quartz silt and the origins of "desert loess". *Earth-Science Reviews* 59, 1-26.

Smykatz-Kloss, B., 2003. Die Lößvorkommen des Pleiser Hügellandes bei Bonn und Neustadt/Wieds sowie der Picardie: Mineralogisch-geochemische und geomorphologische Charakterisierung. Verwitterungs-Beeinflussung und Herkunft der Löss. Dissertation, University of Bonn. URL: http://hss.ulb.uni-Bonn.de/diss_online/math_nat_fak/2003/smykatz-kloss_bettina

Sprafke, T., Terhorst, B., Peticzka, R., Thiel, C., 2013. Paudorf locus typicus (Lower Austria) revisited – the potential of the classic loess outcrop for Middle to Late Pleistocene landscape reconstructions. *Quaternary Science Journal (E&G)* 62, 59-72.

Sprafke, T., Obreht, I., 2016. Loess: Rock, sediment or soil – What is missing for its definition?. *Quaternary International* 399, 198-207.

Sun, J., 2002. Provenance of loess material and formation of loess deposits on the Chinese Loess Plateau. *Earth and Planetary Science Letters* 203, 845-859.

Stahl, A.F.V., 1923. Zur Frage der Lößbildung. *Zeitschrift der Deutschen geologischen Gesellschaft* 74, 320-325.

Stephan, S., 2000. Bt-Horizonte als Interglazial-Zeiger in den humiden Mittelbreiten: Bildung, Mikromorphologie, Kriterien. *Eiszeitalter und Gegenwart* 50, 95-106.

Stevens, L.R., Djamali, M., Andrieu-Ponel, V., de Beaulieu, J.L., 2012. Hydroclimatic variations over the last two glacial/interglacial cycles at Lake Urmia, Iran. *Journal of Paleolimnology* 47, 645-660.

Stevens, T., Adamiec, G., Bird, A. F., Lu, H., 2013. An abrupt shift in dust source on the Chinese Loess Plateau revealed through high sampling resolution OSL dating. *Quaternary Science Reviews* 82, 121-132.

Stockhecke, M., Timmermann, A., Kipfer, R., Haug, G.H., Kwiecien, O., Friedrich, F., Menviel, L., Litt, T., Pickarski, T., Anselmetti, F.S., 2016. Millennial to orbital-scale variations of drought intensity in the Eastern Mediterranean. *Quaternary Science Reviews* 133, 77-95.

Stoops, G. (2003): Guidelines for analysis and description of soil and regolith thin sections. 184 pp., Soil Sci. Soc. of America, Madison, Wisconsin.

Sun, J., 2002. Provenance of loess material and formation of loess deposits on the Chinese Loess Plateau. *Earth and Planetary Science Letters* 203, 845-859.

Svirčev, Z., Marković, S.B., Stevens, T., Codd, G.A., Smalley, I., Simeunović, J., Obreht, I., Dulić, T., Pentelić, D., Hambach, U., 2013. Importance of biological loess crusts for loess formation in semi-arid environments. *Quaternary International* 296, 206-215.

Svitoch, A.A., 2013. The Pleistocene Manych straits: Their structure, evolution and role in the Ponto-Caspian basin development. *Quaternary International* 302, 101-109.

Taheri, M., Khormali, F., Wang, X., Amini, A., Wie, H., Kehl, M., Frechen, M., Chen, F., 2017. Micromorphology of the lower Pleistocene loess in the Iranian loess Plateau and its palaeoclimatic implications. *Quaternary International* 429, 31-40.

Taylor, S.R., McLennan, S.M., McCulloch, M.T., 1983. Geochemistry of loess, continental crustal composition and crustal model ages. *Geochimica et Cosmochimica Acta* 47, 1897-1905.

Taylor, S.R., McLennan, S.M., 1985. *The continental crust: Its Composition and Evolution*. Blackwell, London.

Taylor, S.R., McLennan, S.M., 1995. The geochemical evolution of the continental crust. *Reviews of Geophysics* 33, 241-265.

Thiel, C., Buylaert, J.-P., Murray, A.S., Terhorst, B., Hofer, I., Tsukamoto, S., Frechen, M., 2011. Luminescence dating of the Stratzing loess profile (Austria) - Testing the potential of an elevated temperature post-IR IRSL protocol. *Quaternary International* 234, 23-31.

Thrasher, I.M., Mauz, B., Chiverrell, R.C., Lang, A., 2009. Luminescence dating of glaciofluvial deposits: A review. *Earth-Science Reviews* 97, 133-146.

Tietze, E., 1877. Ueber Lössbildung und ueber die Bildung von Salzsteppen. *Verhandlungen der Kaiserlich Königlich geologischen Reichsanstalt* 15, 264-268.

Torrent, J., Cabedo, A., 1986. Sources of iron oxides in reddish brown soil properties from calcarenites in southern Spain. *Geoderma* 37, 57-66.

Tsoar, H., Pye, K., 1987. Dust transport and the question of desert loess formation. *Sedimentology* 34, 139-153.

Tudryn, A., Chlić, F., Lavrushin, Y.A., Antipov, M.P., Spiridonova, E.A., Lavrushin, V., Tucholka, P., Leroy, S.A.G., 2013. Late Quaternary Caspian Sea environment: late

Khazarian and early Khvalynian transgressions from the lower reaches of the Volga River. *Quaternary International* 292, 193-204.

Újvári, G., Varga, A., Balogh-Brunstad, Z., 2008. Origin, weathering and geochemical composition of loess in southwestern Hungary. *Quaternary Research* 69, 421-437.

Vandenberghe, J.F., Múcher, H.J., Roebroeks, W., Gemke, D., 1985. Lithostratigraphy and palaeoenvironment of the Pleistocene deposits at Maastricht-Belvédère, southern Limburg, the Netherlands. *Mededelingen Rijks Geologische Dienst* 39 (1), 7-29.

Vandenberghe, J., Zhisheng, An., Nugteren, G., Huayu, L., Huissteden, K. van, 1997. New absolute time scale for the Quaternary climate in the Chinese loess region by grain-size analysis. *Geology* 25(1), 35-38.

Vandenberghe, J., Renssen, H., Huissteden, K.v., Nugteren, G., Konert, M., Lu, H., Dodonov, A., Buylaert, J.P., 2006. Penetration of Atlantic westerly winds into Central and East Asia. *Quaternary Science Reviews* 25, 2380-2389.

Viscarra Rossel, R.A., Walvoort, D.J.J., McBartney, A.B., Janik, L.J., Skjemstad, J.O., 2006. Visible, near infrared, mid infrared or combined diffuse reflectance spectroscopy for simultaneous assessment of various soil properties. *Geoderma* 131, 59-75.

Vlaminck, S., Kehl, M., Lauer, T., Shahriari, A., Sharifi, J., Eckmeier, E., Lehndorff, E., Khormali, F., 2016. Loess-soil sequence at Toshan (Northern Iran): Insights into late Pleistocene climate change. *Quaternary International* 399, 122-135.

Voelker, A.H.L., workshop participants, 2002. Global distribution of centennial-scale records for Marine Isotope Stage (MIS) 3: a database. *Quaternary Science Reviews* 21, 1185-1212.

Wacha, L., Pavlaković, S. M., Frechen, M., Crnjaković, M., 2011. The Loess Chronology of the Island of Susak, Croatia. *Quaternary Science Journal* 60, 153 – 169.

Wang, X., Wei, H., Taheri, M., Khormali, F., Danukalova, G., Chen, F., 2016a. Early Pleistocene climate in western arid central Asia inferred from loess-palaeosol sequences. *Scientific Reports* 6, 1-9.

Wang, X., Wei, H., Khormali, F., Taheri, M., Kehl, M., Frechen, M., Lauer, T., Chen, F., 2017. Grain-size distribution of Pleistocene loess deposits in northern Iran and its palaeoclimatic implications. *Quaternary International* 429, 41-51.

Weltje, G.J., 1997. End-Member Modeling of Compositional Data: Numerical-Statistical Algorithms for Solving the Explicit Mixing Problem. *Mathematical Geology* 29(4), 503-549.

Whalley, W.B., Marshall, J.R., Smith, B.J., 1982. Origin of desert loess from some experimental observations. *Nature* 300, 433-435.

Wintle, A.G., 1973. Anomalous fading of thermoluminescence in mineral samples. *Nature* 245, 143-144.

Wolf, D., Baumgart, P., Meszner, S., Fülling, A., Haubold, F., Sahakyan, L., Meliksetian, K., Faust, D., 2016. Loess in Armenia – stratigraphic findings and palaeoenvironmental indications. *Proceedings of the Geologists' Association* 127, 29-39.

Wright, J., Smith, B.J., Whalley, B., 1998. Mechanisms of loess-sized quartz silt production and their relative effectiveness: laboratory simulations. *Geomorphology* 23, 15-34.

Wright, J.S., 2001. "Desert" loess versus "glacial" loess: quartz silt formation, source areas and sediment pathways in the formation of loess deposits. *Geomorphology* 36, 231-256.

Wright, J.S., 2001a. Making loess-sized quartz-silt: data from laboratory simulations and implications for sediment transport pathways and the formation of 'desert' loess deposits associated with the Sahara. *Quaternary International* 76/77, 7-19.

Wright, J.S., 2007. An overview of the role of weathering in the production of quartz silt. *Sedimentary Geology* 202, 337-351.

Yaalon, D.H., Dan, J., 1974. Accumulation and distribution of loess-derived deposits in the semi-desert fringe areas of Israel. *Annals of Geomorphology*, suppl. Volume 20, Gebrüder Bornträger, Berlin, Stuttgart.

Yang, S.L., Ding, Z.L., 2003. Color reflectance of Chinese loess and its implications for climate gradient change during the last two glacial-interglacial cycles. *Geophysical research letters* 30 (20), 1-4.

Yanina, T.A., 2012. Correlation of the Late Pleistocene paleogeographical events of the Caspian Sea and Russian Plain. *Quaternary International* 271, 120-129.

Yanina, T. A., 2014. The Ponto-Caspian region: Environmental consequences of climate change during the Late Pleistocene. *Quaternary International* 345, 88-99.

Zech, M., Andreev, A., Zech, R., Müller, S., Hambach, U., Frechen, M., Zech, W., 2010. Quaternary vegetation changes derived from a loess-like permafrost palaeosol sequence in northeastern Siberia using alkane biomarker and pollen analyses. *Boreas* 39(3), 540-550.

Zech, M., Krause, T., Meszner, S., Faust, D., 2013. Incorrect when uncorrected: Reconstructing vegetation history using *n*-alkane biomarkers in loess-palaeosol sequences – A case study from the Saxonian loess region, Germany. *Quaternary International* 296, 108-116.

Zeeden, C., Hambach, U., Veres, D., Fitzsimmons, K., Obrecht, I., Böskén, J., Lehmkuhl, F., 2017 (in press). Millennial scale climate oscillations recorded in the Lower Danube loess over the last glacial period. *Palaeogeography, Palaeoclimatology, Palaeoecology*. [dx.doi.org/10.1016/j.palaeo.2016.12.029](https://doi.org/10.1016/j.palaeo.2016.12.029)

Zickel, M., Becker, D., Verheul, J., Yener, Y., Willmes, C., 2016. Paleocoastlines GIS dataset. CRC806-Database, doi: 10.5880/SFB806.20.

Eigenbeteiligung an Veröffentlichungen

1. **Vlaminck, S.**, Kehl, M., Lauer, T., Shahriari, A., Sharifi, J., Eckmeier, E., Lehndorff, E., Khormali, F., 2016. Loess-soil sequence at Toshan (Northern Iran): Insights into late Pleistocene climate change. *Quaternary International* 399, 122-135.
Geländearbeit: 65%
Erhebung der Daten im Labor: 85 %
Auswertung und Interpretation: 95 %
Verfassen der Publikation: 95 %
2. Lauer, T., **Vlaminck, S.**, Frechen, M., Rolf, C., Kehl, M., Sharifi, J., Lehndorff, E., Khormali, F., 2017. The Agh Band loess-palaeosol sequence – A terrestrial archive for climatic shifts during the last and penultimate glacial-interglacial cycles in a semiarid region in northern Iran. *Quaternary International* 429 Part B, 13-30.
Geländearbeit: 65%
Erhebung der Daten im Labor: 50 %
Auswertung und Interpretation: 55 %
Verfassen der Publikation: 55 %
3. **Vlaminck, S.**, Rolf, C., Franz, S.O., Lauer, T., Kehl, M., Lehndorff, E., Frechen, M., Khormali, F., (2016). Geochemical and rock magnetic properties of the Toshan loess-soil sequence (NE Iran): 130 ka record of loess and palaeosol formation (under review).
Geländearbeit: 65%
Erhebung der Daten im Labor: 75 %
Auswertung und Interpretation: 95 %
Verfassen der Publikation: 95 %
4. **Vlaminck, S.**, Kehl, M., Köhler, T., Frechen, M., Lehndorff, E., Khormali, F., (2017). The loess-soil sequence at Neka-Abelou and its palaeoclimatic implications: towards a pedostratigraphic model of northeastern Iran (manuscript).
Geländearbeit: 65%
Erhebung der Daten im Labor: 25 %
Auswertung und Interpretation: 80 %
Verfassen der Publikation: 90 %

Erklärung

Ich versichere, dass ich die von mir vorgelegte Dissertation selbständig angefertigt, die benutzten Quellen und Hilfsmittel angegeben und die Stellen der Arbeit – einschließlich Tabellen, Karten und Abbildungen –, die anderen Werken im Wortlaut oder dem Sinn nach entnommen sind, in jedem Einzelfall als Entlehnung kenntlich gemacht habe; dass diese Dissertation noch keiner anderen Fakultät oder Universität zur Prüfung vorgelegen hat; dass sie – abgesehen von unten angegebenen Teilpublikationen – noch nicht veröffentlicht worden ist, sowie, dass ich eine solche Veröffentlichung vor Abschluss des Promotionsverfahrens nicht vornehmen werde. Die Bestimmungen der Promotionsordnung sind mir bekannt. Die von mir vorgelegte Dissertation ist von PD Dr. Martin Kehl betreut worden.

[1] Vlaminck, S., Kehl, M., Lauer, T., Shahriari, A., Sharifi, J., Eckmeier, E., Lehndorff, E., Khormali, F., 2016. Loess-soil sequence at Toshan (Northern Iran): Insights into late Pleistocene climate change. *Quaternary International* 399, 122-135.

[2] Lauer, T., Vlaminck, S., Frechen, M., Rolf, C., Kehl, M., Sharifi, J., Lehndorff, E., Khormali, F., 2017. The Agh Band loess-palaeosol sequence – A terrestrial archive for climatic shifts during the last and penultimate glacial-interglacial cycles in a semiarid region in northern Iran. *Quaternary International* 429, Part B, 13-30.

[3] Vlaminck, S., Rolf, C., Franz, S.O., Lauer, T., Kehl, M., Lehndorff, E., Frechen, M., Khormali, F., (2016). Geochemical and rock magnetic properties of the Toshan loess-soil sequence (NE Iran): 130 ka record of loess and palaeosol formation [**under review**].

[4] Vlaminck, S., Kehl, M., Köhler, T., Frechen, M., Lehndorff, E., Khormali, F., (2017). The loess-soil sequence at Neka3 and its palaeoclimatic implications: towards a pedostratigraphic model of northeastern Iran [**manuscript**].

Curriculum vitae

02.01.1982	geboren in Köln
08/1993 bis 07/2001	Abitur am Hölderlin Gymnasium, Köln
08/2001 bis 07/2004	Ausbildung zum Versicherungskaufmann (DEVK-Versicherung)
08/2004 bis 03/2005	Zivildienst
04/2005 bis 12/2011	Studium der Geographie (Universität zu Köln), Nebenfächer Geologie (Universität zu Köln) und Bodenkunde (Rheinische Friedrich-Wilhelm Universität Bonn), Abschluss: Diplom-Geographie (Note: 1,0)
01/2012 bis 10/2012	Nebentätigkeiten
12/2012 bis jetzt	Wissenschaftlicher Mitarbeiter in der AG Kehl, Geographisches Institut der Universität zu Köln